AGH University of Science and Technology

FACULTY OF MECHANICAL ENGINEERING AND ROBOTICS

DEPARTMENT OF POWER SYSTEMS AND ENVIRONMENTAL PROTECTION FACILITIES

DOCTORAL THESIS

Thermodynamic modelling of modern low-emission power units with a gas turbine

Author: Navaneethan Subramanian, M.Sc.

Supervisor: Paweł Madejski, PhD., DSc., Eng.

Completed in: Faculty of Mechanical Engineering and Robotics

Kraków, 2025

"தாமின் புறுவது உலகின் புறக்கண்டு
காமுறுவர் கற்றறிந் தார்"

- குறள் 399, திருக்குறள் (300 BCE - 5 CE)

”Those who gain joyful knowledge recognize its positive impact on the world and are motivated to keep learning for the fulfillment it brings”

- Kural 399, Thirukkural (300 BCE - 5 CE)

Acknowledgement

I would like to express my deepest gratitude to my supervisor, Prof. Paweł Madejski, for his guidance, support, and for granting me this opportunity. His insights and encouragement have been instrumental in shaping this work. I also extend my sincere thanks to my colleague, Tomasz Kuś, and the POLNOR project partners for their collaboration and assistance throughout this journey. In addition, I am grateful to faculty members whose support has significantly contributed to my academic growth.

I dedicate this thesis to my late uncle and guardian, Mannar Maran Dhandayuthapani, whose wisdom and enduring presence continue to inspire me. My heartfelt gratitude goes to my parents, Prabha and Subramanian, for their unwavering love, sacrifices, and constant encouragement. I also sincerely thank my extended family for their support, which has played a crucial role in my journey. Thanks to all the people who supported me during this time and made a difference with their presence.

The research leading to these results has received funding from the Norway Grants 2014-2021 via the National Centre for Research and Development. Work has been prepared within the frame of the project: ”Negative CO_2 emission gas power plant” - NOR/POLNORCCS/NEGATIVE-CO2-PP/0009/2019-00 which is co-financed by programme “Applied research” under the Norwegian Financial Mechanisms 2014-2021 POLNOR CCS 2019 - Development of CO_2 capture solutions integrated in power and industry processes.

Abstract

The growing global demand for energy and anthropogenic activities to satisfy demand has led to a significant increase in greenhouse gas emissions, contributing to global warming and climate change. Addressing these challenges requires the development of high-efficiency energy systems with low carbon dioxide (CO_2) emissions, as the energy sector is a leading contributor to global CO_2 emissions. The main objective of this research is to perform a comprehensive thermodynamic analysis of gas and steam power cycles, with a focus on improving the operational efficiency of low-emission combined cycle gas turbine (CCGT) power plants. Based on the concept of bioenergy with carbon capture and storage (BECCS) technology, the study aims to determine the properties of the fuel that allows the transition of a large-scale gas plant to a carbon-free CCGT power plant using CO_2-neutral fuels.

The study evaluates the performance of CO_2-neutral fuels, which involves a mixture of gaseous fossil fuels such as pure methane and nitrogen-rich natural gas in certain proportions with syngas derived from biomass sources such as sewage sludge. A detailed analysis of CCGT power plant integrated with CO_2 capture systems is performed to determine achievable levels of CO_2 capture. A thermodynamic modelling of a reference power plant is developed considering the critical components of large-scale power plants integrated with CO_2 capture installations. Flue gases generated from various fuel compositions are processed under different load conditions using solvents such as monoethanolamine (MEA) and a mixture of 2-amino-2-methyl-1-propanol (AMP) with piperazine (PZ). Since steam is extracted for amine regeneration from the power plant, the performance of the CCGT power plant varies depending on the fuel composition and the type of solvent, which impacts the overall efficiency of the system.

CCGT performance analyses with and without integration of district heating network (DHN) show that combining fossil fuels with syngas and implementing CO_2 capture under varying load conditions allow the potential to achieve negative emissions. When syngas is mixed with fossil fuels, methane mixtures show better performance in power plant operation and N_2 rich gas mixtures are more effective in reducing emissions. Syngas proportions of 50% or more with methane and all proportions of syngas mixed with N_2 rich gas show the potential to achieve negative emissions when CO_2 capture systems operate under full or 90% load conditions. The results of the thermodynamic modelling are analyzed through key performance indicators, such as energy, economic, and environmental indicators. Economic analyses confirm the viability of the reference case system in real-world applications. The results confirm the potential for the integrating syngas with fossil fuels and using CO_2 capture technologies to achieve environmental targets while maintaining economic feasibility.

Streszczenie

Rosnący globalny popyt na energię oraz antropogeniczne działania podejmowane w celu jego zaspokojenia doprowadziły do znacznego wzrostu emisji gazów cieplarnianych, co przyczynia się do globalnego ocieplenia i zmian klimatycznych. Zmierzenie się z tymi wyzwaniami wymaga opracowania wysokoefektywnych systemów energetycznych o niskiej emisji dwutlenku węgla (CO_2), ponieważ sektor energetyczny jest jednym z głównych źródeł globalnej emisji CO_2. Głównym celem tych badań jest przeprowadzenie kompleksowej analizy termodynamicznej obiegów gazowo-parowych, koncentrując się na poprawie efektywności operacyjnej niskoemisyjnych elektrowni gazowo-parowych (CCGT). W oparciu o koncepcję bioenergii z wychwytem i składowaniem dwutlenku węgla (BECCS), badanie ma na celu określenie właściwości paliw umożliwiających przekształcenie dużych elektrowni gazowych w bezemisyjne jednostki CCGT wykorzystujące paliwa neutralne pod względem emisji CO_2.

Wyniki badań pozwalają ocenić efektywność stosowania paliw neutralnych pod względem emisji CO_2, które obejmują mieszaniny gazowych paliw kopalnych, takich jak czysty metan i gaz ziemny bogaty w azot w określonych proporcjach, wraz z gazem syntezowym pochodzącym z biomasy, na przykład z osadów ściekowych. Przeprowadzono szczegółową analizę elektrowni CCGT zintegrowanej z systemami wychwytu CO_2, aby określić możliwe do osiągnięcia poziomy wychwytu CO_2. Opracowano modele termodynamiczne elektrowni referencyjnej, uwzględniając kluczowe elementy dużych elektrowni zintegrowanych z instalacjami wychwytu CO_2. Gazy spalinowe generowane z różnych składów paliw są przetwarzane w różnych warunkach obciążenia za pomocą czynników takich jak monoetanoloamina (MEA) oraz mieszaniny 2-amino-2-metylo-1-propanolu (AMP) z piperyzyną (PZ). Ponieważ para jest ekstrahowana z elektrowni do regeneracji amin, wydajność elektrowni CCGT zmienia się w zależności od składu paliwa i rodzaju rozpuszczalnika, co wpływa na ogólną efektywność systemu.

Analizy wydajności CCGT z i bez integracji z siecią ciepłowniczą (DHN) wykazują, że mieszanie paliw kopalnych z gazem syntezowym oraz wdrażanie wychwytu CO_2 w zmiennych warunkach obciążenia umożliwiają osiągnięcie ujemnych emisji. Mieszanki metanowe wykazują lepszą wydajność w pracy elektrowni, podczas gdy mieszanki gazowe bogate w azot są bardziej efektywne w redukcji emisji. Proporcje gazu syntezowego wynoszące 50% lub więcej z metanem, jak również wszystkie proporcje gazu syntezowego mieszane z gazem bogatym w azot, mają potencjał osiągnięcia ujemnych emisji, gdy systemy wychwytu CO_2 działają przy pełnym lub częściowym obciążeniu równym 90%. Wyniki modelowania termodynamicznego zostały przeanalizowane pod kątem kluczowych wskaźników efektywności, takich jak wskaźniki energetyczne, ekonomiczne i środowiskowe. Analizy ekonomiczne potwierdzają wykonalność systemu referencyjnego w rzeczywistych zastosowaniach. Wyniki potwierdzają potencjał

integracji gazu syntezowego z paliwami kopalnymi oraz zastosowania technologii wychwytu CO_2, aby osiągnąć cele środowiskowe przy zachowaniu opłacalności ekonomicznej.

Contents

List of Acronyms

1GDH	First Generation District Heating
2GDH	Second Generation District Heating
3GDH	Third Generation District Heating
4GDH	Fourth Generation District Heating
5GDHC	Fifth Generation District Heating and Cooling
ADM	Archer Daniels Midland
AMP	AminoMethyl Propanol
ASU	Air Separation Unit
bcm	billion cubic meters
BECCS	Bioenergy with carbon capture and storage
BECCU	Bioenergy with carbon capture and utilization
BSST	Bidirectional SubSTation
CCGT	Combined Cycle Gas Turbine
CCR	CO_2 capture ratio
CCS	Carbon Capture and Storage
CCU	Carbon Capture and Utilization
CCUS	Carbon Capture, Storage and Utilization
CDR	Carbon dioxide removal
CHP	Combined Heat and Powe
CLC	Chemical Looping Combustion
CO_2	Carbon dioxide
COP	Conference of Parties
CSP	Concentrated solar power

DEA	Diethanolamine
DH	District Heating
DHN	District Heating Networks
EC	Primary Energy Cost, €/kWh
EJ	Exajoules
EOP	Energy Output Penalty, kWh/tCO_2
EOR	Enhanced Oil Recovery
EPP2040	Energy Policy of Poland until 2040
EU	European Union
FWP	Feed Water Pump
GDP	Gross Domestic Product
GHG	Greenhouse Gas
GP	Grid electricity price, PLN/MWh
GW	Gigawatt
HDGT	Heavy-Duty Gas Turbine
HIS	Heat Integrated Stripper
HP	High Pressure
HRSG	Heat Recovery Steam Generator
HSP	Heat Supply Price, PLN/GJ
IEA	International Energy Agency
IP	Intermediate Pressure
IPCC	Intergovernmental Panel on Climate Change
IRENA	International Renewable Energy Agency
ISO	International Standard Organization
LCOE	Levelized Cost of Electricity
LHV	Lower Heating Value
LMTD	Logarithmic Mean Temperature Difference, ℃
LP	Low Pressure
LTDH	Low-Temperature District Heating
LVR	Lean Vapour Recompression

mbpd	million barrels per day
MDEA	Methyl diethanolamine
MEA	Monoethanolamine
MTDH	Medium-Temperature District Heating
NZE	Net Zero Emission
OECD	Organization for Economic Cooperation and Development
ORC	Organic Rankine Cycle
PCCS	Post-combustion Carbon Capture and Storage
PGE	Polska Grupa Energetyczna
PZ	Piperazine
RES	Renewable Energy Sources
RSP	Rich Solvent Preheating
SO_x	Sulphur oxide
SPECCA	specific primary energy consumption for CO_2 avoided, kWh/kgCO_2
$SPECCA_{cost}$	cost of specific primary energy consumption for CO_2 avoided
STEPS	Stated Policies Scenario
TES	Thermal Energy Storage
UNFCCC	United Nations Framework Convention on Climate Change
WGS	Water Gas Shift
WWTP	Wastewater Treatment Plant

Nomenclature

χ	CO_2 emission index, $kgCO_2/kJ$
δP_{cc}	pressure drop inside the combustion chamber
δP_{gt}	pressure drop in gas turbine
$\dot{m}g_{amine}$	CO_2-rich loading, kg/kg
$\dot{m}_{14}$	mass flow of lean solvent at absorber inlet, kg/s
$\dot{m}_{15}$	mass flow of rich solvent at stripper inlet, kg/s
$\dot{m}_{17}$	total mass flow of lean solvent at stripper outlet, kg/s
$\dot{m}_{19}$	amount of lean solvent required for CO_2 capture, kg/s
$\dot{m}_{22}$	mass flow of captured CO_2 with vapour at the outlet of the stripper, kg/s
$\dot{m}_{23}$	mass flow of CO_2 vapour at the outlet of stripper, kg/s
$\dot{m}_2$	mass flow of flue gas at the inlet of the absorber, kg/s
$\dot{m}_{31}$	mass flow of captured CO_2 to storage, kg/s
$\dot{m}_3$	mass flow of flue gas at absorber inlet, kg/s
$\dot{m}_4$	mass flow of treated flue gas at absorber outlet, kg/s
$\dot{m}_9$	mass flow of rich amine at absorber outlet, kg/s
$\dot{m}_{air}$	mass flow of air, kg/s
$\dot{m}_{CO_{2,capt}}$	mass flow of CO_2 captured, t/h
$\dot{m}_{CO_{2,gen}}$	mass flow of CO_2 generated, t/h
$\dot{m}_{CO_2}$	mass flow of CO_2 emitted into the atmosphere, kg/s
$\dot{m}_{D,cs}$	mass flow rate of cold stream on DHN component, kg/s
$\dot{m}_{D,hs}$	mass flow rate of hot stream on DHN component, kg/s

$\dot{m}_{fg.CO_2}$	mass flow rate of CO_2 in flue gas, kg/s
$\dot{m}_{fg}$	mass flow rate of flue gas, kg/s
$\dot{m}_f$	mass flow rate fuel, kg/s
$\dot{m}_{gen.CO_2}$	mass flow of generated CO_2, t/h
$\dot{m}_{lpsteam}$	mass flow rate of LP steam, kg/s
$\dot{m}_s$	mass flow rate of steam, kg/s
$\dot{m}_{vapour}$	mass flow rate of vapour present at the outlet stream of stripper, kg/s
$\dot{Q}$	rate of chemical energy, kW
$\dot{Q}_{21}$	reboiler duty required for the carbon capture process, MW
$\dot{Q}_{\text{amine}}$	reboiler duty of the amine, kJ/kg CO_2
$\dot{Q}_{\text{DHN}}$	heat transfer rate of selected component of DHN, MW
$\dot{Q}_{\text{HRSG}}$	heat transfer rate of selected component of HRSG, MW
$\dot{Q}_{cyc}$	heat supplied to the system, MW
$\dot{W}_{\text{ACi}}$	input work of the air compressor, MW
$\dot{W}_{\text{ACo}}$	output work of the air compressor, MW
$\dot{W}_{\text{cyc}}$	Net power available on the gas cycle, MW
$\dot{W}_{\text{GTi}}$	work input of gas turbine, MW
$\dot{W}_{\text{GTo}}$	work input of gas turbine, MW
$\dot{W}_{\text{ist}}$	work input of steam turbine, MW
$\dot{W}_{\text{ost}}$	work input of steam turbine, MW
η_{cap}	$CO_2 capture efficiency$
η_{CCGT}	net power efficiency of the CCGT
η_{cc}	efficiency of the combustion chamber of the gas turbine
η_{cyc}	efficiency of the gas cycle
η_{el}	electrical efficiency of the generator
η_{iST}	isentropic efficiency of the steam turbine
η_{is}	isentropic efficiency of the air compressor

η_{ms}	mechanical efficiency of the steam tubrine
η_{m}	mechanical efficiency of the air compressor
η_{net}	net efficiency of the power produced
$\eta_{\mathrm{p,ccs}}$	efficiency of the power plant with capture
η_{ref}	efficiency of the reference power plant
e_{cost}	CO_2 emission cost, €/MWh
$Capital_t$	capital construction costs
$Carbon_t$	carbon cost
D_t	decommissioning and waste management cost
DHN_{cost}	cost of DHN heat, PLN/GJ
DHN_h	income from DHN heat supply, PLN/h
DHN_{supply}	DHN heat supply, MW
e_{CO_2}	specific emission of carbon dioxide, kgCO_2/kWh
$e_{CO_{2,ref}}$	specific emission from the reference plant, kgCO_2/kWh
$e_{CO_{2p,ccs}}$	specific emission from the plant with CO_2 capture, kgCO_2/kWh
e_rCO_2	relative emissivity of CO_2, kgCO_2/kWh
E_S	income from electricity sale, PLN/h
EC_{CO_2}	CO_2 emission cost, €/t
f_{cost}	gas fuel price, PLN/MWh
$Fuel_t$	fuel cost
h_1	enthalpy of compressor inlet air, kJ/kg
h_{21}	enthalpy of steam at reboiler inlet, kJ/kg
h_{22}	enthalpy of steam at reboiler outlet, kJ/kg
$h_{2\mathrm{s}}$	isentropic enthalpy of compressor outlet air, kJ/kg
h_2	enthalpy of compressor outlet air, kJ/kg
h_3	enthalpy of flue gas at combustion chamber outlet, kJ/kg
h_4	enthalpy of flue gas at gas turbine exhaust, kJ/kg

h_5	enthalpy of steam at the inlet of steam turbine, kJ/kg
h_{6s}	isentropic enthalpy of steam turbine outlet, kJ/kg
h_6	enthalpy of steam at the outlet of steam turbine, kJ/kg
$h_{fg,t}$	enthalpy of flue gas at the target temperature, kJ/kg
h_{fi}	enthalpy of flue gas at the inlet of the heat exchanger, kJ/kg
h_{fo}	enthalpy of flue gas at the outlet of the heat exchanger, kJ/kg
h_i	enthalpy of the selected gas component, kJ/kg
h_{si}	enthalpy of steam at the inlet of the heat exchanger, kJ/kg
h_{so}	enthalpy of steam at the outlet of the heat exchanger, kJ/kg
$HR_{p,CCS}$	heat rate of power plant with PCCS, kJ/kWh
HR_{ref}	heat rate of power plant without PCCS, kJ/kWh
N_{CCGT}	net electricity output CCGT power plant, MW
N_{GT}	electricity output of gas cycle, MW
N_{net}	net energy generated by power plant, kW
$N_{PP.CCS}$	net power produced by reference power plant with CCS, MW
$N_{PP.ref}$	net power produced by reference power plant without CCS, MW
N_{SE}	power reduced due to steam extraction, MW
N_{ST}	net electricity output of steam cycle, MW
$O\&M_t$	operation and maintenance cost
P_1	inlet pressure of the air compressor, bar
P_2	outlet pressure of the air compressor, bar
P_3	pressure at the outlet of the combustion chamber, bar
P_4	pressure at the outlet of the gas turbine, bar
$PP_{f,cost}$	price of the fuel used in power plant, PLN/h
PP_{income}	total income of the power plant after expenses, PLN/h
Q	heat input by fuel, kJ
Q_{RE}	PCCS reboiler heat consumption, MW

r	real discount rate corresponding to capital cost
r_c	pressure ratio of the air compressor
t	years
T_{ci}	temperature of cold stream inlet, ◦C
T_{co}	temperature of cold stream outlet, ◦C
T_{hi}	temperature of hot stream inlet, ◦C
T_{ho}	temperature of hot stream outlet, ◦C
X_i	mass fraction of the gas component, %
i	gas component

List of Figures

List of Tables

Chapter 1

Introduction

1.1 Low-emission heat and power generation

1.1.1 Energy & Electricity - Supply and Demand

The Total Energy Supply data from the International Energy Agency (IEA) from 2000 to 2023 show significant changes in global energy production. In 2023, countries worldwide produced 642 exajoules (EJ) of energy, including fuel conversion and electricity production, which is 2% higher compared to 2022 [1]. In 2021, China, the United States, and India are the leading contributors with 25.3%, 14.5% and 6.4% respectively to the total energy supply. As shown in Figure 1.1, the global energy supply continues to increase each year to meet the growing demand, except that in 2020 a 3.7% decline in energy supply compared to the previous year was observed due to the COVID pandemic. Despite advances in renewable energy sources, fossil fuels remain the primary energy sources. The global energy supply per capita has increased 12.86% since 2000 to 78418.7 MJ/Capita in 2021 [2].

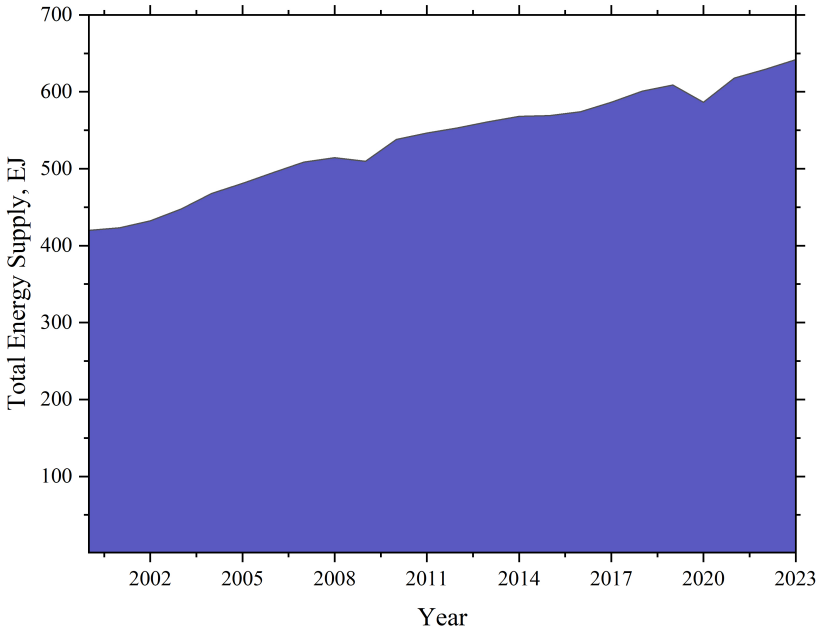

Figure 1.1: Total energy supply in the World (2000 - 2021) [1], [2].

In 2023, global electricity generation has reached 36,400 TWh with more than half the share of renewable energy sources, low-emission power generation technologies, and the integration of carbon capture technologies with fossil fuels [1]. As illustrated in Figure 1.2 of the global energy supply by sources, oil remained the dominant energy source in 2021, accounting for 29.5% of the global energy supply. Subsequently, coal and natural gas contributed 27.2% and 23.6%, respectively. Approximately 28,000 TWh of electricity was generated worldwide in 2021, with coal (35.9%) and natural gas (23%) being the primary fuels for power generation. Renewable energy and other alternative sources together contributed 28.8% to global electricity production, highlighting a significant growth toward net zero emissions. The global energy in 2021 was categorized by varying consumption according to different sectors. The most global energy is consumed by the industrial sector, accounting for 30.1% of the total, closely followed by the transport sector at 26.7% and the residential sector at 21.5% of the global energy. These patterns of energy use are highly dependent on geographical location and economic development, and more industrialized regions generally show higher consumption in the industrial and transport sectors [2].

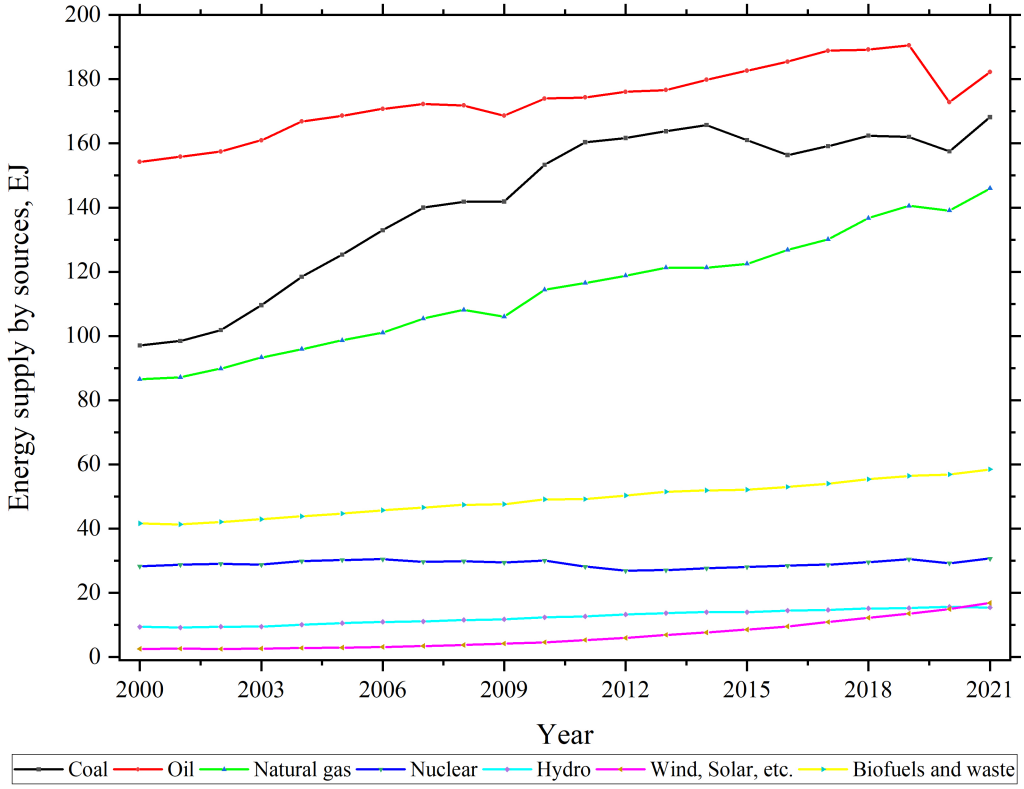

Figure 1.2: Total energy supply in the World by sources (2000 - 2021) [2].

As shown in Figure 1.3, the industrial sector consumed 127 EJ of energy in 2021, while the transport sector used 112 EJ. Notably, between 2016 and 2019, energy consumption by both the industry and transport sectors remained stable, showing consistent demand in these vital areas of the global economy. However, the specific types of fuels used and the purposes of consumption vary widely between the sectors, depending on factors such as technological advancements, regional energy policies, and economic activities [2]. A forecast of the global total energy demand states that the demand will increase up to 670 EJ by 2030 and continue to increase till 2050, with a 16% growth in emerging markets and a 9% decrease in

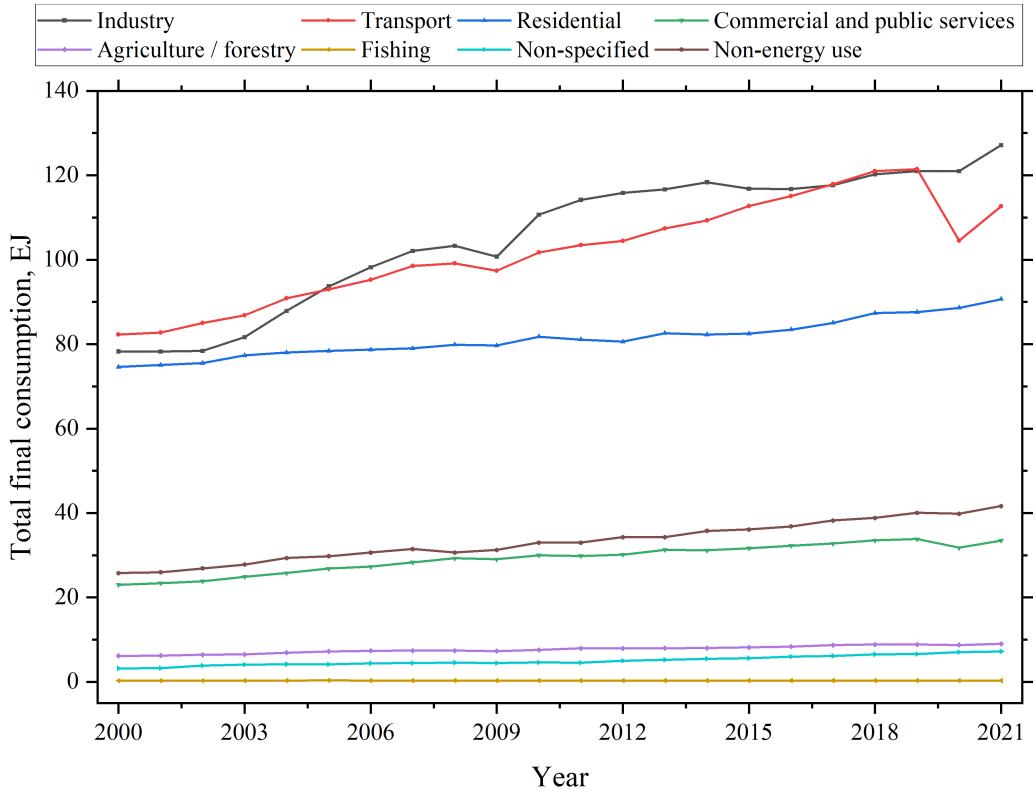

Figure 1.3: Total final energy consumption by sector (2000 - 2021) [2].

advanced economies. However, it is predicted that fossil fuels such as coal, oil and natural gas will achieve a peak before the decline in demand, with an increase in demand for renewable sources and nuclear by 2030, as an impact to achieve Net Zero Emissions (NZE) scenario. Currently, the building and industry sectors account for over 90% of global electricity consumption, including household, cooling, and heating usage. However, the increasing demand with the limited availability of critical minerals essential for power generation and electric vehicles, poses a risk to future electrification [3]. According to the IEA report in 2024, the electricity demand has increased by 2.4% and 2.3% in 2022 and 2023 respectively. The demand is forecasted to increase to 2.4% by the year 2026 [4]. As per British Petroleum's World Energy Statistics Reports, after the COVID-19 epidemic in 2020, global electricity production increased to 28.47 trillion kWh in 2021, which is 6.2% higher compared to electricity production in 2020 [5]. Due to the fossil fuel reserves depletion and the forecast of double the increase in electricity demand by the year 2050 than the current level, the role of renewable energy is increasing in power generation as many countries are focusing on sustainable energy generation. However, due to barriers such as geographical location and weather conditions, the large-scale deployment of renewable energies is restricted [6], [7]. A 2024 mid-year update of the electricity report by the IEA states that the global economic crisis, slowdowns in business activities and weather conditions across the globe have reduced the electricity demand from 2.7% in 2022 to 2.5% in 2023. Despite this, the electricity consumption in 2024 was forecasted to reach 4% growth [8]. The IEA's Stated Policies Scenario (STEPS) states that the electricity demand will rise to 5,900 TWh by the year 2030 with industrial and economic expansions in emerging markets and an increase in the use of electric transportation in advanced economies. Despite the current high use of coal in many countries, the use of

coal decline to 26% by 2030 due to energy security and high prices of natural gas, as a part of renewable growth and NZE scenario. The use of batteries in electric transports will increase the demand for critical minerals from 7 Mt in 2021 to 11 Mt in 2030 since the applications of minerals expand including solar PV, batteries and grids [9]. The electricity analysis and forecast in the 2026 report by IEA indicates that the annual growth rate of electricity demand is declining in advanced economies and increasing in emerging market countries, as shown in Table 1.1. The demand for electricity in various countries is significantly influenced by factors such as manufacturing slowdowns and cooling demand reductions in the United States, as well as energy-saving measures in Japan. Conversely, increased electricity consumption in China's industrial sector and economic expansion in India have driven up demand. Looking ahead, it is anticipated that electrification in the transport and heating sectors of advanced economies, industrial recovery in the European Union, and economic growth in emerging markets will further elevate demand [10].

Table 1.1: Annual electricity demand analysis and forecast to 2026 as per countries [10]

Countries	Actual		Forecast		
	2022	2023	2024	2025	2026
China	3.7%	6.4%	5.1%	4.9%	4.7%
India	8.6%	7%	6.5%	6.5%	6.5%
USA	2.6%	1.6% ↓	2.5%	1%	1%
Japan	1%	3.7% ↓	1.2%	0.2%	0.2%
EU	3.1% ↓	3.2% ↓	1.8%	2.5%	2.5%

Since 1800 to till date, the energy sources have undergone a significant transition from biofuels to coal, coal to oil and oil to gas. While nuclear and other renewable sources have slowly developed during the past two centuries, fossil fuels are still the dominating energy sources. As the demand grows, the moderate increase in renewable energy sources is not impacting the use of fossil fuels, as it requires 13 units of non-fossil fuels to replace 1 unit of fossil fuel source [11]. Despite the growth in European policies aimed to address the problems caused by fossil fuels, such as global warming and air pollution, 24 European countries remain heavily dependent on fossil fuel energy sources, with 10 countries having more than 80% of their total energy consumption derived from coal, oil, and natural gas. This dependency shows the challenges in transitioning to renewable energy, as fossil fuels play a major role in energy security [12]. Poland's recent energy policies emphasize increasing electrification and reducing carbon emissions in alignment with EU climate goals. These policies aim to decarbonize the energy sector while maintaining energy security and providing affordable electricity to consumers. However, despite the efforts, coal remains the dominant energy source for electricity production. In 2022, coal contributed 70.43% of the total 178.25 TWh of electricity generated in the country. Following coal, wind energy contributed 10.9% and natural gas contributed 6.62% of the energy mix in 2022 [13]. With China increasing coal production output by 3.4% and India by 12% in response to growing concerns over energy security, the countries significantly boosted their coal production in 2023. Indonesia increased by 13% due to export demand. These increases

contributed to a global coal production growth of 3.1%, bringing total production to 8970 million tonnes in 2023. However, factors including inflation, the energy crisis and unpredictable fluctuations in energy prices have created a more uncertain outlook for coal production in 2024. As a result, global production is forecasted to decline to 8939 million tonnes [14]. The largest coal-fired power plant in the world is Tuoketuo power station located in Hohhot, Inner Mongolia, China. With an installation capacity of 6700 MW, it produces 33,317 TWh of electricity annually. The power plant was initially commissioned with a capacity of 5.4 GW in 2012 and underwent significant expansion in 2017 to its current capacity. Following Tuoketuo, the Taean and Dangjin power stations in South Korea are the second and third largest coal-fired power plants with a capacity of 6,100 MW and 6,040 MW respectively. The Taean power plant consists of 8 X 500 MW of supercritical units and 2 X 1050 MW ultra-supercritical units, which operate with bituminous coal as a primary source of energy. These units operate at efficiency levels ranging from 37.3 % to 40.15 % depending on the unit [15], [16], [17]. Similarly, The largest natural gas-fired power plant in the world is the Jebel Ali power and desalination plant in the United Arab Emirates has a power generation capacity of 9.55 GW. The plant is also a CHP plant, where the steam from the turbine is used for the desalination process [18]. The second largest gas-fired power plant is the Surgut-2 power station in Russia and the largest oil-fired power plant in Saudi Arabia is the Shoaiba power station with an installed capacity of 5.59 GW and 5.6 GW respectively [19]. The global oil and gas consumption in 2022 is 97 million barrels per day (mbpd) and 4,150 billion cubic meters (bcm) respectively. Due to the net zero transition, this rate is expected to decline in 2050 to 55 mbpd and 2,400 bcm after reaching a peak in 2030 [20].

1.1.2 District Heating System

The District Heating (DH) system is globally recognized for its safety, affordability and efficiency. In 2022, 63.5% of the total energy consumed by European Union (EU) households is dedicated to space heating to satisfy the energy need for various purposes[21], [22]. A report by IEA states that the integration of heat pumps, solar thermal and renewable energy sources with DH systems makes an enormous contribution to achieving net zero emissions by 2050. As a key step, the aim is to establish 350 million connections globally by 2030 including 400 million solar thermal collectors and 600 million heat pumps [23]. As of 2021, the EU has 17,000 District Heating Networks (DHN) with an installed capacity of 300 GW [24]. The first generation DH (1GDH) system in the 1880s employed steam as a heat-transferring medium through concrete steam pipes. The system faced major challenges such as heat loss and accidents due to steam explosions, making it less reliable and a safety risk. The second generation DH (2GDH) system in the 1930s used pressurized hot water with a temperature above 100 ℃. The system faced a lot of problems including high heat losses, high maintenance costs due to the need for large heat exchangers and inefficiency in meeting heat demand. The 3rd generation DH (3GDH) system, which is the current system that started emerging in the 1980s, made significant improvements by addressing the problems from the past. The 3GDH uses CHP enhanced with natural gas and biomass as energy sources. In the 3GDH, pressurized hot water below 100 ℃ is used as heat carriers circulated through insulated stainless steel pipes, heat losses and enhancing system efficiency. The 3GDH replaced the second-generation DH system due to its efficiency improvements, use of cheaper fuels and ability to match the heat demand. The 4th generation DH (4GDH) system, also called a smart energy

system, is designed considering the greenhouse gas emission and global warming crisis and can integrate with multiple energy sources. The system utilizes waste heat using heat pumps, solar thermal collectors and geothermal heat as sources of energy, enabling a transition to 100% renewable energy sources. By using the 4GDH, it is possible to reduce CO_2 emission and shift towards environmentally friendly heating solutions [25]. The 5th Generation District Heating and Cooling (5GDHC) system is an innovative concept that is currently being explored and tested in pilot-scale operations across several regions of Europe. The 5GDHC offers both heating and cooling simultaneously, depending on the needs of individual consumers. The 5GDHC reduces energy waste by using sensors and control systems with a combination of thermal and electrical networks to continuously monitor and balance energy demand and supply, hence it is referred to as a "smart energy system." The use of hybrid substations connected to heat pumps allows highly efficient local energy transfers, which improves system efficiency and helps in decarbonization efforts by reducing reliance on fossil fuels. The integration of renewable energy sources, such as solar thermal collectors or Combined Heat and Power (CHP) systems, enhances the performance of the system. By operating at lower temperatures, the 5GDHC system reduces heat losses and allows for more efficient energy recovery, particularly when integrated with renewables or waste heat sources. The flexibility and efficiency offered by the 5GDHC play a crucial role in the energy transition towards zero carbon emission [26].
The concept of Bidirectional SubSTation (BSST) developed in the 4GDH, the local consumers referred to as prosumers, which are both heat producers and heat consumers, are equipped with solar thermal collectors. The exchange of heat is carried out in two-way DHN, where the DHN heat is used if the heat from solar collector is not sufficient and the excess unused heat from solar collector is sent to DHN [27]. The BSST DHN also uses a centralized heat pump to extract heat from buildings or recover waste heat, which reduces the demand for heat [28]. The direct integration of heat pumps with DHN offers considerable advantages in terms of energy efficiency and low-emission heat production. Using renewable energy sources, heat pumps can replace conventional fossil fuel-based systems, significantly reducing greenhouse gas emissions. This not only improves global decarbonization goals but also increases the overall sustainability of urban heating infrastructure. Heat pumps are particularly well-suited for small-capacity DH systems. Medium- and large-capacity DH systems are better when integrated with CHPs. However, this condition can evolve technology with improvements in characteristics [29]. The integration of CHP with DH systems has the great advantage of being used as an energy storage system. During demand hours, the energy from the DH system is used for power generation and later, during lower load, it can be restored [30]. During peak hours of CHP operations, the DHN can be dissociated from the CHP to make the operation more flexible. DHN already exists in most of the urban areas. Hence, the modification does not require much investment and further improvements in the system yield more profit [31].

1.1.3 Cogeneration

Cogeneration systems enhance the production of thermal and electrical energy with greater efficiency, reduced energy consumption, and lower emissions compared to conventional power generation technologies. According to Directive 2012/27/EU, cogeneration is recognized for its ability to deliver highly efficient heat and power generation and is considered a key technology for energy savings. As part of the

EU's energy efficiency initiatives, the directive aims for an 11.7% energy savings target by 2030 [32]. The share of CHP in electricity production worldwide accounts for up to 15% in 2020 contributing 4,119 TWh of electricity. Of the total production, the CHP in Europe shares 693 TWh, which is 19% of the total production. Natural gas, coal and biofuels are major sources of fuel. For cost-saving and environmental benefit purposes, cogeneration plays a crucial role in most production industries applications such as paper, sugar, petrochemical, cement, textile and iron & steal industries [33]. Cogeneration offers high energy efficiency, energy security, possibilities to reduce Carbon dioxide (CO_2) emission, use of a wide range of fuels and integration with cooling and heating systems [34]. Compared to the conventional systems with 35% efficiency, cogeneration has a high level of efficiency of 85%, since the excess energy after electricity production is used for heat generation, which reduces the overall operational cost and lowers Greenhouse Gas (GHG) emissions [35]. For the exact amount of heat and electricity produced, the cogeneration unit consumes 20 to 30% less fuel compared to a conventional power plant [36]. CHP systems offer the flexibility to integrate with various renewable energy sources, such as solar, biomass, and in some cases geothermal energy. This integration not only enhances the sustainability of CHP systems but also leads to significant cost reductions by reducing reliance on fossil fuels. The adaptability of CHP with renewable sources positions it as a critical component in the transition to a 100% renewable energy future. Even with the fossil fuel reserves depleted, CHP systems can continue to operate efficiently with renewable energy sources. By integrating renewable energy sources, CHP will play a key role in achieving carbon neutrality and lowering operational costs [37]. The combined cycle with CHP offers significant advantages across various operational aspects, particularly in meeting peak-hour demands. One of the aspects is its operational flexibility, which allows the plant to operate efficiently even at minimum load conditions, a characteristic feature of gas turbines. This flexibility of the plant can adjust its output based on fluctuating energy demands, optimizing both performance and efficiency. The system also provides product flexibility, in which the use of steam in the turbine can be regulated. This allows the plant to switch between electricity generation and heat production for DHN, depending on the immediate demand. For example, during periods of high electricity demand or when the electricity price is higher, more steam can be directed to the turbine for power generation, while in heat demand or during winter, the steam can be increased to the DHN to maximize heat output. The integration of TES further enhances the system's flexibility by storing the thermal energy for later use. The overall efficiency of the Combined Cycle Gas Turbine (CCGT) power plant is highly improved through the utilization of heat recovery for steam production and DHN, which reduces fuel consumption by maximizing the use of energy already generated. This leads to the concept of "avoided CO_2 emissions," where less fuel is burned providing high efficiency, resulting in reduced fuel cost and CO_2 cost. Additionally, the integration of renewable energy sources into the system offers further benefits. By using CCGT as a backup only when renewable energy is unavailable, the plant can maintain a high level of efficiency while reducing both fuel costs and emissions, making it a highly sustainable and cost-effective solution for modern energy systems [38].

In 2022, Poland has an increasing power production from renewable energy sources (RES) from 32% in the previous year to 38.3%. Meanwhile, the rise in global natural gas prices led to a reduction in domestic natural gas production. Currently, Poland does not have any operational nuclear power plants, but is

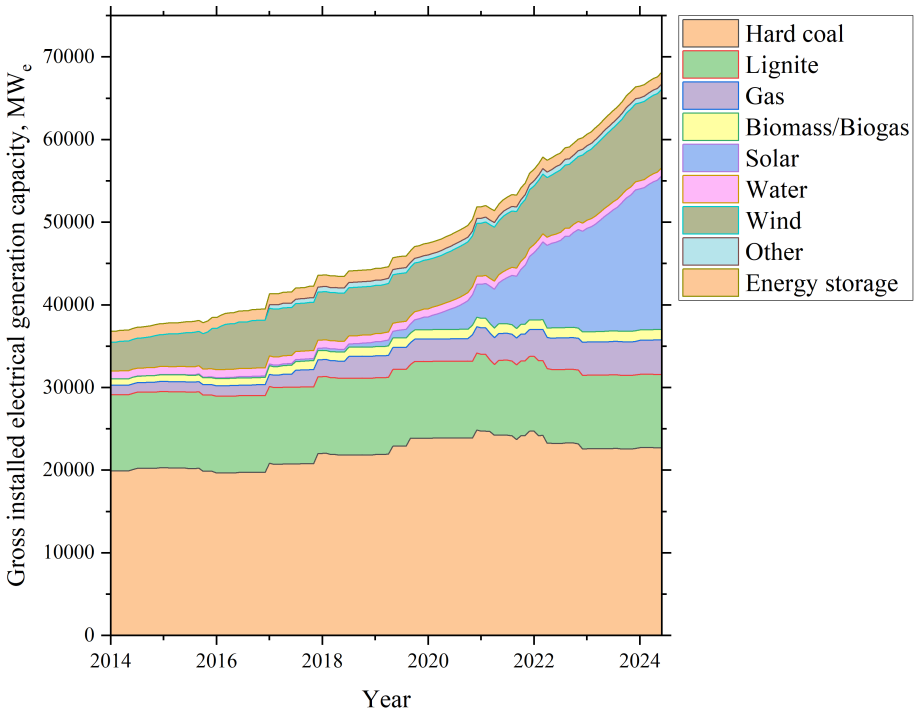

Figure 1.4: Gross installed electrical generation capacity in Poland by sources (2014 - 2024) [40].

planning to build six nuclear reactors with a combined capacity of 6 to 9 GW. With the first reactor planned to be completed by 2033, the other reactors are scheduled to be operational by 2043 [39]. Figure 1.4 illustrates the electricity generation in Poland by sources from 2014 to 2024 [40]. Figure 1.5 shows the CHP plants of state-owned and private enterprises in Poland. The Instrat power plant database provides comprehensive information on the development and current status of CHP plants from 1941 to 2024 in Poland. Of the 115 CHP plants in Poland, 104 remain operational, while two new plants are planned to be operational by 2025, and the rest have been decommissioned due to retirement. CHP plants have an average net electric efficiency of 52.1%, which is higher than the efficiency of other types of power plants with performance ranges between 37.4% and 37.6%. In addition to CHP plants, there are 105 other types of power plant, 80 of which are still operational, with 7 more planned for future development. Most CHP plants in Poland operate on hard coal as their primary fuel source, with only about 5% using biomass, demonstrating the continuous use of fossil fuels by the country in this sector. However, all the power plants planned to be built in the future in Poland are gas-fired. A total of 8 gas-fired power plants are planned between 2025 and 2027, with 1 CHP and 7 other types of power plants. This indicates that the country is reducing its dependency on coal and shifting to lower-emission energy sources, which improves its energy security. Polska Grupa Energetyczna (PGE) leads the market, managing 36 of the country's operational CHP plants. PGE also has plans to commission a new plant by 2025. Despite ongoing advancements, the future of CHP operations in Poland faces challenges, as nearly 34 of the currently active CHP plants are scheduled to decommission by 2030. Figure 1.5 illustrates the distribution of CHP plants in Poland by producer, highlighting PGE's dominance in the sector [41]. In 2022, PGE and Tauron are Poland's two largest energy companies, with installed capacities of 17.9 GW and 5.1 GW, respectively. Together, these firms supply energy to approximately 10.4 million people throughout the country. In

response to Poland's commitment to transitioning to 100% renewable energy, both PGE and Tauron have developed ambitious long-term strategies with milestones set for 2030 and 2050. PGE has committed to increasing the share of renewable energy in its energy mix to 50% by 2030, with the aim of reducing 120 million tons of CO_2 emissions. By 2050, the company's goal is to achieve net zero emissions, aligning with Poland's broader decarbonization goals. Similarly, Tauron aims to increase renewable energy capacity to 3.7 GW and 1.6 GW with a CO_2 emission reduction of 160 kg/MWh and 200 kg/MWh in 2030 and 2050 respectively. As an initial step toward these goals, Tauron plans to install 1 GW of onshore wind power by 2025 [42], [43], [44], [45].

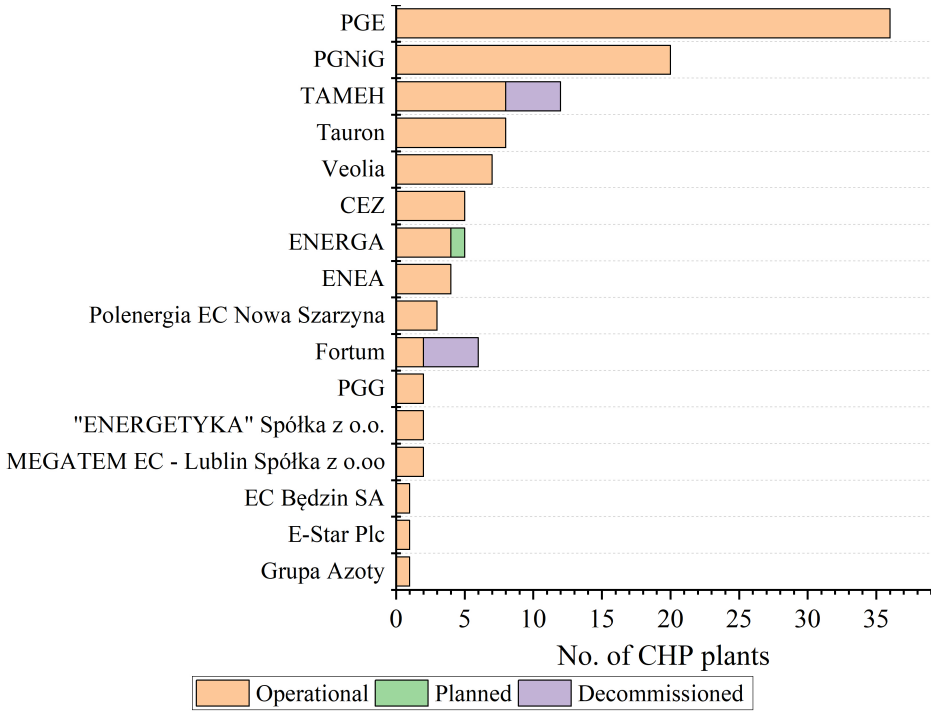

Figure 1.5: No. of CHP plants owned by enterprises in Poland [41]

The Energy Policy of Poland until 2040 (EPP2040) is a framework approved by the Polish government that aligns with the goals of the Paris Agreement and the European Union's climate and energy policies. It includes a strategic pathway to achieve low-emission energy generation by improving energy security and economic performance with a reduction in GHG emissions. The EPP2040 progresses by transiting from coal-based power generation to renewable energy sources and nuclear power. The policy sets transition targets following improvements in renewable energy by 2030 and nuclear power by 2033. This transformation of energy is based on three key pillars: 1) transition of energy production from coal to renewable and nuclear, 2) achieve net zero emission by promoting renewable and nuclear energy, and 3) improve air quality by reducing emissions [46].

1.1.4 CO_2 emission

The use of fossil fuels as a major source to satisfy demand has increased the emission of CO_2, one of the GHG, into the atmosphere [47]. The anthropogenic activities made to satisfy the needs of humankind

for a few decades have influenced the risk of climate change and global warming and the necessity to mitigate the rising problems. Numerous recent incidents have increased the awareness of the reduction of greenhouse gas emissions and the adaptation of clean energy [48]. From the beginning of the past century to today, the effects of climate-related issues have cost 4.13 trillion dollars of the global economy due to natural disasters [49]. In both advanced economies and emerging markets, the increase in population, economic growth, and industrialization impact the increase in energy intensity, leading to higher CO_2 emissions. Especially in countries of the Organization for Economic Cooperation and Development (OECD), the transport sector plays an important role along with Gross Domestic Product (GDP) and energy consumption in increasing CO_2 emissions. However, increasing the energy intensity of renewable energy and increasing energy efficiency can reduce CO_2 emissions [50]. Global CO_2 emissions have reached 37.7 Gt in 2023 with emissions from the global energy sector increasing by 1. 3% in 2023, which is 1 Gt more emissions than in 2019 [1]. However, due to the thriving of clean energy, a slowdown of CO_2 emissions is observed compared to the past decades. The deployment of clean energy such as solar photovoltaic energy, wind and nuclear and the reduction in industrial activities compensated for the increase in emissions, contributing to the slowdown. The reduction in hydroelectric power generation due to droughts, climate changes in certain areas leading to an increasing demand for heating and cooling temperatures, and the resuming of transport and aviation activities by China after the pandemic have increased global CO_2 emissions [51]. Figure 1.6 illustrates the global CO_2 emission from energy production from 2000 to 2024 [52].

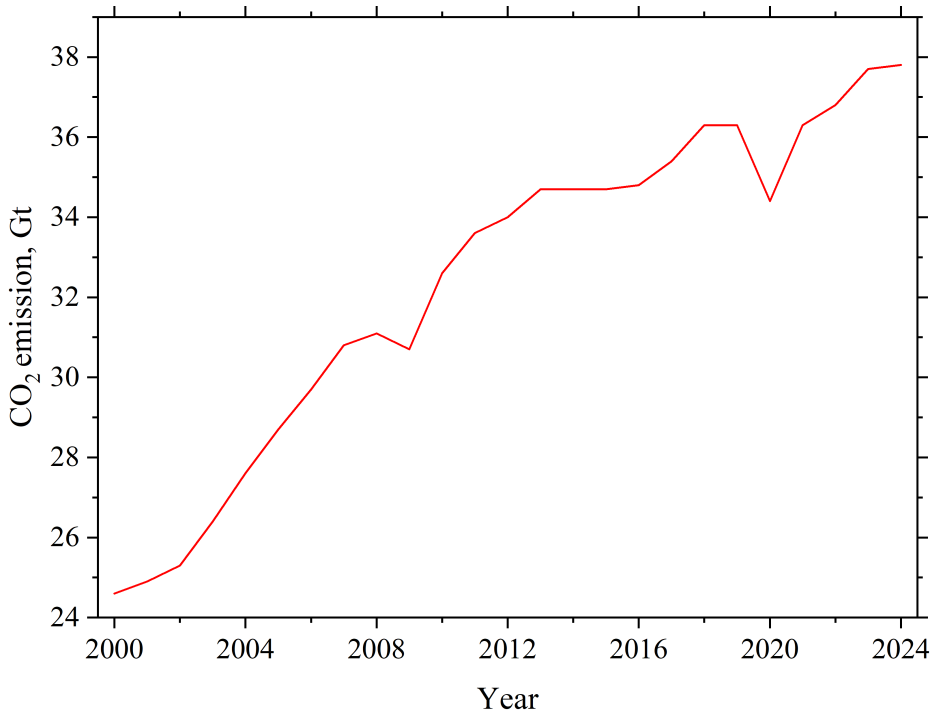

Figure 1.6: Global energy-related CO_2 emission (2000 - 2024) [52]

Global energy-related CO_2 emissions increased by 1.7% in 2017 compared to the previous year, by 2. 7% in 2018 and remained the same in 2019. The restrictions during the COVID pandemic reduced energy consumption and the use of public transport at the beginning of 2020, which has reduced 1.55 billion

tons of CO_2 emissions. This is only temporary, as the ease of restrictions has increased the emissions to previous conditions [53]. The emission from the power sector has increased by 261 Mt in the year 2021 to 2022, keeping it the largest contributor of CO_2 emission compared to other sectors such as transport, industry and buildings. In the same period, the increase in emissions from the power and transport sector was partly compromised by reduced industrial activities and low heat demand, causing reduced emissions in the building sector. Among the energy-producing sectors, a large part of the emissions come from electricity and heat generation. Due to the recent demand for natural gas, oil and coal contributed more CO_2 emissions increasing by 2.5% and 1.6% respectively. Sector-wise emissions for the period 2019 to 2022 are illustrated in Figure 1.7 [54].

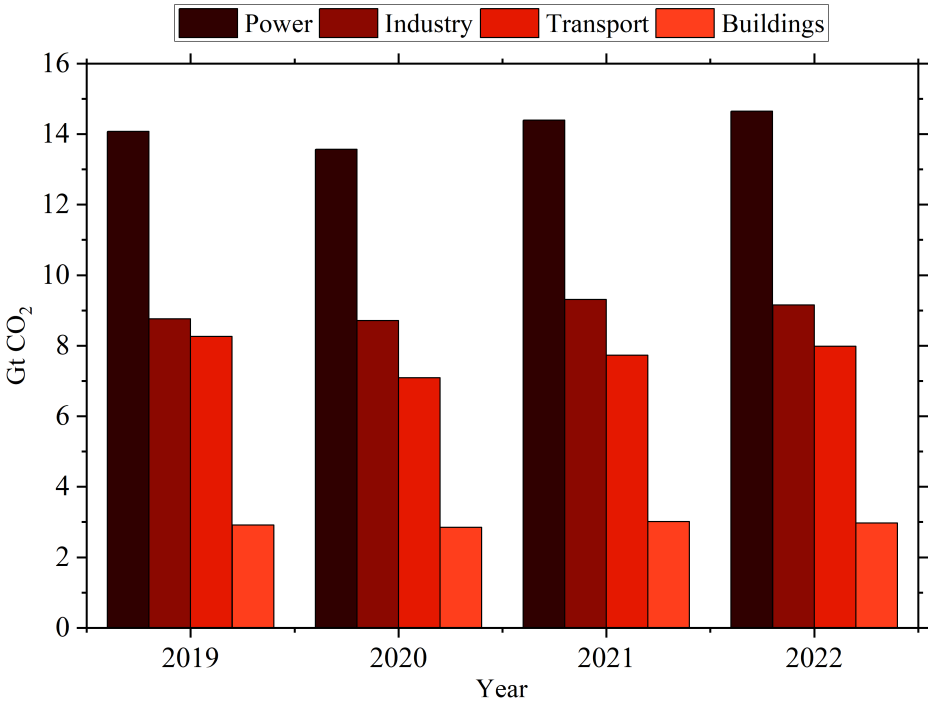

Figure 1.7: Global CO_2 emission by sectors (2019 - 2022) [54]

The energy sector remains one of the largest contributors to atmospheric pollutants such as CO_2, SO_x, NO_x, and particulate matter. The choice of fuel in power plants is critical in determining the type and amount of emissions. Pollutants such as SO_x and NO_x are generally originated from coal combustion, while natural gas combustion produces fewer of these pollutants. Many coal-fired power plants are equipped with desulfurisation and denitrification systems to mitigate emissions. With the use of lower carbon fuels, such as natural gas, and improved overall efficiency, power plants can reduce CO_2 emissions. Although CO_2 capture is possible after combustion, the low concentration of CO_2 in natural gas flue gases poses challenges for capture, and the energy required for the capture process can reduce the overall efficiency of the plant [55]. China, India, and the United States are the world's top CO_2 emitting countries. The countries with the highest global per capita CO_2 emissions are Middle Eastern countries such as Qatar and the United Arab Emirates with low populations and high oil production, which contribute to lower global total emissions. However, other oil-producing countries such as the US, Australia, and Canada with high populations have higher per capita CO_2 emissions and contribute more to global total emission [56].

According to individual power plant emissions data, the Tuoketuo Power Station alone emits 31,435 kt/year of CO_2 annually. The Taean and Dangjin power stations also contribute significantly to global emissions, with annual CO_2 emissions of 35,877 kt/year and 33,859 kt/year respectively [57]. In 2022, the Taean and Dangjin power stations emitted CO_2 of 32.24 Mt and 30.92 Mt, making them the largest contributor to global CO_2 emission among coal power plants [58]. The largest gas-fired power plant, the Surgut-2 power station annually emits 23.5 million tons of CO_2 [59].

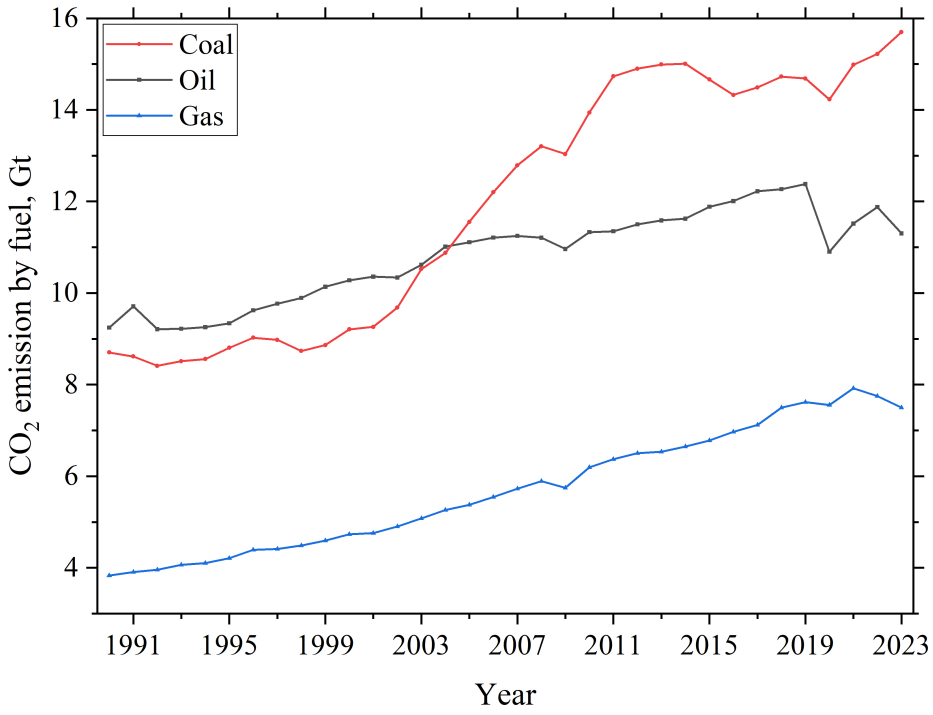

Figure 1.8: Global CO_2 emission by fuel (1990 - 2023) [1], [60]

Coal has been used as the main fuel for the past three centuries in industries and still dominates the energy industry. Coal is currently responsible for the highest CO_2 emissions among the different types of fuel used in industries. Of the total CO_2 emissions made by the energy sector in 2023, coal contributes 41.6% of emissions, followed by oil and gas at 30% and 20% respectively. From the past to the current scenario, gas produces much less CO_2 emission compared to both coal and oil, in which the emission from coal is double times more than the emission from gas. Figure 1.8 shows the global CO_2 emission by fuels used widely in industries from 1990 to 2023 [1], [60].

1.1.5 Negative CO_2 emission

To mitigate the CO_2 emission and limit the global average temperature to below 2℃, about 196 countries formed the Conference of Parties (COP) and joined the Paris Agreement at the United Nations Climate Change Conference held by the United Nations Framework Convention on Climate Change (UNFCCC) in 2015 [61]. It is projected that without the mitigation policy, by the year 2100, the global GDP will be reduced by 7%. The main goal of the Paris Agreement and the Glasgow climate pact is to bring about sustainable development and limit the global average temperature to 1.5℃ [62]. One of the

ways to maintain the temperature below 1.5℃ is to keep fossil fuels unearthed. 58% of oil, 56% of gas, and 90% of coal must be kept unextracted by 2050. The Middle East countries and Russia are the largest holders of oil and gas reserves, respectively [63]. To achieve this goal and limit the temperature to around 1.7℃ by the year 2100, the IEA suggested that the four pillars of action must be followed [64]:

- Energy sector – decarbonization, improving energy efficiency, electrification.
- Preventing deforestation.
- Reduction of emissions other than CO_2, such as methane and HFCs.
- Improve carbon capture and storage (CCS)/carbon removal from the atmosphere.

In the energy sector, decarbonization is achieved through various methods, such as the deployment of renewable energy, carbon capture technology in fossil fuel power plants, and nuclear power plants. According to current policy settings, 44 Mt of CO_2 was captured in 2022. However, to achieve the NZE scenario, by 2030 this capture rate should be increased to 1.2 Gt. Carbon Capture Storage (CCS) and Carbon Capture and Utilization (CCU) in power plants with the use of sustainable fuels and low-emission fuels, and carbon dioxide removal (CDR) provide the possibility to achieve negative emissions [64]. To achieve a Net Zero Emission (NZE) scenario by 2050, the IEA proposed pathways in 2021 for the Global Energy Sector. The NZE scenario includes increasing energy efficiency, reducing methane emissions from fossil fuels, and deploying renewable energy installed capacity of up to 11 TW by 2030 along with proposals for policy improvements. The importance of the scenario is the increased use of renewables such as solar PV, wind, nuclear, heat pumps and electric cars, which increases electrification and reduces the demand for fossil fuels by 80% by the time of achieving NZE. According to the NZE scenario, following the pathways should reduce 35% of CO_2 emissions and 75% of methane emissions in the energy sector by 2030 by increasing the use of renewables, low-emission fuels, nuclear and CO_2 capture technologies. The introduction of NZE pathways reduced the cost of clean energy and improved policies, which resulted in the reduction of the projected global average temperature by 2100 to 2.4℃ from 3.4℃, which was projected before the Paris Agreement in 2015 [65]. In 2021, the International Renewable Energy Agency (IRENA) introduced a 1.5℃ scenario, a similar scenario to NZE for achieving negative CO_2 emissions, which has pathways similar to NZE, except complete elimination of fossil fuel use and use of renewable energy 100% by 2050. The complete phase-out of fossil fuel limits the use of CCS only in production industries such as cement and steel production[66]. The acceleration of clean energy in 2019 has increased the generation of low-emission electricity to 1800 TWh. The deployment of clean energy has drastically reduced the global demand for fossil fuels by 5% in 2023 [67]. In recent years, the G7 countries that include some of the EU countries such as Germany, Italy, and France, also include the United Kingdom, the US, Canada, and Japan are focusing more on the implementation of green technology, considering it as a way to reduce CO_2 emissions and climate-related issues. However, implementation depends upon further research and development, capabilities to handle advanced technologies, providing funding and initial initiatives [68]. The concept of bioenergy with carbon capture and storage (BECCS) introduced in 1996 states that combining energy production using biomass with CCS provides the possibility of achieving negative

emission [69]. The concept received more attention in 2011 when the Intergovernmental Panel on Climate Change (IPCC) reported that BECCS is one of the potential technologies available to achieve negative emissions, and the development of this technology depends on its available land and water resources and the carbon accounting of the biomass used [70]. However, the use of biomass produced in an unsustainable way in BECCS is still considered comparable to emissions from fossil fuels. The IPCC Guidelines for National GHG Inventory in 2006 stated that the emission made from the combustion of biomass-related fuels without CO_2 capture is considered zero. Including a CCS and performing capture results in negative CO_2 emission [71], [72]. About 20 projects were announced with a capture rate of 15MtCO_2/year. Despite reports and attention, the deployment of these projects is in a very low phase so that only 50 MTCO_2/year can be reached by 2030 [73]. Figure 1.9 shows the current installed capacity of BECCS and the planned installation capacity of BECCS compared to the NZE scenario. Currently, only 1 Mt-CO_2/year of BECCS available. The installation of BECCS technology depends on several factors, including the availability of biomass, CO_2 storage facility, and investments [74], [75].

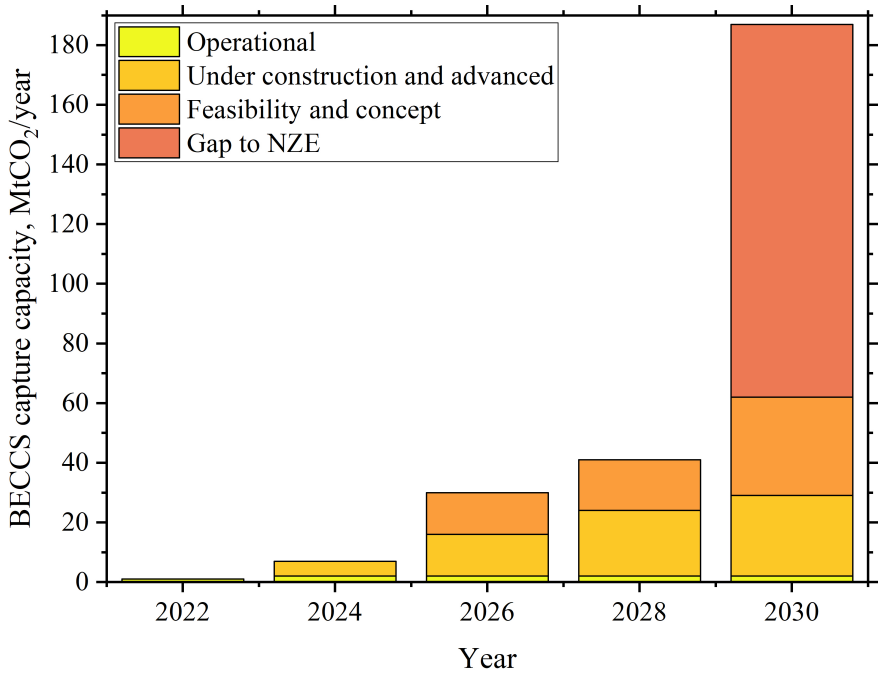

Figure 1.9: Planned and operational BECCS capacity and NZE scenario capacity[74]

1.2 Current status of the research

Gas turbines offer improved efficiency, flexibility, and lower emissions than coal power plants. They are highly responsive to rapid load changes and can start up quickly, making them suitable for fluctuating operating conditions. Coal power plants have higher CO_2 emissions from 50% to 100% more than gas turbines. The Frame-F heavy-duty gas turbine (HDGT) is one of the largest and most powerful in operation, with a firing temperature range of 1300–1400℃ and capable of generating 334 MW of electricity with an efficiency of 40.5% in a simple cycle. When integrated into a combined cycle the turbine can produce up to 475 MW with an efficiency of 58.2%. The lower emissions profile and higher efficiency compared

to coal make the F-class HDGT a crucial component in modern power systems for transitioning towards cleaner energy solutions [76]. Further advancements in CHP systems have been proposed to enhance both power generation and environmental performance. This involves integrating a Combined Cycle with an Organic Rankine Cycle (ORC) and thermoelectric units. In the combined cycle, electricity generation is performed by utilizing exhaust gases from the gas turbine in the evaporator to produce steam for the steam cycle. After the evaporator, the flue gas passes through thermoelectric generators to produce additional electricity. After power generation in the Rankine cycle, the exhaust steam from the steam turbine is used as a converter in the ORC, where it heats the organic working fluid that drives an OR turbine for electricity production. The thermoelectric units supply energy to the auxiliary equipment. This system is capable of producing an annual power output of 749 GWh, although production can vary based on weather conditions [77]. A study by Zaporowski highlights the significant advantages of natural gas-fired CHP achieving high efficiency and low emissions when compared to coal or biomass-fired CHP systems. Various operational parameters of the CHP systems were compared, focusing on the impact of different pressure levels in the Heat Recovery Steam Generator (HRSG). It was found that a gas-fired CHP with three pressure levels such as High Pressure (HP), Intermediate Pressure (IP), and Low Pressure (LP) performs better compared to systems with fewer pressure levels. Specifically, the system with three pressure levels achieved an electrical efficiency of 55% and an overall efficiency of 77.6%, which are higher than the systems with two or single pressure level systems. In terms of cogeneration heat efficiency, the single pressure level HRSG demonstrated a high efficiency of 32.42%, due to the lower amount of electricity produced, which allowed for more efficient heat recovery [78]. The CCGT offers high operational flexibility, increased power generation capacity, lower GHG emissions, and provides an efficiency more than 60%. With more research and development, this efficiency can be improved further. Recent research on the Nishi-Nagoya combined cycle power plant in Japan shows that by improving subcritical and supercritical steam parameters, and optimizing the pressure levels in the HRSGs, the efficiency of the power plant can be improved further. The Nishi-Nagoya plant operates with 3 gas turbines and 3 HRSGs, producing steam to power a steam turbine to generate a total power output of 1.19 GW. In 2018, this power plant set a Guinness World Record for achieving a gross efficiency of 63.08%. Further research shows that efficiency could be improved to 64.45% with a power output of 1.21 GW. However, this improvement would require additional investment in advanced materials for HP pipelines, HRSGs, and turbines, including increasing the stages of the steam turbine and improving the wall thickness of the HRSG [79]. After six years, the record was surpassed by the Keadby 2 power station in the UK, which achieved a gross efficiency of 64.18% [80].

A comparative analysis with three different scenarios is performed to analyse the flexibility of CHP-DHN operation in response to fluctuation of the heat supply. Scenarios such as CHP integrated with a Thermal Energy Storage (TES) system, CHP connected to a DHN, and CHP integrated with DHN using TES as buffer tank are used. The CHP system is modelled to operate at an electrical power output of 370 MW, providing a maximum heat output of 500 MW to the DHN. In a static model of the first scenario, where CHP is combined with a TES system, the TES compensates for the temperature fluctuations of the CHP system. To manage a fluctuation of the heat output of 50 MW, the required volume of TES is calculated to be 5640 m^3. In the second scenario, where the CHP relies only on the DHN for heat distribution, the temperature

gradient cannot be balanced by the DHN alone, as the network itself is used as thermal storage, limiting its ability to respond to changes in demand. The third scenario, which integrates the TES as a buffer tank with the DHN, offers the most efficient solution. To handle the same 50 MW heat fluctuation, the buffer tank requires a smaller volume of just 833 m^3. This improved performance in managing heat frequency reserves compared to the other two scenarios. This configuration optimises system flexibility by efficiently buffering thermal fluctuations while minimizing space and infrastructure needs, making it the most effective option among the scenarios analysed [81]. A low temperature district heating concept (LTDH) is developed, which operates at a supply and return temperature of 55/25℃ is developed with the end user receiving a supply temperature of 45℃ at a minimum limit hot water temperature to residents. LTDH compared to Medium Temperature District Heating (MTDH) operating at 80/40℃ using energy and exergy study shows a significant improvement in LTDH in terms of performance, energy and exergy efficiency. The DH systems operated under two different substations with indirect heating using heat exchangers and direct heating. The comparison shows that the energy efficiency LTDH is 43.5 % and 43 % for direct and indirect heating operations, respectively. In comparison, the energy efficiency of MTDH is 27.1% and 26.2% for the direct and indirect heating operations, respectively. The analysis results in LTDH systems with reduced heat and energy loss, which makes it more suitable for low-quality heat demand and supply [82].
The CCS technology introduced a few decades ago had a lower capture efficiency and difficulties in integrating it with existing complex facilities. After extensive research and development of the first generation of CCS, the second and third generation CCS were introduced with improved efficiency and low cost. Some of it is possible to integrate with existing complex systems. Despite that, most of these developments are still on a pilot scale and very few are commercialized [83]. Carbon capture in the energy industry is performed using 3 different methods [84]:

- Pre-combustion carbon capture: CO_2 is removed before the combustion process through gasification, where solid fuel is converted into syngas with a high hydrogen composition (H_2) and carbon monoxide (CO). While CO in syngas is converted to CO_2 using the Water Gas Shift (WGS) reaction and separated, H_2 is used for combustion.

- Oxy-combustion carbon capture: The air separation unit (ASU) is used to supply oxygen for combustion, producing flue gas consisting of CO_2 and water vapour. The CO_2 is then separated after condensation of the water vapour.

- Post-combustion Carbon Capture and Storage (PCCS): It involves capturing CO_2 after the combustion process using methods such as adsorption, absorption, chemical looping combustion (CLC) or cryogenic techniques.

In the PCCS process, physical absorption utilises polymeric and ceramic materials, while CO_2 adsorption involves materials such as activated carbon and zeolites. In PCCS, CLC uses a carbonator, where CO_2 from the flue gas reacts with calcium oxide (CaO) to form calcium carbonate ($CaCO_3$). Using the application of heat in the calciner, CO_2 is released from $CaCO_3$. For chemical absorption, solvents such as monoethanolamine (MEA), methyl diethanolamine (MDEA), diethanolamine (DEA), and sometimes a blend of solvents are used. Depending on the type of solvent and the regeneration efficiency, solvent-based

PCCS can capture up to 95% of CO_2 from flue gas [84]. Integrating CCGT and PCCS can increase the chances of achieving low emissions and high electricity output while allowing the potential to achieve negative CO_2 emission. However, the low concentration of CO_2 in flue gas requires a higher energy intensity for the capture process and increased capture cost [85]. The selection of a solvent for CO_2 capture is influenced by several factors, including CO_2 solubility, the energy required for solvent regeneration and reaction kinetics of the chemical process [86]. In addition, the corrosion rate, solvent volatility, and size of the absorber should also be considered, which impacts the reaction kinetics. To improve the CO_2 absorption capacity and reaction rates, primary and secondary amines are mixed with tertiary amines [87]. This mixture of solvents improves the capture process by balancing the properties of each solvent, which improves the overall results of the process [88].

The integration of PCCS with CCGT can also reduce the net power generation of CCGT since PCCS equipment such as CO_2 compressors and pumps consumes CCGT electricity. Moreover, steam from the CCGT steam cycle is extracted for solvent regeneration. The modelling of 495 MW natural gas fired CCGT with solvent CO_2 capture technology using a parabolic solar collector and TES to operate the PCCS reboiler shows significant improvements. To overcome the problem of low CO_2 concentration in flue gas, part of the flue gas at the exit of the HRSG is recirculated to the gas turbine, which increased the CO_2 concentration by 1.9 mol% and reduced 20% the duty of the boiler. The implementation of flue gas recirculation and the use of the TES system reduced the Levelized Cost of Electricity (LCOE) by 1.17 $/MW of thermal energy and CO_2 avoidance cost by 4.52 $/t-$CO_2$ [89]. Another modelling analysis of 770 MW CCGT integrated with PCCS using solvent method with advanced configurations in CO_2 capture process resulted in reducing 0.094 MJ/kg-CO_2 of power consumption of the PCCS and increasing 0.5% of power generation in CCGT. Initially, CCGT exhaust gas is recirculated in the power plant to increase the CO_2 content in the flue gas. Lean Vapour Recompression (LVR) introduced to the PCCS separates the vapour from the lean solvent of the reboiler and is used to preheat the rich amine in the amine heat exchanger, which benefits the solvent regeneration. Introducing the LVR and preheating rich amine using the condensate from the reboiler reduces 7.3% of PCCS energy consumption. [90].

The use of biomass in BECCS is expected to contribute to a reduction of 2 GT/year of CO_2 by 2050. In this process, biomass undergoes thermal conversion methods such as combustion, gasification, liquefaction, and pyrolysis, which produce syngas, hydrogen, biochar, and bio-oil, which can be used for energy generation. The integration of CCS within this technology allows the possibility of achieving negative emissions. However, the cost and feasibility of this technology depend on several factors, including biomass availability, transportation costs, storage costs, the cost of CCS deployment, and carbon prices. Thus, government support is crucial for implementation. Of the five BECCS facilities that operate globally, the largest is the Archer Daniels Midland (ADM) ethanol plant in Illinois, which captures 1 Mt of CO_2 annually, which is financially supported by the US Department of Energy. On average, the cost of BECCS ranges from $15 to $400 per ton of CO_2 [91]. Europe is slowly progressing in BECCS and Bioenergy with Carbon Capture and Utilization (BECCU) by utilizing the captured CO_2 in biomethane & bioethanol production, syngas production, Enhanced Oil Recovery (EOR), blue hydrogen and other industrial uses. With 3 existing plants including a biomass power plant with CO_2 capture for polymers

production in the UK and two waste-to-energy plants with CO_2 capture capacity of 7500 t-CO_2/year and 100 kt-CO_2/year, European countries including Germany, Norway, Belgium and the Netherlands have planned biomass/waste-to-energy plants with CO_2 capture in the future. The EU produced electricity of 129.3 TWH and 61.7 TWh utilizing biomass/municipal waste and biogas, respectively in 2018. Considering the availability of biomass, biogas production and biofuel plants in Europe, the total capture capacity of 1.6 Mt-CO_2/year is planned. In addition to this, the EU also focuses on producing jet fuels from biomass and blue hydrogen production, which reduces greenhouse gas emissions [92].

1.3 Research hypothesis

It is possible to develop a large-scale unit of a combined cycle gas turbine power plant (based on the Rankine and Brayton cycles) with zero/negative emission of CO_2, thanks to combined post-combustion methods and zero-emission fuels. Integration and operation of the CCS installation in the CCGT power plant and analysis of suitable solvent allow the reduction of CO emission$_2$ from the power plant with high carbon capture efficiency and low regeneration requirement. Results of thermodynamic modelling of gas-fired power plant operation allow for identifying the properties of gas fuels with achievable carbon capture rate and allow to determine operating conditions and regimes for efficient electricity and heat generation in CCGT power plant.

1.4 Structure of the dissertation

This dissertation is organised into the following chapters:

Chapter 1 provides a comprehensive overview of the literature on energy systems and CO_2 capture installations. It outlines the current challenges and trends related to the focus of the research, which are the motivation and direction of the research.

Chapter 2 provides the main objectives of this research and a detailed description and specifications of the energy systems and CO_2 capture installations analyzed in this study, which are used for developing the thermodynamic models. The input data necessary for the thermodynamic analysis of the power plant and carbon capture technology were collected from various industrial sources and the existing literature. While the designed CCGT comprises real-time operational data from an existing power plant, the PCCS was designed based on literature-derived parameters. The fuels considered in this analysis are based on real-time data and experimental findings from Poland. These data sources ensure that the study reflects the actual fuel composition, availability and operational conditions in the region.

Chapter 3 presents a comprehensive thermodynamic analysis of the combined cycle power plant and the CO_2 capture unit. It provides a detailed description and evaluation of the critical components, including gas turbines, the steam turbine, heat recovery steam generators and district heating network. In addition, the chapter explains the calculations for the mass and energy balance of CO_2 capture streams, which are essential to estimate the properties of the stream required for thermodynamic modelling. Furthermore, the chapter introduces key performance indicators (KPIs) used to assess the feasibility and efficiency of the proposed system. These indicators include energy, environmental, and economic evaluations. A detailed

discussion on these KPIs ensures a thorough technical assessment of the designed system, which provides a detailed understanding of its operational performance and sustainability potential.

Chapter 4 presents the main assumptions of energy systems and CO_2 capture installations, derived from real-world data and the relevant literature. Using the data, a thermodynamic model is developed to accurately reflect real-world operating conditions. To ensure the reliability of the model, the developed model is validated by comparing the energy unit results with operational data of an existing power plant and the results of the CO_2 model with the experimental CO_2 capture data and process simulation results. This validation is crucial to assess the feasibility and accuracy of the system. Furthermore, both the energy system and the CO_2 capture unit are integrated to analyze their combined performance and operational effectiveness.

Chapter 5 provides a comprehensive analysis of the results obtained from thermodynamic modelling. The study examines the use of different types of fuels and various fuel blends in gas turbines, which impacts the overall performance of the power plant and CO_2 capture installations. Detailed discussion on the system performance with and without integration of the district heating network and CO_2 capture facilities is presented. The KPI evaluation provides an assessment of the system's capabilities, which describes performance aspects such as efficiency, emissions reduction, and operational flexibility. Moreover, the chapter explores opportunities to achieve negative CO_2 emissions by identifying potential strategies for carbon reduction and techno-economic assessments. The chapter also explores opportunities to achieve negative CO_2 emissions using the proposed design and identifies the challenges and limitations associated with its implementation.

Chapter 6 summarizes the research findings and provides a short summary of the dissertation, highlighting the outcomes of the study. It describes the feasibility of achieving negative CO_2 emissions and analyzes how the performance of the power plant varies under specific conditions across different scenarios. Additionally, it summarizes the influence of various solvents on the performance of power plant and the technical assessment results of the system.

Chapter 2

Object of the research

As part of the POLNORCCS project on "Negative CO_2 Emission Gas Power Plant" in Work Package 2 (Task 4), the following considerations are taken into account for this research study [93]. The main objective of this research is to evaluate the possibility of achieving negative CO_2 emissions in a gas power plant. To assess the technical feasibility of this analysis, the input and boundary conditions for the thermodynamic analysis and modelling are based on the existing Gorzów CCGT power plant in Gorzów Wielkopolski, Poland [94]. The following sections provide a comprehensive description of the considered case, including the specifications of technology, thermodynamic analysis, model boundary conditions, and analysis results. The main objectives of the research are as follows.

- Perform comprehensive analysis of CCGT integrated with PCCS technology using solvent method.
- Develop a detailed thermodynamic model of CCGT and PCCS on the basis of the results of the analysis.
- Perform complex simulations of CCGT integrated with PCCS using fossil fuels, biogas and mixture of fuels, to analyze the operational performance of CCGT with and without PCCS and measure the technical assessment factors.
- Based on the BECCS concept, evaluate the feasibility of achieving negative CO_2 emission using biogas in the reference power plant.

Due to its high efficiency, low emissions, low operational costs, reliability, and flexible operations, the CCGT system was selected for this case study. Figure 2.1 shows the overall layout of the CCGT power plant operating with two Siemens SGT-800 gas turbines, a Siemens SST-400 steam turbine, two HRSGs and a DHN system. The exhaust produced from the combustion of the air and fuel mixture in the gas turbines is passed to HRSGs that operate at two different pressure levels. To maximize thermal energy utilization, the flue gas and steam flows operate under countercurrent exchange in HRSG components. The steam produced in the pressure levels of the HRSGs is used in the steam turbine for power generation. The extractions from the steam turbine are used in the DHN heat exchanger for water heating, PCCS for amine regeneration, and deaerator for the deaeration process. When the pinch point is achieved in HRSG, which is the minimum temperature difference between the exit of the evaporator flue gas and the fluid

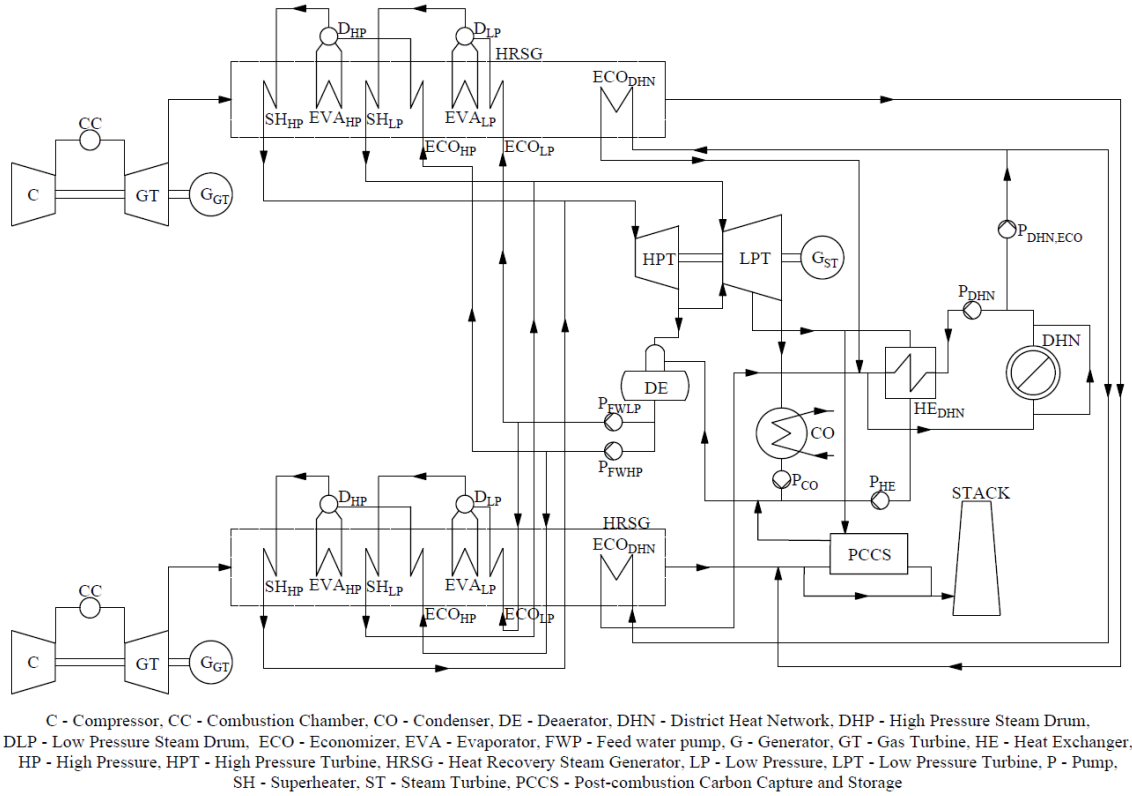

C - Compressor, CC - Combustion Chamber, CO - Condenser, DE - Deaerator, DHN - District Heat Network, DHP - High Pressure Steam Drum, DLP - Low Pressure Steam Drum, ECO - Economizer, EVA - Evaporator, FWP - Feed water pump, G - Generator, GT - Gas Turbine, HE - Heat Exchanger, HP - High Pressure, HPT - High Pressure Turbine, HRSG - Heat Recovery Steam Generator, LP - Low Pressure, LPT - Low Pressure Turbine, P - Pump, SH - Superheater, ST - Steam Turbine, PCCS - Post-combustion Carbon Capture and Storage

Figure 2.1: Layout of the reference case combined cycle gas turbine power plant integrated with post-combustion carbon capture considered for this study [95].

inlet, the thermal energy in the flue gas is further utilized by economizer and DHN. After the utilization of thermal energy in the DHN economizer, the flue gas is sent to PCCS to perform CO_2 capture.
While 68% of the natural gas used in Poland is imported from other countries and 32% of natural gas is produced domestically. Natural gas is primarily found in the western part of Poland, widely in the Greater Poland region, and some in the southeast of Poland, and is supplied to other regions through pipelines. Most of the deposits found in the western part have a high nitrogen content, which is known as nitrogen-rich natural gas, consisting of only 30% to 80% methane. In some parts of the deposits, nitrogen in the N_2 rich gas will be up to 90% [96], [97]. The natural gas found in Poland is classified as E, Ls, Lw, Ln, and Lm. Although type E has a high content of methane, Ls and Lw have nitrogen in the range of 27% and 20%, respectively. The Ln and Lm types have a nitrogen content of around 32% [98], [99]. A model study by Grzymislawski et al. (2023) [100], shows that the increase in the nitrogen content of the fuel used in the combustion chamber of a gas turbine model has decreased NO emissions by more than half compared to burning pure methane. However, increasing the nitrogen content can also decrease the combustion temperature, showing the effect of using N_2-rich fuels in gas turbines for combustion.

Sewage sludge is a residue obtained from wastewater treatment plants used to be disposed as landfills. However, due to the presence of high water content, heavy metals, and organic matter, Directive 2008/98/EC of the EU restricted this method of disposal and Directive 86/278/EEC established limits on the heavy metal content of sewage sludge that can be disposed of as landfills [101], [102]. The wastewater treatment plants (WWTP) in Poland contribute to 337 GWh of electricity, where sewage

sludge is converted to biogas for the generation of electricity. The sludge produced by WWTPs is utilized for various applications such as fertilization, incineration, and landfills [103]. In recent years, due to EU regulations, the use of sludge in landfills in Poland has decreased with an increase in its use for thermal treatment. Figure 2.2 shows the percentage of sludge used for various purposes from the total sludge produced in Poland from 2010 to 2022 [104]. Sewage sludge is considered a type of biomass and is viewed as an alternative to replace fossil fuels. Therefore, syngas produced by the thermochemical conversion of sewage sludge is considered a renewable energy source. The gasification of the sewage sludge offers a reduction in its volume and conversion of the sludge into usable gas fuel [105]. A notable gasification of sewage sludge is the plasma gasification process, where an electric arc is generated between two electrodes to reach a high temperature up to 4500℃. At these temperatures, the organic matter in the sewage sludge is converted to syngas, and the inorganic components are converted to slag. This process has the advantages of producing clean syngas with low toxic components, with lower tar removal and higher gas yield [106],[107].

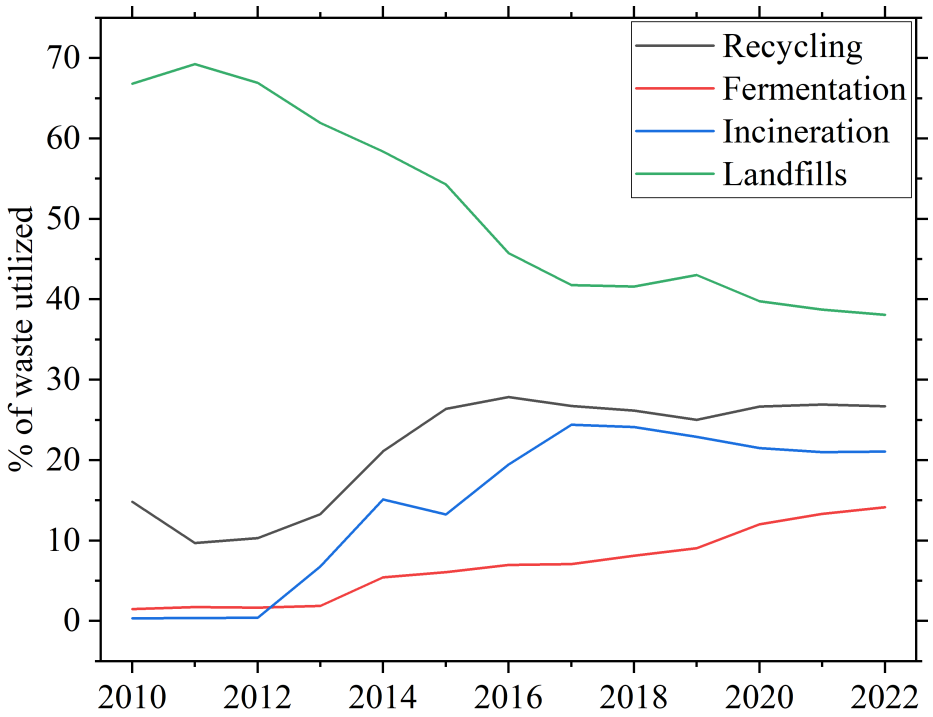

Figure 2.2: Percentage of sewage sludge utilized for thermal treatment from the total municipal waste generated in Poland from 2010 to 2022 [104].

To match the existing scenario, the N_2 rich fuel used in the Gorzów CCGT power plant [108] is considered as another fuel. Based on the concept of BECCS, the syngas produced from the sewage sludge is selected as one of the fuels used in the power plant to achieve negative CO_2 emissions. This syngas composition is obtained as a result of the experimental plasma gasification of sewage sludge. To compare the performance of power plant using different fuels, pure methane is chosen. The composition of the different fuels used for the analysis is shown in Table 2.1. The required fuel flow rate for one gas turbine

varies according to each fuel depending on the lower heating value (LHV)[1] of the fuel, such as 50.55 MJ/kg, 18.62 MJ/kg and 17.47 MJ/kg for methane, N_2-rich gas and syngas, respectively.

Table 2.1: Properties of fuels used in the CCGT gas turbine

Component	Molecular formula	Methane		N_2-rich gas [108]		Syngas	
		mass%	molar%	mass%	molar%	mass%	molar%
Nitrogen	N_2	-	-	62.12	52.92	-	-
Methane	CH_4	100	100	26.87	39.97	11.46	13.2
Hydrogen	H_2	-	-	-	-	5.1	46.74
Carbon monoxide	CO	-	-	-	-	13.31	8.78
Propane	C_3H_8	-	-	6.48	3.51	8.03	3.36
Ethane	C_2H_6	-	-	4.53	3.6	-	-
Carbon dioxide	CO_2	-	-	-	-	59.31	24.9
Ammonia	NH_3	-	-	-	-	2.79	3.03

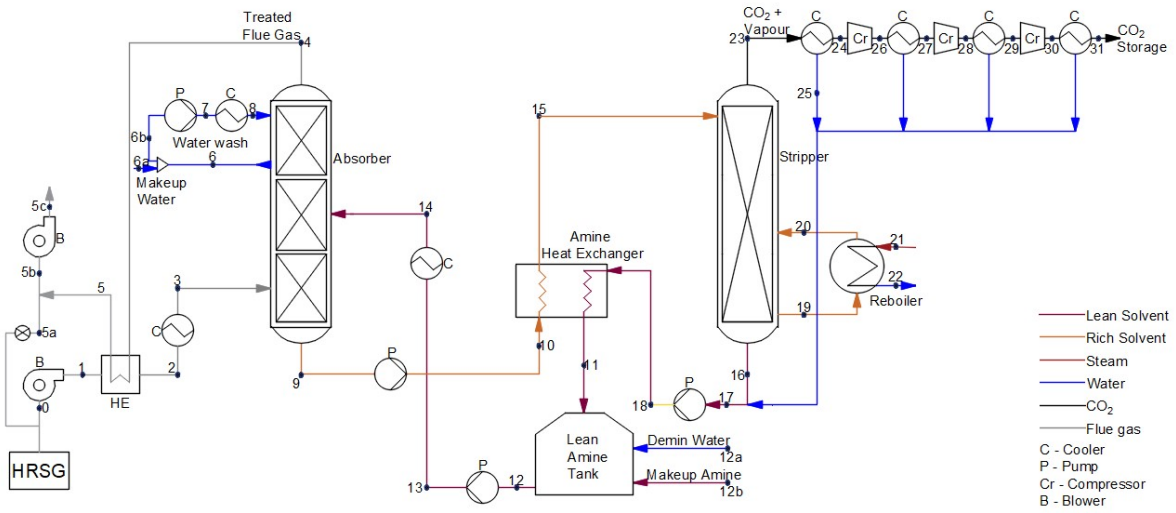

Figure 2.3: Layout of Post-combustion Carbon Capture and Storage technology using solvent method with reference points [95].

Figure 2.3 illustrates the components and layout of the PCCS, including the absorber, stripper/desorber and amine heat exchanger. The exhaust gas from the power plant is pressurised and cooled to the operating conditions of the absorber - 1 bar pressure and 45℃. Amine under the same operating conditions enters the absorber in the middle and reacts with CO_2 in the flue gas. Given the absorbing capacity of amine, the amine absorbs 90% CO_2 in flue gas and exits the absorber, at this stage referred to as rich amine. To minimise amine emission, the treated flue gas is water-washed before being released into the atmosphere, and the flue gas is used further to cool the hot flue gas from the power plant. The pressure of the rich amine is increased to the operating pressure of the stripper and then preheated in an amine heat exchanger

[1]LHV based on ISO 6976:1995(E) at 15 ℃ and 1 atm for gas mixtures

before entering the stripper, where it is further heated to the stripper's operating temperature of 120℃. Recirculation of the amine to the reboiler further increases the temperature using steam at 135℃ and 3 bar, leading to the separation of CO_2 from the amine when the amine flows back to the stripper. The separated CO_2 is then cooled, compressed using the CO_2 handling system, and stored. The lean amine exits the stripper heat rich amine in an amine heat exchanger and repeat the capture process. The reference points on each stream of the PCCS help perform a comprehensive thermodynamic analysis for the calculations of mass balances. These reference points are used to monitor properties such as pressure, temperature, mass flow, and composition to analyze the efficient operation of the PCCS [95]. Table 2.2 shows the chemical properties of amines such as MEA, AMP and PZ used for the PCCS CO_2 capture process [109].

Table 2.2: Properties of solvents used in PCCS process [109].

Parameter	Unit	MEA	AMP	PZ
Chemical formula	-	C_2H_7NO	$C_4H_{11}NO$	$C_4H_{10}N_2$
Molecular weight	g	61.08	89.14	86.14
Boiling point	°C	170	165	145 - 146
Density @ 25°C	g/mL	1.012	0.934	1.1
Flashpoint	°F	200	153	65
Storage temperature	°C	15 to 25	<30	<30
pH	-	12.1	9 - 10.5	11 - 12.5

Chapter 3

Thermodynamic description of technology

3.1 Gas cycle

The Siemens SGT-800 industrial gas turbine was selected for this study due to its exceptional efficiency, operational flexibility, and low emissions. These characteristics make the SGT-800 particularly suited for integration into both cogeneration and combined cycle power plants, including applications in district heating systems. Table 3.1 provided outlines the specific parameters of the SGT-800 used in the analysis, highlighting its suitability for such energy systems.

Table 3.1: Specifications of industrial gas turbine Siemens SGT-800 [110]

Parameter	Unit	Value
Power generation	MW	ISO 50.5
Electrical efficiency	%	38.3
Frequency	Hz	50
Heat rate	kJ/kWh	9407
Speed	rpm	6608
NO_x emission	ppmV	<15
Fuel supply pressure requirement	bar	27-30
Compressor pressure	-	21.1:1
Exhaust gas flow	kg/s	134.2
Exhaust gas temperature	℃	553

The gas turbine operates under standard conditions of the International Standard Organization (ISO), which are crucial to the performance and reliability of the operation of gas turbines. The ISO conditions define standardized parameters such as inlet air pressure, temperature, and relative humidity. The performance of gas turbines can vary significantly depending on environmental conditions, which fluctuate depending on location, altitude, and weather. Hence, standardization is very important for the

gas turbine. As mentioned Figure 3.1, the ISO-rated point of the SGT-800 is set to a compressor air input temperature of 15℃ to achieve a maximum output power of 50.5 MW. This temperature is critical because it represents the performance of the turbine under different operating conditions to deliver optimal efficiency and power output in a range of scenarios.

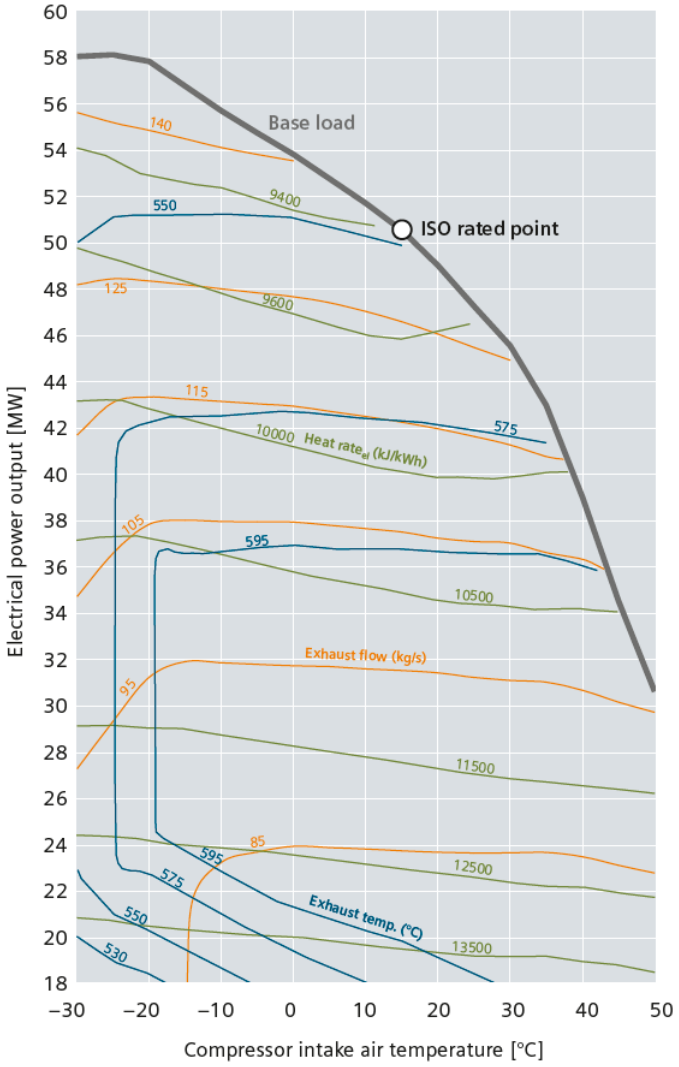

Figure 3.1: ISO rated point for Siemens SGT 800, 50.5 MW [110].

The following equations are used to perform various thermodynamic analyses of the gas cycle of the CCGT plant considered as the reference. In the gas cycle, the outlet pressure of the gas turbine compressor, P_2 (bar), is measured using Equation (3.1) considering the pressure ratio of the compressor (r_c) and the input pressure of the compressor, P_1 (bar).

$$P_2 = r_c \cdot P_1 \tag{3.1}$$

The isentropic efficiency of the compressor (η_{is}) is calculated using equation (3.2).

$$\eta_{is} = \frac{h_{2s} - h_1}{h_2 - h_1} \tag{3.2}$$

Where h_1 is the enthalpy of air at the inlet of the compressor (kJ/kg) calculated for the temperature of the air at the inlet of the compressor T_1 (℃). Considering the isentropic entropy of air at the inlet and outlet of

the compressor are same (s_1=s_2), the isentropic temperature of air at the outlet of the compressor T_{2s} (℃) is calculated using the pressure P_2 and entropy of the compressor outlet air, s_2 (kJ/kg-K), which is used to calculate the isentropic enthalpy of compressor outlet air h_{2s} (kJ/kg). To calculate the outlet temperature of the compressor air, T_2 (℃), the enthalpy of the air at the outlet of the compressor, h_2 is calculated with the above equation written as Equation (3.3).

$$h_2 = \frac{h_{2s} - h_1}{\eta_{is}} + h_1 \tag{3.3}$$

Using the mass flow of air, $\dot{m}_{air}$ (kg/s) and the enthalpy of the air at the inlet and outlet of the compressor, the output work of the air compressor, $\dot{W}_{ACo}$ (MW) is calculated using Equation (3.4).

$$\dot{W}_{ACo} = \dot{m}_{air} \cdot (h_2 - h_1) \tag{3.4}$$

The work input of the air compressor, $\dot{W}_{ACi}$ (MW) is calculated using the mechanical efficiency of the air compressor, η_m using Equation (3.5).

$$\dot{W}_{ACi} = \frac{\dot{W}_{ACo}}{\eta_m} \tag{3.5}$$

The air at the outlet of the air compressor and fuel is passed to the combustion chamber for combustion. Considering the pressure loss inside the combustion chamber, δP_{cc}, the pressure at the outlet of the combustion chamber, P_3 (bar) is calculated using Equation (3.6).

$$P_3 = P_2 \cdot (1 - \delta P_{cc}) \tag{3.6}$$

Equation (3.7) is used to calculate the efficiency of the combustion chamber of the gas turbine using enthalpy of flue gas at the outlet of the combustion chamber, h_3 (kJ/kg).

$$\eta_{cc} = \frac{(\dot{m}_{air} + \dot{m}_f)\, h_3 \cdot \dot{m}_{air}\, h_2}{\dot{m}_f \cdot LHV} \tag{3.7}$$

To estimate the mass flow of fuel, $\dot{m}_f$ (kg/s) with a Lower Heating Value (LHV) of the fuel (kJ/kg) used for combustion, Equation (3.8) is used.

$$\dot{m}_f = \frac{\dot{m}_{air} \cdot (h_3 - h_2)}{\eta_{cc} \cdot LHV - h_3} \tag{3.8}$$

To estimate the mass flow of flue gas, $\dot{m}_{fg}$ (kg/s) produced at the combustion chamber, Equation (3.9) is used.

$$\dot{m}_{fg} = \dot{m}_{air} + \dot{m}_f \tag{3.9}$$

The flue gas produced at the combustion chamber is passed to the gas turbine for power generation. The outlet pressure of the gas turbine, P_4 (bar) is measured using Equation (3.10) considering the pressure loss in the gas turbine (δP_{gt}).

$$P_4 = P_1 - \delta P_{gt} \tag{3.10}$$

The work input ($\dot{W}_{GTi}$) and the work output of the gas turbine ($\dot{W}_{GTo}$) (MW) is calculated by the Equation (3.11) & Equation (3.12) respectively.

$$\dot{W}_{GTi} = \dot{m}_{fg} \cdot (h_3 - h_4) \tag{3.11}$$

$$\dot{W}_{GTo} = \dot{W}_{GTi} \cdot \eta_m \tag{3.12}$$

Where η_m is the mechanical efficiency of the gas turbine and h_4 (kJ/kg) is the enthalpy of the flue gas at the outlet of the gas turbine. The Net power available on the gas cycle $\dot{W}_{cyc}$) (MW) is measured by the difference between the work output of the gas turbine and the work input of the air compressor as in Equation (3.13)

$$\dot{W}_{cyc} = \dot{W}_{GTo} - \dot{W}_{ACi} \tag{3.13}$$

The net electrical output of the gas cycle, N_{GT} (MW) is measured by Equation (3.14) using the electrical efficiency of the generator, η_{el}.

$$N_{GT} = \dot{W}_{cyc} \cdot \eta_{el} \tag{3.14}$$

The heat supplied to the system $\dot{Q}_{cyc}$ (MW) is calculated using Equation (3.15).

$$\dot{Q}_{cyc} = \dot{m}_f \cdot \mathrm{LHV} \tag{3.15}$$

The efficiency of the gas cycle is calculated using the Equation (3.16).

$$\eta_{cyc} = \frac{N_{GT}}{\dot{Q}_{cyc}} \tag{3.16}$$

3.2 Steam cycle

The Siemens SST-400 is a highly efficient industrial steam turbine with a wide range of applications that are used in various energy systems. The SST-400 is widely used in cogeneration plants with district heating systems, combined cycle power plants, concentrated solar power plants (CSP), and geothermal power facilities. Due to the properties of SST-400 as in Table 3.2, operational flexibility, adaptability to rapid load changes, and meeting specific steam extraction requirements [111], make the SST-400 turbine an ideal for this study. This section of the chapter shows the various equations of the steam cycle considered to measure the performance of the steam turbine.

The isentropic efficiency of the steam turbine, η_{iST} is calculated by Equation (3.17). Using this equation, it is possible to calculate the enthalpy of steam at the outlet of the steam turbine, h_6 (kJ/kg) using Equation (3.18).

$$\eta_{iST} = \frac{h_5 - h_6}{h_5 - h_{6s}} \tag{3.17}$$

Where h_5 is the enthalpy of steam at the inlet of steam turbine (kJ/kg) and h_{6s} is the isentropic enthalpy of steam at steam turbine outlet (kJ/kg) for entropy of steam at the inlet and outlet of steam turbine are idem ($s_1 = s_2$) measured in kJ/kg.K.

$$h_6 = h_5 - \eta_{iST}\,(h_5 - h_6) \tag{3.18}$$

Equation (3.19) & Equation (3.20) are used to calculate the work input $\dot{W}_{ist}$ and output $\dot{W}_{ost}$ of the steam turbine (MW) respectively.

$$\dot{W}_{ist} = \dot{m}_s \cdot (h_5 - h_6) \tag{3.19}$$

$$\dot{W}_{ost} = \dot{W}_{ist} \cdot \eta_{ms} \tag{3.20}$$

Table 3.2: Properties of Siemens SST-400 steam turbine [111]

Parameter	Unit	Value
Power output	MW	up to 65
Frequency	Hz	50
Speed	rpm	3000 - 8000
Live steam temperature	℃	540
Live steam pressure	bar	up to 140
Reheat steam temperature	℃	up to 450
Reheat steam pressure	bar	up to 30
Turbine extraction steam pressure	bar	up to 60
Controlled extraction pressure	bar	up to 45
Controlled extraction temperature	℃	450
Exhaust steam back pressure	bar	up to 25
Exhaust steam to district heating	bar	up to 3
Exhaust steam to condensing	bar	up to 0.6

Where $\dot{m}_s$ is the mass flow of steam to the steam turbine (kg/s) and η_{ms} is the mechanical efficiency of steam turbine. The net power produced by the steam turbine, N_{st} (MW), is calculated using Equation (3.21). The N_{st} includes the net power produced by both the HP turbine and the LP turbine.

$$N_{ST} = \dot{W}_{ost} \cdot \eta_{el} \tag{3.21}$$

3.3 Combined cycle

Since the reference case considered for the modern CCGT power plant consists of two gas turbines and one steam turbine, Equation (3.22) & Equation (3.23) are used to calculate the total net power produced by the CCGT, N_{CCGT} (MW) and the net power efficiency of CCGT, η_{CCGT} respectively.

$$N_{CCGT} = 2 \cdot N_{GT} + N_{ST} \tag{3.22}$$

$$\eta_{CCGT} = \frac{N_{CCGT}}{2 \cdot \dot{Q}_{cyc}} \tag{3.23}$$

Table 3.3 presents the key operational parameters of the CCGT SCC-800 2X1 configuration, demonstrating its ability to high electricity production and flexible operation at various load conditions. This CCGT configuration is similar to the reference case CCGT considered for this study, which includes 2 Siemens SGT-800 gas turbines, a Siemens SST-400 steam turbine and 2 HRSG. The data of CCGT in the table are derived from [94], which provides real-world operational parameters of the Gorzów CCGT power plant with a similar arrangement of CCGT equipment and [112] discusses the extensive application of Siemens SGT-800 gas turbines, which highlights the advantages of high efficiency and flexibility at lower loads when included in a CCGT.

Table 3.3: SCC-800 2x1 CCGT modes on operation with overall performance

CCGT Parameter	Unit	Value	
		[94]	[112]
Net plant efficiency	%	55.1	54.7 - 58.6
Net power output	MW	ISO ISO 143.6	ISO 135.4 – ISO 163.1
Net plant heat rate	kJ/kWh	-	6583 - 6143
Net plant output on condensation mode	MW	139.4	-
Gross plant output on condensation mode	MW	141.7	-
Net efficiency of plant on condensation mode	%	53.1	-
Net plant output on cogeneration mode	MW	134.7	-
Gross plant output on cogeneration mode	MW	136.9	-
Net efficiency of plant on cogeneration mode	%	84.3	-
Overall efficiency in winter period	%	82	-
Overall efficiency in summer period	%	52	-
Annual CO_2 emission	g/kW	520	-

3.4 Heat Recovery Steam generator

Figure 3.2 illustrates the detailed configuration of the HRSG used in the analysis. The HRSG is designed with two pressure levels such as HP and LP levels with different pressure values. Each pressure level is equipped with its own economizer, evaporator, steam drum, and superheater. The use of multiple pressure levels in the HRSG improves the overall efficiency of the power plant. Increasing the number of pressure levels in HRSG can extract more heat from the flue gas, increasing the power generation of the steam cycle. The effectiveness of the HRSG is further improved by maximizing heat utilization and minimizing the temperature difference between the flue gas and the generated steam. However, adding more pressure levels is not feasible, if the temperature difference between the flue gas and steam is reduced to 15℃, which would not provide significant heat recovery benefits. Instead, in CHP plants, the remaining heat in the flue gas can be utilized by the DHN economizer connected to the final stage of HRSG [95].

Water is supplied to the economizer by the HP and LP feed water pumps (FWP) after it is preheated in the deaerator. The exhaust gas from the gas turbine is passed through the HRSG duct arrangement used to provide the necessary heat to the components. The preheated water from the economizer is passed into the steam drum, where the separation of water and steam takes place. The steam separated in the cyclone separator is further heated in the superheater tubes to become superheated steam, which is then directed to the steam turbine for power generation. Meanwhile, the water from the steam drum flows through the evaporator and riser tubes, where it is heated by the flue gas before passing through the separator and further through the superheaters, as shown in Figure 3.3. As the flue gas passes through various stages of the HRSG, the temperature of the flue gas decreases with increasing the water/steam temperature at the HRSG components [95].

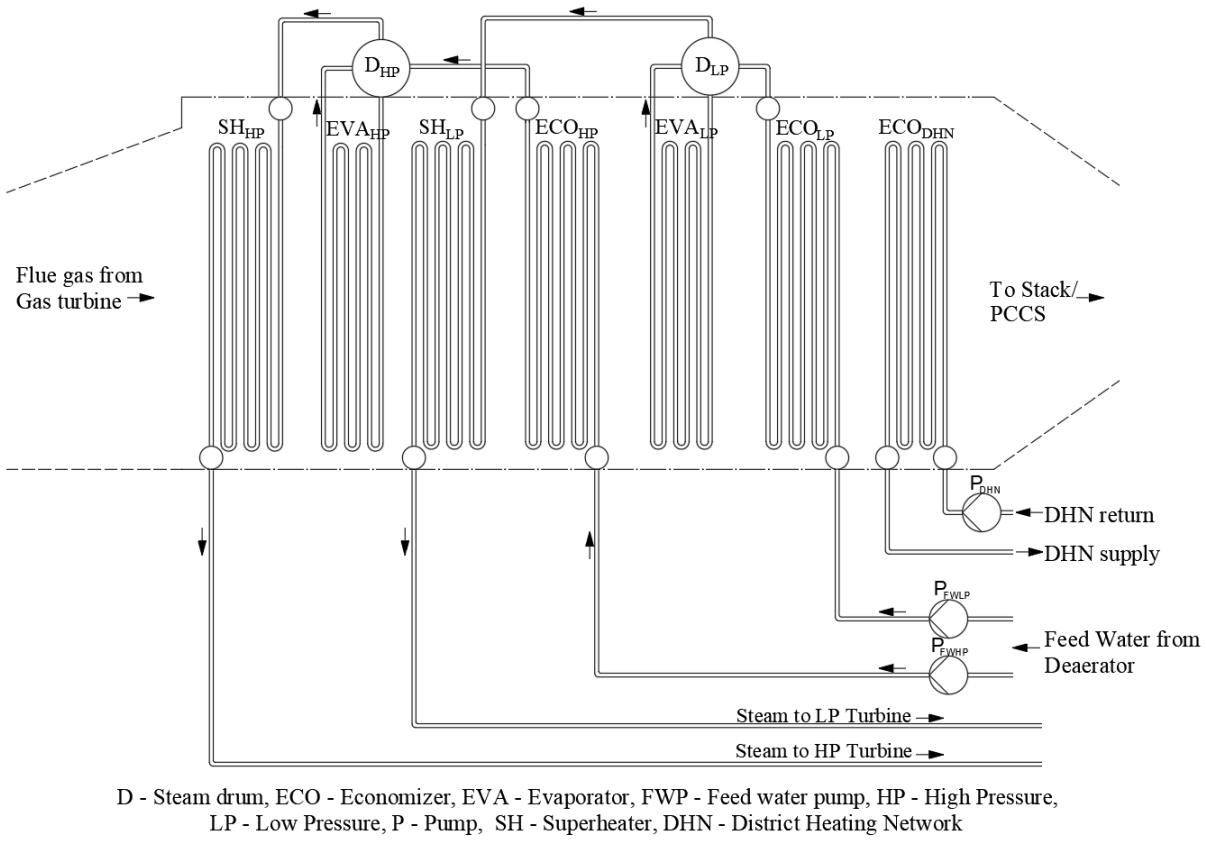

Figure 3.2: Detailed configuration of Heat Recovery Steam Generator with two pressure levels used in the CCGT [95].

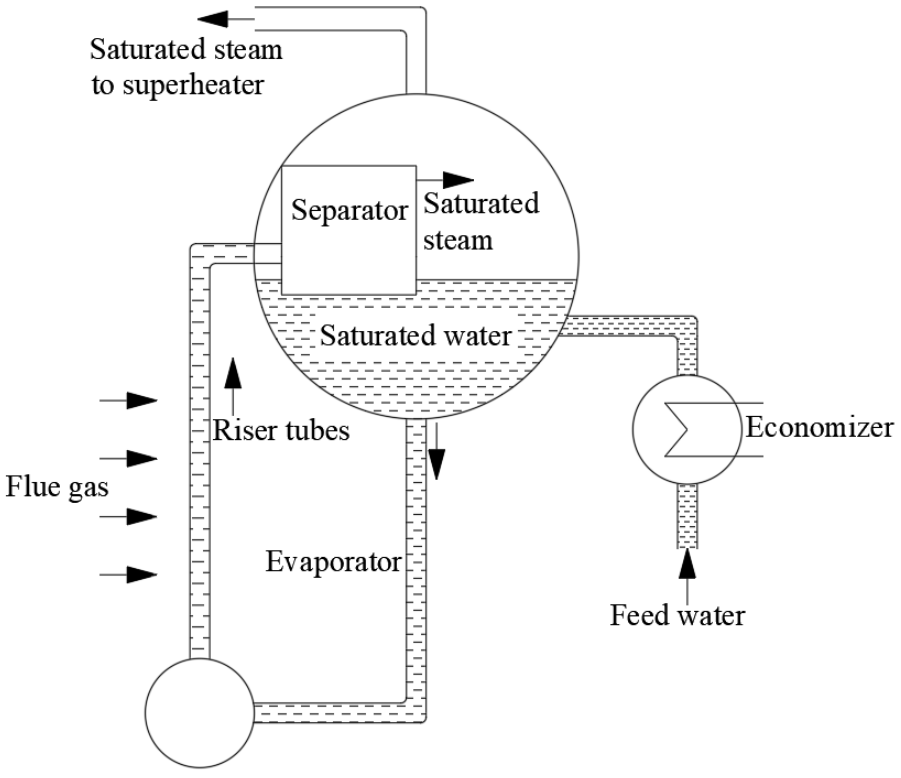

Figure 3.3: Water separation process from saturated steam inside steam drum of the HRSG [95].

The enthalpy of the flue gas at various temperatures, $h_{fg,t}$ (kJ/kg) when using different fuels in HRSG is determined by Equation (3.24) using the mass fraction of the target gas component, X_i and the enthalpy of the gas component at the target temperature of the flue gas (h_i) [95].

$$h_{fg,t} = \sum_{i}^{N} X_i \cdot h_i \tag{3.24}$$

Where t is the target temperature (℃) and i is the chosen gas component. To determine the driving force temperature of the components of HRSG, the logarithmic mean temperature difference (LMTD) (℃) is calculated using Equation (3.25) [95].

$$\text{LMTD} = \frac{\Delta T_A - \Delta T_B}{\ln\left(\frac{\Delta T_A}{\Delta T_B}\right)} \tag{3.25}$$

Where ΔT_A & ΔT_B (℃) are calculated using Equation (3.26) & Equation (3.27) respectively with the inlet and outlet temperature of the hot fluid stream T_{hi} & T_{ho} and cold fluid stream T_{ci} & T_{co}.

$$\Delta T_A = T_{hi} - T_{co} \tag{3.26}$$

$$\Delta T_B = T_{ho} - T_{ci} \tag{3.27}$$

Equation (3.28) is used to calculate the heat exchange rate, $\dot{Q}_{HRSG}$ (MW) of the components of the HRSG in both the flue gas and steam streams using the enthalpy of the targeted temperature [95].

$$\dot{Q}_{HRSG} = \dot{m}_{fg} \cdot (h_{fi} - h_{fo}) = \dot{m}_s \cdot (h_{so} - h_{si}) \tag{3.28}$$

The heat transfer rate is calculated using the enthalpy of flue gas at inlet and outlet h_{fi} & h_{fo} and enthalpy of steam at inlet and outlet h_{si} & h_{so} (kJ/kg) of the components of the HRSG.

3.5 District Heating Network

The figure shows the arrangement of the DHN in reference CCGT power plant. The return water from the DHN is split into two streams and reheated. One stream flows through the DHN economizer at the final stage of the HRSGs and recovers usable waste heat from the exhaust flue gas. The other stream flows through the DHN heat exchanger, where the LP steam extracted from the steam turbine is utilized to increase the return water temperature. These two streams are mixed before they pass to the DHN system. The water supply temperature of DHN is set at 110℃. Three pumps are used in the DHN system, in which two pumps are used to recirculate the return water from the DHN to the heat exchanger and the economizers in the HRSGs, respectively, and one pump to transfer the condensed water from the heat exchanger to the deaerator. Equation (3.29) is used to calculate the rate of heat exchange in the equipment of the DHN, $\dot{Q}_{DHN}$ (MW) such as economizer, heat exchanger, and the overall heat consumption of the DHN, based on the mass flow rates of the hot and cold streams, $\dot{m}_{D,hs}$ & $\dot{m}_{D,cs}$ (kg/s) and the enthalpy values at the inlet and outlet of each component. While flue gas serves as the hot stream in the DHN economizer, the LP steam serves as the hot stream in the DHN heat exchanger. For the overall DHN system, the supply water acts as the hot stream. In all cases, the return water serves as the cold stream.

$$\dot{Q}_{DHN} = \dot{m}_{D,hs} \cdot (h_{fi} - h_{fo}) = \dot{m}_{D,cs} \cdot (h_{so} - h_{si}) \tag{3.29}$$

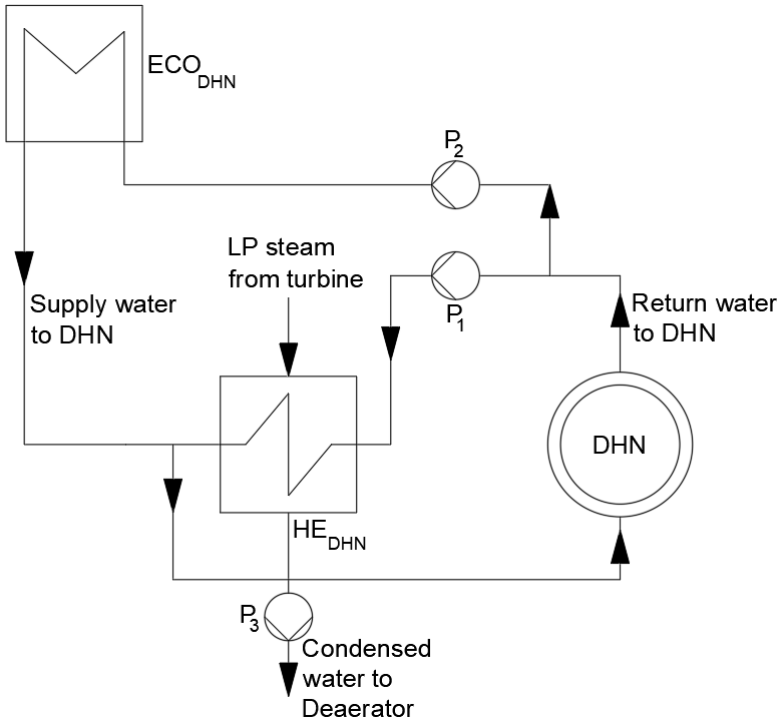

Figure 3.4: Arrangement of District Heating Network in the reference CCGT power plant.

3.6 Post-combustion Carbon Capture and Storage Technology using solvent method

Figure 3.5a presents the detailed arrangement and flow scheme of the PCCS absorber column referred to in [113]. Before passing the flue gas to the absorber, a blower is used to increase the flue gas pressure to match the operating pressure of 1 bar and a cooler is used to cool the flue gas temperature to the operating temperature of the absorber at 40℃. The absorber unit is designed with two inlets: one for the flue gas stream and the other for the aqueous amine solution. Similarly, there are two outlets for clean flue gas and the rich amine solution, which consists of a high CO_2 content after the absorption process. The absorber column is divided into two sections, the lower section, where the chemical absorption of CO_2 by amine occurs. This section is packed with structured packing materials to maximize the surface contact area between the flue gas and the solvent, enhancing mass transfer efficiency. As of [114], the packing materials such as ceramic, stainless steel structures, pall rings, and Mellapak are used based on their thermal stability, corrosion resistance, and surface area characteristics. Two different pumps are used to supply amine to absorber and water to the water wash section. Because of the volatile nature of amine, the upper section of the absorber is the water wash zone, which is used to minimize solvent degradation by capturing entrained amine vapours from the treated flue gas. Here, water is sprayed to cool the cleaned flue gas and prevent amine emissions. Given the exothermic nature of the CO_2 absorption reaction, the water wash section also helps to control the temperature of the outlet gas, reducing it to approximately 40.4℃. In addition, the clean flue gas is used to cool the flue gas stream to the absorber and is further mixed with the diverted stream. The rich amine from the bottom of the absorber is pumped to the top section

of the stripper column. As in Figure 3.5b referred from [115], the stripper with multiple trays facilitates contact between the rising CO_2 vapours and the rich amine flowing, gradually heating the amine to the operating temperature of 120℃. Further heating occurs in the reboiler using steam from the LP turbine, which breaks the bond between CO_2 and solvent. When the solvent flows back into the stripper, the regeneration of the solvent occurs by releasing the captured CO_2. The released CO_2 flows upwards to the CO_2 handling system, where it is cooled to <30℃ and compressed to storage of 110 bar. The CO_2 handling system accounts for approximately 30 - 40% of the total power consumption of the PCCS, mainly due to the three-stage compression of CO_2.

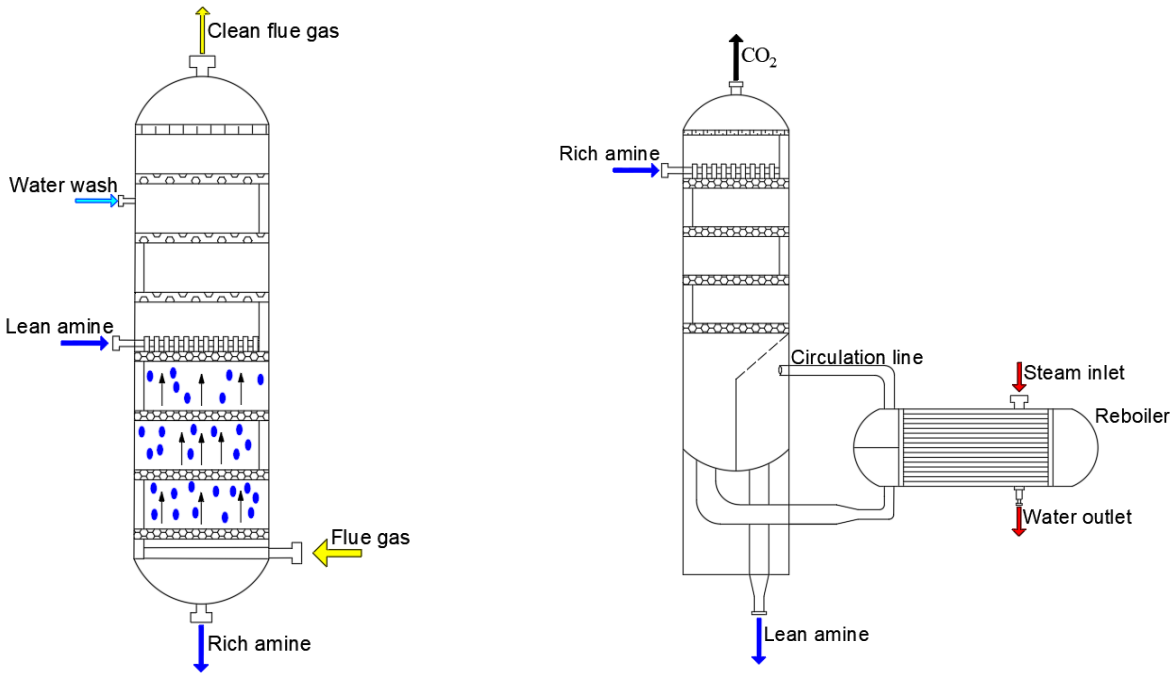

(a) Arrangement of PCCS absorber

(b) Arrangement of PCCS stripper

Figure 3.5: Construction of critical components of PCCS using solvent method.

Due to the high CO_2 capture efficiency, high potential to achieve negative emission when combined with bioenergy and the advantage of retrofitting with existing power plant without complications, the PCCS using solvent method is considered for this analysis. Solvents such as MEA and the AMP-PZ (Aminomethyl propanol-Piperazine) mixture are considered for the study of PCCS process. The following description of CO_2 capture using solvent shows the mass balance and energy calculations, which are used to perform thermodynamic analysis and better understanding for creating the model. The zwitterion mechanism introduced by M. Caplow in 1968 [116] and considered by P.V.Danckwerts in 1978 [117] states the absorption process between the primary and secondary amine (R-NH_2) with CO_2 is an exothermic reaction that forms stable carbamate (R-NHCOO-) as in Equation (3.30). The desorption process is the reversible reaction, in which the bond between amine and CO_2 breaks with the application of heat as in Equation (3.31) [95].

$$2\,\mathrm{R{-}NH_2} + \mathrm{CO_2} \longrightarrow \mathrm{R{-}NH_3^+} + \mathrm{NHCOO^-} + \mathrm{heat} \tag{3.30}$$

$$\mathrm{R{-}NH_3^+} + \mathrm{NHCOO^-} + \mathrm{heat} \longrightarrow 2\,\mathrm{R{-}NH_2} + \mathrm{CO_2} \tag{3.31}$$

The CO_2 absorbing capacity with amine is limited to 0.5 mol-CO_2/1 mol-amine in absorber due to the presence of other gas components and operating conditions such as temperature and pressure. Due to this limit, it requires 2 mol of amine to react with 1 mol of CO_2. For this study, an aqueous solution of 70 wt% of H_2O with 30 wt% MEA is chosen for the capture process, which achieves a capture efficiency of 90%. After the exothermic reaction with CO_2, the amine is referred to as rich amine. The regeneration process in stripper involves the separation of CO_2 from rich amine, which requires a reboiler duty of 3.8 MJ/kg-CO_2 for MEA. The lean amine after the regeneration process at the exit of stripper has a lean CO_2 loading of MEA is 0.17 mol-CO_2/mol-MEA, refers to the proportion of CO_2 in lean amine, which requires a lot of energy to remove. The mass conversion of the absorbing capacity of 0.5 mol-CO_2/mol-MEA is calculated to be 360 g-CO_2/kg-MEA. The blend AMP-PZ amine with similar properties of MEA is taken into consideration in this study for comparison purposes. The aqueous mixture of 16 wt% AMP, 14 wt% PZ and 70 wt% H_2O is used for the process, which achieves 90% CO_2 capture has a rich loading of 0.62 mol-CO_2/mol-AMP and 0.86 mol-CO_2/mol-PZ. In mass conversion, the rich loading is calculated to be 0.306 kg-CO_2/kg-AMP and 0.439 kg-CO_2/kg-PZ. The lean loadings are 0.37 mol-CO_2/mol-AMP and 0.20 mol-CO_2/mol-PZ. The regeneration process for the AMP-PZ solvent requires slightly less energy, with a reboiler duty of 3.7 MJ/ kg-CO_2 [95]. This makes the AMP-PZ mixture competitive for CO_2 capture, balancing effective absorption with lower energy demands during regeneration. To build the model of PCCS using solvent method and to determine the input parameters for the model, it is necessary to perform a theoretical and mass balance analysis of PCCS. This theoretical analysis followed by calculations provides data about the required mass flow of solvent and steam for the capture process. The following equations refer to the reference points provided in Figure 2.3 on each stream of the PCCS process diagram, which provides a better understanding of the working principle of PCCS. After the creation of the model using boundary conditions, it is necessary to give input of the mass flow of lean amine required for the CO_2 capture and mass flow of steam required for the regeneration process. Once the calculated mass flows are given to the model, the model adjusts the flow of amine & steam according to the CO_2 at the inlet of the absorber and stripper respectively. The total mass flow of amine, $\dot{m}_{14}$ (kg/s) required for capturing mass flow of CO_2 in flue gas, $\dot{m}_{fg.CO_2}$ (kg/s) is calculated using Equation (3.32) [95].

$$\dot{m}_{14} = \dot{m}_{fg.CO_2} \cdot \dot{mg}_{amine} \tag{3.32}$$

Where $\dot{mg}_{amine}$ is the rich amine loading in kg/kg. The amine used in the model has a capture rate of 90%, which indicates the PCCS capturing 90% of CO_2 in flue gas passing through it. The total mass flow of CO_2 captured by the amine, $\dot{m}_{cap.CO_2}$ (kg/s) at the absorber is calculated by Equation (3.33) [95].

$$\dot{m}_{cap.CO_2} = 0.9 \cdot \dot{mg}_{fg.CO_2} \tag{3.33}$$

After the CO_2 removal process in the PCCS absorber, the treated flue gas which consists of a small amount of CO_2 escapes through the top of the absorber after water wash. Using Equation (3.34), the mass flow of treated flue gas, $\dot{m}_4$ (kg/s) is calculated using the mass flow of flue gas, $\dot{m}_3$ (kg/s) at the inlet of the PCCS absorber [95].

$$\dot{m}_4 = \dot{m}_3 - \dot{m}_{cap.CO_2} \tag{3.34}$$

While the treated flue gas escapes through the top of the absorber, the rich amine with CO_2 content passes through the bottom of the absorber. The mass flow of rich amine, $\dot{m}_9$ (kg/s) at the bottom of the absorber is calculated using Equation (3.35).

$$\dot{m}_9 = \dot{m}_{14} + \dot{m}_{cap.CO_2} \tag{3.35}$$

The mass balance in the absorber inlet and outlet is given as in Equation (3.36).

$$\dot{m}_3 + \dot{m}_{14} = \dot{m}_4 + \dot{m}_9 \tag{3.36}$$

The rich amine at the outlet of the absorber is pressurized to 2.05 bar and the temperature is increased by passing through the amine heat exchanger and enters the stripper as mass flow of rich amine, $\dot{m}_{15}$ (kg/s). The steam used for amine regeneration in reboiler is the LP steam from CCGT, which is extracted from the same line of steam supplied for DHN. Hence, the LP steam used in PCCS has an operating condition of 135 ℃ and 3 bar. Inside reboiler, the steam has a pressure drop of 0.1 bar and condensed water at the outlet of the reboiler has 132.37 ℃ and 2.9 bar (as per the saturated steam properties). The enthalpy of steam and water at the inlet, h_{21} and outlet, h_{22} of reboiler are 2728.22 kJ/kg and 556.6 kJ/kg respectively. The reboiler duty, $\dot{Q}_{21}$ (kJ/kg-CO_2) required for the model is calculated using Equation (3.37) [95].

$$\dot{Q}_{21} = \dot{Q}_{amine} \cdot \dot{m}_{cap.CO_2} \tag{3.37}$$

Where, $\dot{Q}_{amine}$ (kJ/kg-CO_2) is the given reboiler duty of the amine used for the capture process. The rate of heat exchange in PCCS reboiler (MW) is calculated using Equation (3.38). To estimate the mass flow of steam, $\dot{m}_{lpsteam}$ (kg/s) required for the regeneration process, this Equation is written as Equation (3.39) [95].

$$\dot{Q}_{21} = \dot{m}_{lpsteam} \cdot (h_{21} - h_{22}) \tag{3.38}$$

$$\dot{m}_{lpsteam} = \frac{\dot{Q}_{21}}{(h_{21} - h_{22})} \tag{3.39}$$

After the regeneration process, the separated CO_2 from amine passes out at the top of the stripper and carries 10% of vapour from the amine. Throughout the various stages of CO_2 compression, the vapour is cooled and mixed back again to the amine at the exit of stripper. The mass flow of captured CO_2 stream with vapour content, $\dot{m}_{23}$ (kg/s) at the top of the stripper and the mass flow of the vapour, $\dot{m}_{vapour}$ (kg/s) escaped along with captured CO_2 is calculated by the equations Equation (3.40) & Equation (3.41) respectively [95].

$$\dot{m}_{23} = \dot{m}_{cap.CO_2} + \dot{m}_{vapour} \tag{3.40}$$

$$\dot{m}_{vapour} = 10\,\% \cdot \dot{m}_{15} \tag{3.41}$$

Using solvent technique in PCCS for CO_2 capture process, a purity of 99.8 (vol%) of CO_2 can be achieved [118]. Considering the CO_2 purity and 0.2% of vapour losses, the mass flow of lean amine at the outlet of the stripper, $\dot{m}_{17}$ (kg/s) is calculated using Equation (3.42) [95].

$$\dot{m}_{17} = \dot{m}_{15} - \dot{m}_{cap.CO_2} - 0.2\,\% \cdot \dot{m}_{vapuor} \tag{3.42}$$

The captured CO_2, $\dot{m}_{17}$ (kg/s) at the final stage of PCCS is compressed to 110 bar pressure through multi-stage compression and cooled the <30℃ and sent to storage. The captured CO_2 with high purity and less amount of vapour is calculated by Equation (3.43) [95].

$$\dot{m}_{31} = \dot{m}_{23} - 99.98\,\% \cdot \dot{m}_{vapuor} \tag{3.43}$$

At the initial stages of modelling, the mass flow of various streams in PCCS process and the heat requirement for reboiler are calculated using the above equation. The pressure and temperature at each reference point of various streams of the model are considered with reference to the works of literature [119], [120], [121], [122], [123] and [124].

3.7 Technology assessment factors

The technology assessment factors of the CCGT integrated with PCCS help to evaluate various factors including performance, efficiency, and cost analysis to achieve negative CO_2 emission. By integrating CCGT with the PCCS installation, the obtained results are used in the assessment indicators to analyse emissions at different levels for the considered model. Indicators such as energy, environmental and economic are used to analyse the technical feasibility, economic viability, policy assessment, and environmental impact of the considered case study.

3.7.1 Energy indicators

The following energy indicators are measured from the developed model used to assess the emission level:

- Gross/Netto efficiency, %
- Gross/Netto power, MW
- Steam cycle power generation, MW
- DHN heat consumption, MW
- Own power consumption, MW
- Power reduced due to steam extraction, MW
- Power load factor, -
- Efficiency output penalty (EOP), kWh/tCO_2

The energy indicators such as power load factor and EOP are calculated using Equation (3.44) and Equation (3.45) respectively.

$$\text{Power load factor} = \frac{N_{SE}}{Q_{RE}} \tag{3.44}$$

Where N_{SE} is the power reduced due to steam extraction (MW) and Q_{RE} is the reboiler heat consumption by PCCS (MW).

$$EOP = \frac{N_{PP.ref} - N_{PP.CCS}}{\dot{m}_{CO_2}} \tag{3.45}$$

Where $N_{PP.ref}$ & $N_{PP.CCS}$ are the Net power produced by power plant without and with CCS (kW) and $\dot{m}_{CO_2}$ is the mass flow of CO_2 captured (t/h).

3.7.2 Environmental indicators

The environmental analysis includes the assessment of the emission levels generated by CCGT with and without the performance of CO_2 capture. In this analysis, the utilization of syngas from sewage sludge is considered as bioenergy. Estimated CO_2 emission during syngas combustion is derived from fuel content (59. 31% CO_2 content). Based on the concept of BECCS, this value is treated as a 'negative emission' since it is produced from biomass fuel. When the proportion of syngas with fossil fuel varies in the mixture fuel, the share of CO_2 in the fuel and the CO_2 produced changes accordingly. According to this approach, negative emission is achieved by mixing syngas with fossil fuel or using only syngas from sewage sludge and performing CO_2 capture [95]. In the case of mixing syngas with fossil fuel before combustion, the mass flow of CO_2 emitted into the atmosphere, $\dot{m}_{CO_2}$ (kg/s) is calculated by Equation (3.46).

$$\dot{m}_{CO_2} = CO_2 \text{ generated} - CO_2 \text{ captured} - \text{share of } CO_2 \text{ in syngas} \tag{3.46}$$

The following formulas are used to calculate the environmental assessment of the designed reference case CCGT with PCCS [84].

The specific emission of carbon dioxide [84], eCO_2 ($kgCO_2$/kWh) is calculated using Equation (3.47) with the Net energy generated, N_{net} (kW).

$$eCO_2 = \frac{\dot{m}_{CO_2}}{N_{net}} \cdot 3600 \tag{3.47}$$

The relative emissivity of carbon dioxide [84], e_rCO_2 ($kgCO_2$/kWh) is calculated with Equation (3.48).

$$e_rCO_2 = \eta_{net} \cdot eCO_2 \tag{3.48}$$

Combining with the specific emission of CO_2 the above equation is written as Equation (3.49) [84].

$$e_rCO_2 = \frac{\dot{m}_{CO_2}}{\dot{Q}} \cdot 3600 \tag{3.49}$$

Where η_{net} is the net efficiency of the power produced in % and $\dot{Q}$ is the rate of chemical energy in kW. The CO_2 capture ratio (CCR) is calculated using Equation (3.50) using mass flow of captured CO_2, $\dot{m}_{CO_2,capt}$ (t/h) and mass flow of generated CO_2, $\dot{m}_{CO_2,gen}$ (t/h) [84].

$$CCR = \frac{\dot{m}_{CO_2,capt}}{\dot{m}_{CO_2,gen}} \tag{3.50}$$

The CO_2 emission index, χ (kg-CO_2/kJ) is calculated using Equation (3.51) with heat input by fuel, Q (kJ) [84].

$$\chi = \frac{\dot{m}_{CO_2,gen}}{Q} \tag{3.51}$$

The CO_2 capture in $kgCO_2/kWh$ is measured using Equation (3.52). Combining the Equation (3.51), the equation is written as Equation (3.53) [84].

$$\mathrm{CO_2\ captured} = \frac{\chi}{\eta_{p,ccs}} \cdot \eta_{cap} \tag{3.52}$$

$$\mathrm{CO_2\ captured} = \frac{\dot{m}_{CO_2,gen}}{\mathrm{Q}} \cdot \frac{\eta_{cap}}{\eta_{p,ccs}} \tag{3.53}$$

Where $\eta_{p,ccs}$ is the efficiency of the power plant with capture and η_{cap} is the CO_2 capture efficiency. The CO_2 emitted in $kgCO_2/kWh$ is calculated using Equation (3.54) [84].

$$\mathrm{CO_2\ emitted} = \frac{\chi}{\eta_{p,ccs}} \cdot (1 - \eta_{cap}) \tag{3.54}$$

The use of HRSG in this case can avoid CO_2 produced during the steam production. The CO_2 avoided ($kgCO_2/kWh$) is measured using Equation (3.55) with the specific emission from the reference plant, $eCO_{2,ref}$ and specific emission from the plant with CO_2 capture, $eCO_{2p,ccs}$ [84].

$$\mathrm{CO_2\ avoided} = \frac{eCO_{2,ref} - eCO_{2p,ccs}}{eCO_{2,ref}} \tag{3.55}$$

Since the term CO_2 avoided is characterized as a reduction in CO_2 emitted, the CO_2 avoided can also be characterized as Equation (3.56) [84].

$$\mathrm{CO_2\ avoided} = \frac{\chi}{\eta_{ref}} - \frac{\chi}{\eta_{p,css}} \cdot (1 - \eta_{cap}) \tag{3.56}$$

Where η_{ref} is the efficiency of the reference power plant. Using Equation (3.57), the specific primary energy consumption for CO_2 avoided, SPECCA ($kWh/kgCO_2$) is calculated [84].

$$\mathrm{SPECCA} = \frac{\mathrm{HR}_{p,CCS} - \mathrm{HR}_{ref}}{eCO_{2,ref} - eCO_{2p,ccs}} = \frac{\frac{1}{\eta_{p,css}} - \frac{1}{\eta_{ref}}}{eCO_{2,ref} - eCO_{2p,ccs}} \tag{3.57}$$

Where $\mathrm{HR}_{p,CCS}$ & HR_{ref} are the heat rate of power plant with and without PCCS unit in kJ/kWh.

3.7.3 Economic indicators

The following equations are used for the economic analysis of the CCGT with and without PCCS. The SPECCA cost is calculated using Equation (3.58) with the primary energy cost, EC (€/t-CO_2) [84].

$$\mathrm{SPECCA}_{cost} = \frac{\mathrm{HR}_{p,CCS} - \mathrm{HR}_{ref}}{eCO_{2,ref} - eCO_{2p,ccs}} \cdot \mathrm{EC} = \frac{\frac{1}{\eta_{p,css}} - \frac{1}{\eta_{ref}}}{eCO_{2,ref} - eCO_{2p,ccs}} \cdot \mathrm{EC} \tag{3.58}$$

The levelized cost of electricity in €/MWh is calculated using Equation (3.59) [84].

$$\mathrm{LCOE} = \frac{\sum (\mathrm{Capital_t} + \mathrm{O\&M_t}) \cdot (1 + \mathrm{r})^{-\mathrm{t}}}{\sum \mathrm{MWh} \cdot (1 + \mathrm{r})^{-\mathrm{t}}} \tag{3.59}$$

Where $\mathrm{Capital}_t$ is the capital construction costs in year t, $\mathrm{O\&M}_t$ is the operation and maintenance cost including the fuel price in year t, MWh is electricity produced annually, r is the real discount rate corresponding to capital cost and t is the year.

The CO_2 emission cost of the power plant, e_{cost} (€/MWh) is calculated using Equation (3.60) with the CO_2 cost, EC_{CO_2}, €/t.

$$e_{\text{cost}} = \frac{\dot{m}_{CO_2}}{3.6} \cdot \text{EC}_{\text{CO}_2} \tag{3.60}$$

The income from the electricity sale of the power plant is calculated using Equation (3.61) with reference to the grid electricity price, GP (PLN/MWh).

$$\text{E}_{\text{S}} = \text{N}_{\text{net}} \cdot \text{GP} \tag{3.61}$$

The income from the DHN heat sale of the power plant, DHN_h (PLN/h) is calculated using Equation (3.62) with reference to the DHN heat supply, DHN_{supply} (MW) and heat supply price, DHN_{cost}, (PLN/GJ).

$$\text{DHN}_h = \frac{\text{DHN}_{supply}}{3.6} \cdot \text{DHN}_{cost} \tag{3.62}$$

The price of fuel consumed by the power plant, $PP_{f,cost}$ (PLN/h) is calculated using Equation (3.63) with the heat input of the fuel, Q (MW) and gas fuel price, f_{cost}, (PLN/MWh).

$$\text{PP}_{f,cost} = \frac{\text{Q}}{1000} \cdot \text{f}_{cost} \tag{3.63}$$

The total income of the power plant after expenses, PP_{income} (PLN/h) is calculated using Equation (3.64), with CO_2 emission cost calculated in (PLN/t).

$$\text{PP}_{income} = \text{E}_S + \text{DHN}_h - e_{cost} \tag{3.64}$$

Chapter 4

Research Methodology & Thermodynamic modelling

4.1 Main assumptions of parameters for thermodynamic analysis of reference case CCGT

With the specifications of the critical components of the reference case CCGT power plant referred to by the Gorzów power plant, the input and boundary conditions are derived from an extensive review of the literature. These operating conditions are used to build the simulation model that is accurately aligned with the existing operational scenario. To improve the accuracy of the model, assumptions are used in the theoretical calculations and the obtained results are analysed. Based on the literature works [94], [110], [125], [126], [127], [128], [129] and the library of Ebsilon Professional®, the main assumption of the basic parameters for the reference case of thermodynamic analysis of the gas cycle is described in Table 4.1. Similarly, the main assumptions of the basic parameters for the thermodynamic analysis reference case for steam cycle are considered with reference to literature [94], [111] and [125], and Ebsilon library as in Table 4.2.

The Ebsilon Professional® performs calculations using the Gauss-Seidel method and performs mass and energy balance to analyse the created thermodynamic model. The software has a large gas turbine library, which allows one to choose the specific gas turbine required for the modelling [130]. In this case, Siemens SGT-800 is chosen as the gas turbine for the reference CCGT model as in Figure 4.1. The input process parameters such as temperature, pressure and compressor & turbine efficiency as in Table 4.1 are given as input to the SGT-800 model. According to the LHV of the fuel given as input to the gas turbines, the model calculates the mass flow of fuel & air required for producing 50.5 MW of power generation.

Assigning reference points to HRSG streams, such as flue gas, water, and steam, as shown in Figure 4.2 enables the distinction of the streams and the thermodynamic analysis based on mass balance calculations for each component in the HRSG. These reference points are critical for theoretical calculations to determine the mean temperature difference and rate of heat exchange of HRSG components. The results obtained from heat and energy distribution data improve the accuracy of the HRSG model. The main assumptions of input data for HRSG & DHN operation are derived from the thermodynamic analyses and

Table 4.1: Main assumption of basic parameters for thermodynamic analysis reference case of gas cycle

Parameter	Unit	Value
Ambient air temperature (ISO)	℃	15
Ambient air pressure (ISO)	bar	1.013
Relative humidity (ISO)	%	60
Air inlet mass flow	kg/s	130
Compressor pressure ratio	-	21.1:1
Compressor isentropic efficiency	%	89.5
Compressor mechanical efficiency	%	99
Compressor discharge temperature	℃	431
Fuel temperature	℃	25
Fuel Pressure (ISO)	bar	30
Combustor inlet water temperature	℃	25
Combustor outlet temperature	℃	1250
GT inlet temperature	℃	1230
GT exhaust temperature	℃	552.9
Generator efficiency	%	98.5
Generator frequency	Hz	50

Table 4.2: Main assumption of basic parameters for thermodynamic analysis reference case of steam cycle

Parameter	Unit	Value
HP/LP steam pressure	bar	80/8
HP/LP steam temperature	℃	510/227
Mass flow of steam to HP steam turbine	t/h	62.4
Mass flow of steam to LP steam turbine	t/h	15
Condenser inlet pressure	bar	0.042
Condenser cooling water inlet temperature	℃	15
Condenser cooling water pressure	bar	5
Condenser cooling water pressure drop	bar	0.5
Make up water temperature	℃	15
Steam turbine isentropic efficiency	%	88
Steam turbine mechanical efficiency	%	99.8
Generator efficiency	%	98.5
Generator frequency	1/min	3000

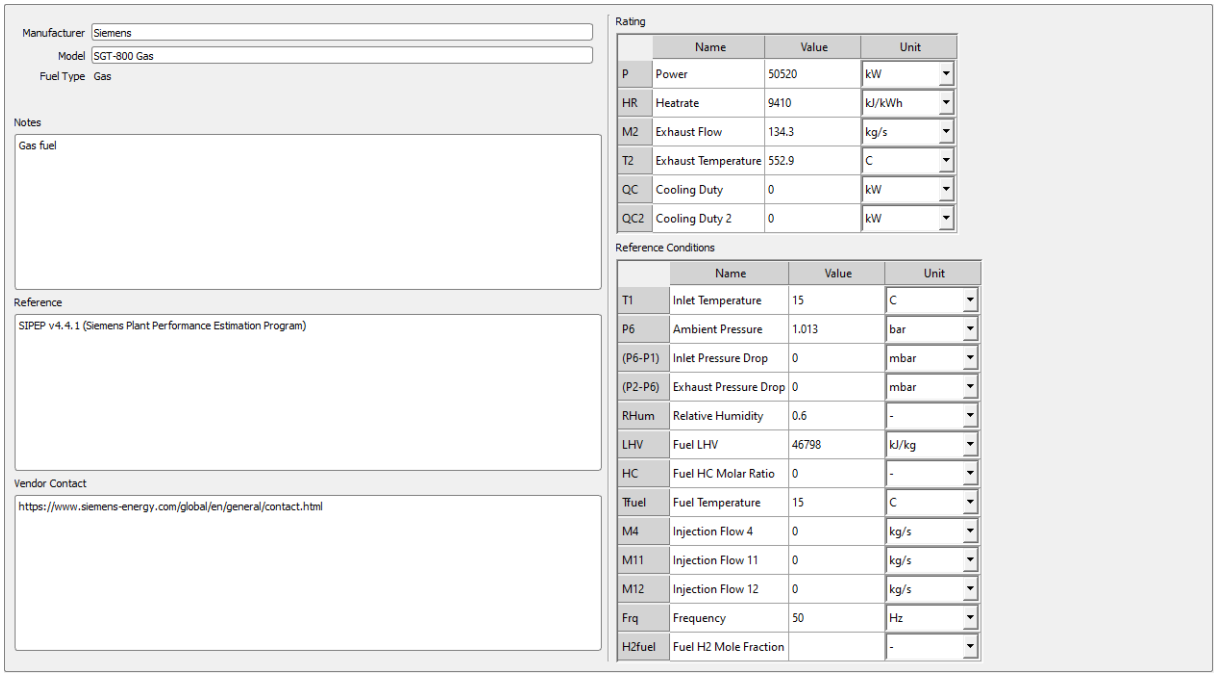

Figure 4.1: Description of SGT-800 gas turbine in Ebsilon Professional®.

operating parameters of both the gas and steam turbines, as summarized in Table 4.3. This table also includes process parameters for auxiliary components, such as the pump and deaerator, which are critical to optimizing the operations of the HRSG and DHN systems and improving efficiency. By analysing the heat distribution and properties of flue gas, water, and steam at various stages, the study aims to optimize HRSG performance, enhancing heat recovery efficiency and overall power plant output.

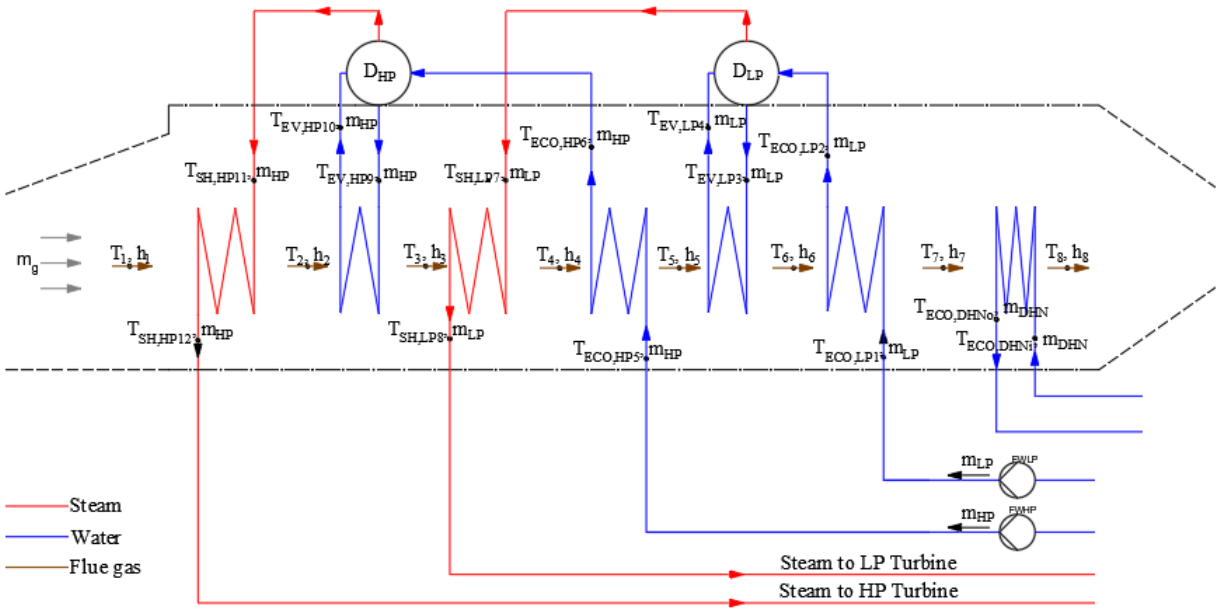

T - Temperature, m - mass flow rate, h - enthalpy, g - flue gas, FW - Feedwater pump, D - steam drum, HP - High Pressure, LP - Low Pressure, SH - Superheater, EV - Evaporator, ECO - Economizer, DHN - District Heating Network

Figure 4.2: Flue gas path and water/steam line of HRSG components with reference points [95].

Table 4.3: Input data and specifications of components of one HRSG & DHN used in the CCGT [95]

Parameter	Unit	Value
Thermal capacity in steam (thermal output)	MW_t	67
Thermal capacity in DHN water heater (thermal output of hot water)	MW_t	10
HRSG components hot and cold liquid streams pressure drop	MPa	0.4
HRSG components hot and cold gas streams pressure drop	%	2
HRSG HP & LP components cold side heat transfer coefficient	W/m^2K	500
HRSG HP & LP components hot side heat transfer coefficient	W/m^2K	50
DHN supply temperature	℃	110
DHN return temperature	℃	70
DHN heat exchanger supply water pressure drop	bar	0.05
Operating pressure of deaerator	bar	7
Boiler feedwater pump isentropic efficiency	%	80
Boiler feedwater pump mechanical efficiency	%	99.8
Boiler feedwater pump speed	rpm	3000

4.2 Model validation of CCGT

Based on the input data given in Section 4.1, a detailed model of CCGT was developed using Ebsilon Professional. As displayed in Figure 4.3, the GT & ST indicate the gas turbines and steam turbine, respectively. The HP & LP steam generated in two HRSGs is mixed at a point and passed to the respective steam turbines. LP steam extracted from the LP turbine is used for water heating in DHN heat exchanger and for the amine regeneration process in PCCS. The CCGT system also includes auxiliary components that consume power from CCGT itself, which include boiler feedwater pumps, one condensate extraction pump, and three DHN water pumps. The results of the CCGT thermodynamic calculations performed using the input data are used to optimize the system and improve overall efficiency. When low LHV fuels and blended fuels are used in the gas turbine, the gas turbine increases the fuel mass flow to achieve its maximum power generation of 50.5 MW. Hence, despite the use of different fuels, the performance of gas turbines remains the same, producing 100.72 MW. The performance of CCGT is measured in different specifications as in Table 4.4. The performance of the CCGT is assessed under three operational conditions: without DHN, with 54 MW of heat supplied to the DHN and with 35 MW of heat supplied to the DHN. The output of the gas turbine remains constant for all fuel types used, indicating that the blend of syngas with other fuels does not affect the overall efficiency of CCGT in the generation of electricity and heat delivery to the DHN. The net power output and net efficiency of the CCGT without DHN process conditions align with the operational ranges of the Gorzów power plant and the SCC-800 2x1 CCGT as shown in Table 3.3. When operating CCGT with a 35 MW heat supply to DHN, the process conditions align closely with the cogeneration mode of SCC-800 2x1 CCGT. This alignment of the results shows that the performance of

model reflects real-world conditions, validating accuracy of the model, and confirming its potential for performance evaluation under various operational scenarios [131].

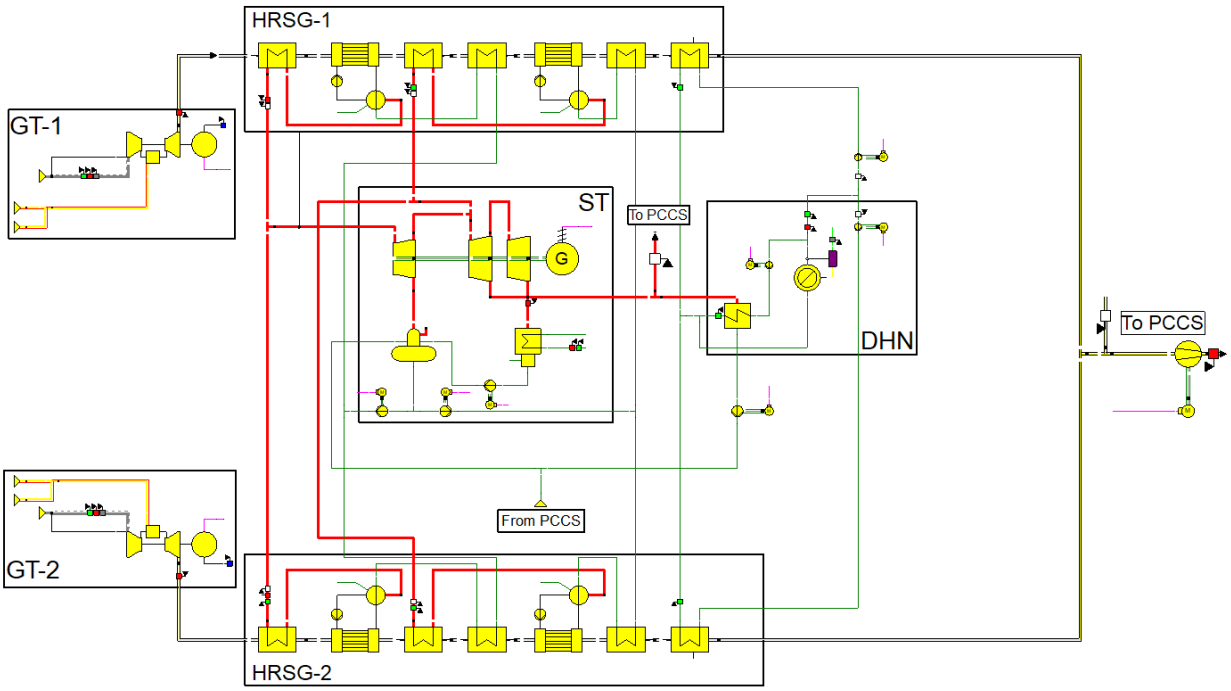

Figure 4.3: Model of CCGT created using Ebsilon Professional with reference input data [131].

Table 4.4: Results of the performance of CCGT obtained from the model

Parameter	Unit	No DHN	DHN - 54 MW	DHN - 35MW
Gross energy output	MW	143.8	138.3	142.3
Net power output	MW	143.4	137.9	141.7
Gross energy efficiency	%	54.5	52.3	53.8
Net power efficiency	%	54.3	52.1	53.6
Plant own consumption	MW	0.46	0.53	0.53

4.3 Main assumptions of PCCS

As mentioned in Section 3.6, the solvents MEA and the AMP-PZ mixture are used in this study for PCCS using the solvent method analysis. From the CO_2 rich loading capacity of MEA, it is calculated that 1 kg of MEA is required to absorb 0.36 kg of CO_2. Using Equation (3.32), the mass flow rate required of aqueous lean MEA to capture 14.73 kg/s of CO_2 in flue gas produced from methane combustion is calculated to be 136.27 kg/s. For the lean loading of MEA after amine regeneration, it is calculated that 5.01 kg/s of CO_2 content will be in the lean solvent flow at the exit of the stripper. The lean aqueous MEA solution recirculated in the PCCS has a composition of 28.4% MEA + 3.68% CO_2 + 67.92% H_2O. A similar

calculation performed for the solvent of the AMP-PZ mixture shows that, from the rich CO_2 loading, a lean AMP of 48.11 kg/s and lean PZ of 33.52 kg/s is required for the treatment of the flue gas. Taking into consideration the aqueous solution with a proportion of AMP-PZ as 16 wt% & 14 wt%, the required lean AMP-PZ for treating the same amount of CO_2 in flue gas is calculated to be 137.68 kg/s, which is slightly higher than MEA. Taking into account the lean CO_2 loading, the composition of the aqueous solution of lean AMP-PZ is calculated to be 14.88% AMP + 12.88% PZ + 4.5% CO_2 + 67.74% H_2O. From the reboiler duty of MEA and AMP-PZ 3.8 MJ/kg-CO_2 and 3.7 MJ/kg-CO_2 respectively, the required mass flow of steam for the reboiler is calculated using Equation (3.39). For the calculated conditions of CO_2 in rich amine and to treat the methane fuel combustion flue gas, the mass flow rate of steam required when regenerating MEA is 23.19 kg/s and for AMP-PZ is 22.58 kg/s. The exhaust gases from gas turbines pass through various stages of HRSGs, transferring heat to produce steam and reaching the exhaust of HRSGs at a temperature and pressure of 104.6℃ & 0.885 bar respectively and mass flow rate of 268.6 kg/s. At this condition, the flue gas is directed into the PCCS. The literature on PCCS [119; 120; 121; 122; 123; 124] are used to provide boundary conditions as in Table 4.5 [95].

Table 4.5: Boundary conditions for modelling PCCS [95]

Parameter	Unit	Value
Absorber operating temperature	℃	40
Absorber operating pressure	bar	1
Absorber pressure drop	bar	0.1
Stripper operating temperature	℃	120
Stripper operating pressure	bar	2
Stripper pressure drop	bar	0.5
Steam temperature to reboiler	℃	135
Steam pressure to reboiler	bar	3
Coolers pressure drop	bar	0.05
Cooling water temperature	℃	15
CO_2 capture efficiency	%	90
CO_2 to storage temperature	℃	<30
CO_2 to storage pressure	bar	110

Apart from the boundary conditions, the temperature and pressure at each point necessary to model the PCCS process were also determined from the literature. Various reference points are provided to the streams of PCCS process using solvent as in Figure 4.4. Reference points help to perform the mass balance of the streams in the PCCS process and estimate the initial input required for the model, such as the mass flow of lean amine and the required amount of steam in the PCCS, which are crucial in building the model and optimizing the operational parameters. The results of the CCGT flue gas and the main assumptions of PCCS are used in Equation (3.32) - Equation (3.43) to calculate the required inputs and theoretically analyse the PCCS process [95].

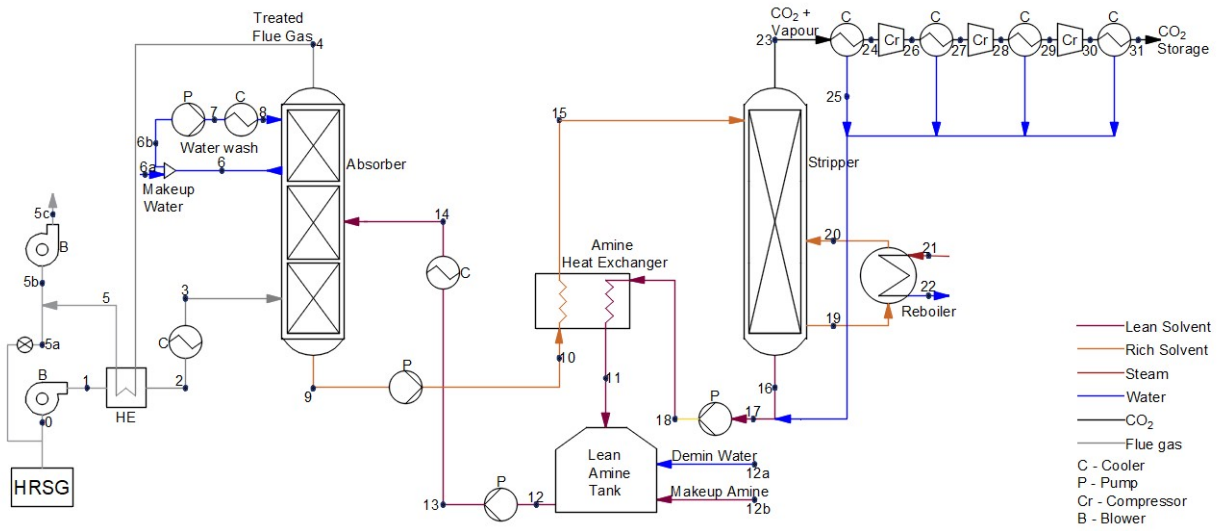

Figure 4.4: Layout of PCCS using solvent method with reference points on each stream [95].

4.4 Model validation of PCCS

Theoretical analysis and mass balance were performed using PCCS input data, and the calculated results were used to build the PCCS model, as shown in Figure 4.5. The estimated two crucial parameters, such as the required mass flow of solvent and steam, are given as initial input to the model depending upon the type of solvent used. The model regulates these parameters according to the CO_2 content in the flue gases produced by different fuels and the CO_2 in the rich amine. These adjustments are necessary because CO_2 loadings and reboiler duties can vary depending on the fuel used in the gas turbine [131].

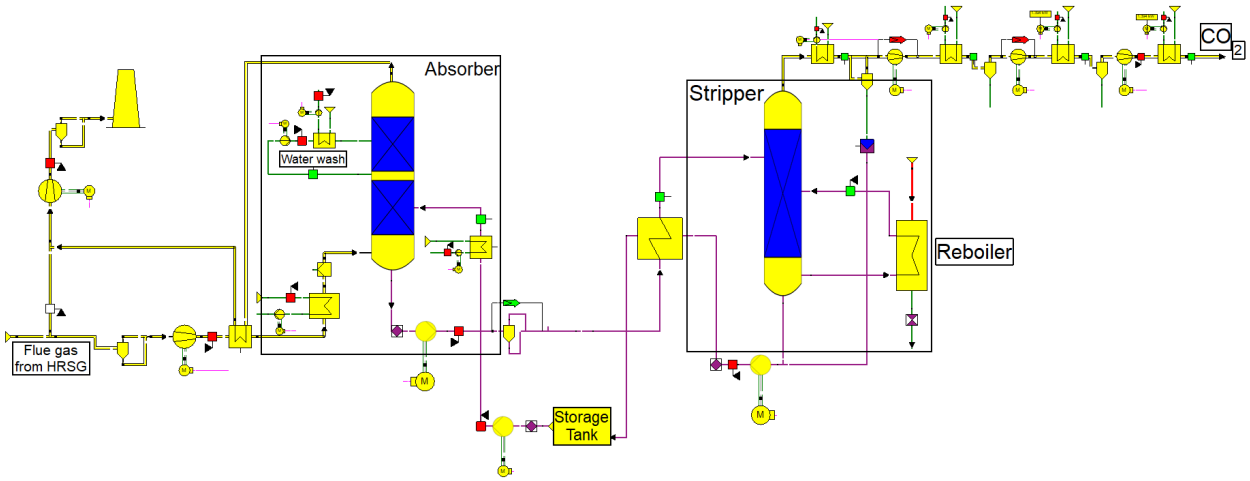

Figure 4.5: Model of PCCS using solvent method created using Ebsilon Professional [131].

The model is created with a focus on performing thermodynamic analysis and integrating the PCCS model with the CCGT model. Due to this, significant attention is given to improving the accuracy of the overall performance of the system in comparison to the chemical interactions within the model. Due to the absence of mass transfer between phases and chemical interactions except combustion, emissions, and

fuel processing in Ebsilon, the reaction mechanism between gaseous CO_2 and liquid amine is manually described in the model. Despite this, the behaviour of the stream completely depends on the composition of the fluid. The aqueous solvent in the model is described as a universal fluid in which the composition of the solvent can be described manually. In absorber, 90% of CO_2 from flue gas is separated and mixed with the solvent, which is reversed in stripper depending upon the lean loading of amine used. To improve the accuracy of the simulation, the model includes a detailed mass balance from the theoretical analysis. For better mass balance within the process and to get a simple approach, the PCCS acts as a closed system, where the amine emission and vapour losses are eliminated. However, a water wash system is included at the top of the absorber to cool the treated flue gas. As shown in the created model of PCCS, the PCCS process consists of an absorber, a stripper with a reboiler, an amine heat exchanger, a CO_2 handling system and cooling systems. To improve the efficiency of the process, the flue gas exiting the HRSG is pressurized and then cooled with treated flue gas from the absorber using a flue gas heat exchanger. The steam required for the reboiler in the stripper is extracted from the LP steam turbine of CCGT. After the steam has been used in the reboiler, it condenses and is returned to the water line of the CCGT. The vapour carried out by the captured CO_2 is condensed and added back to the lean aqueous solvent. Theoretical analysis of PCCS is used to optimize overall efficiency of the system while maintaining effective CO_2 capture [131]. To verify the accuracy of the developed model, a model of PCCS developed in Aspen Plus and results are compared. For the validation of the developed model, the results of the PCCS model are compared with the experimental results of PCCS used at the Łaziska Power Plant in Łaziska Górne, Poland.

4.4.1 Experimental validation

A. Tatarczuk et al. (2023) published the results of the analysis of PCCS pilot-scale plant at Łaziska Power Plant in Poland as 'Thermodynamic analysis of a post-combustion carbon dioxide capture process in a pilot plant equipped with a heat integrated stripper', which is crucial for validating the developed model of PCCS in Ebsilon. The Łaziska Power Plant is a 225 MW hard coal power plant, in which an advanced PCCS pilot facility with a Heat Integrated Stripper (HIS) is integrated. The pilot plant uses an aqueous solution of 30% MEA with CO_2 capture efficiency of 85% to 95%. The HIS system uses an electrical heater to supply the necessary heat to the reboiler. In this pilot experiment, flue gas with a mass flow rate of 200 m^3/h at 33.5 kPa and 35℃ passes through the absorber and reacts with amine. The lean solvent is supplied to absorber in two different streams and rich solvent in three different streams to stripper. The stripper consists of two internal recuperators that utilize the heat of lean amine at the exit of the stripper by recirculating, minimizing the requirement for heat for the process. The experimental setup uses three amine heat exchangers (E-210, E-213, and E-214) to preheat the streams of rich amine from absorber using lean amine streams from stripper. Of the three rich solvent streams, one is directly passed, second through the E-210 heat exchanger and the final stream through E-213 & E-214 heat exchangers to the stripper. A water wash section is integrated at the top of the absorber to minimize amine losses. The energy required for the reboiler in the standard process is 3.21 MJ/kgCO_2, which is reduced to 3 MJ/kgCO_2 when using the HIS system. This setup increases CO_2 capture efficiency to 91% [132]. For a more accurate comparison with experimental data and validation of the PCCS model, the model is adjusted to a smaller setup similar

to that used at the Łaziska Power Plant. Two amine heat exchangers are added to the PCCS model as in Figure 4.6. To keep a simple approach, no modifications are made in the stripper. The outlet streams to absorber and stripper from heat exchangers are combined. The model uses MEA 30 wt% solvent with reboiler duty of 3 MJ/kgCO_2 and the CO_2 loading of 0.4764 mol-CO_2/mol-MEA. The capture efficiency is 90%, the mass flow of treated flue gas is 20.97 kg/s and the CO_2 content in treated flue gas is 0.011 mol in both model and experiment. The required lean MEA is calculated to be 0.131 kg/s and the required steam flow to reboiler is calculated to be 0.017 kg/s, which are given as input to the model. The model is designed in a way that with reference to the input calculated value, the model will increase or decrease the solvent flow and steam flow according to the CO_2 content in flue gas and rich solvent. The captured CO_2 is compressed and cooled to pressure and temperature of 41.8℃ and 98 bar. Comparing the simulation and the pilot plant the parameters in absorber and stripper remains same. In the built model, the chemical reaction between the amine and CO_2 is manually described, due to the absence of chemical interaction and gas phase to liquid phase mass transfer. Due to the same reason the amine emission in treated flue gas is neglected.

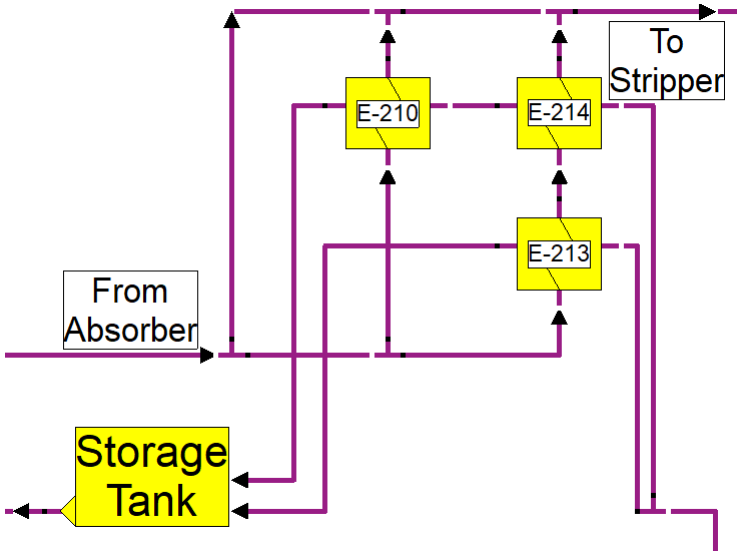

Figure 4.6: Modified model of PCCS amine heat exchangers in Ebsilon similar to PCCS in Łaziska power plant.

Table 4.6 shows the detailed comparison of the PCCS modelling results with experimental data. The model output showed a strong correlation with experimental data in case of process parameters such as pressure, temperature, mass flow, and molar composition in various streams. Differences in temperature can be observed at some points of the model compared to pilot plant such as rich solvent outlet temperature of heat exchangers E-213 & E-214 and lean solvent flow outlet temperature at E-213 & E-214 heat exchangers. This is due to the difference in the density of the solvent used in the model and the density of the solvent used in the experiment is unknown. According to the model, the density of the MEA solvent is noted to be 0.461 g/cm^3 at temperature 35℃ and 1.325 bar pressure. The change in density impacts the flow rate of the solvent in the heat exchangers, which will align with the temperature of solvent at the outlet of the heat exchangers. The variations are due to differences in the stripper configurations, in

which the experiment used HIS stripper. However, the relative error calculated with the experimental data and simulation results shows a range of 0 - <5%, which indicates acceptable values. Despite these minor differences, the operational values of the absorber flue gas treated, captured CO_2 and vapour at the outlet of stripper show similar results, indicating that the overall modelling results align with the experimental data. This supports the validation of integrating the model with other types of energy units and scaling up the model to higher capacities.

Table 4.6: Comparison of experimental data with simulation results

Parameter	Unit	Experiment [132]	Simulation	Error (%)
Treated flue gas				
Mass flow	kg/h	239.58	239.58	0
Pressure (ΔP)	kPa	129	129	0
Temperature	℃	48.7	48.7	0
CO_2 in treated flue gas	mol	0.0115	0.0111	3.48
O_2 in treated flue gas	mol	0.09	0.09	0
Captured CO_2				
Mass flow	kg/h	41.8	41.8	0
Pressure	kPa	98	98	0
Temperature	℃	21	21	0
Rich solvent E-210				
Inlet temperature	℃	49.9	49.9	0
Outlet temperature	℃	83.6	83.6	0
Rich solvent stripper i/l				
Temperature	℃	91	90.7	0.33
Lean solvent at stripper o/l				
Temperature	℃	107	107	0
Lean solvent E-213				
Inlet temperature	℃	94	94	0
Lean solvent E-214				
Inlet temperature	℃	94.9	94.9	0
Gas at stripper outlet				
Mass flow	kg/h	47.3	47.16	0.3
Pressure	kPa	128.8	128.8	0
Temperature	℃	71.2	71.5	0.42
Ambient air pressure	kPa	99	99	0

4.4.2 Model-to-Model Benchmarking: Ebsilon Professional® vs. Aspen Plus

Aspen Plus V12 was selected for benchmarking model results due to its ability to perform complex chemical reactions and mass transfer processes across different phases. The software accurately analyzes CO_2 capture using amine by adjusting to changes in operating conditions and monitoring reactions between CO_2 and amine to measure the impact on PCCS performance [133], [134].

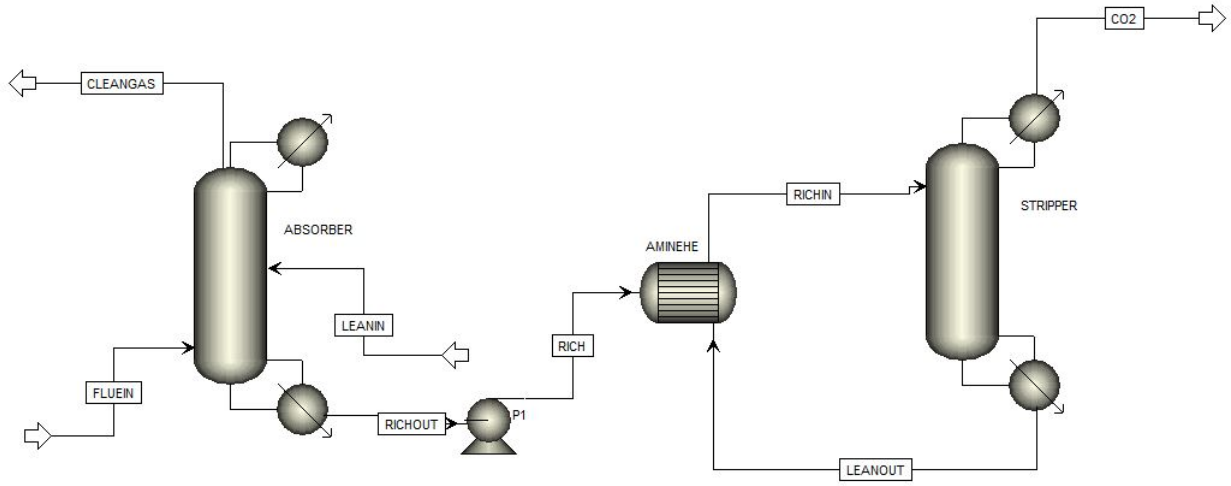

Figure 4.7: Developed model of PCCS using solvent method in Aspen Plus.

This model uses a rate-based simulation framework that includes both equilibrium and kinetic reaction mechanisms to accurately describe the multicomponent mass and energy transfer between the gas and liquid phases in the PCCS system. The use of MEA solvent with a CO_2 capture efficiency of 90% needs the detailed thermodynamic models to simulate the absorption and regeneration processes. The model includes specific mass transfer coefficients, interfacial area calculations and reaction kinetics for the carbamate formation. Parameters are optimized within Aspen Plus (Figure 4.7) to reflect process behavior and to benchmark the model against Ebsilon results under identical flue gas boundary conditions from methane combustion. The absorber column is configured with 30 stages to enhance gas–liquid contact and promote CO_2 absorption, while the stripper column includes 20 stages to ensure effective thermal regeneration of the solvent. These configurations reflect those used in the Ebsilon PCCS. The absorber and stripper use the following specific equilibrium and kinetic reactions (Equation (4.1) - Equation (4.9)) [134], primarily involving MEA and CO_2, including the formation of MEA–carbamate and the bicarbonate buffer system. This detailed representation enables accurate prediction of solvent loading, energy consumption, and overall capture efficiency.

$$\mathrm{MEAH^+ + H_2O \leftrightarrow MEA + H_3O^+ + heat} \tag{4.1}$$

$$\mathrm{2\,H_2O \leftrightarrow H_3O^+ + OH^-} \tag{4.2}$$

$$\mathrm{HCO_3^- + H_2O \leftrightarrow CO_3^{-2} + H_3O^+} \tag{4.3}$$

$$\mathrm{H_2O + H_2S \leftrightarrow HS^- + H_3O^+} \tag{4.4}$$

$$H_2O + H_2S \leftrightarrow S^{2-} + H_3O^+ \tag{4.5}$$

$$CO_2 + OH^- \leftrightarrow HCO_3^- \tag{4.6}$$

$$HCO_3^- \leftrightarrow CO_2 + OH^- \tag{4.7}$$

$$MEA + CO_2 + H_2O \leftrightarrow MEACOO^- + H_3O^+ \tag{4.8}$$

$$MEACOO^- + H_3O^+ \leftrightarrow MEA + CO_2 + H_2O \tag{4.9}$$

During simulation in Aspen Plus, the resulting compositions are delivered with accurate chemical details due to the ability of the model and reaction kinetics associated with CO_2 absorption by MEA. This includes the formation of ion such as protonated MEA ($MEAH^+$), bicarbonate (HCO_3^-), and carbamate ($MEACOO^-$), as well as water and dissolved CO_2. The progression of these reactions across different column stages provides a stage-wise insight into mass and energy transfer behaviour. Operating conditions such as temperature and pressure were found to be in close alignment with those calculated in Ebsilon, validating the boundary conditions used for benchmarking. However, differences are observed in the mass flow rates of key streams due to the difference in modelling approaches. Aspen Plus includes detailed chemical equilibrium and kinetic models, while Ebsilon relies on thermodynamic balance and heat integration assumptions. Mass flow rate directly influences solvent circulation rate, reboiler duty, lean amine makeup, and steam extraction for DHN. The comparative analysis presented in Table 4.7 shows that the relative differences in stream flow rates between Aspen Plus and Ebsilon in an acceptable range of 0.27% to 3.61%. The differences in mass flow rates indicate that the reaction kinetics and two-phase mass transfer slightly affect flow rate. Despite this, the strong correlation in flow data confirms the accuracy of Ebsilon PCCS model results and its suitability. The alignment confirms that the thermodynamic modelling approach used in Ebsilon is sufficient for simulating CO_2 capture and the overall process behaviour of PCCS, especially when supported by calibrated data from a rate-based model like Aspen Plus.

Table 4.7: Comparision of mass flow rate (kg/s) of crucial streams of PCCS obtained from Ebsilon Professional and Aspen Plus model

Stream No.	Ebsilon Professional	Aspen Plus	Relative Difference (%)
Flue gas at absorber i/l	266.9	267.67	0.27
Treated flue gas	253.8	262.96	3.61
Rich amine at absorber o/l	149.8	145.28	3.02
Lean amine to storage tank	136.57	134.63	1.42
Lean amine at absorber i/l	136.68	134.63	1.5
Rich amine at stripper i/l	149.85	145.28	3.05
Lean amine at stripper o/l	127.16	126.88	0.22
CO_2 vapour at stripper o/l	22.68	23.34	2.91

4.5 Modelling of CCGT integrated with PCCS

The validation and benchmarking of CCGT and PCCS models makes the model more reliable for the continued use of the developed model for further analysis. The model outputs are closely aligned with real-world data, making it possible to modify the developed model. The developed PCCS model has the advantage of possible integration with various types of power plants to analyse the behaviour with different setups. The developed CCGT and PCCS models in Figure 4.3 and Figure 4.5 are connected by directing flue gases from the CCGT outlet to the PCCS inlet as shown in Figure 4.8.

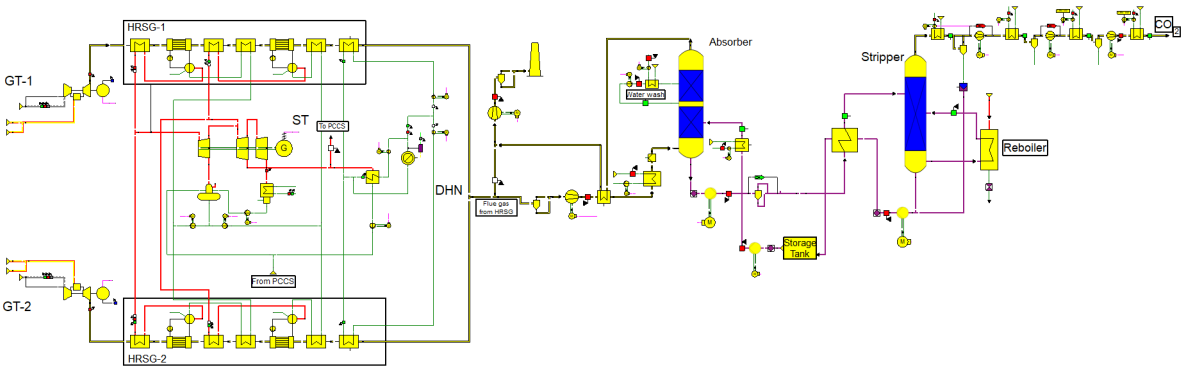

Figure 4.8: Integrated model of CCGT and PCCS in Ebsilon [131].

To assess the potential for achieving negative emissions, the PCCS is operated under varying load conditions by diverting a portion of flue gas flow directly to the atmosphere. This approach enables the CCGT to maintain full operation while adjusting the PCCS load as needed. To evaluate the performance of CCGT integrated with PCCS, N_2-rich fuel is used in the CCGT model. Flue gas at full load condition is passed to the PCCS to perform CO_2 capture. The performance results of PCCS with MEA are compared with AMP-PZ solvent as shown in Table 4.8.

Table 4.8: Performance results of CCGT using N_2-rich fuel integrated with PCCS using MEA and AMP-PZ solvents at full load condition

Parameter	Unit	CCGT with PCCS	
		using MEA	using AMP-PZ
Gross energy output	%	62.5	62.61
Net energy output	%	43.62	43.75
Net electricity generation	MW	115.21	115.5
Heat supplied to DHN	MW	34	34
CO_2 captured	kg/s	13.68	13.68
Lean amine flow	kg/s	142.12	142.17
Rich amine flow	kg/s	155.8	155.86
Steam flow o reboiler	kg/s	24.8	24.1
Own power consumption	MW	24.77	24.77

As previously mentioned, AMP-PZ requires less steam for regeneration than MEA, which impacts the overall operation of CCGT. Even while maintaining a 34 MW heat supply to the DHN in both scenarios, the performance of CCGT has slightly declined when operating with PCCS using MEA. The slightly higher steam demand for MEA regeneration reduces both the overall power output and efficiency of the CCGT compared to AMP-PZ. In addition to this, the CO_2 capture flow rate and internal power consumption remain the same in both cases. Similar to the assessed case of using N_2-rich fuel in CCGT, the operational assessment of CCGT using different fuels and mixture of fuels, and PCCS using MEA and AMP-PZ are performed in this study.

Chapter 5

Results & discussions of the thermodynamic analysis

5.1 Evaluation of different gas fuel properties, its mixtures, and impact on combustion in industrial gas turbines and HRSG

To achieve negative CO_2 emission from the selected reference case power plant using syngas obtained from sewage sludge, the syngas is mixed with methane and N_2 rich fuel, as the composition provided in Table 2.1. Upon analysing overall fuel consumption of gas turbine model, the proportion of syngas in the mixture is regulated by mixing syngas with the other gas fuels in different proportions such as 25%, 50% and 75%. As fuel mixture ratios vary as shown in Figure 5.1 for methane with syngas and Figure 5.2 N_2 rich gas with syngas respectively, properties such as composition, combustion characteristics and LHV change accordingly. Blended fuels with different proportions of syngas are used in the gas turbine model at 30 bar and 25℃. Based on the LHV of the fuels and the flue gas flow rate, the model calculates the necessary mass flow rates of fuel and air required to achieve the total power generation by the turbines. Figure 5.3 & Figure 5.4 shows the required mass flow rate of the blended fuels for methane and N_2 rich in syngas, respectively, used in a CCGT gas turbine. With higher proportions of syngas, the LHV of the fuel decreases due to the CO_2 present in syngas, which reduces the energy content. In this case, syngas consist of a CO_2 content and a lower LHV among the fuels used, the LHV decreases with an increase in CO_2 content in the fuel when the proportion of syngas increases in the blended fuel.

After the combustion of fuels and blend of fuels in gas turbines, the composition of flue gases produced varies as shown in Table 5.1 for fuels methane, N_2-rich natural gas, and syngas fuels. Syngas combustion results in flue gas with higher CO_2 levels, due to the initial CO_2 content in the syngas itself. At the gas turbine outlet, the flue gas reaches a temperature of 553℃ and 1.02 bar pressure. Regardless of the fuels and blended fuels used in gas turbines, the behaviour of gas turbines remains the same, and the flue gases produced from the turbines are 268.6 kg/s for all cases. The exhaust of both turbines is directed to the HRSGs, where the remaining energy from the flue gases is utilized to generate steam for further power production. This utilization of heat in flue gas increases the overall efficiency of the CCGT system by producing more power with low emissions. Similarly to single-fuel modelling, blend fuel mixtures are

analysed to determine the composition of the flue gas and CO_2 emissions. The flue gases produced from the blended fuels have properties similar to those of single fuels in terms of temperature, pressure, and mass flow at the turbine outlet.

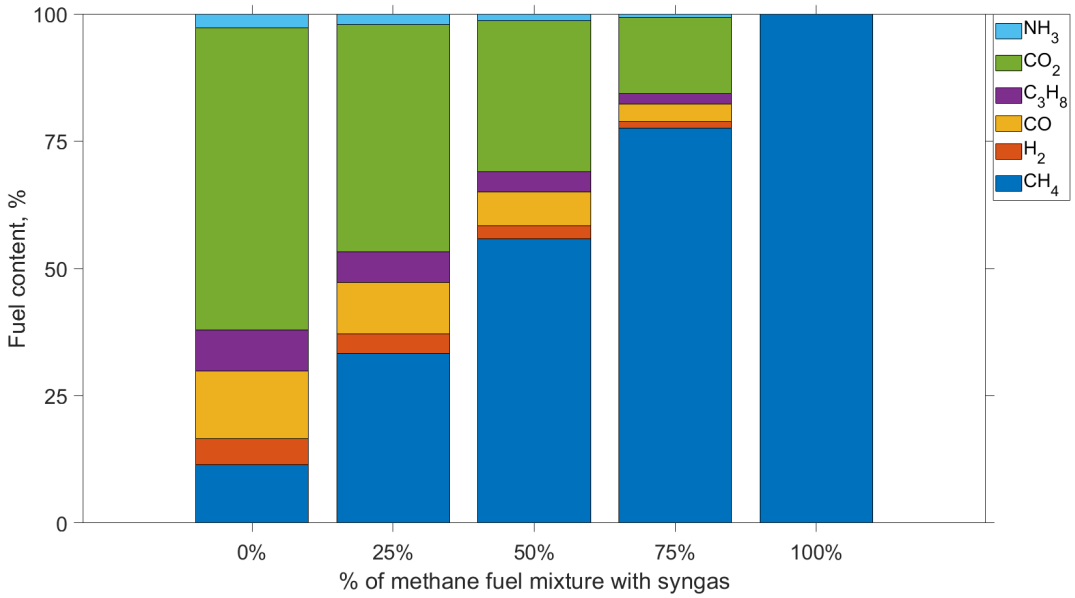

Figure 5.1: Change in composition of methane fuel mixed with syngas at different proportions.

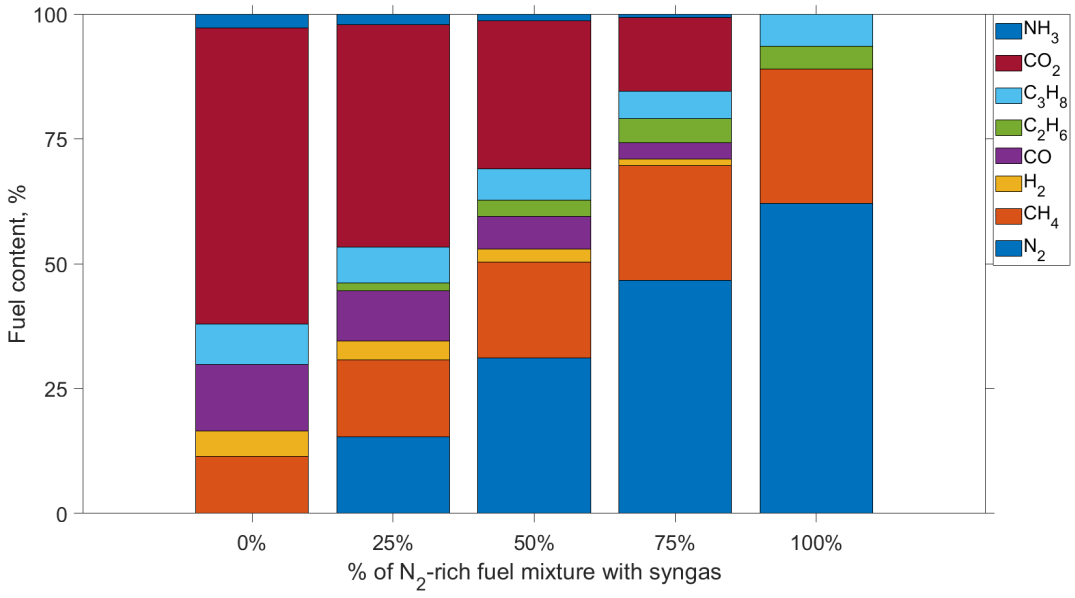

Figure 5.2: Change in composition of N_2-rich gas mixed with syngas at different proportions.

The CO_2 produced from syngas combustion is higher compared to all fuels used, which is considered as 'negative CO_2 emission' due to the use of sewage sludge and capturing CO_2 produced from syngas. Hence, the mixing of syngas with fossil gas fuels reduces the overall emissions produced by the blended fuels. The performance of PCCS and CCGT is measured by passing flue gases to PCCS under different load conditions,

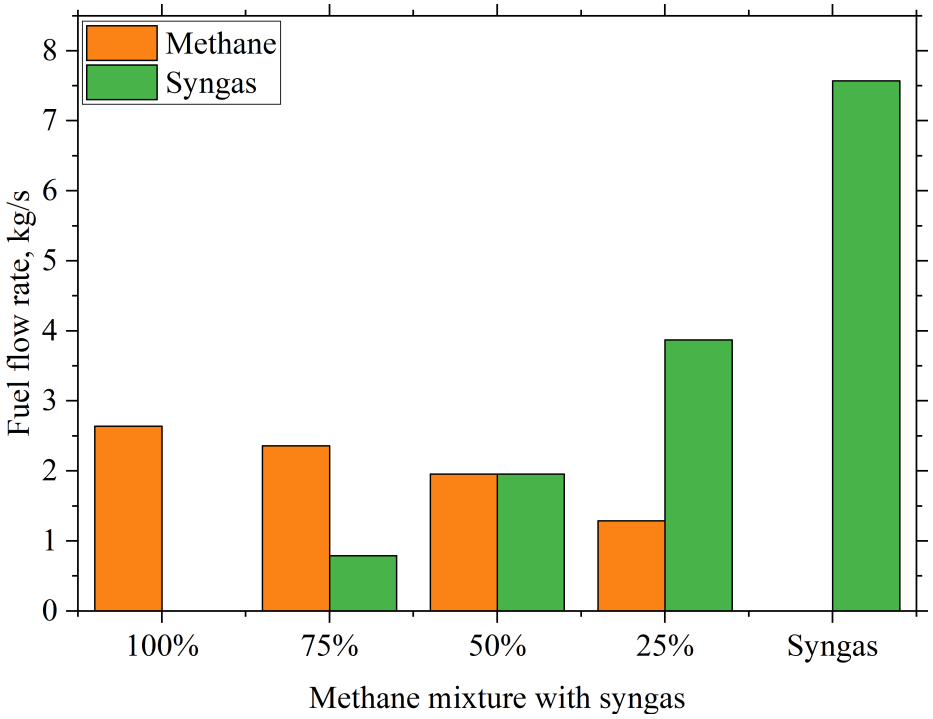

Figure 5.3: Flow rate of methane and syngas blended fuels at different proportions used in one gas turbine.

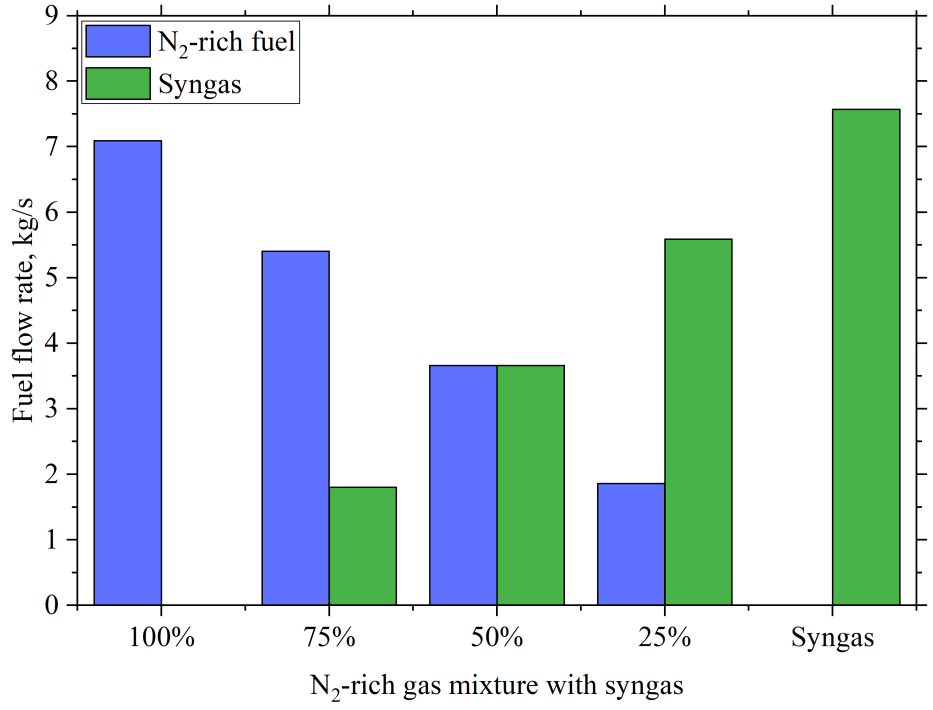

Figure 5.4: Flow rate of N_2-rich gas and syngas blended fuels at different proportions used in one gas turbine.

Table 5.1: Detailed composition of the exhaust gas from the SGT-800 turbine determined with Ebsilon (10 ppmv dry level, 15% O_2)

Component	Molecular formula	Methane		N_2-rich gas		Syngas	
		mass%	molar%	mass%	molar%	mass%	molar%
Nitrogen	N_2	74.3274	75.1939	75.0942	76.0611	71.6727	72.8608
Oxygen	O_2	14.7585	13.0711	14.0323	12.4427	14.6017	12.9949
Argon	Ar	0.4314	0.3059	0.4165	0.2958	0.4152	0.296
Water vapour	H_2O	5.0355	7.9213	4.7927	7.5485	5.6072	8.8637
Carbon dioxide	CO_2	5.4456	3.5067	5.6622	3.6507	7.7016	4.9836
Nitrogen oxides	NO_x	0.0016	0.0011	0.0018	0.0012	0.0016	0.001

from 50% to 100%. Changing the load conditions in PCCS, the CO_2 content at the inlet of the PCCS varies depending on the fuel used in gas turbines. Figure 5.5 illustrates the CO_2 flow rate at the inlet of the PCCS in varying flue gas load conditions from different fuels and blended fuels used in gas turbines [131].

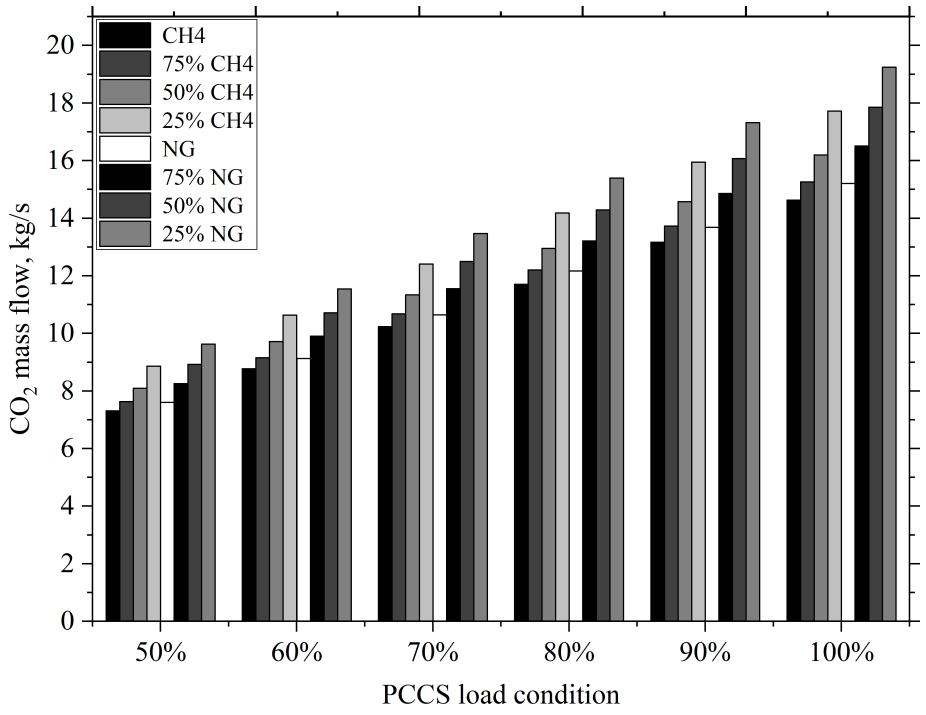

Figure 5.5: CO_2 at the inlet of PCCS when operated in different load conditions [131].

Methane and syngas were selected to evaluate the thermodynamic performance of one HRSG of the reference case CCGT because of their greater difference in LHV. The analysis for one HRSG applies to the other HRSG, as both have same boundary conditions and geometrical configurations. The analysis is performed by calculating various thermodynamic properties such as the enthalpy of flue gases at different stages, the rate of heat exchange, LMTD and heat distribution between HRSG components, using equations Equation (3.24) - Equation (3.28). Using the developed CCGT model, the gas turbine produces a constant

power output of 50.5 MW when using fuel flow rates of 2.64 kg/s for methane and 7.572 kg/s for syngas, with airflow rates of 131.66 kg/s and 126.73 kg/s, respectively. The exhaust gases produced from the combustion of these fuels are utilized by HRSG by transferring heat to water and converting it into HP and LP steam. Due to constant pressure drops given to HRSG components, pressure differences between inlet and outlet remained the same for both fuels, although temperature variations were observed at component inlets and outlets. The heat exchange rate of the components varies depending on the flow and temperature of the stream mass as shown in Figure 5.6 and calculated LMTD as shown in Table 5.2 [95].

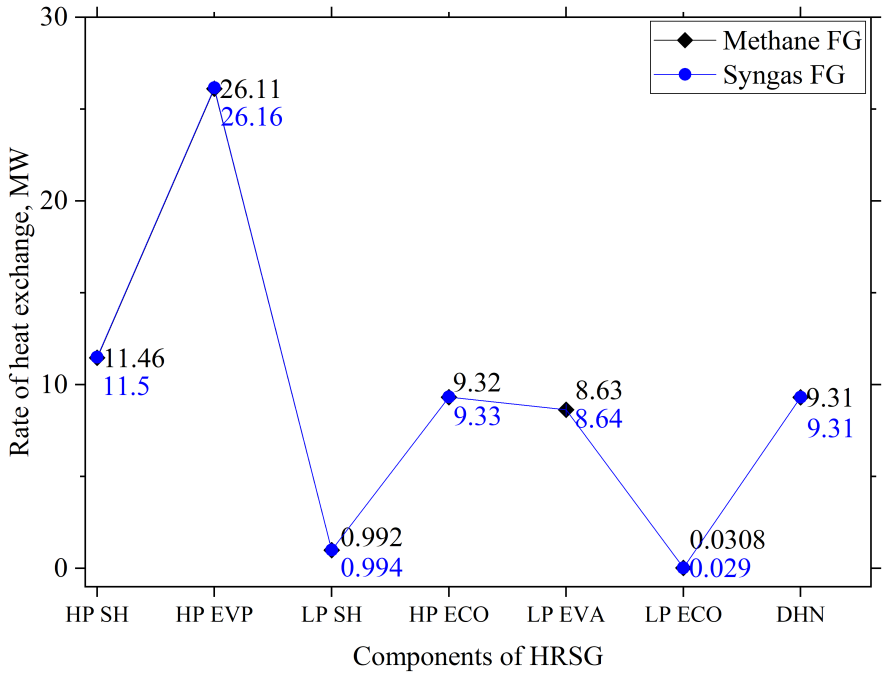

Figure 5.6: Variation in Rate of heat exchange of each component of HRSG with flue gases from methane and syngas [95].

Table 5.2: Calculated LMTD of the components of HRSG with reference to Figure 4.2 [95]

HRSG components	LMTD (℃)	
	Methane	Syngas
HP ECO	36.5	37.8
HP EVP	76.9	78.7
HP SH	96.8	97
LP ECO	14.45	14.65
LP EVA	33.02	33.7
LP SH	67.3	67.3

The evaporator has the highest heat exchange rate in both HP and LP levels, followed by the superheaters of all components. The 9 MW heat exchange rate in DHN economizer shows the efficiency and effectiveness of HRSGs, improving the overall efficiency of the power plant. The LMTD values are higher in HP

superheater with 96.8℃ and 97℃ and lower in 14.45℃ and 14.65℃ in LP economizer for methane and syngas fuels, respectively. Based on the composition and temperature of the flue gas, the enthalpy values for various stages of HRSG referring to Figure 4.2 were calculated as illustrated in Figure 5.7 & Figure 5.8. As noted in the figures, with various heat exchange rates of HRSG components, the temperature differences using methane and syngas fuels are very slight. Despite the use of fuels with different LHV, the presence of high N_2 and low CO_2 in methane flue gas compromised the temperature variations of syngas flue gas with low N_2 and high CO_2 content, resulting in similar enthalpy values at various stages of HRSG. Therefore, the performance of HRSGs in CCGT remains the same regardless of the fuel used, which can be observed from Figure 5.9 for methane and & Figure 5.10 for syngas showing the temperature distribution throughout the HRSG [95].

From the calculated steam and flue gas temperature, the HRSG pinch point when using methane and syngas is estimated to be 23.1℃ and 24.16℃ respectively. The addition of DHN changes the overall temperature profile of HRSG by reducing the flue gas temperature at the exit of HRSG to 81℃. The improvement in DHN economizer heat exchange rate and the lower flue gas temperature at the HRSG exit is due to the additional heat extraction by DHN, which leads to the pinch point.

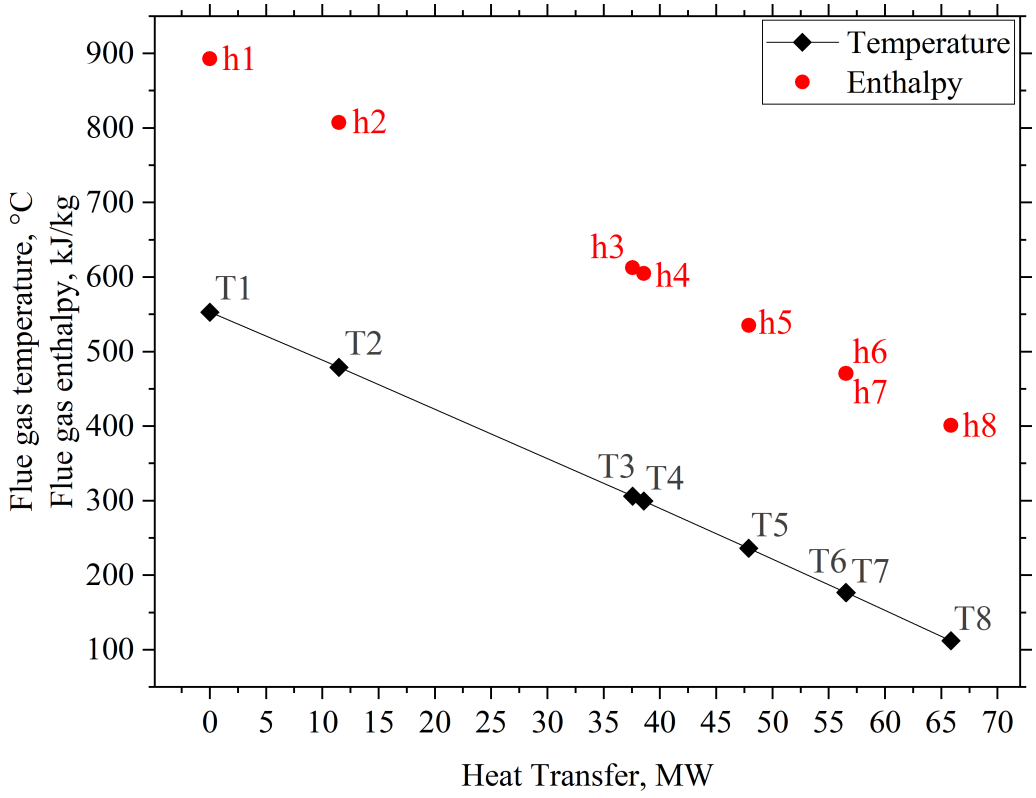

Figure 5.7: Enthalpy of flue gas from methane at various stages of HRSG temperature points referred to Figure 4.2 [95].

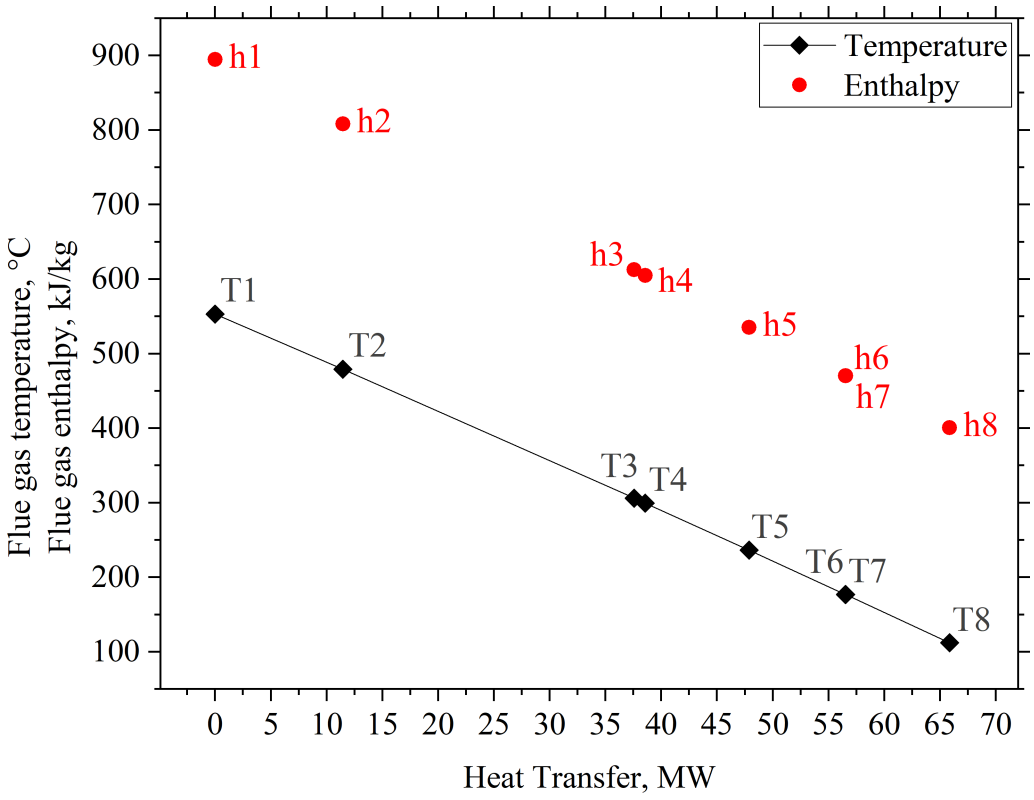

Figure 5.8: Enthalpy of flue gas from syngas at various stages of HRSG temperature points referred to Figure 4.2 [95].

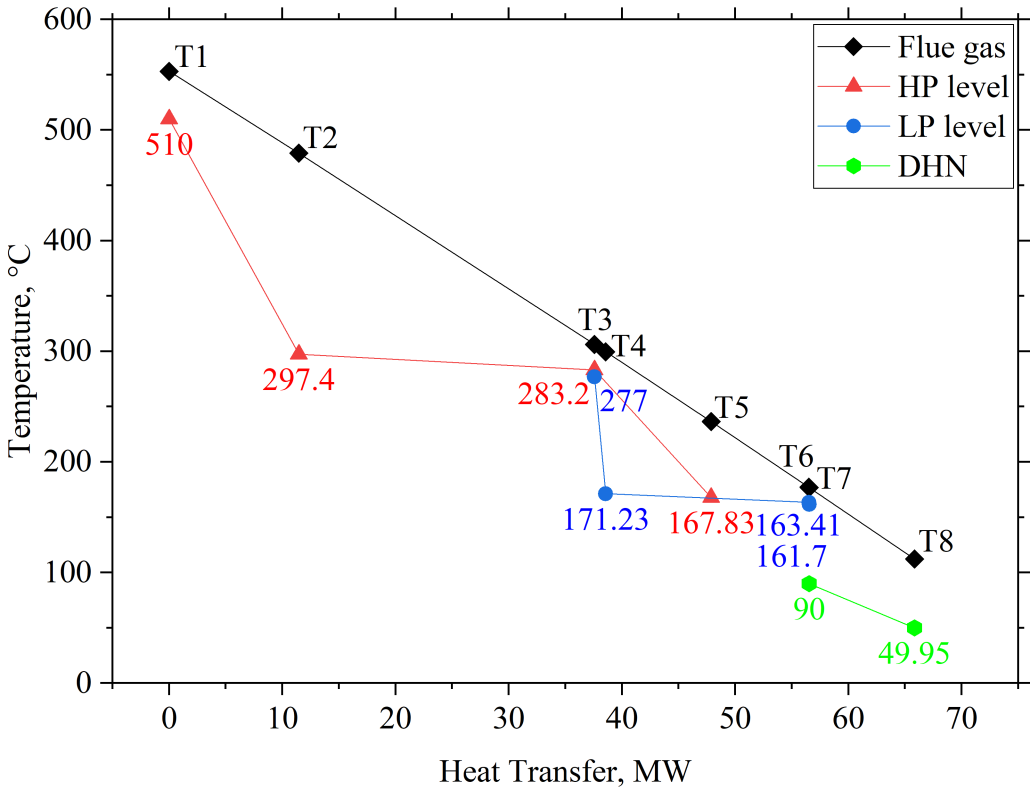

Figure 5.9: Heat distribution in HRSG with flue gas from methane fuel [95].

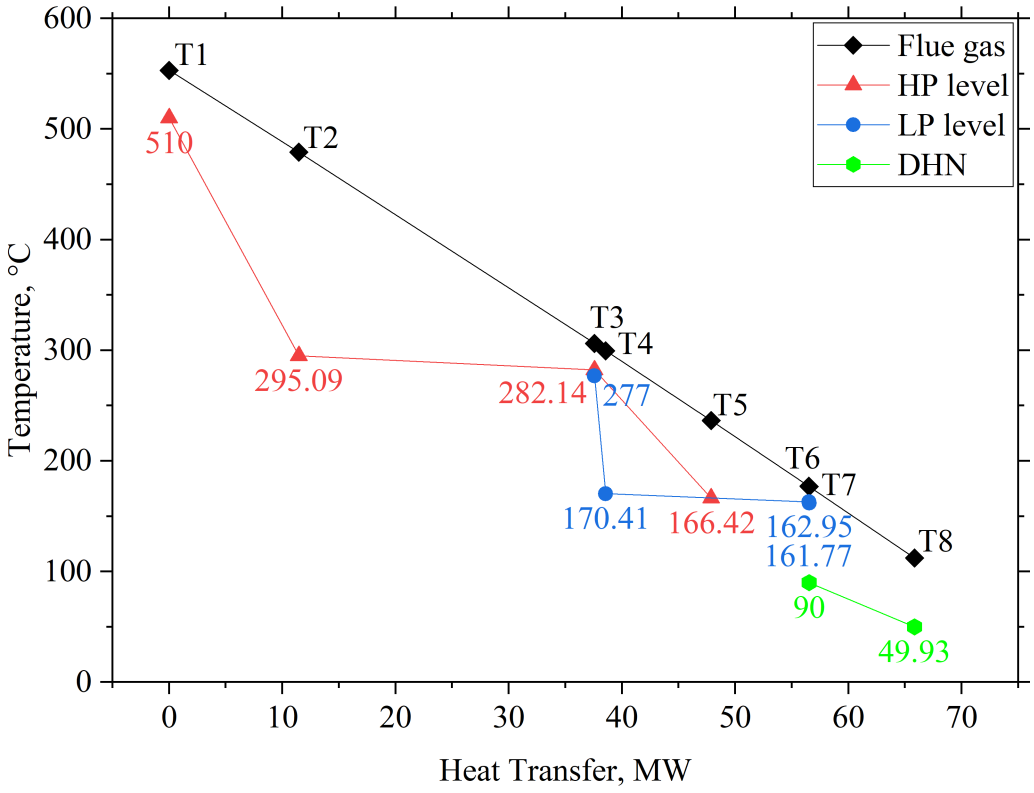

Figure 5.10: Heat distribution in HRSG with flue gas from syngas fuel [95].

5.2 Results of CCGT integrated with PCCS using different solvents

The fuel and flue gas analysis in the reference case CCGT shows that the overall behaviour of gas turbines and HRSGs remains unchanged regardless of the use of single and blended fuels. The use of different fuels has slight impacts on the temperature profile of the HRSG and more impact on the CO_2 emission produced, depending upon the fuel. In this system, the steam power generation, heat supply to DHN and steam extraction for amine regeneration in PCCS are in thermal equilibrium. Since the steam for solvent regeneration and DHN water heating is taken from the LP steam turbine extract, it impacts the steam cycle power and overall power generation. Steam extraction for various uses makes less steam available in the steam cycle for power generation. This extraction depends on the CO_2 produced from the fuel, type of amine used for PCCS, amine regeneration rate, and DHN heat demand. Lower heat demand and low amine regeneration rate consume less steam extraction. The balance of the system is explained in detail for PCCS operation at full load conditions and varying load conditions with input of CO_2 content given to PCCS as referred to in Figure 5.5.

5.2.1 Performance of CCGT using different fuels with PCCS operation at full load condition

To make better comparisons between gas fuels and solvents used in this process, the gross power generation of CCGT is maintained between 130 MW and 131 MW by adjusting the heat supplied to DHN. The extraction in the PCCS cannot be adjusted as it must meet the specific regeneration requirements of

the PCCS configuration. Parameters considered crucial for analysing the thermal balance of CCGT such as gross power generation, steam cycle power generation and DHN heat supply are measured. Due to the reasons for avoiding CHP's operational inefficiency, improving fuel efficiency, reducing condenser operational load and HRSG's steam production configuration, the heat supply to DHN is limited between 28 MW to 54 MW. Exceeding or reducing the limit causes an imbalance in the system. Although 54 MW of heat is supplied to DHN without PCCS condition, after integration with PCCS and required steam supplied to its operation, the heat supply to DHN is adjusted between 28 MW to 36 MW to maintain the gross power generation. For both PCCS operations with MEA and AMP-PZ, the same heat transfer rate to DHN is used as in Figure 5.11. Due to steam extraction in DHN and PCCS that affect the power generation of the steam cycle as in Figure 5.12, variations in gross power generation are observed when using different fuels[131].

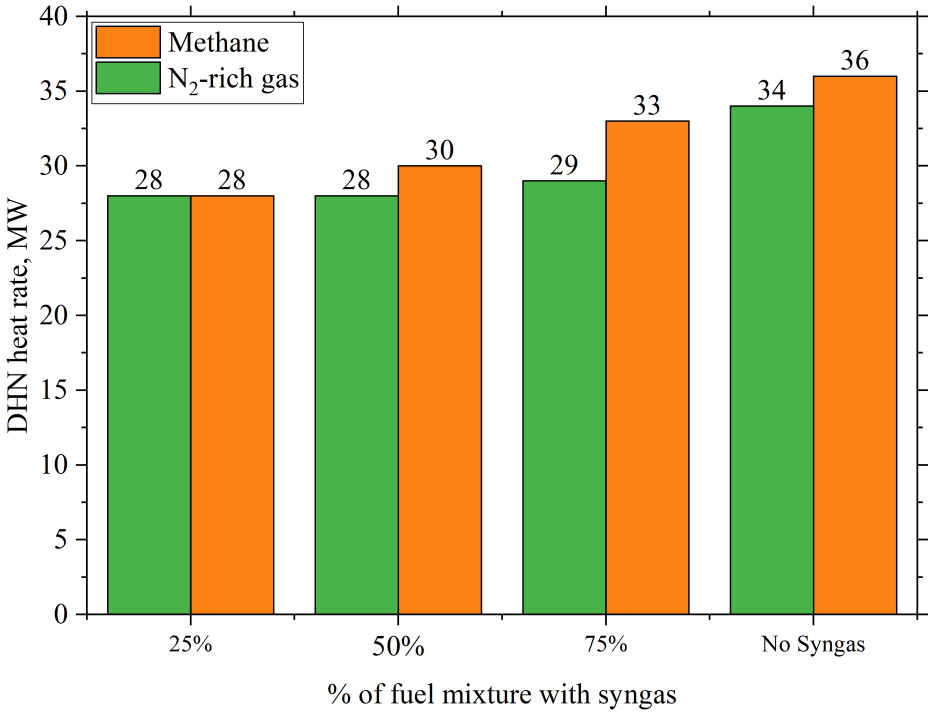

Figure 5.11: Performance of DHN of CCGT when operating PCCS at full load condition [131].

For the given condition, the DHN heat supply using methane and various proportions of methane blended with syngas is higher compared to N_2-rich fuel and its blend with syngas. This is due to the high LHV of methane fuel and the lower CO_2 emission produced by methane, which requires less steam for amine regeneration and more steam to maintain the nominal power generation and heat supply to DHN. As the proportion of syngas increases in blend fuel, the CO_2 emission increases causing more supply of steam to PCCS. Hence, at 75% of syngas mixture with fuels, 28 MW of heat is supplied to the DHN with the lowest power generation rate. Following changes in DHN heat supply, the variations in CCGT gross power generation using different fuels and blended fuels integrated with PCCS operated in full load condition using MEA and AMP-PZ solvents are shown in Figure 5.13 and Figure 5.14, respectively. As observed with both solvents, the steam cycle power generation is lower when using fuels with no syngas compared to a 75% or 50% syngas mixture. Due to the higher heat supply to the DHN in the no syngas condition, a large

amount of steam is directed to the DHN heat exchanger, reducing the power generation in the steam cycle compared using other fuel composition.

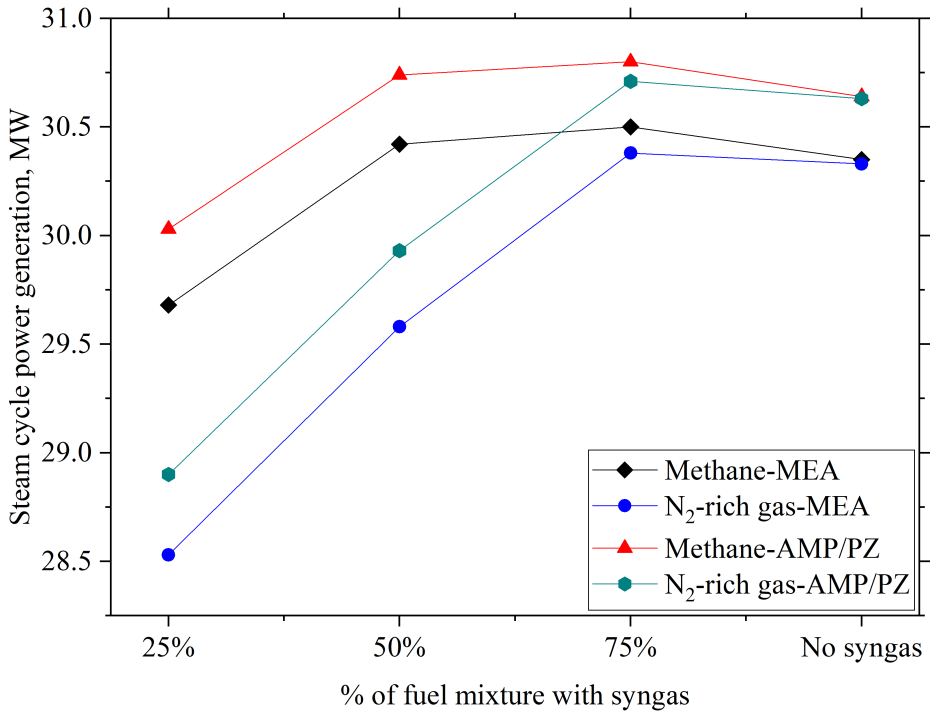

Figure 5.12: Power generation in steam cycle of CCGT when operating PCCS at full load condition.

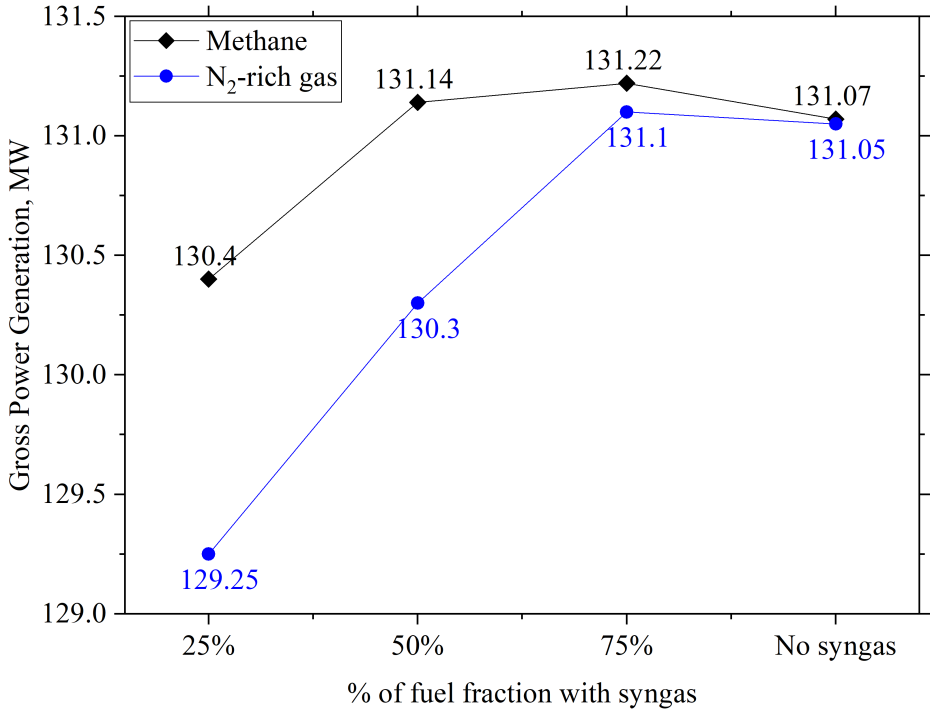

Figure 5.13: Gross power generation by CCGT using different fuel mixtures and treating flue gases in PCCS using MEA [131].

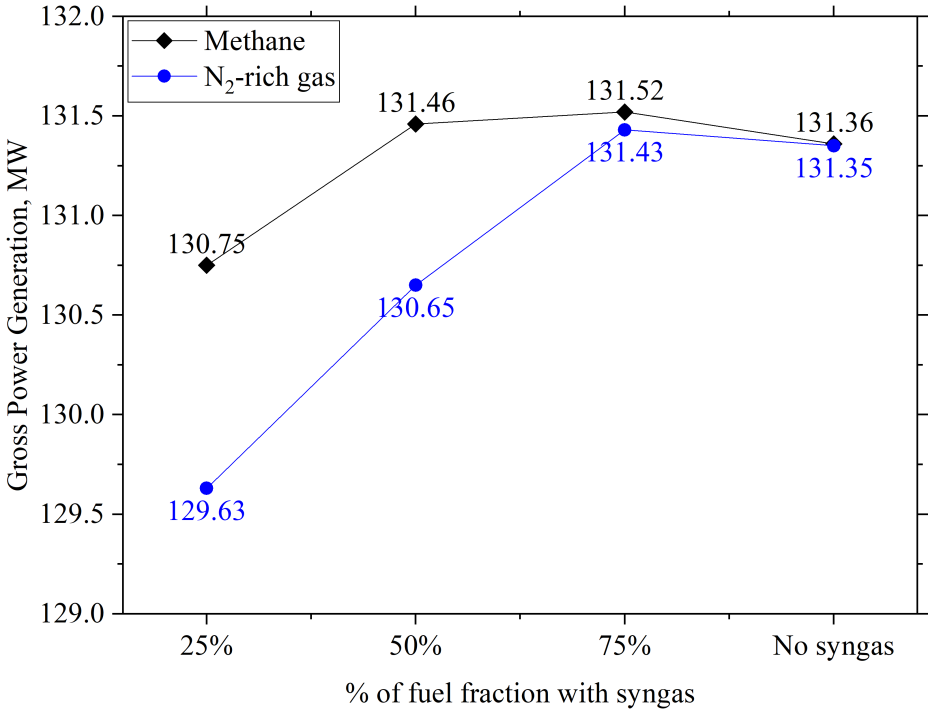

Figure 5.14: Gross power generation by CCGT using different fuel mixtures and treating flue gases in PCCS using AMP-PZ [131].

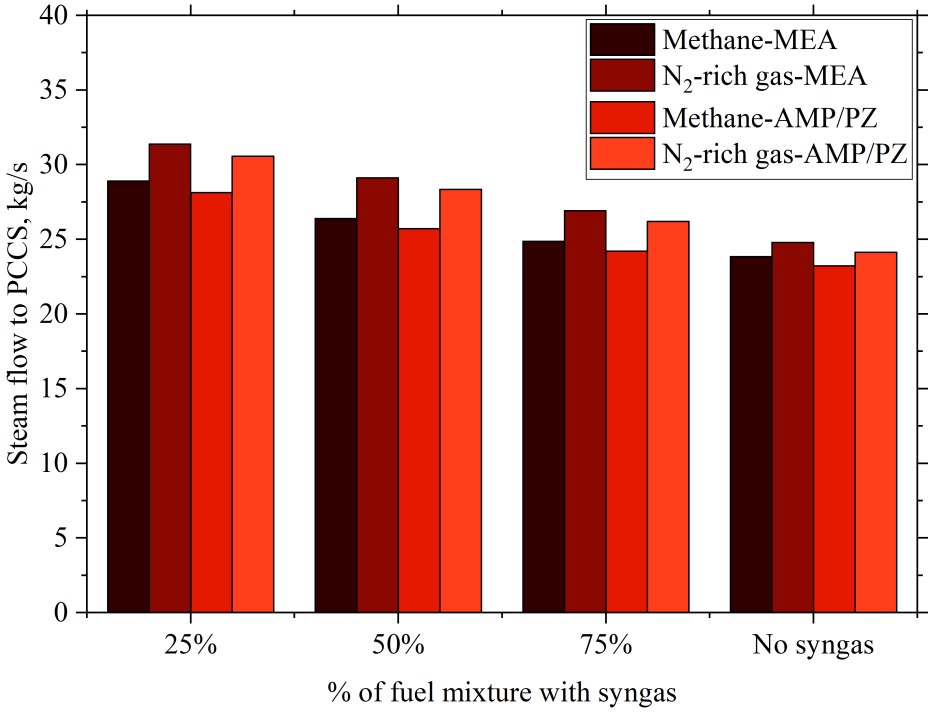

Figure 5.15: Steam requirement by PCCS for treating flue gases from different fuels and blended fuels using MEA and AMP-PZ solvents.

Due to the LHV of methane and N_2-rich gas and lower CO_2 produced from the fuels, it is possible to achieve higher power generation and high DHN heat supply using these fuels. The mixing of syngas increases the

requirement for steam in PCCS, which decreases the DHN heat supply and reduces the generation of steam cycle power [131]. The AMP-PZ solvent consumes steam for regeneration slightly lower compared to MEA as shown in Figure 5.15, while treating flue gases from different fuel compositions. This results in increased steam power production, which improves overall power production when AMP-PZ is used for the same heat supplied to DHN as while using MEA. Hence, the power generation in CCGT is higher when using AMP-PZ in PCCS than when using MEA. Figure 5.16 shows the mass flow of lean amine required for the PCCS process and rich amine at the outlet of the absorber.

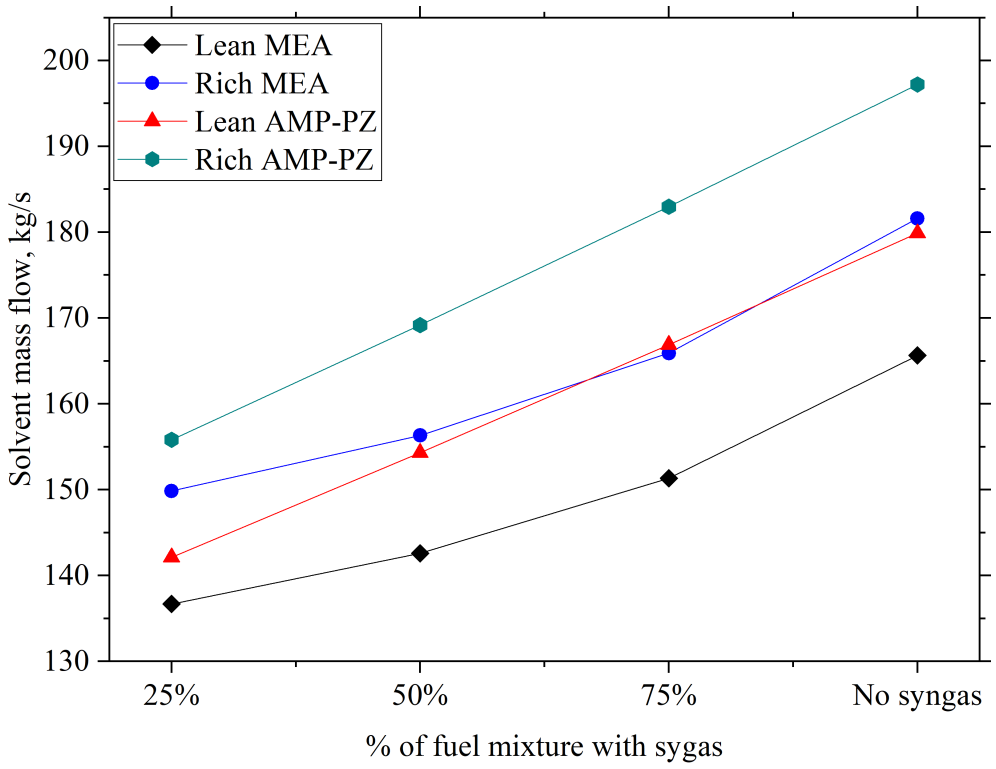

Figure 5.16: Mass flow of lean & rich amine at the inlet and outlet of PCCS absorber when treating flue gases from different fuels compositions.

5.2.2 Performance of CCGT with PCCS operation at variable PCCS load conditions

While operating PCCS under varying flue gas load conditions, a reduction in steam demand improved the operations and efficiency of CCGT. However, a larger amount of CO_2 will be emitted into the atmosphere under reduced load conditions. Despite changes in PCCS flue gas load, the CCGT continues to operate under full load conditions. The adjustment of flue gas load to PCCS reduced the requirement of amine mass flow, which lowers the steam requirement for the solvent regeneration process. A similar method to adjust the DHN heat rate as in Figure 5.17 is used to maintain the gross power generation between 130 MW and 131 MW for PCCS under different load conditions to treat flue gases of different fuel compositions using MEA and AMP-PZ. The results obtained for the gross power generation by PCCS operation under different load conditions using MEA and AMP-PZ are shown in Figure 5.18 and Figure 5.19. As PCCS load conditions are gradually reduced, more steam becomes available in the steam

cycle, providing the possibility of supplying to DHN. Therefore, under the PCCS 50% load condition, the DHN heat supply can reach a maximum of 54 MW by maintaining the gross power generation of more than 130 MW in the CCGT [131].

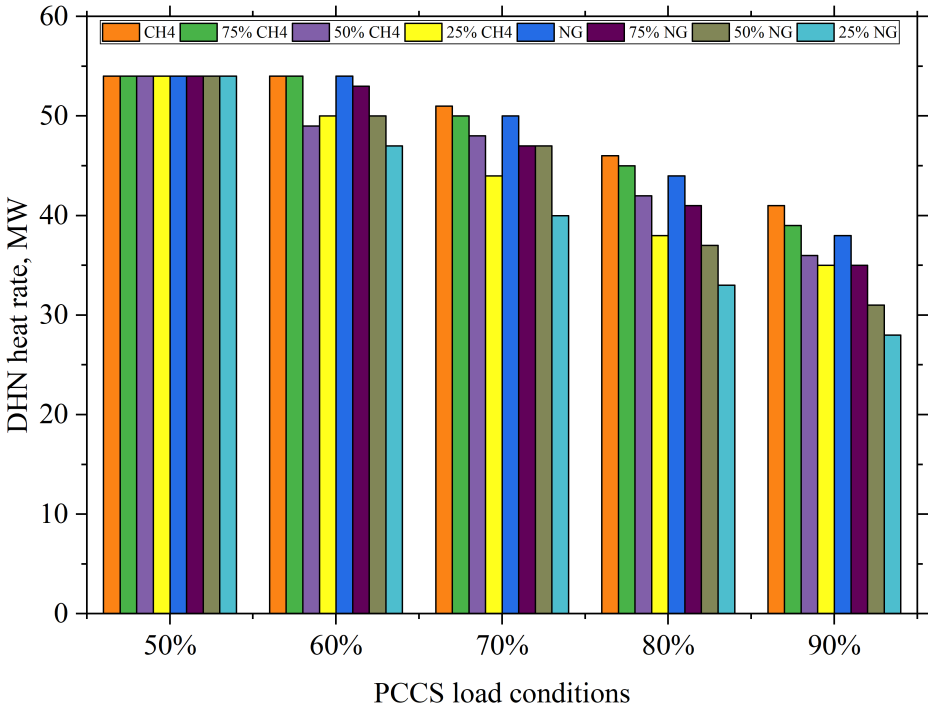

Figure 5.17: Percentage of nominal DHN heat supply when operating PCCS at variable load conditions.

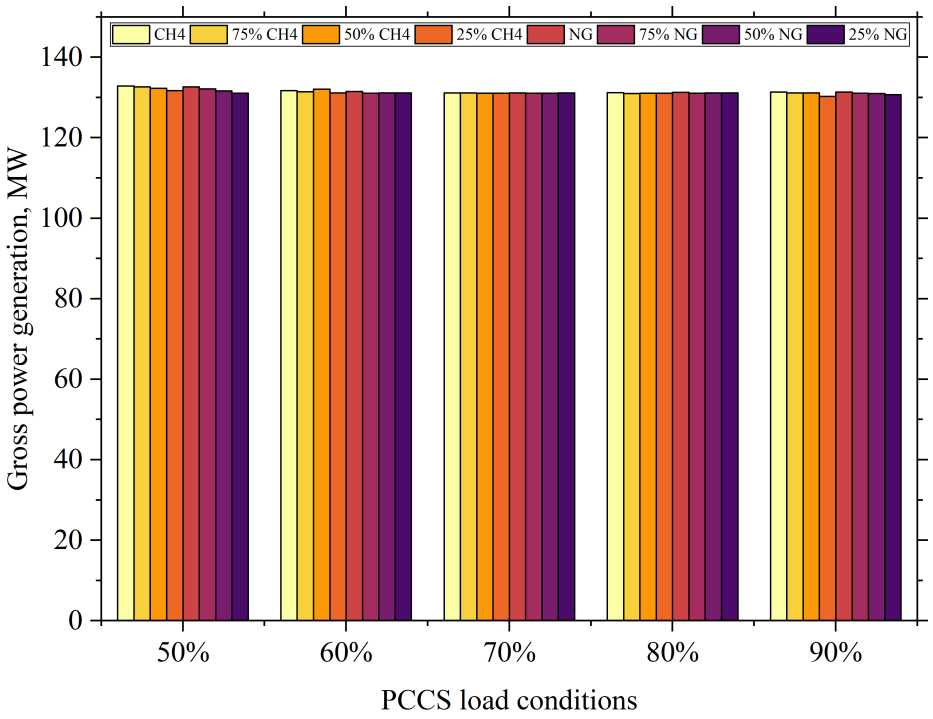

Figure 5.18: Gross power generation by CCGT using different fuel mixtures and treating flue gases in PCCS using MEA at variable load conditions.

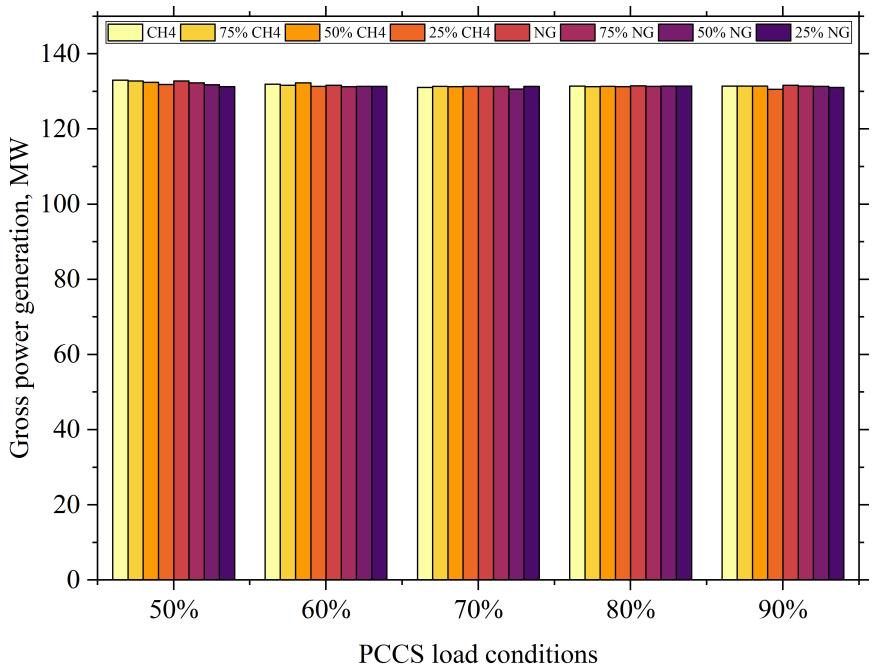

Figure 5.19: Gross power generation by CCGT using different fuel mixtures and treating flue gases in PCCS using AMP-PZ at variable load conditions.

As shown in Figure 5.20 & Figure 5.21 for MEA and AMP-PZ steam consumption for the reboiler, respectively, the steam consumed during regeneration of AMP-PZ is less than MEA, which increased the overall performance of the CCGT when PCCS operates with AMP-PZ. Although the PCCS process with MEA and AMP-PZ delivers a highly efficient CO_2 capture, the overall efficiency achieved with AMP-PZ is high. This efficiency is reflected in the DHN, so for fixed DHN heat supply, AMP-PZ has an enhanced performance. Figure 5.22 & Figure 5.23 illustrates the mass flow of lean required for PCCS process of treating flue gases from different fuel compositions under different load conditions [131]. The detailed parameters of PCCS performance using MEA and AMP-PZ are listed in Appendix A & Appendix B respectively.

5.3 Determination of energetic, environmental and economic effects in gas power plant during electricity and heat production with CO_2-neutral fuels and CCS installation

Based on the development of model and performance analysis of CCGT integrated with PCCS, the various parameters are estimated for the analysis. The analysis of CCGT performance varies when using different compositions of gas fuels and when operating PCCS under different flue gas load conditions using different solvents. Key performance indicators such as energy, environmental, and economic indicators are used to assess the system's capability to achieve negative CO_2 emissions. Energy indicators show a detailed performance measure and the impacts of using different fuel compositions and performing carbon capture process under various load conditions. Environmental indicators focus on assessing the emissions

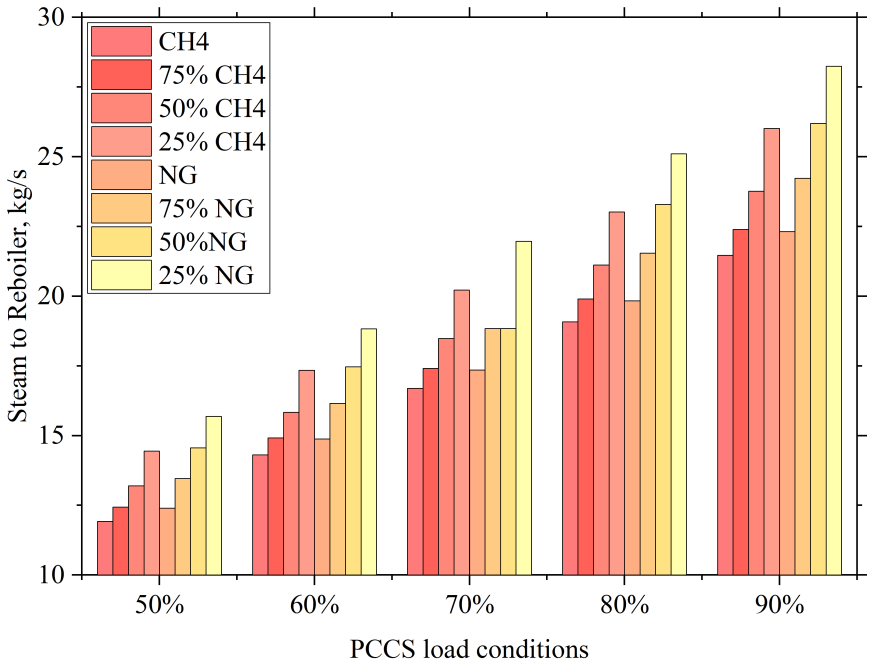

Figure 5.20: Steam consumed by PCCS reboiler for MEA solvent regeneration [131].

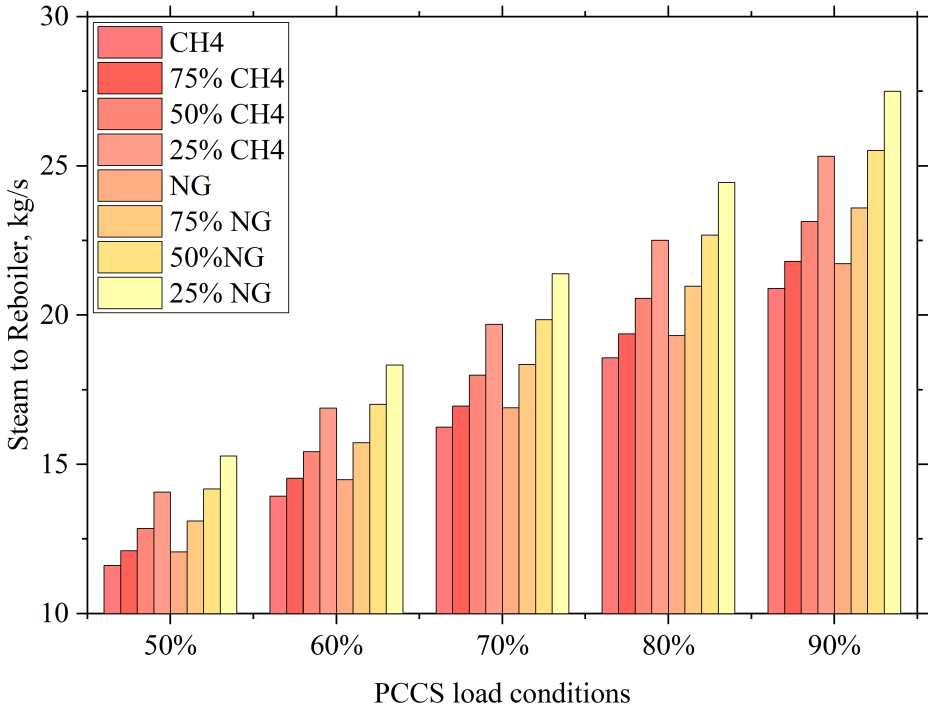

Figure 5.21: Steam consumed by PCCS reboiler for AMP-PZ solvent regeneration [131].

factors including CO_2 capture rate and the impact on power generation while using capture process. Economic indicators provide a detailed understanding about the costs and revenue of operating CCGT with PCCS, which measures key factors such as fuel consumption costs, construction costs, operational and maintenance costs and income from power generation and heat supply.

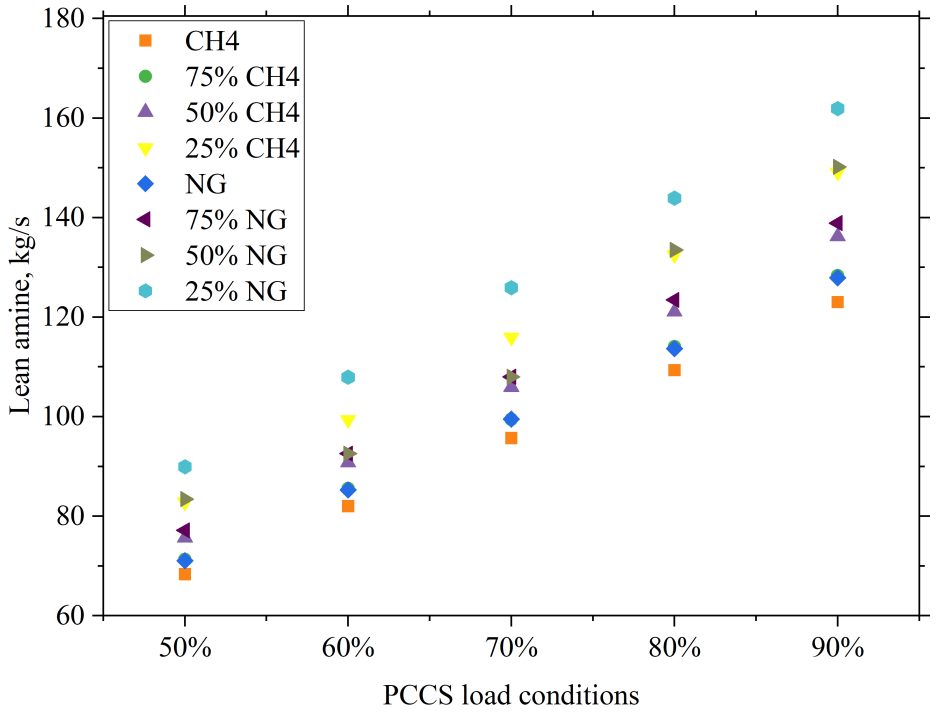

Figure 5.22: Mass flow of lean MEA required for PCCS process of treating flue gases from different fuel compositions at different load conditions [131].

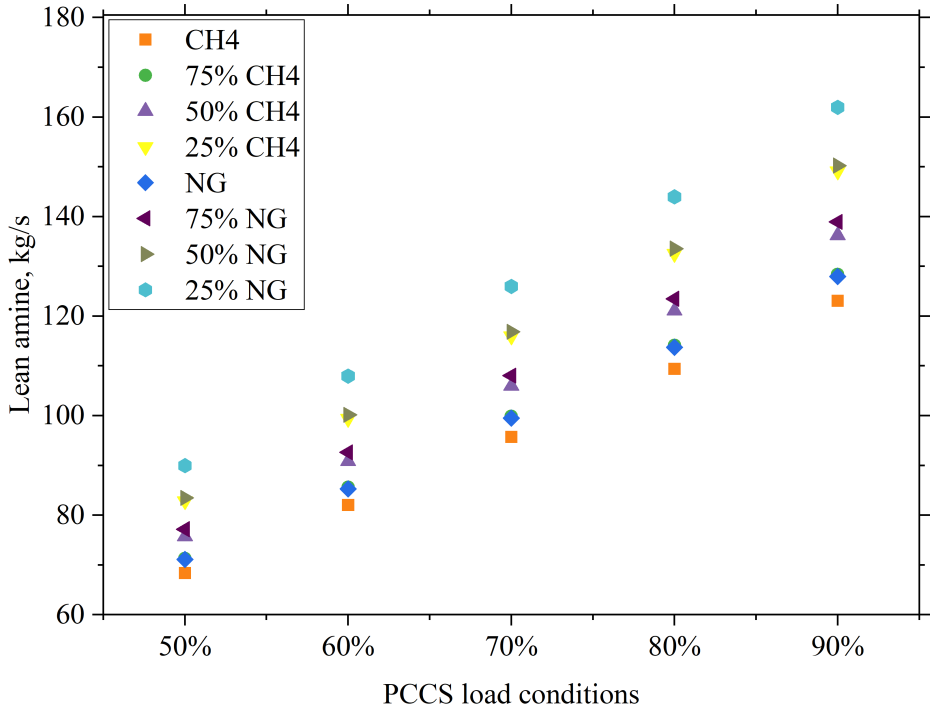

Figure 5.23: Mass flow of lean AMP-PZ required for PCCS process of treating flue gases from different fuel compositions at different load conditions [131].

5.3.1 Energy indicators

Various thermodynamic properties of CCGT using different fuel compositions and the impacts of integrating with PCCS and performing flue gas treatment using two different solvents are measured and investigated. This study shows that the performance of CCGT depends on the fuel used in gas turbines as well as the amine used in PCCS. The LHV of the fuel and the emission produced from the combustion of fuel combined with steam and electrical production to satisfy the DHN and PCCS operations affect the performance of the CCGT. As the flue gas load to the PCCS increases, both gross and net efficiencies of the CCGT decrease. This decrease in results is also associated with an increase in proportion of syngas in the fuel mixture as illustrated in Figure 5.24 and Figure 5.25, which shows gross and net efficiency differences for different fuel compositions with treating flue gases using MEA and AMP-PZ respectively under variable load conditions. When analysing the efficiency differences between solvents, it is observed that the gross energy efficiency of CCGT varies between 60% to 70.7%, while net energy efficiency varies from 49.3% to 50.3%, depending on both the fuel composition and the solvent used in PCCS. Eventhough both MEA and AMP-PZ solvents made an impact on performance of CCGT, the overall efficiency with the AMP-PZ solvent is higher compared with the MEA solvent. This higher efficiency is due to the requirement of AMP-PZ of a less steam to perform the reboiler heat duty. The methane-syngas blend performs better compared to N_2-rich fuel mixture, due to its LHV. The 25% N_2-rich gas mix with syngas has the lowest performance due to its high CO_2 emission and low calorific value among the fuel compositions used. Figure 5.26 & Figure 5.27 shows the net power output calculated from the gross power generation and the own power consumption of the CCGT and PCCS using MEA and AMP-PZ, respectively. Slight fluctuations were noted in Figure 5.28 & Figure 5.29of own power consumption of power plant with PCCS, which affect the net efficiency and power output. These fluctuations are due to an adjustment of the steam flow rates by the model considering the amine outlet temperature in the reboiler depending on the amine used. To optimize heat transfer rate in PCCS reboiler, the model regulates steam flow according to the content, mass flow and temperature of rich solvent considering the thermodynamic properties [131].

A certain amount of steam extraction for amine regeneration caused a decline in net power generation. Since steam extraction to DHN is mandatory in the case analysed, the power reduction due to steam extraction to PCCS is calculated with the gross power output of CCGT without PCCS and the gross power output of CCGT with PCCS. As described in the performance of the integrated CCGT with PCCS, AMP-PZ regeneration consumes less steam than MEA. Hence, the power reduction due to steam extraction when using MEA as in Figure 5.30 is higher compared to AMP-PZ as in Figure 5.31. In CCGT without steam extraction, the power reduction is calculated only considering the net power produced by CCGT and the power consumed by the equipment of CCGT. For MEA, the steam cycle power reduction ranges from 8 MW to 5.5 MW for methane mixture fuels and from 9.1 MW to 5.7 for N_2-rich gas mixtures. In case of AMP-PZ, the steam power reduction ranges from 7.7 MW to 5.3 MW for methane mixture fuels and from 8.7 MW to 5.5 MW for N_2-rich gas mixture fuels.

Due to steam extraction and power supply to PCCS, the EOP of CCGT varies according to the flue gas load conditions as in Figure 5.32 & Figure 5.33 for PCCS using MEA and AMP-PZ, respectively. The EOP increases with an increase in the load conditions of PCCS, which shows that more than the required amount

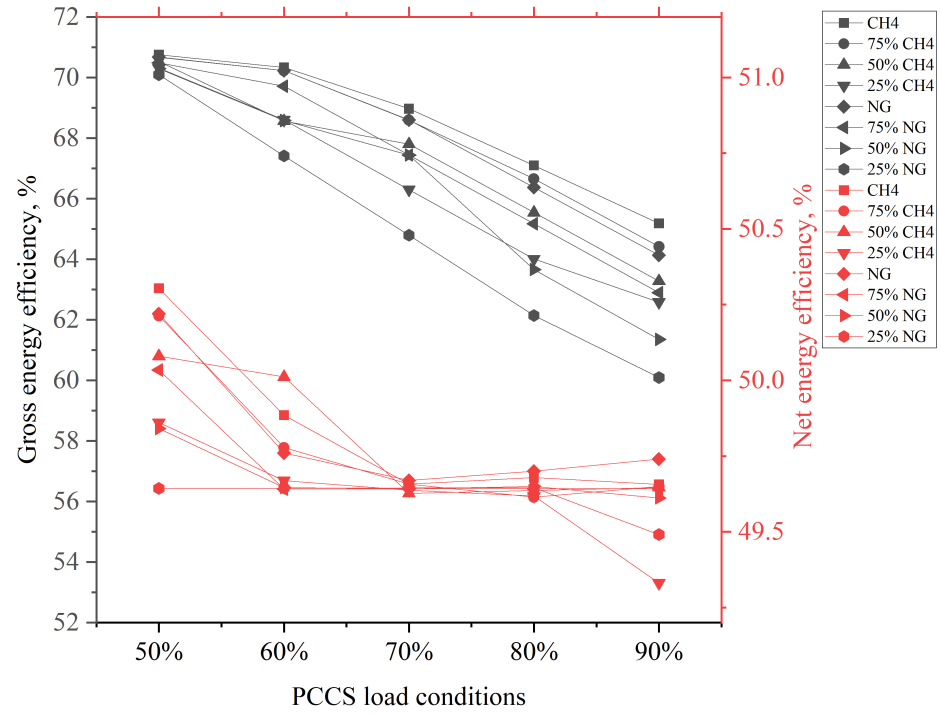

Figure 5.24: Gross & Net energy efficiency of CCGT using different fuel mixtures and treating flue gases in PCCS using MEA at variable load conditions [131].

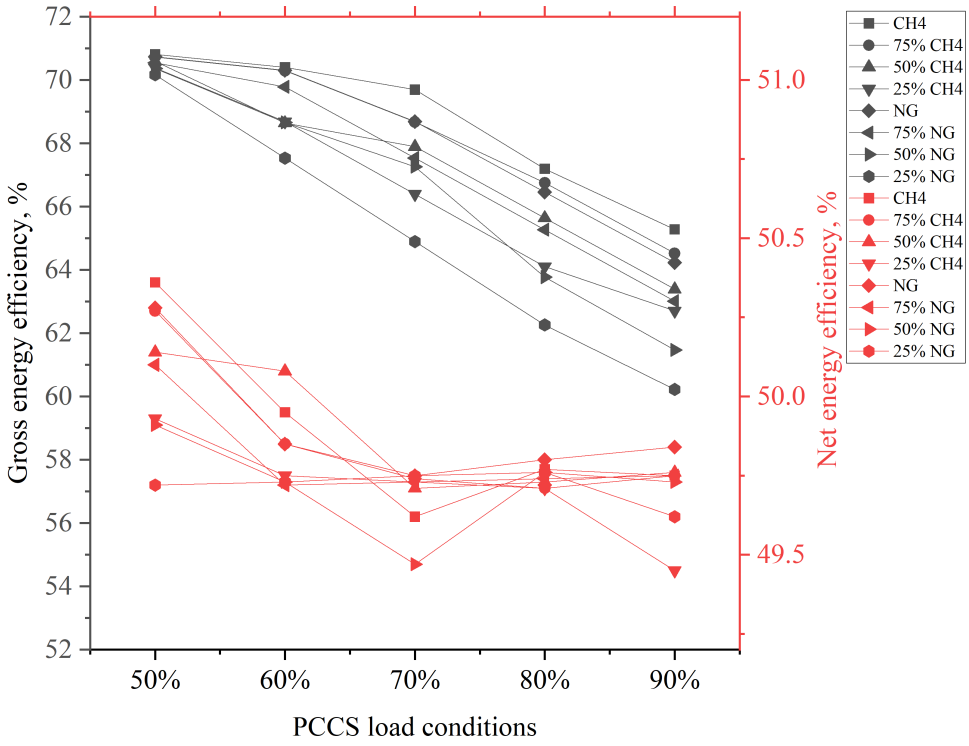

Figure 5.25: Gross & Net energy efficiency of CCGT using different fuel mixtures and treating flue gases in PCCS using AMP-PZ at variable load conditions [131].

of energy is spent on PCCS during reduced load conditions, increasing power output and EOP causing operational inefficiency.

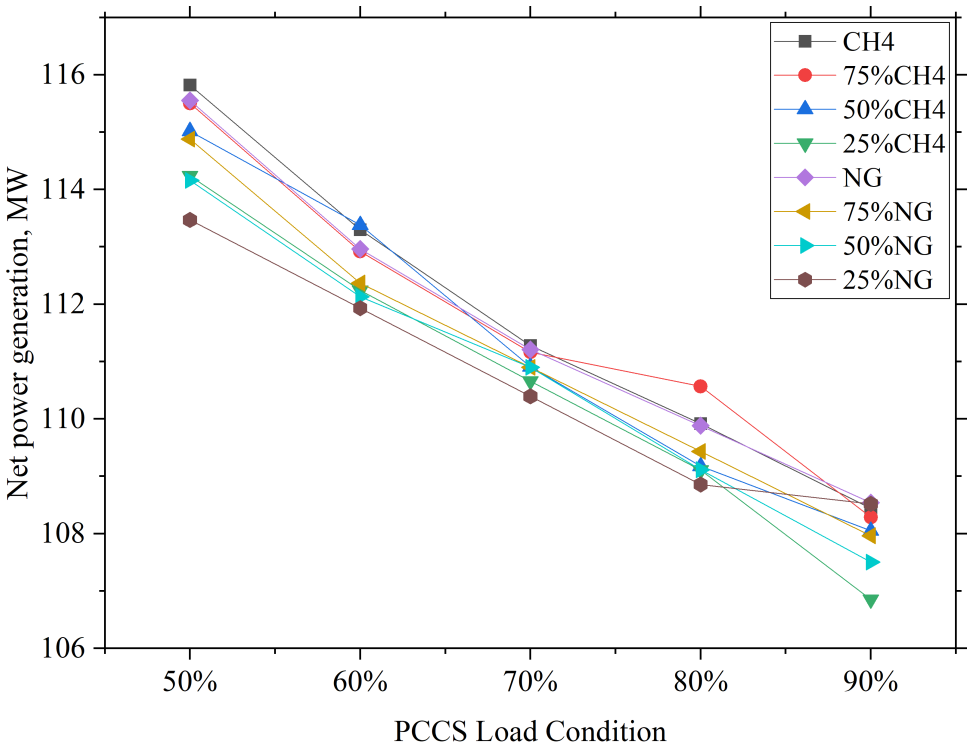

Figure 5.26: Net power generation in CCGT using different fuel mixtures and treating flue gases in PCCS using MEA at variable load conditions.

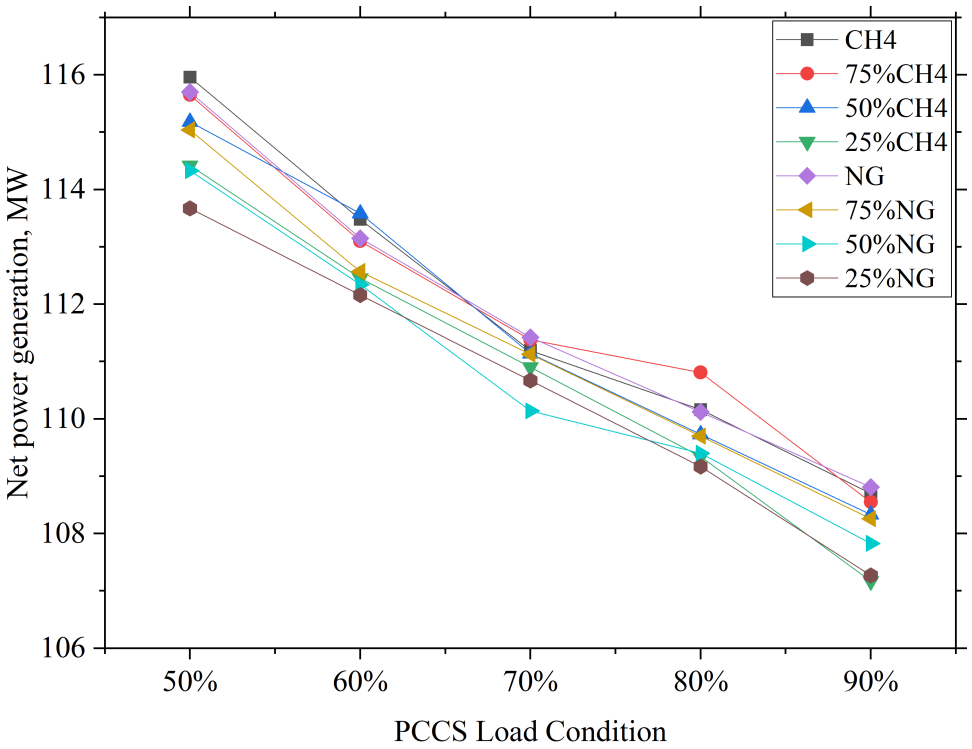

Figure 5.27: Net power generation in CCGT using different fuel mixtures and treating flue gases in PCCS using AMP-PZ at variable load conditions.

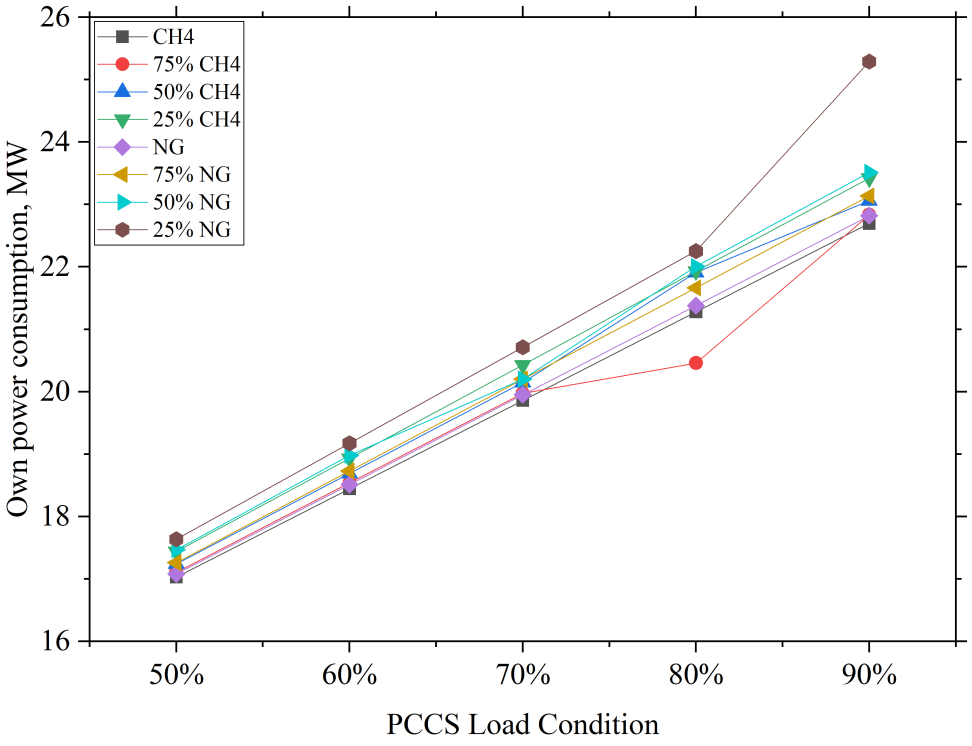

Figure 5.28: Own power consumption of CCGT using different fuel mixtures and flue gases in PCCS using MEA at variable load conditions [131].

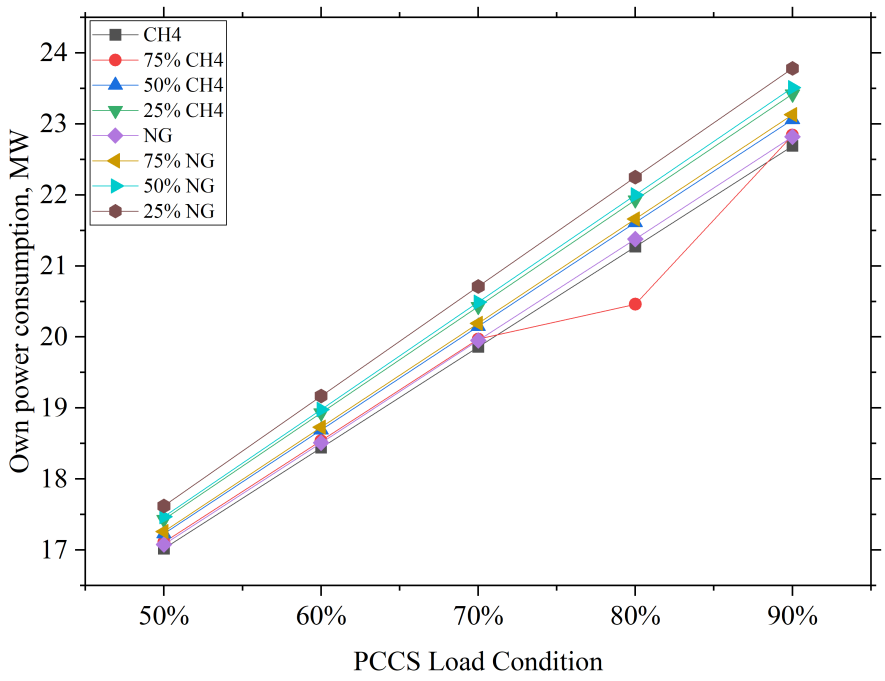

Figure 5.29: Own power consumption of CCGT using different fuel mixtures and flue gases in PCCS using AMP-PZ at variable load conditions [131].

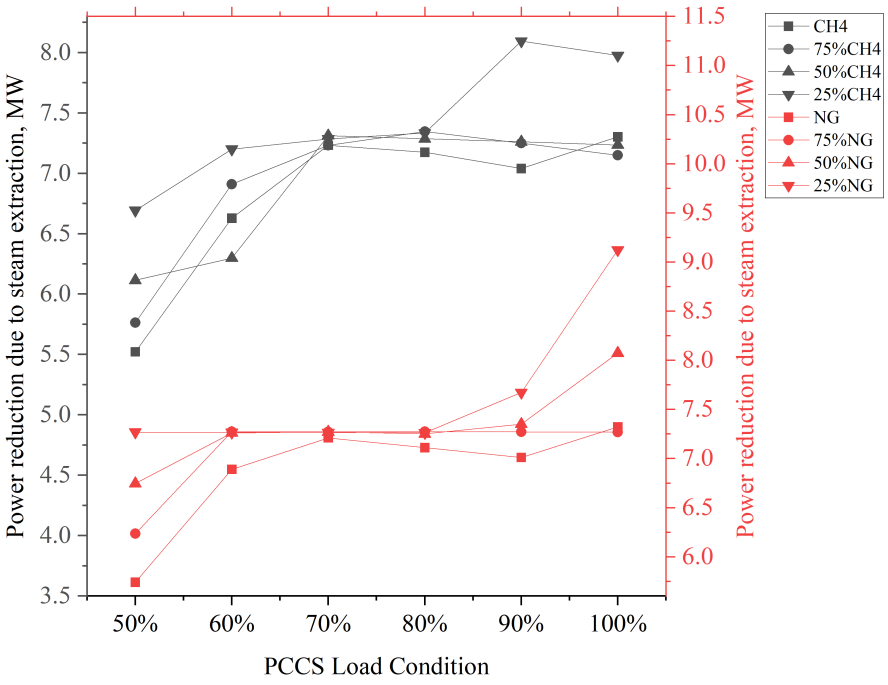

Figure 5.30: Power reduction in CCGT due to steam extraction for MEA regeneration in PCCS.

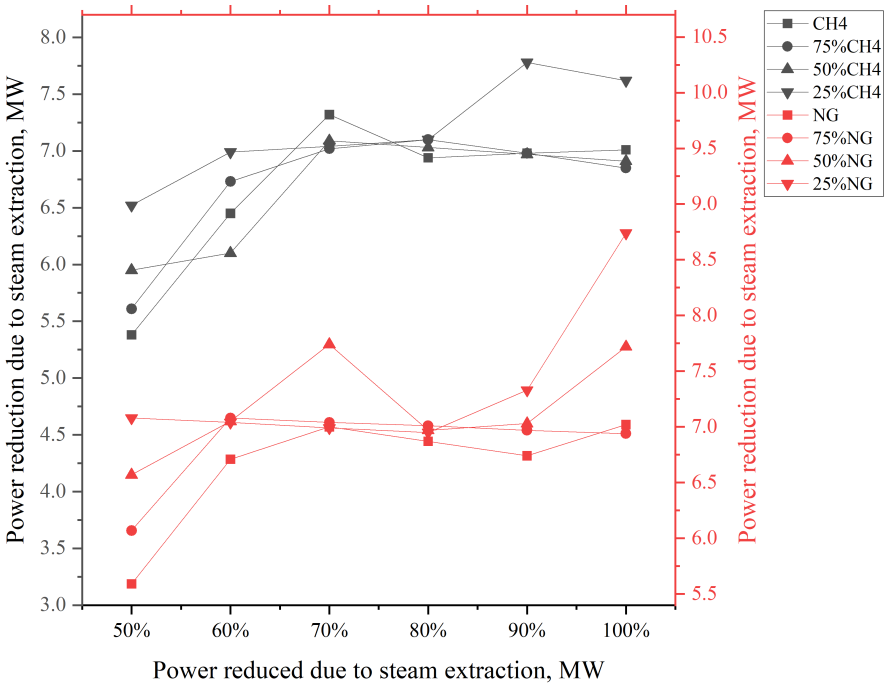

Figure 5.31: Power reduction in CCGT due to steam extraction for AMP-PZ regeneration in PCCS.

5.3.2 Environmental indicators

Environmental indicators are necessary for evaluating the performance of a CCGT integrated with PCCS, which provides a detailed assessment of environmental impact of the system. These indicators are useful for calculating carbon emissions reduction, energy penalties, and efficiency losses, which provides the possibility of achieving the negative CO_2 emission efficiently. While specific emissions show the

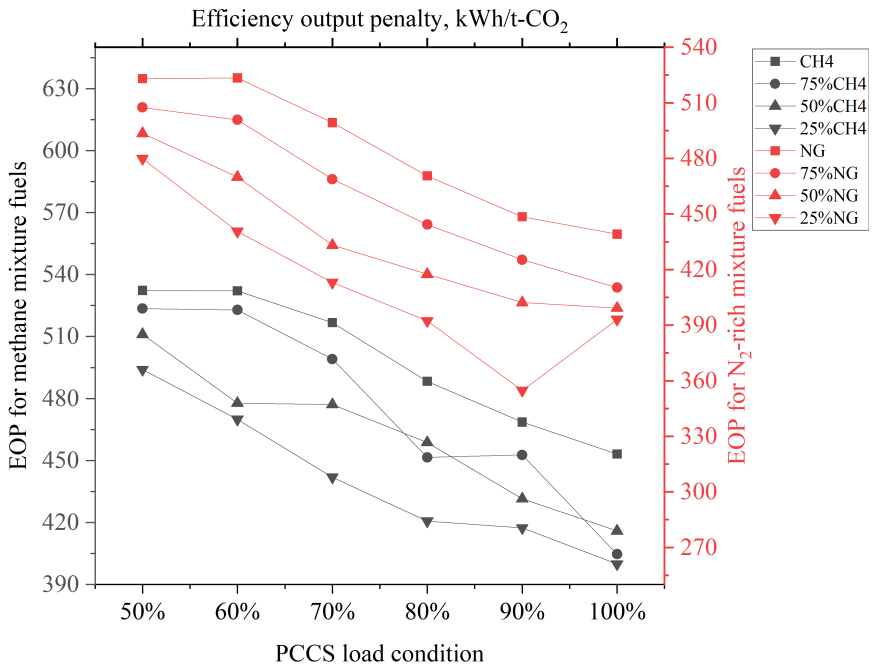

Figure 5.32: Efficiency output penalty of CCGT using different fuels and operating PCCS using MEA.

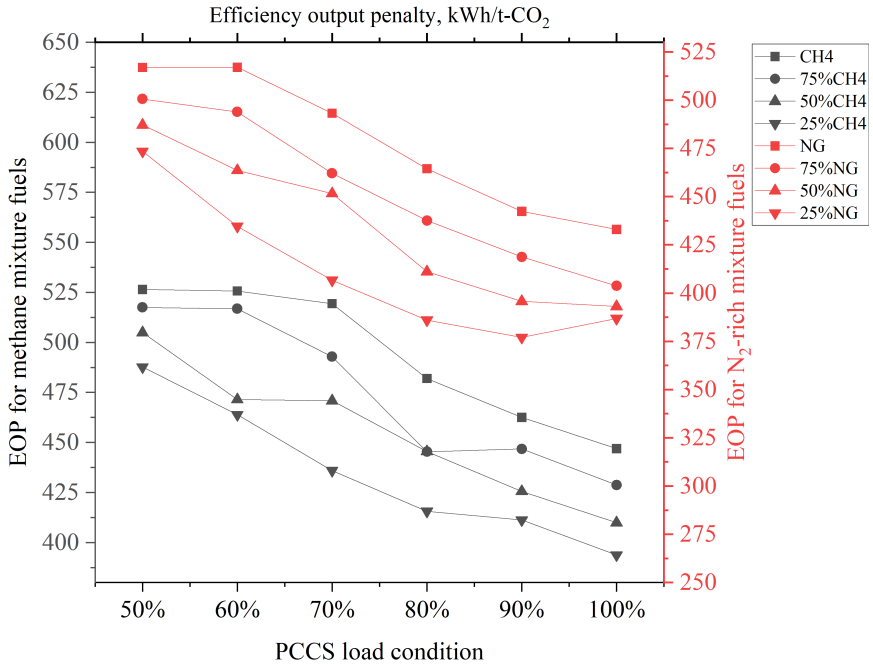

Figure 5.33: Efficiency output penalty of CCGT using different fuels and operating PCCS using AMP-PZ.

amount of CO_2 emitted per kWh of power produced by the CCGT, relative emissivity compares the emission performance of a reference power plant. Figure 5.34 & Figure 5.35 show the specific emissions and relative emissivity respectively for the reference CCGT operating with different fuel compositions integrated with PCCS using solvents under variable load conditions [131].

Due to minor differences in power production when using MEA and AMP-PZ solvents, the specific emissions and relative emissivity remain the same for both cases. However, as power production in

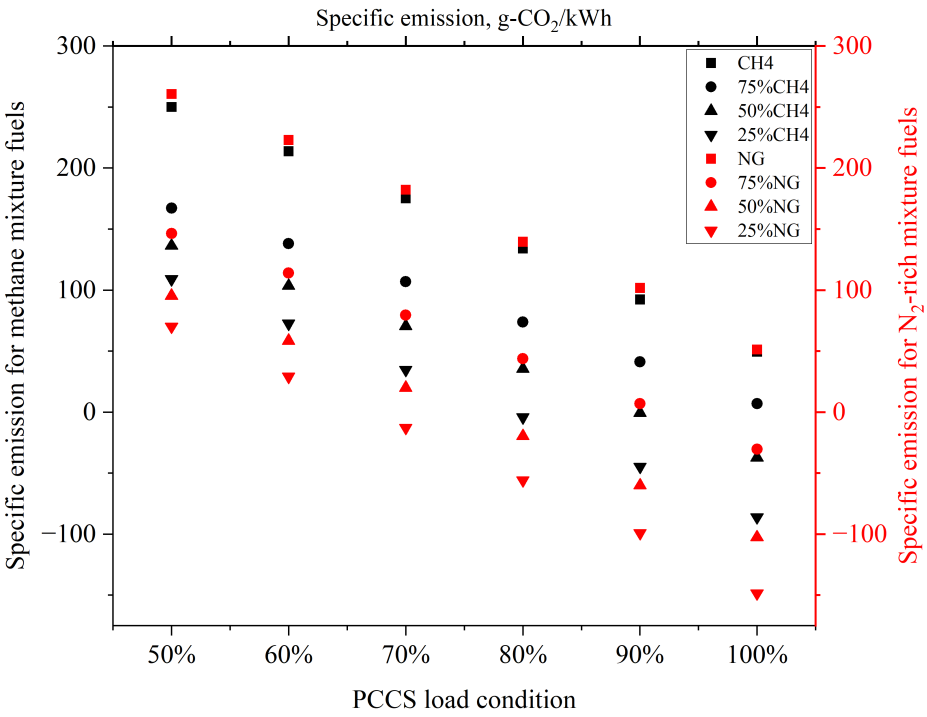

Figure 5.34: Specific emission of reference case CCGT using different compositions of fuels and integrated with PCCS using solvents operating at different load conditions [131].

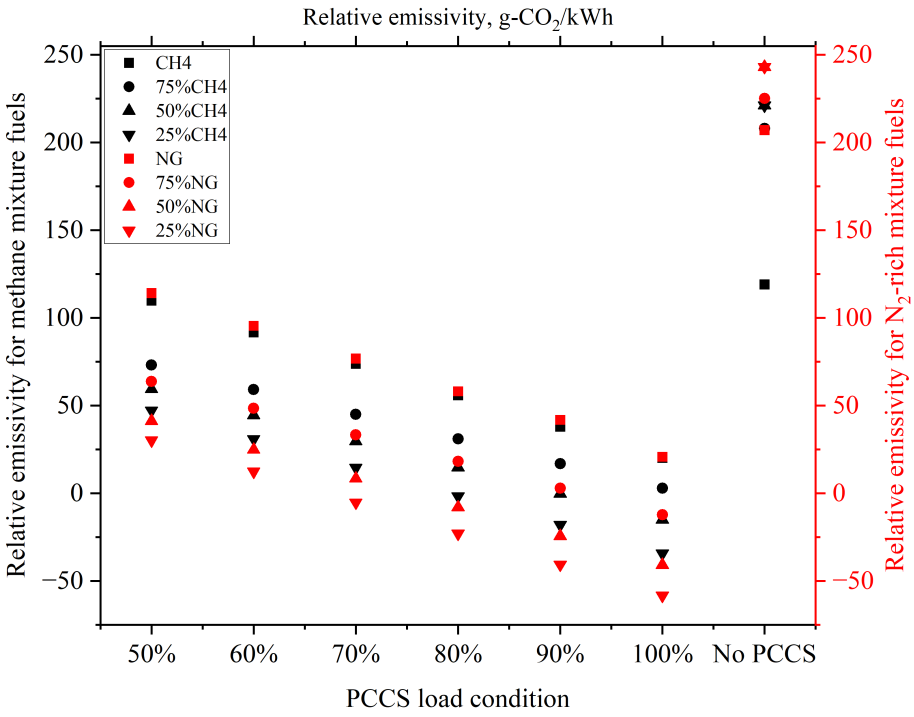

Figure 5.35: Relative emissivity of reference case CCGT using different compositions of fuels and integrated with PCCS using solvents operating at different load conditions [131].

the steam cycle increases under variable PCCS load conditions, the CO_2 emitted into the atmosphere also increases with load, increasing specific emissions and relative emissivity. This indicates that PCCS

consumes more energy and steam than required, which shows inefficiency in energy utilisation. Hence, the utilisation of PCCS at its maximum capacity provides higher energy efficiency than variable load conditions. Compared with relative emissivity, CCGT without PCCS shows higher emissivity, which is the expected outcome due to lack of emission control. In this case, the flue gases of methane and its blends show better performance compared to N_2-rich fuel blends, as specific emissions and relative emissivity are lower. Since the CO_2 capture rate is constant in PCCS, the CCR for variable load conditions remains the same for all fuel compositions used. CO_2 emission index calculated with generated CO_2 and heat input by fuel for all fuels used in the CCGT as in Figure 5.36 shows the increase in the use of energy by PCCS according to the fuel used. An increase in the proportion of syngas in the fuel increases the CO_2 intensity of flue gas produced, which increases the CO_2 emission index. Regardless of the changes in PCCS load, the emission index remains the same for the fuel used.

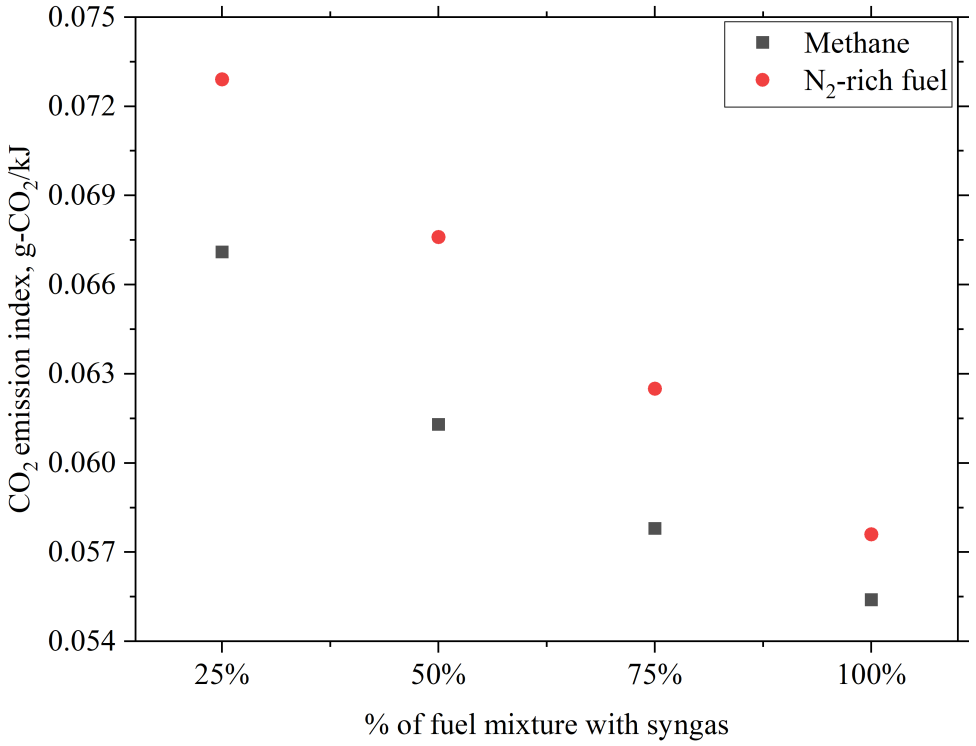

Figure 5.36: CO_2 emission index of CCGT using different fuel compositions integrated with PCCS.

Since PCCS has a CO_2 removal efficiency of 90%, CO_2 captured and CO_2 emitted as in Figure 5.37 & Figure 5.38 are the same under different CCR for both solvents used. The higher value of CO_2 captured under full load conditions indicates that the PCCS operates efficiently by reducing emissions under energy penalties. The integration of HRSG and DHN with CCGT improved the amount of CO_2 avoided by eliminating the need for auxiliary fuel to supply steam to DHN and PCCS. The increase in CO_2 avoided as in Figure 5.39 shows that the HRSG optimizes the steam to both the PCCS and DHN as well as effective CO_2 capture is performed in the PCCS. As the energy penalty is a consequence of this high performance in CO_2 capture, reducing emissions is an important factor to consider in this process. Figure 5.40 illustrates the calculated SPECCA of CCGT using different composition of fuels. The SPECCA values for 100% methane and N_2-rich natural gas are higher than those for syngas-blended fuels. The SPECCA decreases with

an increase in the proportion of syngas gas in fuel, indicating that the primary energy consumption for the capture process has reduced with CO_2 emission and an increase in energy efficiency. At full load conditions, the SPECCA for fuels with varying syngas compositions ranges from 1.39 kWh/kgCO_2 to 1.11 kWh/kgCO_2. When blended fuels were introduced, the SPECCA dropped to values from 0.99 kWh/kgCO_2 to 0.62 kWh/kgCO_2, depending on the specific fuel mixture. These results show the efficiency improvements achieved by introducing syngas into the fuel blend.

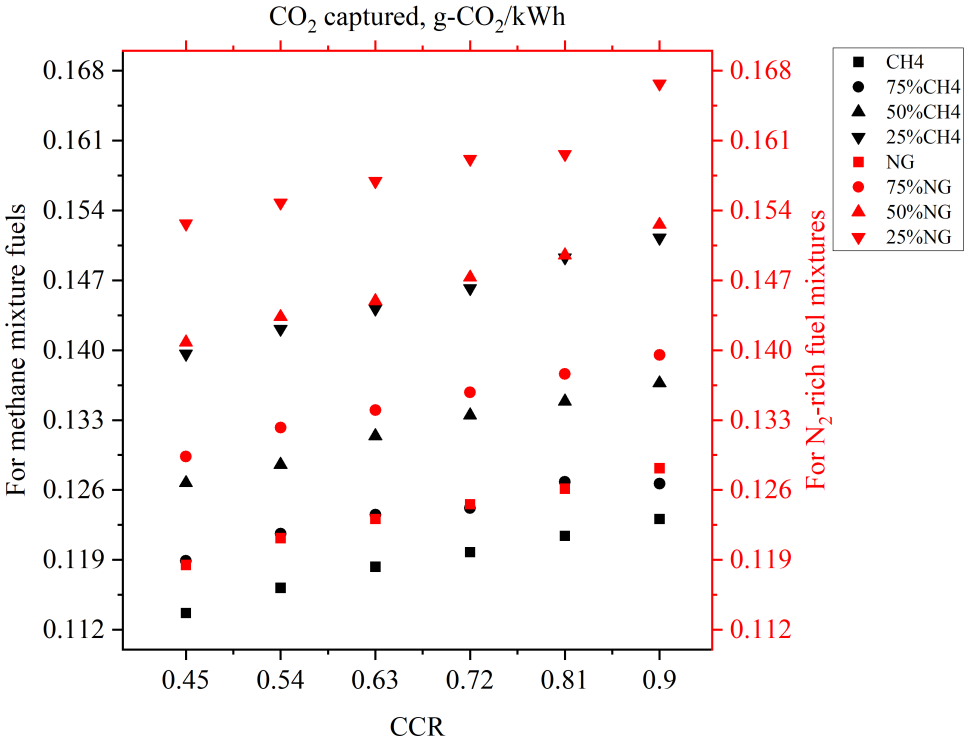

Figure 5.37: Change in captured CO_2 in gCO_2/kWH according to the carbon capture rate of PCCS.

After CO_2 captured in PCCS as in Figure 5.41, the CO_2 emission as in Figure 5.42 [131] for the given reference case CCGT with PCCS is estimated by reducing the content of CO_2 in syngas and CO_2 captured in PCCS from the generated CO_2 from fuel combustion. This means that the emission is reduced with an increase in the syngas composition in the fuel.

However, under partial load conditions such as 50% and 60%, negative CO_2 emissions were not achieved. This limitation occurs due to only a portion of the flue gases are processed by PCCS and the rest are passed into the atmosphere. At full load and 90% load conditions, the system shows promising potential for achieving negative CO_2 emissions, except when using 100% fossil fuels and methane mixture with 25% syngas. Moreover, the comparison between methane mixtures and N_2-rich mixtures shows that the N_2-rich gas performs better in achieving negative CO_2 emissions when blended with syngas. This is due to the share of CO_2 produced from the fuel being higher from syngas in N_2-rich mix.

5.3.3 Economic indicators

Economic indicators are essential to evaluate the performance of CCGT with and without PCCS, such as emissions, energy generation, and electricity production, assessment of financial feasibility, and

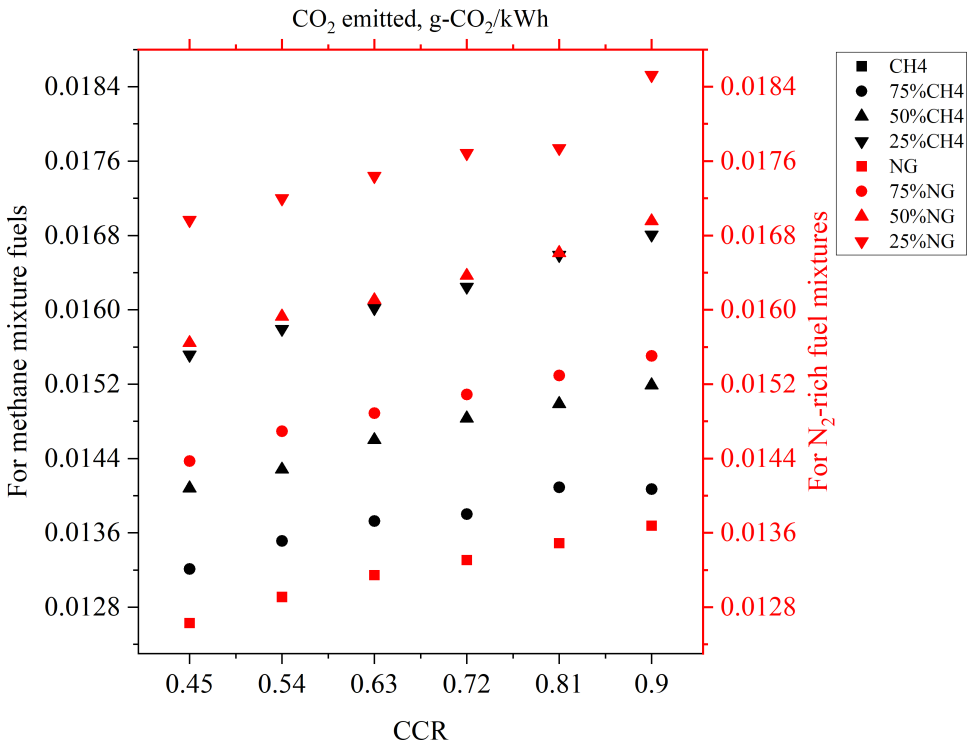

Figure 5.38: CO_2 emitted in gCO_2/kWH according to the carbon capture rate of PCCS.

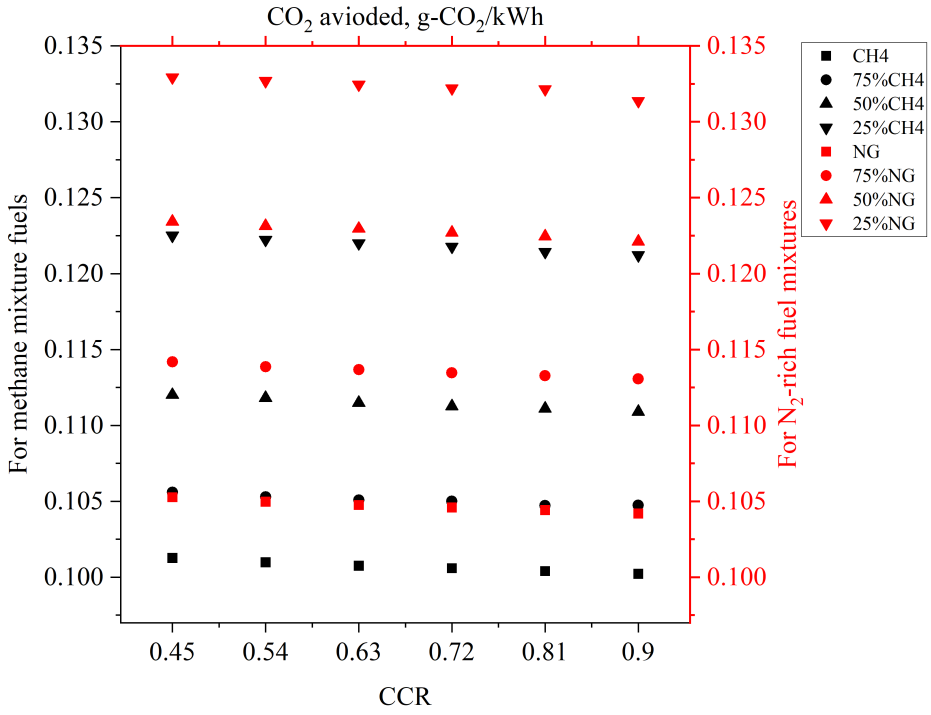

Figure 5.39: CO_2 avoided in gCO_2/kWH according to the carbon capture rate of PCCS.

influence of prices from the energy market on power plant operations. This ensures cost efficiency in achieving negative carbon emissions from the reference CCGT system. From the CO_2 emission analysis, it is apparent that operating PCCS under full load conditions offers the potential to achieve negative CO_2 emissions. Taking this into account, the SPECCA is calculated for CCGT systems using different fuel

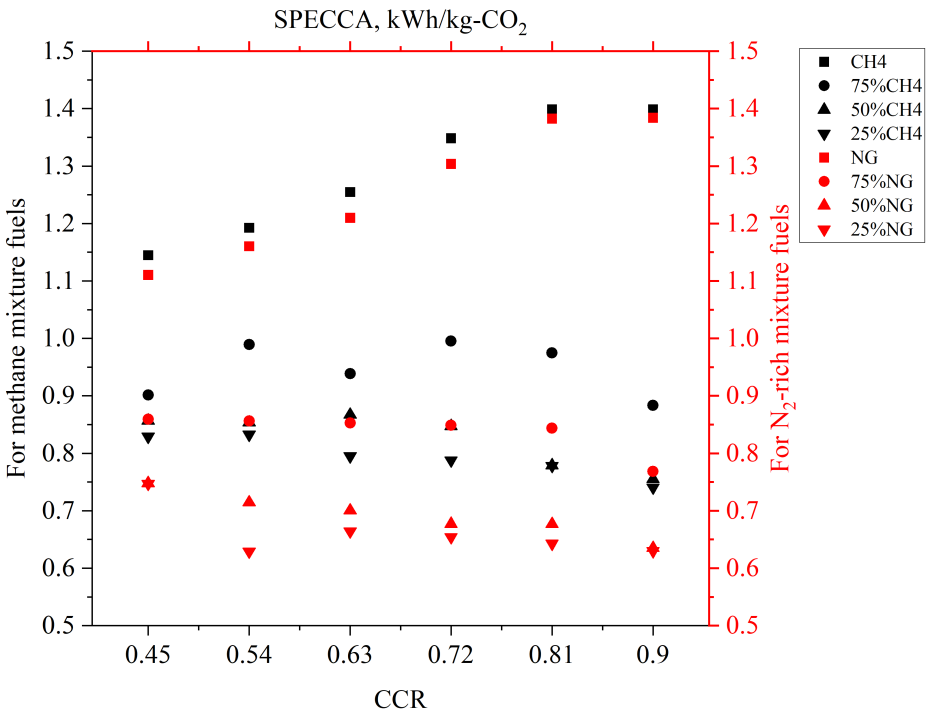

Figure 5.40: Specific Primary Energy Consumption for CO_2 Avoided of CCGT using different fuel compositions and integrated with PCCS.

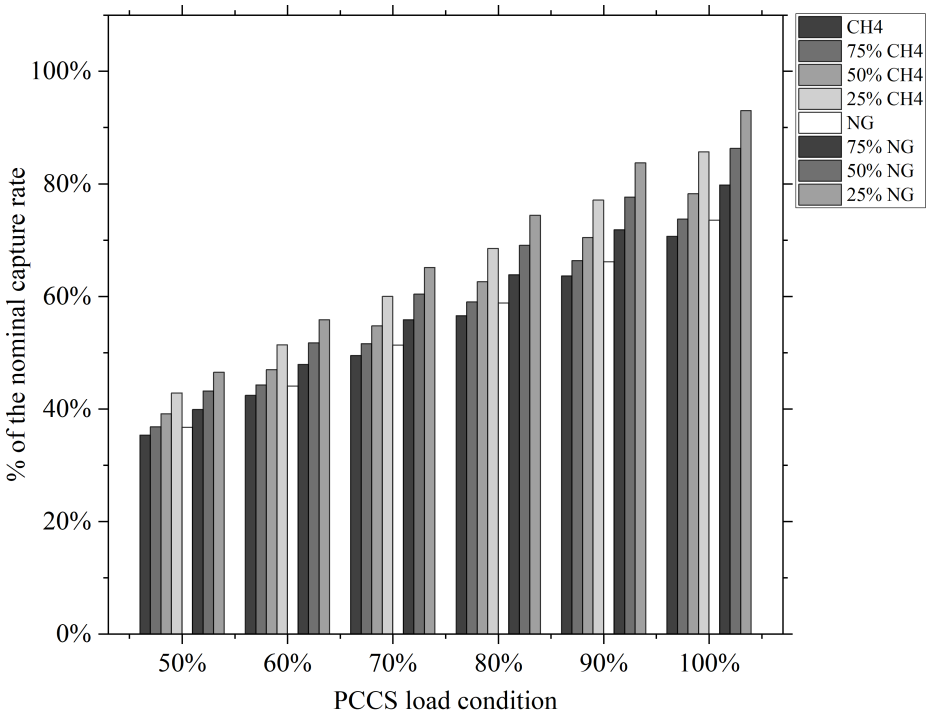

Figure 5.41: Percentage of nominal CO_2 capture rate in PCCS operated in different load condition [131].

compositions and integrated with PCCS under full load conditions, as illustrated in Table 5.3. SPECCA is calculated using Equation (3.58) with a primary energy cost of 0.1769 €/kWh referred from [135]. The calculated SPECCA cost analysis shows variations based on fuel composition. For CCGT systems using

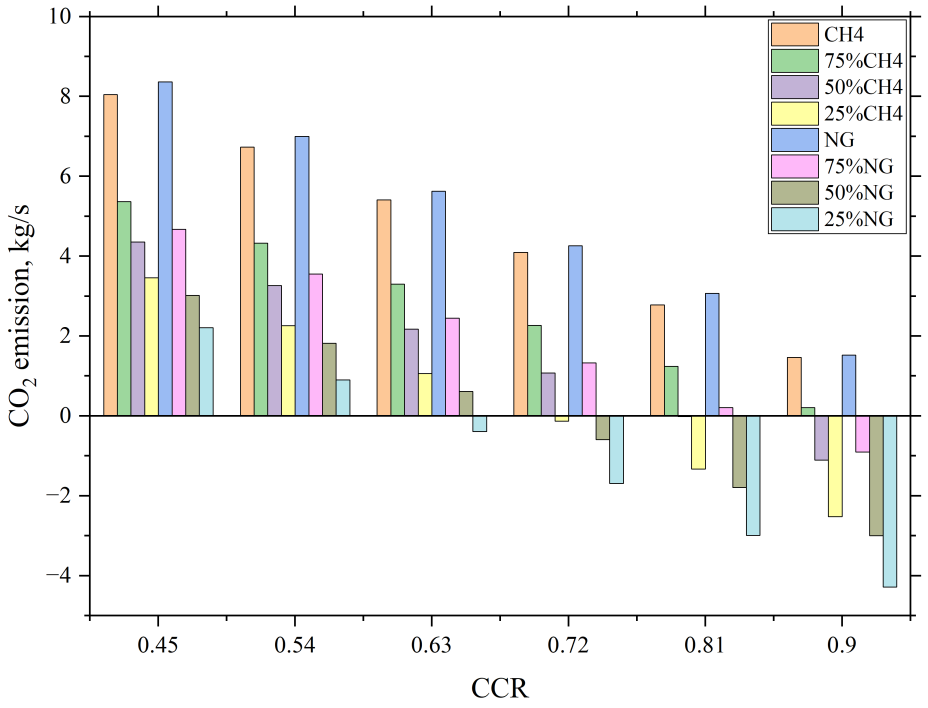

Figure 5.42: CO_2 emission from the reference case CCGT using different fuel compositions and integrated with PCCS [131].

100% fossil fuels, the SPECCA cost for methane is calculated to be 202.53 €/t-CO_2 and 196.42 €/t-CO_2 for N_2-rich gas. When syngas is blended with fossil fuels, the cost of SPECCA gradually decreases as the proportion of syngas increases in the fuel mix. The cost of SPECCA for blended fuels ranges from 159.43 €/t-CO_2 to 132.16 €/t-CO_2, showing cost reductions compared to fossil fuel use. This shows that a lower primary energy is required for the carbon capture process with reduced operational costs, which improves the energy efficiency and economic viability of the PCCS. These results emphasize the potential of using syngas as a fuel to improve the performance and cost effectiveness of CCGT systems integrated with PCCS.

Table 5.3: SPECCA cost analysis for CCGT with PCCS at full load condition

Fuel composition	SPECCA, €/t-CO_2
Methane 100%	202.53
Methane 75% + 25% syngas	159.43
Methane 50% + 50% syngas	151.59
Methane 25% + 75% syngas	146.68
N_2-rich gas 100%	196.42
N_2-rich gas 75% + 25% syngas	151.99
N_2-rich gas 50% + 50% syngas	132.30
N_2-rich gas 25% + 75% syngas	132.16

The assumptions for calculating the LCOE for a CCGT integrated with PCCS were determined as part of the POLNOR project on the 'Negative CO_2 Power Plant'. The LCOE for CCGT without PCCS and with PCCS using MEA and AMP-PZ are calculated as in Table 5.4. The assumptions are considered for an operational lifetime of 25 years of CCGT with an annual operation of 8000 hours, a real discount rate of 7% referred to from [136]. The annual CCGT fuel price is already included in the O& M cost considered for the calculation. With the assumed data and using Equation (3.59), the LCOE for CCGT without PCCS is estimated to be €64.33/MWh. When included with PCCS, the calculated LCOE is €91/MWh and €95/MWh for MEA and AMP-PZ, respectively [137]. For the real discount rate considered, the calculated LCOE of CCGT is aligned with the projected LCOE sensitivity of IEA [138], which states the stability and competitiveness of the cost of CCGT at a high discount rate. This LCOE highlights the economic feasibility of integrating PCCS technology with CCGT systems.

Table 5.4: Assumptions and calculated LCOE for CCGT with and without PCCS [137]

Parameter	Unit	without PCCS	with PCCS using MEA	with PCCS using AMP-PZ
Capital construction costs	M€/year	22.3	41.5	37.7
O&M cost	M€/year	54.29	64	94.25
LCOE	**€/MWh**	**64.33**	**91**	**95**

Based on the electricity output, heat supply and emission from the power plant, the revenue and expenses of the power plant are calculated. To calculate the income from electricity sales and heat sales of the CCGT using different fuels, the market price of electricity sales is 234.37 PLN/MWh referred from Polskie Sieci Elektroenergetyczne [139] and heat supply price from CHP is 15.95 PLN/GJ referred from Polish Energy Regulatory Office [140]. Figure 5.43 & Figure 5.44 show the income from electricity sales and heat sales from the CCGT using different fuel compositions and integrated with PCCS using different load conditions. When CCGT is operated without integration of PCCS, it generates an electricity output of 128.43 MW, which is supplied to the grid, along with a heat output of 54 MW to the DHN. Therefore, the income generated by the CCGT without PCCS is 94,041.58 PLN/h from electricity sales and 2,264.25 PLN/h from heat sales. When integrated with PCCS, the income from electricity sales ranges from 84,808 PLN/h to 76,094 PLN/h and from heat sales varies between 2,264 PLN/h and 1,174 PLN/h, depending on the fuel type and PCCS load conditions. As described previously, during the low load condition, more steam is utilized in the steam cycle, which increases the electricity output from the CHP and increased heat production for DHN, which results in higher income for the CCGT. However, this has a risk of emitting higher levels of CO_2 into the atmosphere. The cost of CO_2 emissions of CCGT is included into this analysis. The emission cost calculated as in Figure 5.45 using a CO_2 price of 68.71 €/t-CO_2 referenced from [141] varies based on operational conditions. Without PCCS, CO_2 emission costs range from 4,417.28 €/h to 3,618.80 €/h and with PCCS the costs decrease ranging between 2,069.13 €/h and 51.90 €/h depending on the load and fuel composition. The emission prices are not applicable for CCGT using fuel mixtures with syngas, which achieved negative emissions. Thus, the carbon emission prices are reduced or neglected for CCGT when

integrated with PCCS. The total income of the power plant is calculated after deducting CO_2 emission costs and fuel expenses. In the case of estimating the price of the fuel, it is assumed that the prices of methane and N_2 rich natural gas share the same price category as natural gas. The price of natural gas is estimated as 234.37 PLN/MWh referred from Towarowa Giełda Energii S.A. gas price [142]. However, the price estimation for syngas from plasma gasification of sewage sludge remains uncertain due to its pilot-scale status. Based on these inputs, the total income for CCGT using methane and N_2 rich natural gas is calculated to be 18,705.81 PLN/h and 18,083.16 PLN/h, respectively.

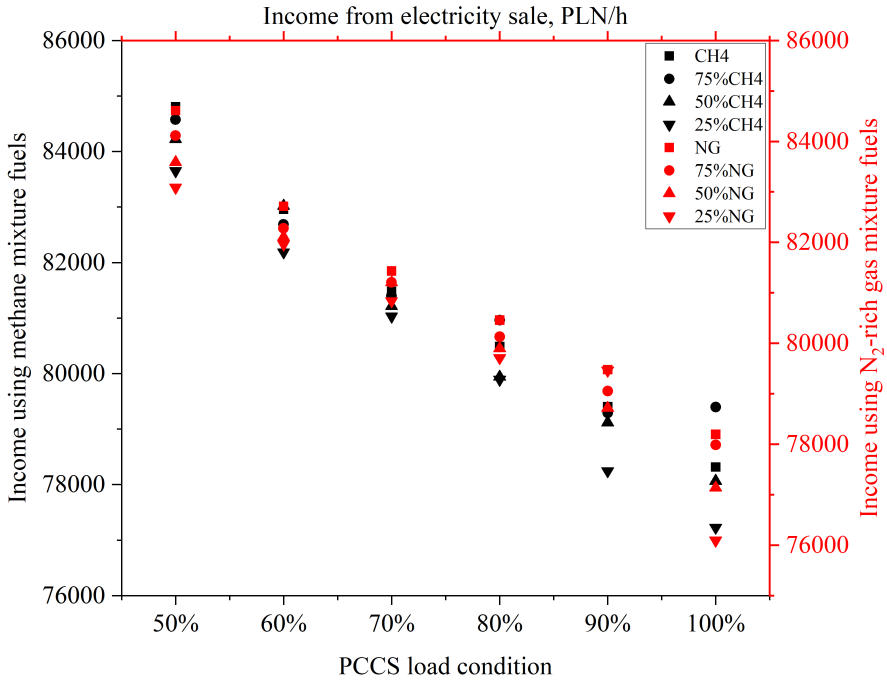

Figure 5.43: Income from electricity sale of CCGT using different fuel compositions.

5.4 Performance CCGT without DHN with CO_2-neutral fuels and CCS installation

An alternative approach was conducted to measure the performance analysis of CCGT without integration with DHN. In this configuration, the LP steam extraction to DHN was closed and the DHN economizers in the HRSGs were removed. The modified model as illustrated in Figure 5.46 was integrated with a developed PCCS and performance was evaluated. For a comparative study, pure methane and methane blends with syngas in 75% and 50% proportions were used as fuel for CCGT and simulations were performed. The PCCS results in this approach were consistent with those of the CCGT integrated with DHN, as the same quantity of flue gas and the CO_2 content was treated in the PCCS. However, the absence of DHN changed the performance of CCGT, as shown in Table 5.5, Table 5.6 & Table 5.7 for using fuels pure methane 75% methane with syngas and 50% methane with syngas respectively some of the crucial energy indicators.

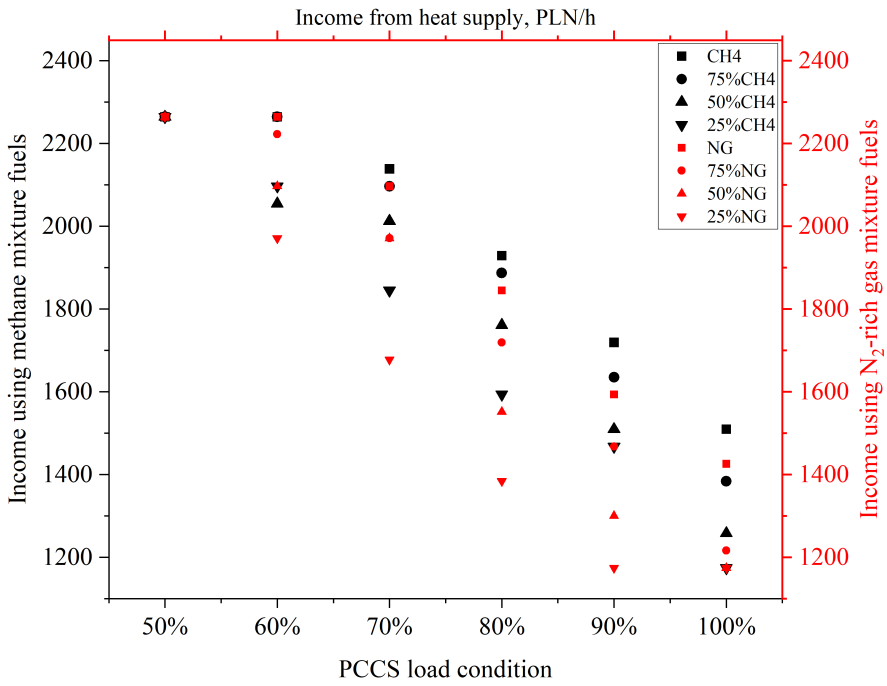

Figure 5.44: Income from heat sale of CCGT using different fuel compositions.

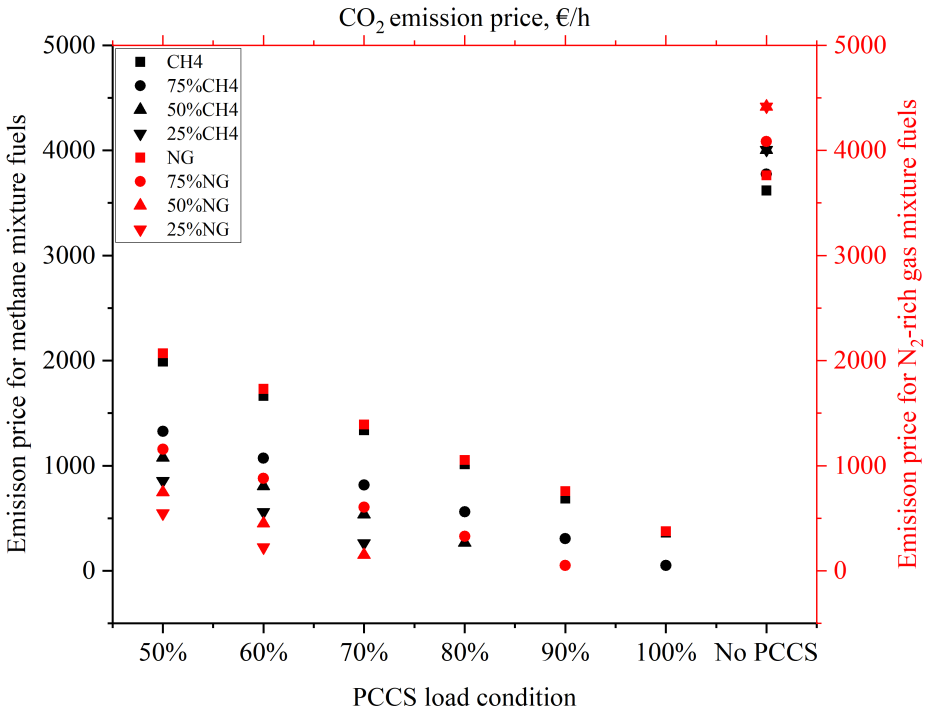

Figure 5.45: CO_2 expenses for CCGT using different fuel compositions as per CO_2 emission price.

Shutting down the steam supply to DHN made additional steam available for power generation, leading to an increase in the gross power output of the CCGT without DHN compared to the system with DHN. Despite this, the power reduction due to steam extraction was significantly higher in CCGT without DHN as shown in Figure 5.47 with the comparison of CCGT with and without DHN using methane mixture fuels. The higher thermal energy recovery achieved through DHN integration cannot be obtained in PCCS steam

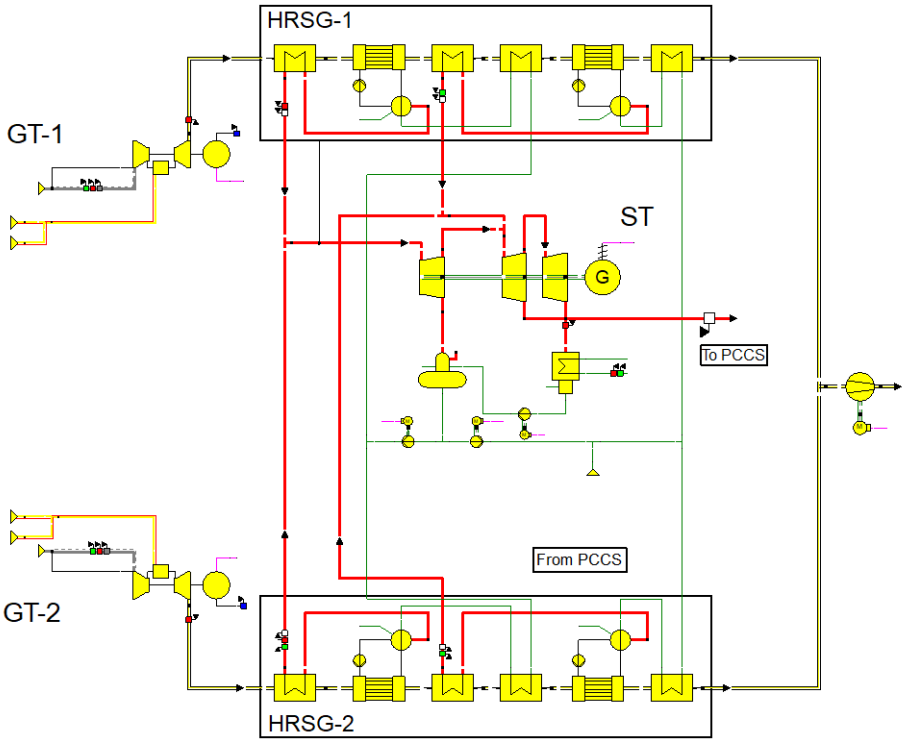

Figure 5.46: Developed model of CCGT without DHN and steam extraction to PCCS.

Table 5.5: Performance of CCGT using methane integrated with PCCS and without DHN

Parameter	Unit	100%	90%	80%	70%	60%	50%
Gross energy efficiency	%	50.3	50.71	51.13	51.55	51.97	52.39
Net electricity efficiency	%	40.59	41.54	42.49	43.44	44.39	45.34
Gross power output	MW	132.83	133.93	135.03	136.14	137.24	138.35
Net power output	MW	107.18	109.69	112.2	114.71	117.23	119.74
Steam cycle power generation	MW	32.11	33.21	34.32	35.42	36.53	37.63
Steam extraction power reduction	MW	11.05	9.95	8.85	7.74	6.64	5.53
EOP	kWh/tCO_2	530.28	530.24	530.49	530.25	530.24	530.65

extraction, since the thermal energy is completely utilised in the reboiler for solvent regeneration, leaving no opportunity for thermal energy recovery. The presence of DHN enabled efficient thermal energy recovery, which contributed to overall system performance. Moreover, the removal of DHN economizers from HRSGs results in thermal inefficiencies and deficient utilisation of waste heat. Another notable parameter is the increased EOP, which is higher than the system with DHN. This indicates that the absence of DHN limits the overall performance of the CCGT.

For the same carbon capture ratio used in the PCCS of CCGT with DHN, the specific emission of the CCGT without DHN is calculated and compared as illustrated in Figure 5.48. Specific emissions are calculated based on the CO_2 emitted and the power generated, showing that CCGT without DHN achieves lower values compared to the system with DHN. This suggests improved performance in carbon capture

Table 5.6: Performance of CCGT using 75% methane with syngas integrated with PCCS and without DHN

Parameter	Unit	100%	90%	80%	70%	60%	50%
Gross energy efficiency	%	50.12	50.55	50.98	51.43	51.86	52.3
Net electricity efficiency	%	40.91	41.32	42.72	43.27	44.24	45.22
Gross power output	MW	132.35	133.5	134.65	135.81	136.96	138.11
Net power output	MW	108.04	109.13	112.81	114.27	116.85	119.42
Steam cycle power generation	MW	31.63	32.78	33.94	35.09	36.24	37.39
Steam extraction power reduction	MW	11.53	10.38	9.23	8.07	6.92	5.77
EOP	kWh/tCO_2	491.02	521.01	493	521.45	521.17	521.95

Table 5.7: Performance of CCGT using 50% methane with syngas integrated with PCCS and without DHN

Parameter	Unit	100%	90%	80%	70%	60%	50%
Gross energy efficiency	%	49.85	50.31	50.77	51.24	51.7	52.16
Net electricity efficiency	%	40.00	41.00	41.89	43.02	44.03	45.04
Gross power output	MW	131.64	132.87	134.09	135.31	136.53	137.76
Net power output	MW	105.61	108.28	110.64	113.61	116.28	118.94
Steam cycle power generation	MW	30.92	32.15	33.37	34.59	35.82	37.04
Steam extraction power reduction	MW	12.24	11.01	9.79	8.57	7.35	6.12
EOP	kWh/tCO_2	509.04	508.77	516.32	509.29	508.86	509.34

efficiency and better utilization of steam in PCCS. Despite these differences, the relative emissivity and CO_2 emission index remain the same between both configurations, since the fuel type, heat input, and PCCS performance in terms of CO_2 captured and generated are same in both cases. Additionally, slight differences are observed in CO_2 captured, emitted, and avoided when comparing the systems. For example, as shown in Figure 5.49 of CO_2 captured & Figure 5.50 of CO_2 emitted and CO_2 avoided for CCGT without DHN, using pure methane the system with DHN achieves 0.1231 gCO_2/kWh compared to 0.1228 gCO_2/kWh without DHN. This trend continues across different fuel compositions and capture ratios, with the DHN-integrated system capturing more and emitting less CO_2 per kWh. However, under lower load conditions, the system without DHN shows better performance in CO_2 avoided.

For CCGT operating without a DHN configuration, the SPECCA is calculated for various fuel types such as pure methane, 75% methane blended with syngas, and 50% methane blended with syngas. SPECCA values were calculated to be 1.34 kWh/kg-CO_2, 1.15 kWh/kg-CO_2, and 1.16 kWh/kg-CO_2 respectively and SPECCA costs were estimated to be 237.25 €/t-CO_2, 202.84 €/t-CO_2, and 204.91 €/t-CO_2, which are higher compared to the configuration with DHN. Without income from heat sales, the income from electricity sales for CCGT without DHN is shown in Figure 5.51 for different PCCS load conditions. By reducing carbon costs and fuel expenses, the net income for the CCGT without DHN is calculated as 35,444.76 PLN/h under no PCCS conditions and 36,282.1 PLN/h under full PCCS load condition, with a net gain of 441.09

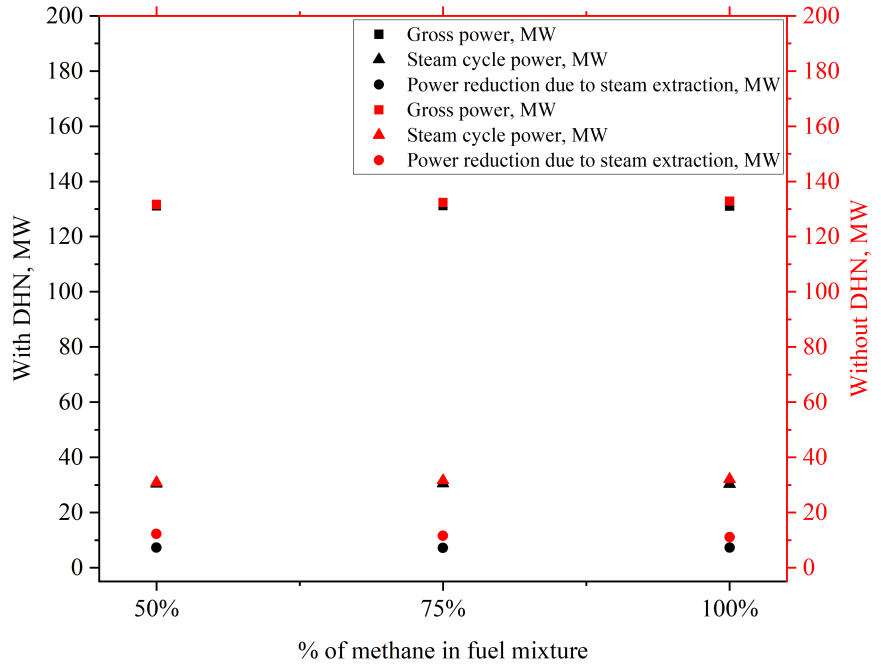

Figure 5.47: Comparison of CCGT parameters with and without DHN using methane blended fuels and integrated with PCCS at different capture ratio.

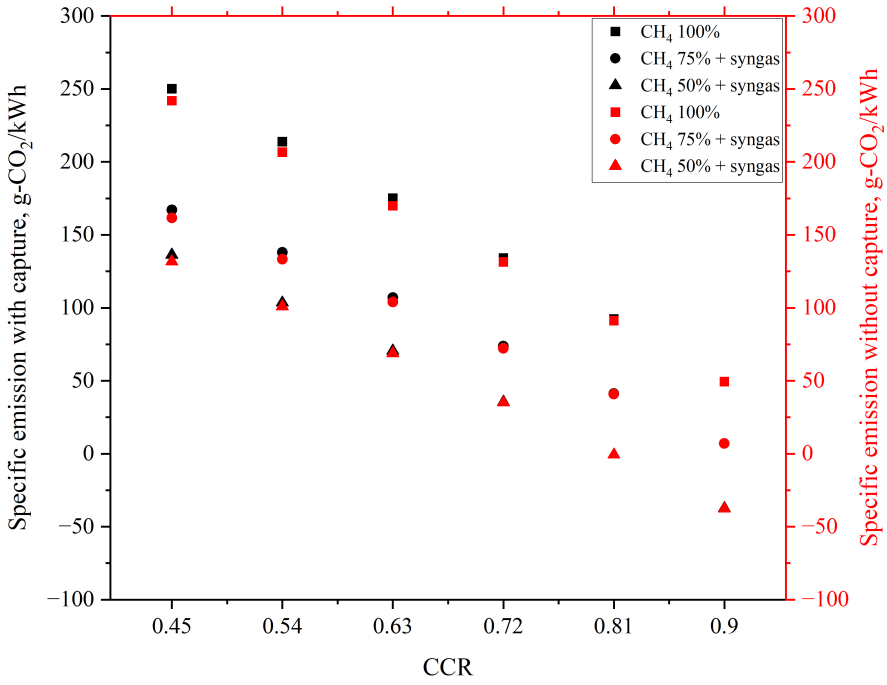

Figure 5.48: Comparison of Specific emission of CCGT with and without DHN using methane blended fuels and integrated with PCCS at different capture ratio.

PLN/h compared to the DHN-integrated configuration. CCGT without DHN shows better performance in energy and economic indicators, such as higher electricity sales and net income, except in terms of thermal energy recovery and SPECCA costs. From an environmental perspective, the DHN-integrated CCGT remains advantageous due to its higher CO_2 capture efficiency.

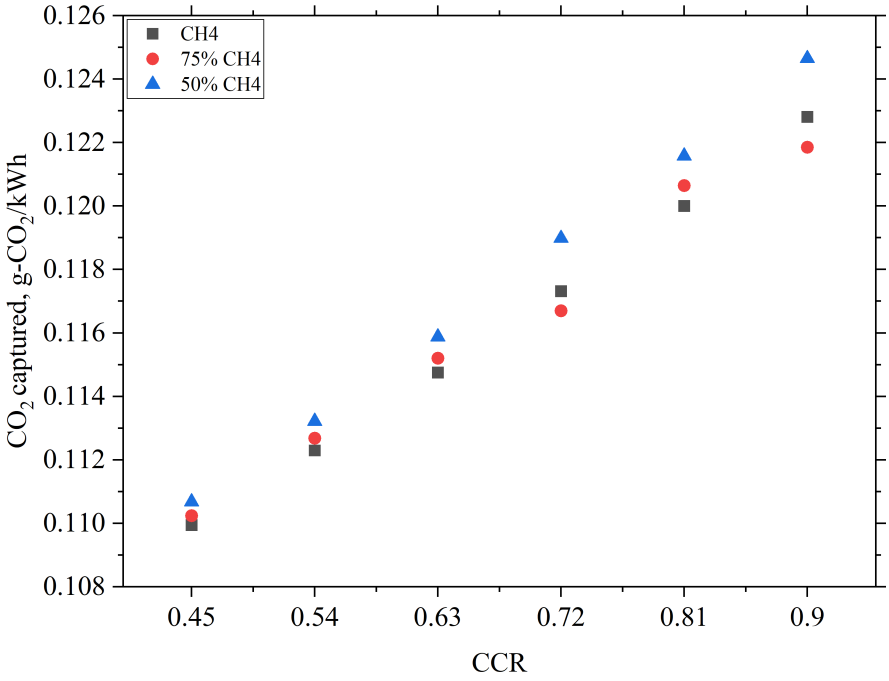

Figure 5.49: CO_2 captured in g-CO_2/kWh in CCGT without DHN using methane blend fuels and integrated with PCCS at different capture ratio.

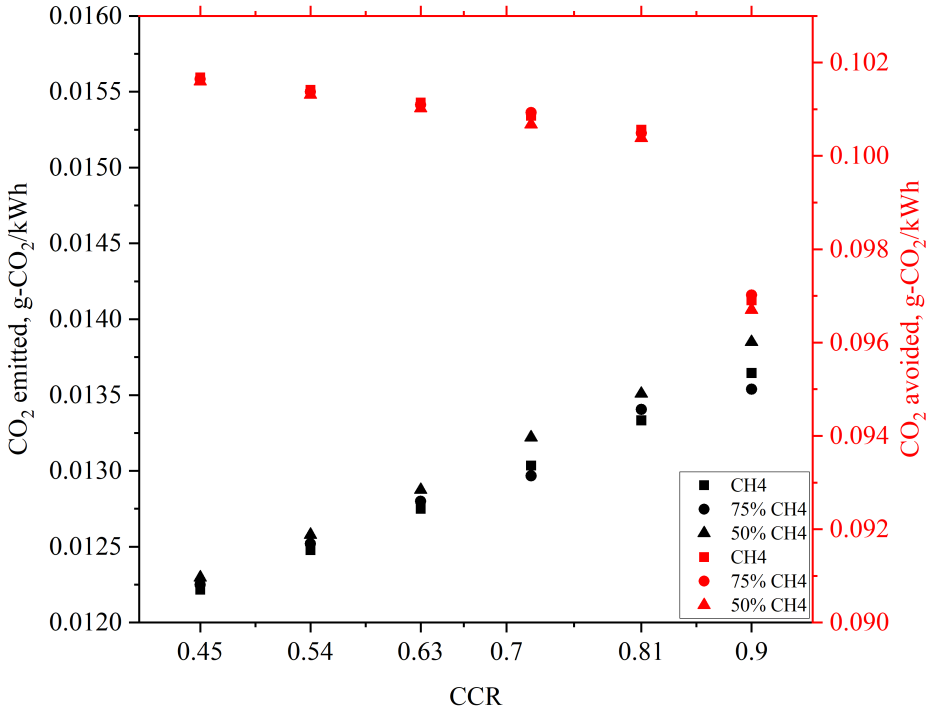

Figure 5.50: CO_2 emitted and CO_2 avoided in CCGT without DHN using methane blended fuels and integrated with PCCS at different capture ratio.

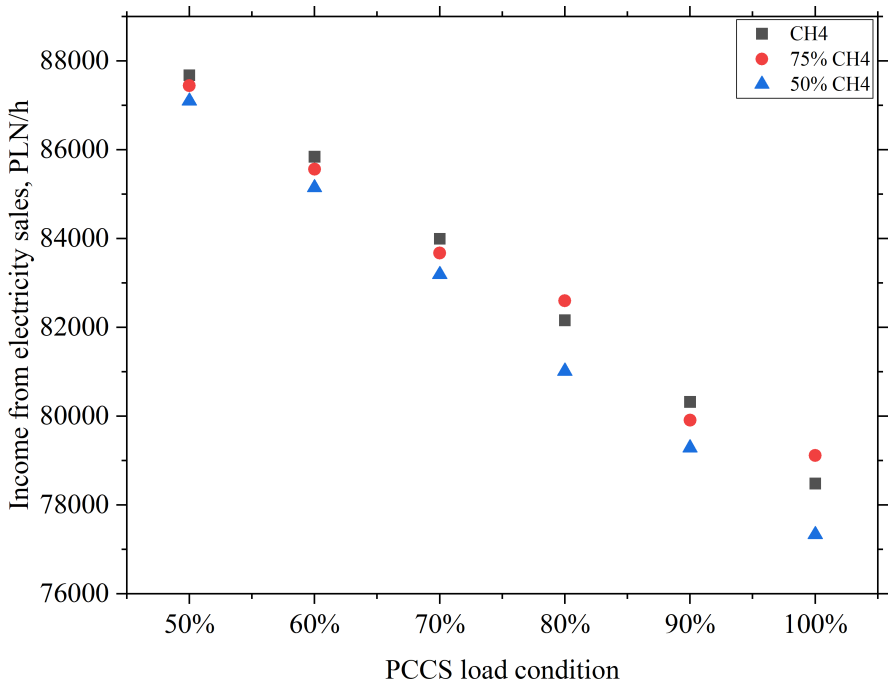

Figure 5.51: Income from electricity sales of CCGT without DHN using methane blended fuels and integrated with PCCS at different load conditions.

5.5 Opportunities and Limitations

An analysis was conducted to evaluate the feasibility of achieving negative emissions in a CCGT system operating entirely on syngas, without blending with fossil fuels. The performance of the integrated PCCS was assessed by gradually reducing its load from 100% to 60%, focusing on energy, environmental, and economic indicators. Figure 5.52 illustrates the gross and net power generation of the CCGT system using syngas with different DHN heat supply integrated with PCCS under varying load conditions.

Similar to the economic analysis for blended fuels, the gross power output of the CCGT was maintained within a range of 130 to 131 MW. However, under PCCS load conditions of 100% and 90%, the steam extraction for the PCCS reboiler limited the DHN heat supply to 28 MW, reducing the gross power output to below 130 MW. Therefore, the gross energy efficiency of the CCGT ranged from 59.13% to 66.3%, while the net power efficiency fluctuated between 38.8% and 42.29% as shown in Figure 5.53. Using syngas as fuel, the gas turbines consumed a mass flow rate of 15.14 kg/s to maintain power generation. However, steam extraction from the steam cycle for PCCS reboiler operations, as shown in Figure 5.54, caused power generation in the steam cycle to vary between 10.21 MW and 7.29 MW, depending on load conditions. The PCCS power consumption ranged from 16.54 MW at 100% load to 9.93 MW at 60% load. Figure 5.55 presents the EOP of the CCGT using syngas with DHN integrated with PCCS under varying load conditions, which ranged from 416.54 to 387.54 kWh/t-CO_2. At 80% PCCS load, the EOP reached its lowest value of 371.42 kWh/t-CO_2, indicating optimal operating conditions and effective heat integration between the PCCS and the DHN system. At higher and lower load conditions, the energy consumption increases due to higher

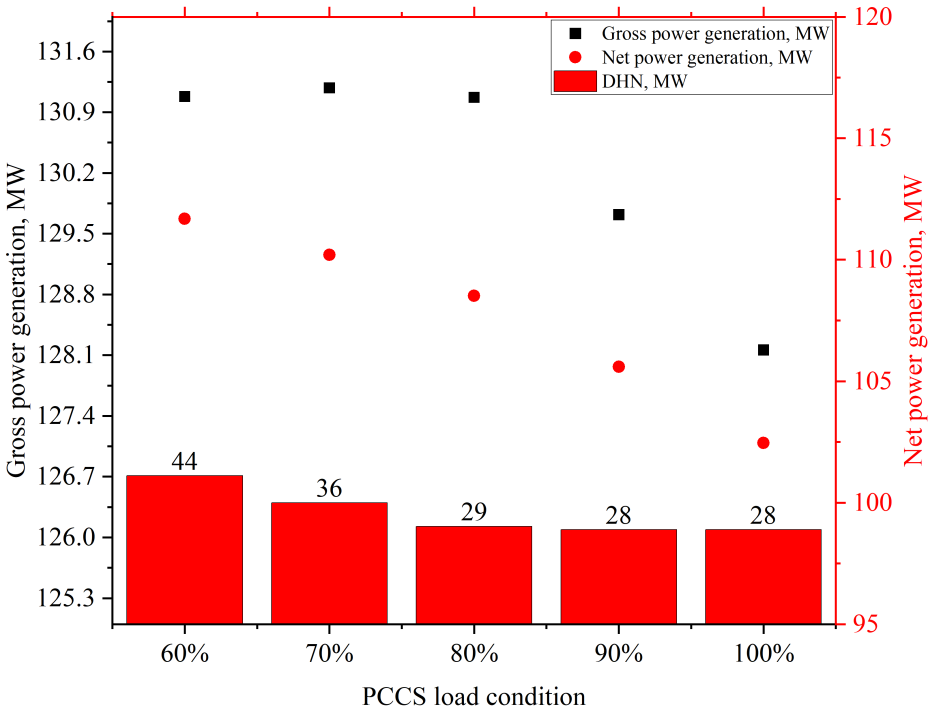

Figure 5.52: Gross and Net power generation of CCGT using syngas with different DHN heat supply and integrated with PCCS at different load conditions.

energy demand at full load and reduced heat recovery efficiency at lower loads. These results show that the CCGT system integrated with PCCS maintains efficient performance.

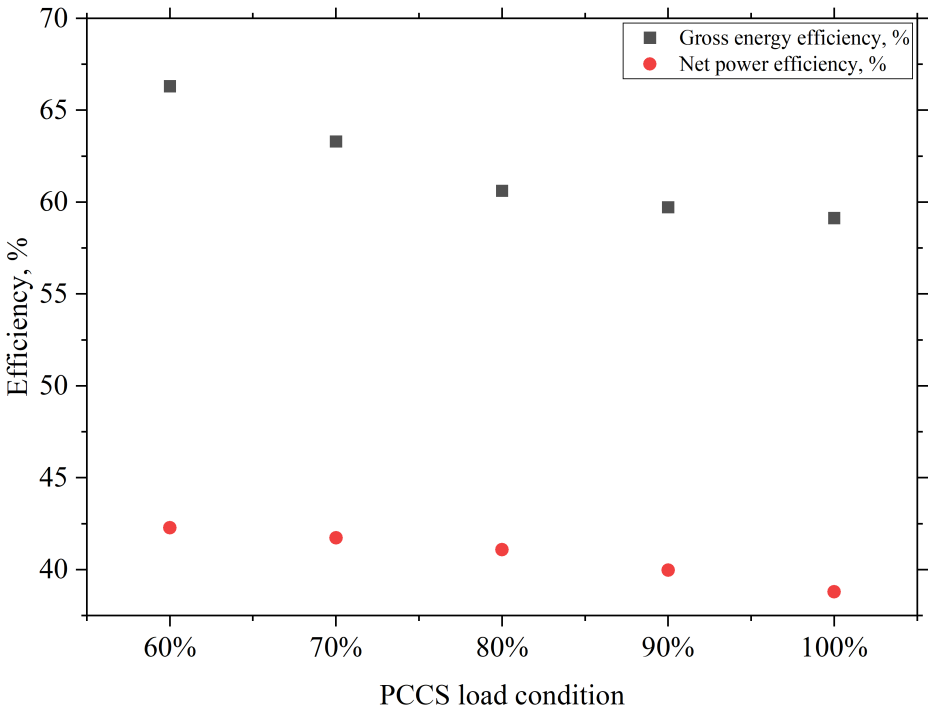

Figure 5.53: Gross energy and Net power efficiency of CCGT using syngas with DHN and integrated with PCCS at different load conditions.

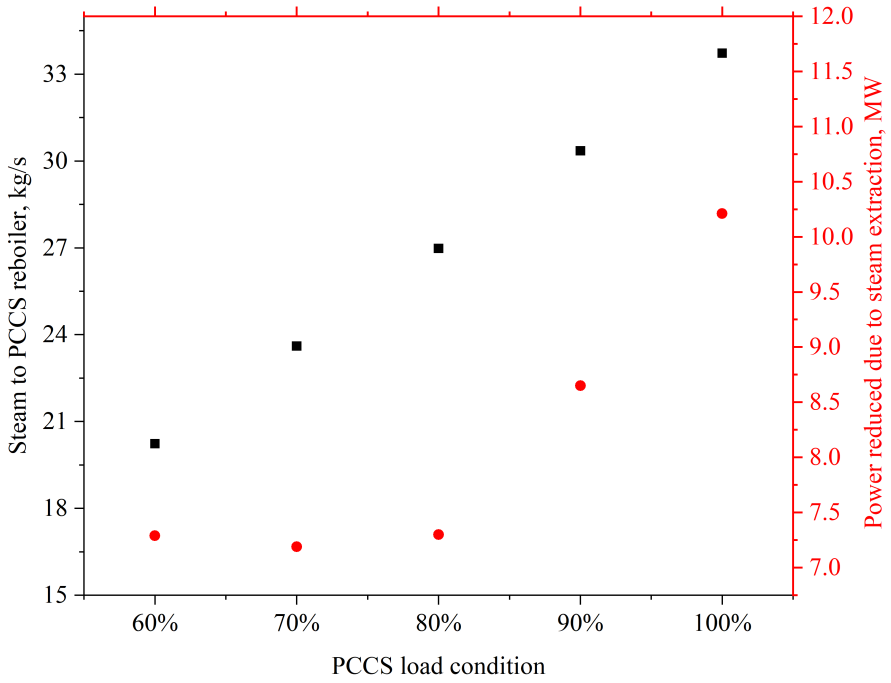

Figure 5.54: Steam supply to PCCS reboiler at different load conditions to treat flue gas from using syngas fuel in CCGT and power reduced in steam cycle due to it.

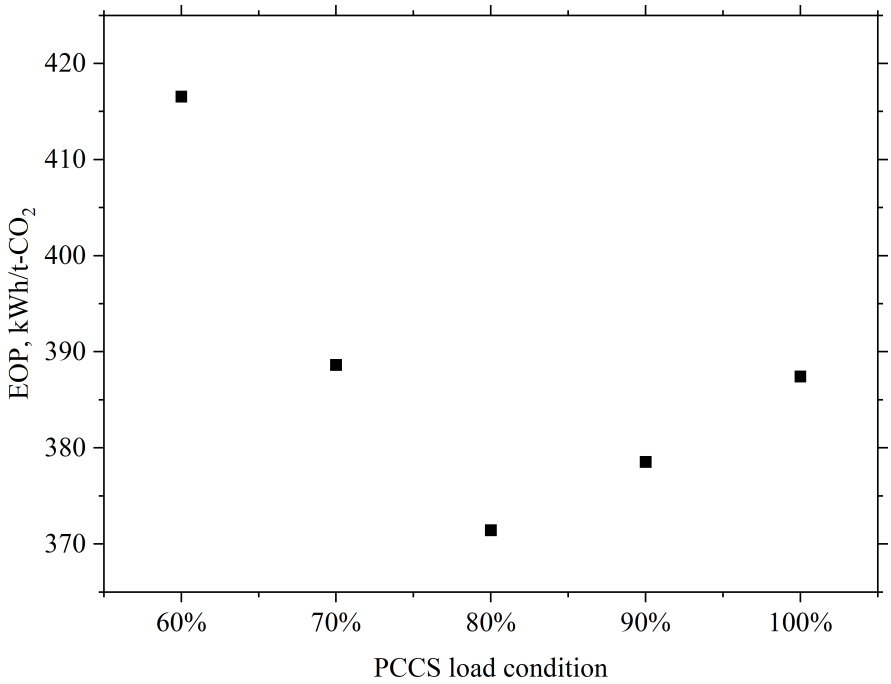

Figure 5.55: Efficiency output penalty of CCGT using syngas with DHN and integrated with PCCS at different load conditions.

In the context of BECCS, CO_2 emissions resulting from the combustion of syngas in CCGT are analyzed under PCCS in variable load conditions as shown in Figure 5.56. Without PCCS, CO_2 emissions are estimated at 20.69 kg/s. However, with the integration of PCCS under different load conditions, the

system achieves negative emissions. This reduces specific emissions and relative emissivity, which are lower compared to blended fuels as illustrated in Figure 5.57.

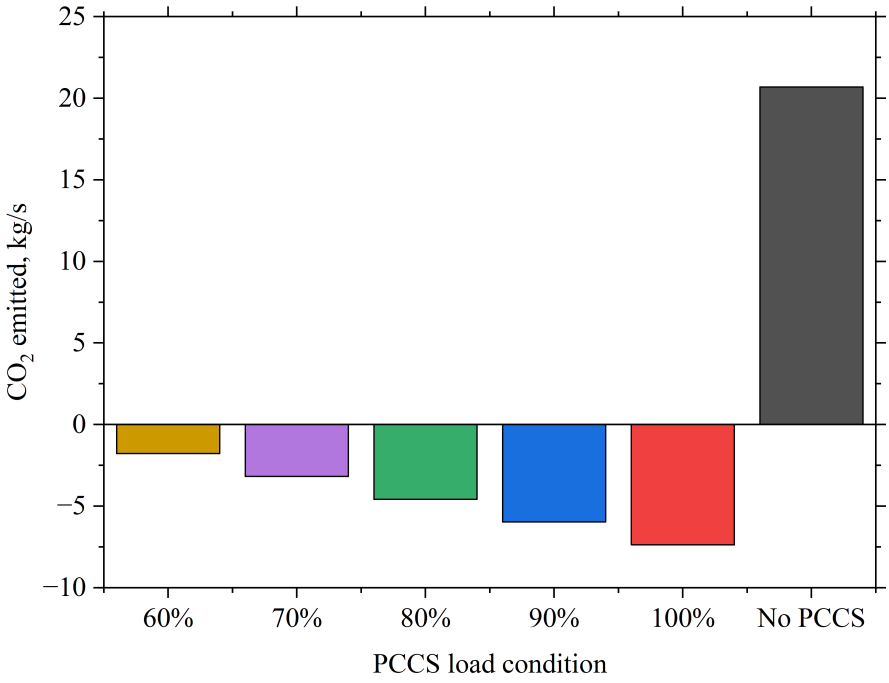

Figure 5.56: CO_2 emission from CCGT using syngas integrated with PCCS under different load conditions.

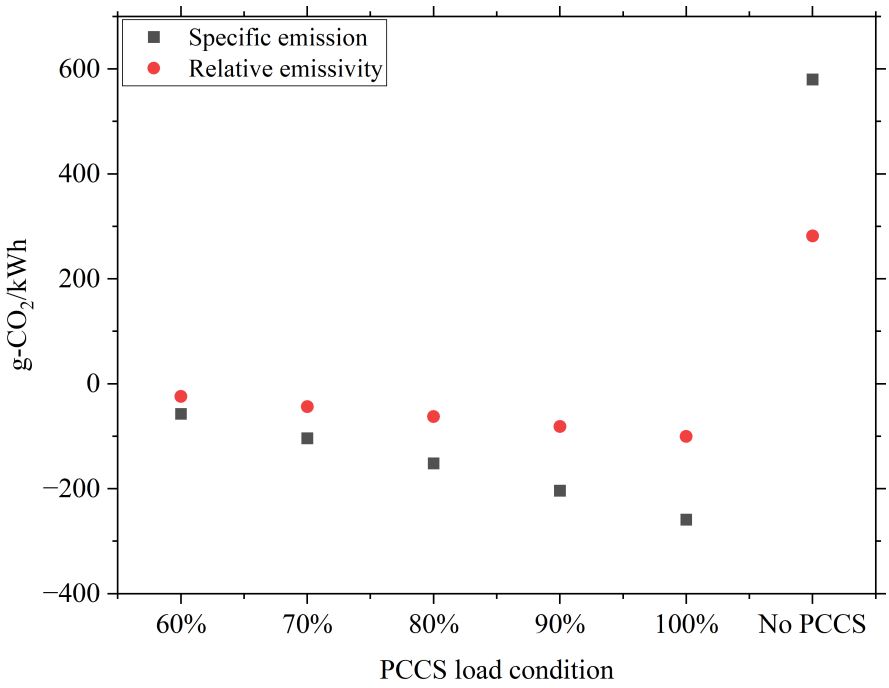

Figure 5.57: Specific emission and relative emissivity of CCGT using syngas integrated with PCCS under different load conditions.

In emission analysis, the CCGT system that uses syngas integrated with PCCS under varying load conditions has a CO_2 capture ratio similar to that of systems using blended fuels, due to the 90% capture

efficiency of the amine used in PCCS. With a CO_2 emission index of 0.0783 g-CO_2/kJ and a CO_2 emission level of 0.161 g-CO_2/kWh under conditions without PCCS, the CO_2 performance indicators for the CCGT using syngas with PCCS under different load conditions are illustrated in Figure 5.58.

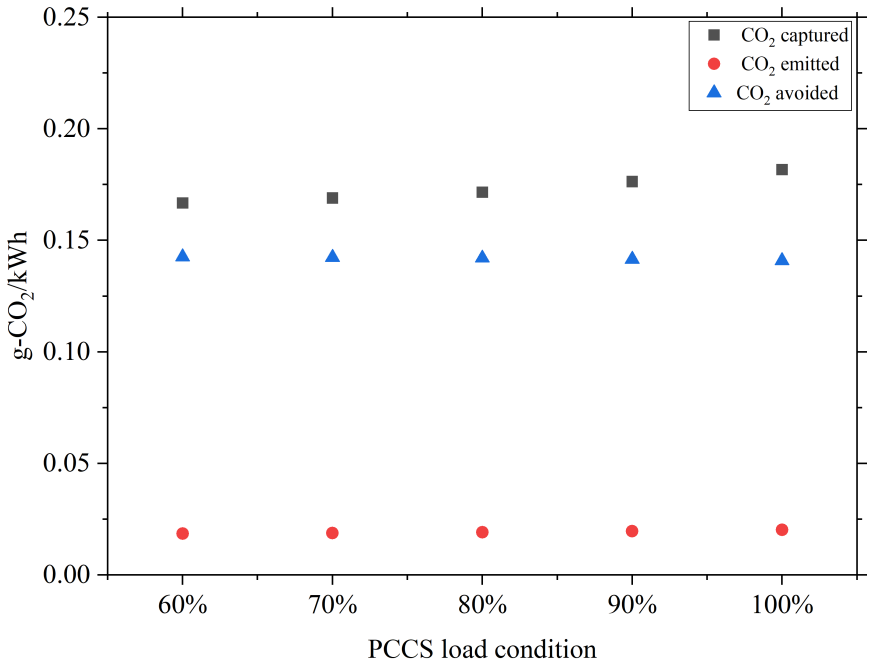

Figure 5.58: CO_2 indicators of CCGT using syngas integrated with PCCS under different load conditions.

The CCGT fueled only with syngas and integrated with PCCS shows better performance under full load conditions compared to part load conditions in terms of power generation. Negative emissions are achieved only when syngas is blended with fossil fuels or used as the sole fuel for combustion, combined with PCCS operation. The potential for achieving negative emissions increases as the proportion of syngas in the fuel mixture increases. However, increasing the syngas content has certain limitations in terms of operational and performance conditions. One significant limitation is the high demand for sewage sludge required for gasification when only syngas is used as fuel. Plasma gasification produces approximately 0.79 kg of syngas from 1 kg of sewage sludge, and the estimated requirement of sewage sludge for the reference CCGT increases proportionally with the syngas content in the fuel mix, as shown in Table 5.9. When syngas is mixed with an N_2-rich gas, the sludge requirement is more than double compared to a mixture of methane and syngas. If syngas is used exclusively, the annual demand for the dry mass of sewage sludge is estimated to be 604,509.36 tons for the proximate and ultimate analysis of sewage sludge [143] in Table 5.8 respectively.

According to the Polish Central Statistics Office [144], Figure 5.59 illustrates the annual production of sewage sludge in dry mass from industrial and municipal wastewater treatment plants in Poland between 2010 and 2023. The generated sewage sludge, including incineration, is utilized for various purposes such as landfills, recycling, and fertilizer production. As of 2023, Poland produced approximately 946.5 thousand. t.d.s of sewage sludge, which slightly exceeds the amount required for the operation of the reference CCGT power plant. However, factors such as the various applications of sewage sludge, transportation

Table 5.8: Proximate and Ultimate analysis of dry mass of sewage sludge considered for the estimation [143]

Proximate Analysis			Ultimate Analysis		
Specification	Unit	Value	Specification	Unit	Value
Fixed Carbon	%	9.21	Carbon	%	27.33
Volatile Matter	%	56.94	Hydrogen	%	6.54
Dried material moisture	%	2.00	Nitrogen	%	4.27
Ash	%	31.85	Sulphur	%	0.28
Net Heat Value	MJ/kg	9.60	Oxygen	%	27.72
Gross Heating Value	MJ/kg	15.39			

Table 5.9: Amount of sewage sludge in dry mass required for syngas production to satisfy the reference case CCGT operations

Fuel composition	Syngas consumption kg/s	Required syngas t/year	Required sewage sludge t/year
Methane 75% + syngas 25%	1.58	49725.96	62944.26
Methane 50% + syngas 50%	3.92	123469.75	156290.82
Methane 25% + syngas 75%	7.74	244158.02	309060.78
N_2-rich gas 75% + syngas 25%	3.6	113627.99	143832.9
N_2-rich gas 50% + syngas 50%	7.32	230975.97	292374.65
N_2-rich gas 25% + syngas 75%	11.17	352219.28	445847.19
Syngas 100%	15.14	477562.39	604509.36

from different regions of Poland, and the conversion process of sludge to syngas limit its availability for use in the reference CCGT.

Another limitation is the plasma gasification of sewage sludge, which is influenced by the varying properties of the sewage sludge. Higher moisture levels reduce the lower heating value (LHV) of the syngas produced. As noted by Zhang et al. [145], improving the LHV of syngas involves pretreatment processes such as crushing, cracking, drying, preheating, and improving the overall quality of the feedstock. In addition to the challenges associated with the processing of wastewater sludge, limitations also occur in the CO_2 capture process. The high operating costs of PCCS integrated with power plants make it impossible to operate continuously at full load. To mitigate costs, the PCCS is sometimes operated under partial load conditions. However, fluctuations in the flue gas entering the PCCS disrupt the mass flow of the solvent and the steam flow to the reboiler, causing instability in the system [146]. At full load, the steam consumption of the PCCS reboiler reduces the power generation capacity of the CCGT, leading to decreased electricity export income and increased operational costs. After the capture process, CO_2 must be transported and stored using various methods, which involves many challenges. Factors such as the

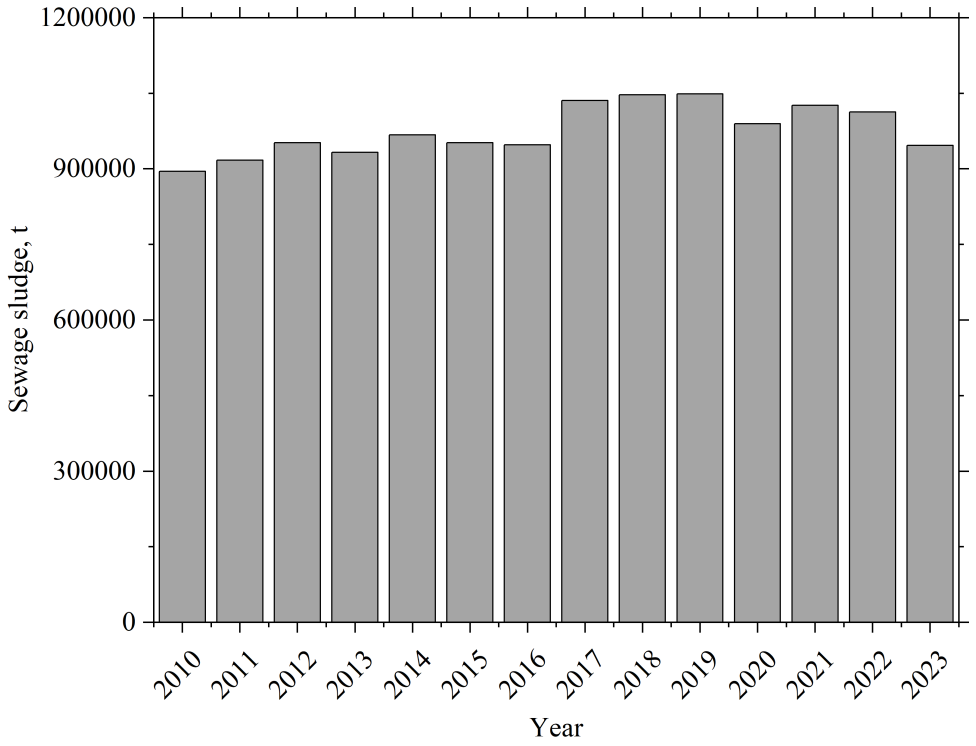

Figure 5.59: Sewage sludge in dry mass produced from industrial and municipal wastewater treatment plants in Poland [144].

purity of captured CO_2, transportation methods, related costs, and the effects of impurities influence the efficiency of the process. Transportation costs depend heavily on the method, such as pipelines and ships. Pipelines are most suitable for shorter distances, while ships are preferred for long-distance transport. These methods are more efficient and environmentally friendly compared to transport by trucks, which generate additional emissions [147], [148]. Transporting CO_2 in liquid form is cost-effective and efficient, as it requires less volume compared to the gaseous state and avoids the need for thicker pipelines required for supercritical states to withstand high pressure. However, impurities in the captured CO_2 can complicate transport, in terms of supercritical state with various temperature and pressure requirements, increase compression costs, and cause corrosion in pipelines. Achieving high CO_2 purity is therefore critical but adds to the overall cost of the process [149], [150], [151].

Chapter 6

Summary and Conclusion

A thermodynamic model of a combined cycle gas turbine power plant integrated with a district heating network and post-combustion carbon capture and storage using a solvent-based method has been developed. Real-world observations and experimental data are used for input parameters and model validation. The properties of various fuel compositions, results from the validated model, and key performance indicators are evaluated. When performing CCGT without PCCS integration, it achieves net power generation of 143.4 MW and a net efficiency of 54.3% , which aligns with the operational benchmarks of an SCC-800 2x1 CCGT configuration and the parameters of the Gorzów power plant, validating the model under proposed operational conditions. However, these operating conditions without CO_2 installation poses a risk of emitting more CO_2 into the atmosphere. Similarly, the PCCS model was validated using pilot-scale PCCS data from the Łaziska Power Plant in Poland with a relative error below 5% and comparing results with Aspen Plus simulation results for benchmarking shows the relative differences in the range of 0% to 3.61%, confirming its precision. Based on the concept of bioenergy with carbon capture and storage (BECCS) to achieve negative CO_2 emissions, syngas derived from plasma gasification of sewage sludge was mixed with fossil fuels such as pure methane and nitrogen-rich natural gas in different proportions. This validation of the developed thermodynamic model shows the reliability of results from further modifications of the model within the thermodynamic constraints. Due to the properties of the gas turbine model, the gas turbine increases or decreases the fuel and air flow according to LHV to maintain constant power generation. Hence, regardless of the fuel used, the power generation of the gas cycle remains constant. However, increasing the proportion of syngas in the fuel leads to an increase in the fuel mass flow rate and CO_2 concentration in the flue gases.

The analysis of flue gases passing through various stages of the HRSG shows that, under the specified boundary conditions, the enthalpy changes in the flue gases remain relatively the same across different fuels. Due to this, the heat transfer rates of the HRSG components at various pressure levels are nearly the same regardless of the fuel type used in the gas turbine, with the highest in the HP evaporator and the lowest in the LP economiser. As a result, when using different fuels, only minor differences are observed in the LMTD and the heat distribution between HRSG components and the HP steam temperature of 510℃ and LP steam temperature of 277℃ at the HRSG outlet remain constant. Given the variability in fuel compositions, maintaining steady operational performance in HRSG steam production is crucial to

ensuring the stability of the system. However, steam power generation is relayed upon stream extraction for DHN heat supply and PCCS solvent regeneration. These systems are observed to operate in an equilibrium state, where changes in the steam flow rate to one system directly affect the other two. Since steam extraction for PCCS is inevitable, it results in penalties for power generation and DHN heat supply. Therefore, the overall performance of the integrated CCGT with PCCS is influenced by the CO_2 content in the flue gases. Energy performance indicators show that CCGT achieves better efficiency with methane-rich fuel mixtures. However, increasing the proportion of syngas in the fuel mix increases the demand for steam, solvent requirements for PCCS, and power consumption in PCCS which in turn reduces the overall energy efficiency, power output, and DHN heat supply of the CCGT.

The lower reboiler duty of the AMP-PZ solvent compared to that of MEA results in reduced steam extraction, which improves the performance of the CCGT in terms of energy output and efficiency, better than that of the MEA-based PCCS system. The improved performance of the AMP-PZ solvent is reflected in the EOP, with lower values for AMP-PZ indicating enhanced overall efficiency and reduced operational costs of the power plant. Of the total power consumed by the PCCS from the CCGT, 99.1% of the power consumed by the CO_2 handling system and the flue gas blower involved in the CO_2 capture process. In full load operation, the PCCS consumes 11.2% to 12.4% of the plant's electricity, depending on the fuel composition. Under variable load conditions, the reduced flow of CO_2 to the PCCS system decreases the consumption of steam and power, improving the performance of the CCGT. In scenarios using nitrogen-rich gas fuel mixtures with syngas, the higher CO_2 content in the fuel leads to a higher CO_2 emission index compared to methane mixtures. However, despite the higher index, N_2-rich fuel mixtures resulted in reduced emissions per kWh of electricity output, which makes it suitable for achieving lower-emission fuel properties. Furthermore, to validate this, the CO_2 emission data in Figure 5.42 shows that the N_2-rich mixture has a greater potential to achieve negative emissions under PCCS load conditions from 80% to 100%. In contrast, syngas-methane blends must exceed more than the 50% syngas proportion, and PCCS should be operated under high load conditions to achieve negative emissions. Even when CCGT performs better with methane-syngas blends, this is limited by low PCCS load conditions and lower proportions of syngas in case of emissions. Although performance differences with N_2-rich-syngas blends are marginally smaller, these mixtures allow flue gases to be processed in varying load conditions while still achieving negative emissions and improving plant performance. However, higher revenues from electricity and DHN heat sales are attained only when the PCCS operates under low-load conditions. Compromising revenue for low-emission power production still ensures operational profitability. Excluding DHN from the CCGT system increases power production and revenue from electricity, but results in reduced thermal energy recovery and waste of sensible heat. The calculated SPECCA and LCOE values for CCGT configurations with and without PCCS demonstrate a balance between emission reduction and economic feasibility for the developed reference CCGT case. Hence, achieving negative CO_2 emissions through the utilization of syngas blended with fossil fuels is possible and economically viable.

Appendix A

PCCS parameters for treating flue gases from different composition of fuels using MEA

Table A.1: PCCS parameters for treating flue gas from pure methane fuel under different load conditions using MEA solvent

Point	Pressure (bar)	Temperature (°C)	Mass flow rate (kg/s)					
			100%	90%	80%	70%	60%	50%
0	0.885	104.64	268.60	241.70	214.88	188.02	161.16	134.30
1	1.15	137.91	268.60	241.70	214.88	188.02	161.16	134.30
2	1.1	65.40	268.60	241.70	214.88	188.02	161.16	134.30
3	1.05	40.00	266.80	240.12	213.44	186.70	160.08	133.40
4	0.895	40.40	253.07	227.76	202.45	177.14	151.84	126.53
5	0.885	117.39	253.07	227.76	202.45	177.14	151.84	126.53
5a	0.885	105.00	0	26.88	26.86	80.58	53.72	134.30
5b	0.885	117.39	253.07	254.62	229.31	257.73	259.28	260.83
5c	1.15	152.23	253.07	254.62	229.31	257.73	205.56	260.83
6	1.00	35.00	198.81	198.81	198.81	198.81	198.81	198.81
7	1.10	35.00	198.81	198.81	198.81	198.81	198.81	198.81
8	1.05	28.68	198.81	198.81	198.81	198.81	198.81	198.81
9	1.05	60.00	156.32	140.68	125.05	109.42	93.79	78.16
10	2.10	60.36	156.32	140.68	125.05	109.42	93.79	78.16
11	1.50	70.36	142.47	128.22	113.98	99.73	85.48	71.30
12	1.01325	70.36	142.59	128.32	114.07	99.42	85.55	71.30
13	1.10	70.78	142.59	128.32	114.07	99.42	85.55	71.30
14	1.05	40.00	142.59	128.32	114.07	99.42	85.55	71.30

Table A.1: PCCS parameters for treating flue gas from pure methane fuel under different load conditions using MEA solvent

Point	Pressure (bar)	Temperature (°C)	Mass flow rate (kg/s)					
			100%	90%	80%	70%	60%	50%
15	2.05	100.00	156.32	140.68	125.05	109.42	93.79	78.16
16	1.96	122.00	132.65	119.38	106.12	92.85	79.59	66.24
17	1.96	119.57	142.47	128.22	113.98	99.72	85.48	71.24
18	2.00	120.29	142.47	128.22	113.98	99.72	85.48	71.24
19	2.03	122.00	156.32	140.68	125.05	109.42	93.79	12.43
20	2.01	125.00	156.32	140.68	125.05	109.42	93.79	12.43
21	3.00	135.00	24.87	22.39	19.90	17.41	14.92	12.44
22	2.90	132.37	24.87	22.39	19.90	17.41	14.92	12.44
23	1.99	125.00	23.67	21.30	18.93	16.56	14.20	12.44
24	1.96	30.00	13.85	12.46	11.08	9.70	8.31	6.86
25	1.96	30.00	9.82	8.83	7.85	6.87	5.89	6.86
26	7.84	150.45	13.85	8.83	11.08	9.70	8.31	6.86
27	7.79	30.00	13.76	12.38	11.00	9.62	8.25	6.86
28	31.16	150.14	13.76	12.38	11.00	9.62	8.25	6.86
29	31.11	30.00	13.73	12.36	10.99	9.61	8.24	6.86
30	110.05	138.57	13.73	12.36	10.99	9.61	8.24	6.86
31	110.00	22.00	13.73	12.36	10.99	9.61	8.24	6.86

Table A.2: PCCS parameters for treating flue gas from 75% methane mixture with syngas under different load conditions using MEA solvent

Point	Pressure (bar)	Temperature (°C)	Mass flow rate (kg/s)					
			100%	90%	80%	70%	60%	50%
0	0.885	104.64	268.60	241.70	214.88	188.02	161.16	134.30
1	1.15	137.87	268.60	241.70	214.88	188.02	161.16	134.30
2	1.1	65.40	268.60	241.70	214.88	188.02	161.16	134.30
3	1.05	40	266.80	240.12	213.44	186.70	160.08	133.40
4	0.895	40.40	253.07	227.76	202.45	177.14	151.84	126.53
5	0.885	117.72	253.07	227.76	202.45	177.14	151.84	126.53
5a	0.885	105	0	26.88	26.86	80.58	53.72	134.30
5b	0.885	117.72	253.07	254.62	229.31	257.73	259.28	260.83
5c	1.15	152.57	253.07	254.62	229.31	257.73	205.56	260.83
6	1	35	198.81	198.81	198.81	198.81	198.81	198.81

Table A.2: PCCS parameters for treating flue gas from 75% methane mixture with syngas under different load conditions using MEA solvent

Point	Pressure (bar)	Temperature (°C)	Mass flow rate (kg/s)					
			100%	90%	80%	70%	60%	50%
7	1.1	35	198.81	198.81	198.81	198.81	198.81	198.81
8	1.05	28.71	198.81	198.81	198.81	198.81	198.81	198.81
9	1.05	60	156.32	140.68	125.05	109.42	93.79	78.16
10	2.1	60.36	156.32	140.68	125.05	109.42	93.79	71.30
11	1.5	70.36	142.47	128.22	113.98	99.73	85.48	71.23
12	1.01325	70.36	142.59	128.32	114.07	99.42	85.55	71.30
13	1.1	70.78	142.59	128.32	114.07	99.42	85.55	71.30
14	1.05	40	142.59	128.32	114.07	99.42	85.55	71.30
15	2.05	100	156.32	140.68	125.05	109.42	93.79	78.16
16	1.96	122	132.65	119.38	106.12	92.85	79.59	66.32
17	1.96	119.57	142.47	128.22	113.98	99.72	85.48	71.24
18	2	120.29	142.47	128.22	113.98	99.72	85.48	71.24
19	2.03	122	156.32	140.68	125.05	109.42	93.79	78.16
20	2.01	125	156.32	140.68	125.05	109.42	93.79	78.16
21	3	135.00	24.87	22.39	19.90	17.41	14.92	12.44
22	2.9	132.37	24.87	22.39	19.90	17.41	14.92	12.44
23	1.99	125	23.67	21.30	18.93	16.56	14.20	11.83
24	1.96	30	13.85	12.46	11.08	9.70	8.31	11.83
25	1.96	30	9.82	8.83	7.85	6.87	5.89	4.91
26	7.84	150.45	13.85	8.83	11.08	9.70	8.31	6.92
27	7.79	30.00	13.76	12.38	11.00	9.62	8.25	6.92
28	31.16	150.14	13.76	12.38	11.00	9.62	8.25	6.88
29	31.11	30	13.73	12.36	10.99	9.61	8.24	6.86
30	110.05	138.57	13.73	12.36	10.99	9.61	8.24	6.86
31	110	22	13.73	12.36	10.99	9.61	8.24	6.86

Table A.3: PCCS parameters for treating flue gas from 50% methane mixture with syngas under different load conditions using MEA solvent

Point	Pressure (bar)	Temperature (°C)	Mass flow rate (kg/s)					
			100%	90%	80%	70%	60%	50%
0	0.885	104.64	268.60	241.74	214.88	188.02	161.16	134.30
1	1.15	137.87	268.60	241.74	214.88	188.02	161.16	134.30

Table A.3: PCCS parameters for treating flue gas from 50% methane mixture with syngas under different load conditions using MEA solvent

Point	Pressure (bar)	Temperature (°C)	Mass flow rate (kg/s)					
			100%	90%	80%	70%	60%	50%
2	1.1	65.40	269.00	241.74	214.88	188.02	161.16	134.30
3	1.05	40.00	266.53	239.88	213.23	186.57	159.95	133.27
4	0.895	40.40	251.96	226.76	201.57	176.37	151.18	125.98
5	0.885	117.72	251.96	226.76	201.57	176.37	151.18	125.98
5a	0.885	105.00	0	26.86	53.72	80.58	107.44	134.30
5b	0.885	117.72	251.96	253.62	255.30	256.95	258.62	260.28
5c	1.15	152.57	251.96	253.62	255.30	256.95	258.62	260.28
6	1.00	35.00	199.00	198.81	198.81	198.81	198.81	198.81
7	1.10	35.00	198.81	198.81	198.81	198.81	198.81	198.81
8	1.05	28.71	199.00	198.81	198.81	198.81	198.81	198.81
9	1.05	60.00	165.90	149.31	132.72	116.13	99.54	82.95
10	2.10	60.36	165.90	149.31	132.72	116.13	99.54	82.95
11	1.50	70.36	151.21	136.19	121.07	105.93	90.80	75.67
12	1.01325	70.36	151.33	136.19	121.07	105.93	90.80	75.67
13	1.10	70.78	151.00	136.19	121.07	105.93	90.80	75.67
14	1.05	40.00	151.00	136.19	121.07	105.93	90.80	75.67
15	2.05	100.00	166.00	149.31	132.72	116.13	99.54	82.95
16	1.96	122.00	140.79	126.70	112.63	98.55	84.47	70.39
17	1.96	119.57	151.21	136.19	121.07	105.93	90.80	75.60
18	2.00	120.29	151.00	136.19	121.07	105.93	90.80	75.60
19	2.03	122.00	166.00	149.31	132.72	116.13	99.54	82.95
20	2.01	125.00	165.90	149.31	132.72	116.13	99.54	82.95
21	3.00	135.00	26.40	23.76	21.12	18.48	15.84	13.20
22	2.90	132.37	26.00	23.76	21.12	18.48	15.84	13.20
23	1.99	125.00	25.00	22.60	20.10	17.58	15.07	12.55
24	1.96	30.00	15.00	13.22	11.76	10.28	8.82	7.35
25	1.96	30.00	10.42	9.37	8.33	7.29	6.25	5.21
26	7.84	150.45	14.70	13.22	11.76	10.28	8.82	7.35
27	7.79	30.00	14.60	13.13	11.67	10.28	8.75	7.35
28	31.16	150.14	15.00	13.13	11.67	10.28	8.75	7.30
29	31.11	30.00	14.57	13.12	11.66	10.20	8.75	7.29
30	110.05	138.57	15.00	13.12	11.66	10.20	8.75	7.29
31	110.00	22.00	14.57	13.12	11.66	10.20	8.75	7.29

Table A.4: PCCS parameters for treating flue gas from 25% methane mixture with syngas under different load conditions using MEA solvent

Point	Pressure (bar)	Temperature (°C)	Mass flow rate (kg/s)					
			100%	90%	80%	70%	60%	50%
0	0.885	104.64	268.60	241.74	214.88	188.02	161.16	134.3
1	1.15	137.87	268.60	241.74	214.88	188.02	161.16	134.3
2	1.1	65.40	268.60	241.74	214.88	188.02	161.16	134.3
3	1.05	40	266.10	239.49	212.88	186.27	159.66	133.05
4	0.895	40.40	250.15	225.13	200.12	175.1	150.10	125.075
5	0.885	117.72	250.15	225.13	200.12	175.1	150.10	125.075
5a	0.885	105	0	26.86	53.72	80.58	107.44	134.3
5b	0.885	117.72	250.15	251.90	253.83	255.68	257.53	259.375
5c	1.15	152.57	250.15	251.90	253.83	255.68	257.53	259.375
6	1	35	198.81	198.81	198.81	198.8076	198.81	198.8076
7	1.1	35	198.81	198.81	198.81	198.8076	198.81	198.8076
8	1.05	28.71	198.81	198.81	198.81	198.8076	198.81	198.8076
9	1.05	60	181.59	163.43	145.27	127.12	108.96	90.797
10	2.1	60.36	181.59	163.43	145.27	127.12	108.96	90.797
11	1.5	70.36	165.51	149.08	132.51	115.95	99.38	82.821
12	1.01325	70.36	165.64	149.08	132.51	115.95	99.38	82.821
13	1.1	70.78	165.64	149.08	132.51	115.95	99.38	82.821
14	1.05	40	165.64	149.08	132.51	115.95	99.38	82.821
15	2.05	100	181.59	163.43	145.27	127.12	108.96	90.797
16	1.96	122	154.10	138.69	123.28	107.87	92.46	77.05
17	1.96	119.57	165.51	149.08	132.51	115.95	99.38	82.821
18	2	120.29	165.51	149.08	132.51	115.95	99.38	82.821
19	2.03	122	181.59	163.44	145.27	127.12	108.96	90.797
20	2.01	125	181.59	163.44	145.27	127.12	108.96	90.797
21	3	135.00	28.90	26.01	23.02	20.22	17.34	14.448
22	2.9	132.37	28.90	26.01	23.02	20.22	17.34	14.448
23	1.99	125	27.49	24.75	21.99	19.25	16.50	13.75
24	1.96	30	16.09	14.48	12.87	11.26	9.65	8.04
25	1.96	30	11.41	10.26	9.12	7.98	6.84	5.7
26	7.84	150.45	16.09	14.48	12.87	11.26	9.65	8.04
27	7.79	30.00	15.98	14.38	12.78	11.26	9.65	7.99
28	31.16	150.14	15.98	14.38	12.78	11.18	9.58	7.99
29	31.11	30	15.95	14.36	12.76	11.17	9.57	7.98
30	110.05	138.57	15.95	14.36	12.76	11.17	9.57	7.98

31	110	22	15.95	14.36	12.76	11.167	9.57	7.976

Table A.5: PCCS parameters for treating flue gas from Nitrogen rich natural gas under different load conditions using MEA solvent

Point	Pressure (bar)	Temperature (°C)	Mass flow rate (kg/s)					
			100%	90%	80%	70%	60%	50%
0	0.885	104.64	268.60	241.74	214.88	188.02	161.16	134.30
1	1.15	137.94	268.60	241.74	214.88	188.02	161.16	134.30
2	1.1	65.40	268.60	241.74	214.88	188.02	161.16	134.30
3	1.05	40.00	267.66	240.90	214.13	187.36	160.60	133.83
4	0.895	40.40	253.98	228.58	203.18	177.78	152.39	126.99
5	0.885	116.96	253.98	228.58	203.18	177.78	152.39	126.99
5a	0.885	105.00	0.00	26.86	53.72	80.58	107.44	134.30
5b	0.885	116.96	253.98	255.44	256.90	258.36	259.83	261.29
5c	1.15	151.76	253.98	255.44	256.90	258.36	259.83	261.29
6	1.00	35.00	198.81	198.81	198.81	198.81	198.81	198.81
7	1.10	35.00	198.81	198.81	198.81	198.81	198.81	198.81
8	1.05	28.65	198.81	198.81	198.81	198.81	198.81	198.81
9	1.05	60.00	155.82	140.23	124.65	109.07	93.49	77.91
10	2.10	60.36	155.82	140.23	124.65	109.07	93.49	77.91
11	1.50	70.36	142.01	127.81	113.61	99.41	85.21	71.01
12	1.01325	70.36	142.13	127.91	113.70	99.49	85.28	71.06
13	1.10	70.78	142.13	127.91	113.70	99.49	85.28	71.06
14	1.05	40.00	142.13	127.91	113.70	99.49	85.28	71.06
15	2.05	100.00	155.82	140.23	124.65	109.07	93.49	77.91
16	1.96	122.00	132.22	119.00	105.78	92.56	79.33	66.11
17	1.96	119.57	142.01	127.81	113.61	99.41	85.21	71.01
18	2.00	120.29	142.01	127.81	113.61	99.41	85.21	71.01
19	2.03	122.00	155.82	140.23	124.65	109.07	93.49	77.91
20	2.01	125.00	155.82	140.23	124.65	109.07	93.49	77.91
21	3.00	135.00	24.79	22.31	19.84	17.36	14.88	12.40
22	2.90	132.37	24.79	22.31	19.84	17.36	14.88	12.40
23	1.99	125.00	23.59	21.23	18.87	16.51	14.15	11.80
24	1.96	30.00	13.80	12.42	11.04	9.66	8.28	6.90
25	1.96	30.00	9.79	8.81	7.83	6.85	5.87	4.89
26	7.84	150.45	13.80	12.42	11.04	9.66	8.28	6.90
27	7.79	30.00	13.71	12.34	10.97	9.60	8.23	6.86

Table A.5: PCCS parameters for treating flue gas from Nitrogen rich natural gas under different load conditions using MEA solvent

Point	Pressure (bar)	Temperature (°C)	Mass flow rate (kg/s)					
			100%	90%	80%	70%	60%	50%
28	31.16	150.14	13.71	12.34	10.97	9.60	8.23	6.86
29	31.11	30.00	13.69	12.32	10.95	9.58	8.21	6.84
30	110.05	138.57	13.69	12.32	10.95	9.58	8.21	6.84
31	110.00	22.00	13.69	12.32	10.95	9.58	8.21	6.84

Table A.6: PCCS parameters for treating flue gas from 75% N_2 rich gas mixture with syngas under different load conditions using MEA solvent

Point	Pressure (bar)	Temperature (°C)	Mass flow rate (kg/s)					
			100%	90%	80%	70%	60%	50%
0	0.885	104.64	268.60	241.74	214.88	188.02	161.16	134.30
1	1.15	137.88	268.60	241.74	214.88	188.02	161.16	134.30
2	1.1	65.40	268.60	241.74	214.88	188.02	161.16	134.30
3	1.05	40	267.09	240.38	213.67	186.96	160.26	133.55
4	0.895	40.40	252.23	227.00	201.78	176.56	151.34	126.12
5	0.885	117.50	252.23	227.00	201.78	176.56	151.34	126.12
5a	0.885	105	0	26.86	53.72	80.58	107.44	134.30
5b	0.885	117.50	252.23	253.87	255.51	257.14	258.78	260.42
5c	1.15	152.35	252.23	253.87	255.51	257.14	258.78	260.42
6	1	35	198.81	198.81	198.81	198.81	198.81	198.81
7	1.1	35	198.81	198.81	198.81	198.81	198.81	198.81
8	1.05	28.70	198.81	198.81	198.81	198.81	198.81	198.81
9	1.05	60	169.17	152.25	135.33	118.42	101.50	84.58
10	2.1	60.17	169.17	152.25	135.33	118.42	101.50	84.58
11	1.5	66.52	154.18	138.76	123.35	107.92	92.51	77.09
12	1.01325	66.52	154.31	138.88	123.45	108.02	92.58	77.15
13	1.1	66.92	154.31	138.88	123.45	108.02	92.58	77.15
14	1.05	40	154.31	138.88	123.45	108.02	92.58	77.15
15	2.05	101	169.17	152.25	135.33	118.42	101.50	84.58
16	1.96	123	143.56	129.20	114.84	100.50	86.13	77.09
17	1.96	119.57	154.18	138.76	123.35	107.92	92.51	77.09
18	2	120.29	154.18	138.76	123.35	107.92	92.51	77.09
19	2.03	123	169.17	152.25	135.33	118.42	101.50	84.58

Table A.6: PCCS parameters for treating flue gas from 75% N_2 rich gas mixture with syngas under different load conditions using MEA solvent

Point	Pressure (bar)	Temperature (°C)	Mass flow rate (kg/s)					
			100%	90%	80%	70%	60%	50%
20	2.01	125	169.17	152.25	135.33	118.42	101.50	84.58
21	3	135.00	26.92	24.23	21.54	18.84	16.15	13.46
22	2.9	132.37	26.92	24.23	21.54	18.84	16.15	13.46
23	1.99	125	25.61	23.05	20.49	17.93	15.37	12.81
24	1.96	30	14.99	13.50	11.99	10.50	15.36	7.49
25	1.96	30	10.63	9.56	8.50	7.44	6.38	5.31
26	7.84	150.45	14.99	13.50	11.99	10.50	8.99	7.49
27	7.79	30.00	14.89	13.40	11.91	10.42	8.93	7.44
28	31.16	150.14	14.89	13.40	11.91	10.42	8.93	7.44
29	31.11	30	14.86	13.38	11.89	10.40	8.92	7.43
30	110.05	138.57	14.86	13.38	11.89	10.40	8.92	7.43
31	110	22	14.86	13.38	11.89	10.40	8.92	7.43

Table A.7: PCCS parameters for treating flue gas from 50% N_2 rich gas mixture with syngas under different load conditions using MEA solvent

Point	Pressure (bar)	Temperature (°C)	Mass flow rate (kg/s)					
			100%	90%	80%	70%	60%	50%
0	0.885	104.64	268.60	241.74	214.88	188.02	161.16	134.30
1	1.15	137.82	268.60	241.74	214.88	188.02	161.16	134.30
2	1.10	65.40	269.00	241.74	214.88	188.02	161.16	134.30
3	1.05	40.00	266.50	240.38	213.67	186.96	160.25	133.55
4	0.895	40.40	250.43	227.00	201.78	176.56	151.34	126.12
5	0.885	118.08	250.00	227.00	201.78	176.56	151.34	126.12
5a	0.885	105.00	0.00	26.86	53.72	80.58	107.44	134.30
5b	0.885	118.08	250.43	252.25	254.06	257.14	258.78	259.52
5c	1.15	152.96	250.00	252.25	254.06	257.14	258.78	259.52
6	1.00	35.00	199.00	198.81	198.81	198.81	198.81	198.81
7	1.10	35.00	198.81	198.81	198.81	198.81	198.81	198.81
8	1.05	28.75	199.00	198.81	198.81	198.81	198.81	198.81
9	1.05	60.00	182.96	164.66	146.36	128.07	109.77	91.48
10	2.10	60.36	182.96	164.66	146.36	128.07	109.77	91.48
11	1.50	70.36	166.75	150.07	133.40	116.72	100.05	82.43

Table A.7: PCCS parameters for treating flue gas from 50% N_2 rich gas mixture with syngas under different load conditions using MEA solvent

Point	Pressure (bar)	Temperature (°C)	Mass flow rate (kg/s)					
			100%	90%	80%	70%	60%	50%
12	1.01325	70.36	166.89	150.20	133.51	116.82	100.13	83.44
13	1.10	70.78	167.00	150.20	133.51	116.82	100.13	83.44
14	1.05	40.00	167.00	150.20	133.51	116.82	100.13	83.44
15	2.05	100.00	183.00	164.66	146.36	128.07	109.77	91.48
16	1.96	122.00	155.26	139.73	124.20	108.68	93.15	77.63
17	1.96	119.57	166.75	150.07	133.40	116.72	100.05	82.43
18	2.00	120.29	167.00	150.07	133.40	116.72	100.05	82.43
19	2.03	122.00	183.00	164.66	146.36	128.07	109.77	91.48
20	2.01	125.00	182.96	164.66	146.36	128.07	109.77	91.48
21	3.00	135.00	29.11	26.20	23.29	18.84	17.47	14.56
22	2.90	132.37	29.00	26.20	23.29	18.84	17.47	14.56
23	1.99	125.00	28.00	24.93	22.16	19.39	16.62	13.85
24	1.96	30.00	16.00	14.58	12.96	11.35	9.73	8.11
25	1.96	30.00	11.49	10.34	9.19	8.04	6.90	5.75
26	7.84	150.45	16.21	14.58	12.96	11.35	9.73	8.11
27	7.79	30.00	16.10	14.49	12.88	11.27	9.66	8.05
28	31.16	150.14	16.00	14.49	12.88	11.27	9.66	8.05
29	31.11	30.00	16.07	14.46	12.86	11.25	9.64	8.04
30	110.05	138.57	16.00	14.46	12.86	11.25	9.64	8.04
31	110.00	22.00	16.07	14.46	12.86	11.25	9.64	8.04

Table A.8: PCCS parameters for treating flue gas from 25% N_2 rich gas mixture with syngas under different load conditions using MEA solvent

Point	Pressure (bar)	Temperature (°C)	Mass flow rate (kg/s)					
			100%	90%	80%	70%	60%	50%
0	0.885	104.64	268.60	241.74	214.88	188.02	161.16	134.30
1	1.15	137.75	268.60	241.74	214.88	188.02	161.16	134.30
2	1.1	65.40	268.60	241.74	214.88	188.02	161.16	134.30
3	1.05	40.00	265.89	239.30	212.72	186.13	159.54	132.95
4	0.895	40.40	248.57	223.71	198.86	198.80	149.14	124.29
5	0.885	118.67	248.57	223.71	198.86	198.80	149.14	124.29
5a	0.885	105.00	0.00	26.86	53.72	80.58	107.44	134.30

Table A.8: PCCS parameters for treating flue gas from 25% N_2 rich gas mixture with syngas under different load conditions using MEA solvent

Point	Pressure (bar)	Temperature (°C)	Mass flow rate (kg/s)					
			100%	90%	80%	70%	60%	50%
5b	0.885	118.67	248.57	250.57	252.58	254.58	256.58	258.59
5c	1.15	153.60	248.57	250.57	252.58	254.58	256.58	258.59
6	1.00	35.00	198.81	198.81	198.81	198.81	198.81	198.81
7	1.10	35.00	198.81	198.81	198.81	198.81	198.81	198.81
8	1.05	28.80	198.81	198.81	198.81	198.81	198.81	198.81
9	1.05	60.00	197.21	177.49	157.77	138.05	118.32	98.60
10	2.10	60.17	197.21	177.49	157.77	138.05	118.32	98.60
11	1.50	69.52	179.74	161.76	143.78	125.82	107.84	89.87
12	1.01325	69.52	179.88	161.89	143.91	125.92	107.93	89.94
13	1.10	69.93	179.88	161.89	143.91	125.92	107.93	89.94
14	1.05	40.00	179.88	161.89	143.91	125.92	107.93	89.94
15	2.05	100.00	197.21	177.49	157.77	138.05	118.32	98.60
16	1.96	122.00	167.35	150.61	133.88	117.14	100.41	83.67
17	1.96	119.57	179.74	161.76	143.78	125.82	107.84	89.87
18	2.00	120.29	179.74	161.76	143.78	125.82	107.84	89.87
19	2.03	122.00	197.21	177.49	157.77	138.05	118.32	98.60
20	2.01	125.00	197.21	177.49	157.77	138.05	118.32	98.60
21	3.00	135.00	31.38	28.24	25.11	21.97	18.83	15.69
22	2.90	132.37	31.38	28.24	25.11	21.97	18.83	15.69
23	1.99	125.00	29.86	26.87	23.88	20.90	17.92	14.93
24	1.96	30.00	17.47	15.72	13.97	12.23	10.48	8.74
25	1.96	30.00	12.39	11.15	9.91	8.67	7.43	6.20
26	7.84	150.45	17.47	15.72	13.97	12.23	10.48	8.74
27	7.79	30.00	17.35	15.62	13.88	12.15	10.41	8.68
28	31.16	150.14	17.35	15.62	13.88	12.15	10.41	8.68
29	31.11	30.00	17.32	15.59	13.86	12.13	10.40	8.66
30	110.05	138.57	17.32	15.59	13.86	12.13	10.40	8.66
31	110.00	22.00	17.32	15.59	13.86	12.13	10.40	8.66

Table A.9: PCCS parameters for treating flue gas from syngas under different load conditions using MEA solvent

Point	Pressure (bar)	Temperature (°C)	Mass flow rate (kg/s)				
			100%	90%	80%	70%	60%
0	0.885	104.64	268.60	241.74	214.88	188.02	161.16
1	1.15	137.68	268.60	241.74	214.88	188.02	161.16
2	1.1	65.40	268.60	241.74	214.88	188.02	161.16
3	1.05	40	265.26	238.74	212.21	185.68	159.16
4	0.895	40.40	246.65	221.98	197.32	172.65	147.99
5	0.885	119.30	246.65	221.98	197.32	172.65	147.99
5a	0.885	105	0	26.86	53.72	80.58	107.44
5b	0.885	119.30	246.65	248.84	251.04	253.23	255.43
5c	1.15	154.27	246.65	248.84	251.04	253.23	255.43
6	1	35	198.81	198.81	198.81	198.81	198.81
7	1.1	35	198.81	198.81	198.81	198.81	198.81
8	1.05	28.92	198.81	198.81	198.81	198.81	198.81
9	1.05	60	211.94	190.74	169.55	148.36	127.16
10	2.1	59.48	211.94	190.74	169.55	148.36	127.16
11	1.5	69.48	193.16	173.84	154.53	135.21	115.90
12	1.01325	69.48	193.32	173.99	154.65	135.32	115.99
13	1.1	69.89	193.32	173.99	154.65	135.32	115.99
14	1.05	40	193.32	173.99	154.65	135.32	115.99
15	2.05	100	211.94	190.74	169.55	148.36	127.16
16	1.96	124	179.85	161.86	143.88	125.89	107.91
17	1.96	119.57	193.16	173.84	154.53	135.21	115.90
18	2	120.29	193.16	173.84	154.53	135.21	115.90
19	2.03	124	211.94	190.74	169.55	148.36	127.16
20	2.01	125	211.94	190.74	169.55	148.36	127.16
21	3	135.00	33.72	30.35	26.98	23.61	20.23
22	2.9	132.37	33.72	30.35	26.98	23.61	20.23
23	1.99	125	32.09	28.88	25.67	22.46	19.25
24	1.96	30	18.78	16.90	15.02	13.14	11.27
25	1.96	30	13.31	11.98	10.65	9.32	7.99
26	7.84	150.45	18.78	16.90	15.02	13.14	11.27
27	7.79	30.00	18.65	16.78	14.92	13.05	11.19
28	31.16	150.14	18.65	16.78	14.92	13.05	11.19
29	31.11	30	18.62	16.76	14.89	13.03	11.17

Table A.9: PCCS parameters for treating flue gas from syngas under different load conditions using MEA solvent

Point	Pressure (bar)	Temperature (°C)	Mass flow rate (kg/s)				
			100%	90%	80%	70%	60%
30	110.05	138.57	18.62	16.76	14.89	13.03	11.17
31	110	22	18.62	16.76	14.89	13.03	11.17

Appendix B

PCCS parameters for treating flue gases from different composition of fuels using AMP-PZ

Table B.1: PCCS parameters for treating flue gas from pure methane fuel under different load conditions using AMP-PZ solvent

Point	Pressure (bar)	Temperature (°C)	Mass flow rate (kg/s)					
			100%	90%	80%	70%	60%	50%
0	0.885	104.64	268.60	241.74	214.88	188.02	161.16	134.3
1	1.15	137.93	268.60	241.74	214.88	188.02	161.16	134.3
2	1.1	65.40	268.60	241.74	214.88	188.02	161.16	134.3
3	1.05	40.00	266.98	240.28	213.58	186.88	160.19	133.49
4	0.895	40.40	253.81	228.43	203.05	177.67	152.28	126.91
5	0.885	117.18	253.81	228.43	203.05	177.67	152.28	126.91
5a	0.885	105	0.00	26.86	53.72	80.58	107.44	134.3
5b	0.885	117.18	253.81	255.3	256.77	258.25	259.73	261.21
5c	1.15	152.00	253.81	255.3	256.77	258.25	259.73	261.21
6	1	35	198.81	198.81	198.81	198.81	198.81	198.81
7	1.1	35	198.81	198.81	198.81	198.81	198.81	198.81
8	1.05	28.67	198.81	198.81	198.81	198.81	198.81	198.81
9	1.05	60	149.90	134.91	119.92	104.93	89.94	74.95
10	2.1	60.36	149.90	134.91	119.92	104.93	89.94	74.95
11	1.5	70.36	136.58	122.96	109.30	95.64	81.97	68.31
12	1.01325	70.36	136.74	123.06	109.39	95.72	82.04	68.37
13	1.1	70.78	136.74	123.06	109.39	95.72	82.04	68.37

Table B.1: PCCS parameters for treating flue gas from pure methane fuel under different load conditions using AMP-PZ solvent

Point	Pressure (bar)	Temperature (°C)	Mass flow rate (kg/s)					
			100%	90%	80%	70%	60%	50%
14	1.05	40	136.74	123.06	109.39	95.72	82.04	68.37
15	2.05	100	149.90	134.91	119.92	104.93	89.94	74.95
16	1.96	122	127.19	144.5	101.86	89.04	76.32	63.6
17	1.96	119.57	136.58	122.96	109.30	95.64	81.97	68.31
18	2	120.29	136.58	122.96	109.30	95.64	81.97	68.31
19	2.03	122	149.90	134.91	119.92	104.93	89.94	74.95
20	2.01	125	149.90	134.91	119.92	104.93	89.94	74.95
21	3	135.00	23.32	20.9	18.57	16.25	13.93	11.61
22	2.9	132.37	23.32	20.9	18.57	16.25	13.93	11.61
23	1.99	125	22.71	20.42	18.15	15.88	13.62	11.35
24	1.96	30	13.31	11.94	10.62	9.29	7.96	6.64
25	1.96	30	9.40	8.47	7.53	6.59	5.65	4.71
26	7.84	150.45	13.31	11.94	10.62	9.29	7.96	6.64
27	7.79	30.00	13.22	11.88	10.54	9.23	7.92	6.59
28	31.16	150.14	13.22	11.88	10.54	9.23	7.92	6.59
29	31.11	30	13.20	11.85	10.53	9.22	7.9	6.58
30	110.05	138.57	13.20	11.85	10.53	9.22	7.9	6.58
31	110	22	13.20	11.85	10.53	9.22	7.9	6.58

Table B.2: PCCS parameters for treating flue gas from 75% methane mixture with syngas under different load conditions using AMP-PZ solvent

Point	Pressure (bar)	Temperature (°C)	Mass flow rate (kg/s)					
			100%	90%	80%	70%	60%	50%
0	0.885	104.64	268.60	241.74	214.88	188.02	161.16	134.3
1	1.15	137.91	268.60	241.74	214.88	188.02	161.16	134.3
2	1.1	65.40	268.60	241.74	214.88	188.02	161.16	134.3
3	1.05	40.00	266.80	240.12	213.44	186.76	160.08	133.4
4	0.895	40.40	253.07	227.76	202.45	177.15	151.84	126.53
5	0.885	117.39	253.07	227.76	202.45	177.15	151.84	126.53
5a	0.885	105	0.00	26.86	53.72	80.58	107.44	134.3
5b	0.885	117.39	253.07	254.62	256.17	257.73	259.28	260.83
5c	1.15	152.23	253.07	254.62	256.17	257.73	259.28	260.83

Table B.2: PCCS parameters for treating flue gas from 75% methane mixture with syngas under different load conditions using AMP-PZ solvent

Point	Pressure (bar)	Temperature (°C)	Mass flow rate (kg/s)					
			100%	90%	80%	70%	60%	50%
6	1	35	198.81	198.81	198.81	198.81	198.81	198.81
7	1.1	35	198.81	198.81	198.81	198.81	198.81	198.81
8	1.05	28.68	198.81	198.81	198.81	198.81	198.81	198.81
9	1.05	60	156.37	140.73	125.09	109.46	93.82	78.18
10	2.1	60.33	156.37	140.73	125.09	109.46	93.82	78.18
11	1.5	70.33	142.48	128.26	114.01	99.76	85.51	71.26
12	1.01325	70.33	142.63	128.37	114.12	99.84	85.58	71.32
13	1.1	70.75	142.63	128.37	114.12	99.84	85.58	71.32
14	1.05	40	142.63	128.37	114.12	99.84	85.58	71.32
15	2.05	100	156.37	140.73	125.09	109.46	93.82	78.18
16	1.96	122	132.67	119.43	106.16	92.88	79.62	66.35
17	1.96	119.57	142.48	128.26	114.01	99.76	85.51	71.26
18	2	120.29	142.48	128.26	114.01	99.76	85.51	71.26
19	2.03	122	156.37	140.73	125.09	109.46	93.82	78.18
20	2.01	125	156.37	140.73	125.09	109.46	93.82	78.18
21	3	135.00	24.33	21.8	19.38	16.95	14.53	12.11
22	2.9	132.37	24.33	21.8	19.38	16.95	14.53	12.11
23	1.99	125	23.69	21.3	18.94	16.57	14.2	11.84
24	1.96	30	13.89	12.48	11.08	9.89	8.31	8.93
25	1.96	30	9.80	8.84	7.86	6.88	5.9	4.91
26	7.84	150.45	13.89	12.48	11.08	9.89	8.31	8.93
27	7.79	30.00	13.80	12.38	11	9.63	8.25	6.88
28	31.16	150.14	13.80	12.38	11	9.63	8.25	6.88
29	31.11	30	13.77	12.36	10.98	9.61	8.24	6.86
30	110.05	138.57	13.77	12.36	10.98	9.61	8.24	6.86
31	110	22	13.77	12.36	10.98	9.61	8.24	6.86

Table B.3: PCCS parameters for treating flue gas from 50% methane mixture with syngas under different load conditions using AMP-PZ solvent

Point	Pressure (bar)	Temperature (°C)	Mass flow rate (kg/s)					
			100%	90%	80%	70%	60%	50%
0	0.885	104.64	268.60	241.74	214.88	188.02	161.16	134.3
1	1.15	137.87	268.60	241.74	214.88	188.02	161.16	134.3
2	1.1	65.40	268.60	241.74	214.88	188.02	161.16	134.3
3	1.05	40.00	266.53	239.88	213.23	186.57	159.92	133.27
4	0.895	40.40	251.96	226.76	201.57	176.37	151.18	125.98
5	0.885	117.72	251.96	226.76	201.57	176.37	151.18	125.98
5a	0.885	105	0.00	26.86	53.72	80.58	107.44	134.3
5b	0.885	117.72	251.96	253.62	255.29	256.95	258.62	260.28
5c	1.15	152.57	251.96	253.62	255.29	256.95	258.62	260.28
6	1	35	198.81	198.81	198.81	198.81	198.81	198.81
7	1.1	35	198.81	198.81	198.81	198.81	198.81	198.81
8	1.05	28.71	198.81	198.81	198.81	198.81	198.81	198.81
9	1.05	60	165.96	149.36	132.76	116.17	99.57	82.98
10	2.1	60.36	165.96	149.36	132.76	116.17	99.57	82.98
11	1.5	69.65	151.21	136.13	121.01	105.88	90.75	75.63
12	1.01325	69.65	151.38	136.24	121.11	105.97	90.83	75.69
13	1.1	70.06	151.38	136.24	121.11	105.97	90.83	75.69
14	1.05	40	151.38	136.24	121.11	105.97	90.83	75.69
15	2.05	100	165.96	149.36	132.76	116.17	99.57	82.98
16	1.96	122	140.81	126.75	112.67	98.58	84.5	70.42
17	1.96	119.57	151.21	136.13	121.01	105.88	90.75	75.63
18	2	120.29	151.21	136.13	121.01	105.88	90.75	75.63
19	2.03	122	165.96	149.36	132.76	116.17	99.57	82.98
20	2.01	125	165.96	149.36	132.76	116.17	99.57	82.98
21	3	135.00	25.82	23.14	20.57	17.99	15.42	12.85
22	2.9	132.37	25.82	23.14	20.57	17.99	15.42	12.85
23	1.99	125	25.14	22.61	20.11	17.59	15.07	12.56
24	1.96	30	14.74	13.23	11.76	10.29	8.82	7.35
25	1.96	30	10.40	9.38	8.34	7.3	6.25	5.21
26	7.84	150.45	14.74	13.23	11.76	10.29	8.82	7.35
27	7.79	30.00	14.64	13.14	11.68	10.22	8.76	7.3
28	31.16	150.14	14.64	13.14	11.68	10.22	8.76	7.3
29	31.11	30	14.62	13.12	11.66	10.2	8.75	7.28

Table B.3: PCCS parameters for treating flue gas from 50% methane mixture with syngas under different load conditions using AMP-PZ solvent

Point	Pressure (bar)	Temperature (°C)	Mass flow rate (kg/s)					
			100%	90%	80%	70%	60%	50%
30	110.05	138.57	14.62	13.12	11.66	10.2	8.75	7.28
31	110	22	14.62	13.12	11.66	10.2	8.75	7.28

Table B.4: PCCS parameters for treating flue gas from 25% methane mixture with syngas under different load conditions using AMP-PZ solvent

Point	Pressure (bar)	Temperature (°C)	Mass flow rate (kg/s)					
			100%	90%	80%	70%	60%	50%
0	0.885	104.64	268.60	241.74	214.88	188.02	161.16	134.3
1	1.15	137.80	268.60	241.74	214.88	188.02	161.16	134.3
2	1.1	65.40	268.60	241.74	214.88	188.02	161.16	134.3
3	1.05	40.00	266.10	239.49	212.88	186.27	159.66	133.05
4	0.895	40.40	250.15	225.13	200.12	175.1	150.09	125.07
5	0.885	118.25	250.15	225.13	200.12	175.1	150.09	125.07
5a	0.885	105	0.00	26.86	53.72	80.58	107.44	134.3
5b	0.885	118.25	250.15	251.99	253.84	255.68	257.53	259.37
5c	1.15	153.14	250.15	251.99	253.84	255.68	257.53	259.37
6	1	35	198.81	198.81	198.81	198.81	198.81	198.81
7	1.1	35	198.81	198.81	198.81	198.81	198.81	198.81
8	1.05	28.76	198.81	198.81	198.81	198.81	198.81	198.81
9	1.05	60	181.65	163.48	145.32	127.15	108.99	90.83
10	2.1	60.36	181.65	163.48	145.32	127.15	108.99	90.83
11	1.5	70.36	165.51	149.01	132.45	115.89	99.34	82.78
12	1.01325	70.36	165.70	149.13	132.56	115.98	99.42	82.85
13	1.1	70.78	165.70	149.13	132.56	115.98	99.42	82.85
14	1.05	40	165.70	149.13	132.56	115.98	99.42	82.85
15	2.05	100	181.65	163.48	145.32	127.15	108.99	90.83
16	1.96	122	154.13	138.74	123.32	107.91	92.49	77.08
17	1.96	119.57	165.51	149.01	132.45	115.89	99.34	82.78
18	2	120.29	165.51	149.01	132.45	115.89	99.34	82.78
19	2.03	122	181.65	163.48	145.32	127.15	108.99	90.83
20	2.01	125	181.65	163.48	145.32	127.15	108.99	90.83
21	3	135.00	28.26	25.32	22.51	19.69	16.88	14.07

Table B.4: PCCS parameters for treating flue gas from 25% methane mixture with syngas under different load conditions using AMP-PZ solvent

Point	Pressure (bar)	Temperature (°C)	Mass flow rate (kg/s)					
			100%	90%	80%	70%	60%	50%
22	2.9	132.37	28.26	25.32	22.51	19.69	16.88	14.07
23	1.99	125	27.52	24.75	21.99	19.25	16.49	13.75
24	1.96	30	16.13	14.48	12.87	11.28	9.64	8.04
25	1.96	30	11.39	10.27	9.13	7.97	6.85	5.71
26	7.84	150.45	16.13	14.48	12.87	11.28	9.64	8.04
27	7.79	30.00	16.03	14.38	12.78	11.19	9.59	7.99
28	31.16	150.14	16.03	14.38	12.78	11.19	9.59	7.99
29	31.11	30	16.00	14.36	12.76	11.17	9.57	7.97
30	110.05	138.57	16.00	14.36	12.76	11.17	9.57	7.97
31	110	22	16.00	14.36	12.76	11.17	9.57	7.97

Table B.5: PCCS parameters for treating flue gas from Nitrogen rich natural gas under different load conditions using AMP-PZ solvent

Point	Pressure (bar)	Temperature (°C)	Mass flow rate (kg/s)					
			100%	90%	80%	70%	60%	50%
0	0.885	104.64	268.60	241.74	214.88	188.02	161.16	134.30
1	1.15	137.94	268.60	241.74	214.88	188.02	161.16	134.30
2	1.1	65.40	268.60	241.74	214.88	188.02	161.16	134.30
3	1.05	40.00	267.66	240.89	214.13	187.37	160.59	133.83
4	0.895	40.40	253.98	228.58	203.18	177.78	152.39	126.98
5	0.885	116.96	253.98	228.58	203.18	177.78	152.39	126.98
5a	0.885	105.00	0.00	26.86	53.72	80.58	107.44	134.30
5b	0.885	116.96	253.98	255.44	256.90	258.36	259.83	261.28
5c	1.15	151.76	253.98	255.44	256.90	258.36	259.83	261.28
6	1.00	35.00	198.81	198.81	198.81	198.81	198.81	198.81
7	1.10	35.00	198.81	198.81	198.81	198.81	198.81	198.81
8	1.05	28.65	198.81	198.81	198.81	198.81	198.81	198.81
9	1.05	60.00	155.86	140.28	124.69	109.10	93.52	77.93
10	2.10	60.33	155.86	140.28	124.69	109.10	93.52	77.93
11	1.50	70.33	142.02	127.85	113.65	99.44	85.23	71.03
12	1.01325	70.33	142.17	127.96	113.74	99.52	85.30	71.09
13	1.10	70.75	142.17	127.96	113.74	99.52	85.30	71.09

Table B.5: PCCS parameters for treating flue gas from Nitrogen rich natural gas under different load conditions using AMP-PZ solvent

Point	Pressure (bar)	Temperature (°C)	Mass flow rate (kg/s)					
			100%	90%	80%	70%	60%	50%
14	1.05	40.00	142.17	127.96	113.74	99.52	85.30	71.09
15	2.05	100.00	155.86	140.28	124.69	109.10	93.52	77.93
16	1.96	122.00	132.25	119.04	105.81	92.58	79.36	66.13
17	1.96	119.57	142.02	127.85	113.65	99.44	85.23	71.03
18	2.00	120.29	142.02	127.85	113.65	99.44	85.23	71.03
19	2.03	122.00	155.86	140.28	124.69	109.10	93.52	77.93
20	2.01	125.00	155.86	140.28	124.69	109.10	93.52	77.93
21	3.00	135.00	24.25	21.73	19.31	16.90	14.48	12.07
22	2.90	132.37	24.25	21.73	19.31	16.90	14.48	12.07
23	1.99	125.00	23.61	21.24	18.88	16.52	14.16	11.79
24	1.96	30.00	13.84	12.43	11.05	9.67	8.29	6.90
25	1.96	30.00	9.77	8.81	7.83	6.85	5.87	4.89
26	7.84	150.45	13.84	12.43	11.05	9.67	8.29	6.90
27	7.79	30.00	13.75	12.34	10.89	9.59	8.23	6.86
28	31.16	150.14	13.75	12.34	10.89	9.59	8.23	6.86
29	31.11	30.00	13.73	12.32	10.95	9.58	8.21	6.84
30	110.05	138.57	13.73	12.32	10.95	9.58	8.21	6.84
31	110.00	22.00	13.73	12.32	10.95	9.58	8.21	6.84

Table B.6: PCCS parameters for treating flue gas from 75% N_2 rich gas mixture with syngas under different load conditions using AMP-PZ solvent

Point	Pressure (bar)	Temperature (°C)	Mass flow rate (kg/s)					
			100%	90%	80%	70%	60%	50%
0	0.885	104.64	268.60	241.74	214.88	188.02	161.16	134.3
1	1.15	137.88	268.60	241.74	214.88	188.02	161.16	134.3
2	1.1	65.40	268.60	241.74	214.88	188.02	161.16	134.3
3	1.05	40.00	267.09	240.38	213.67	186.96	160.26	133.55
4	0.895	40.40	252.23	227.01	201.78	176.56	151.34	126.12
5	0.885	117.50	252.23	227.01	201.78	176.56	151.34	126.12
5a	0.885	105	0.00	26.86	53.72	80.58	107.44	134.3
5b	0.885	117.50	252.23	253.87	255.51	257.14	258.78	260.42
5c	1.15	152.35	252.23	253.87	255.51	257.14	258.78	260.42

Table B.6: PCCS parameters for treating flue gas from 75% N_2 rich gas mixture with syngas under different load conditions using AMP-PZ solvent

Point	Pressure (bar)	Temperature (°C)	Mass flow rate (kg/s)					
			100%	90%	80%	70%	60%	50%
6	1	35	198.81	198.81	198.81	198.81	198.81	198.81
7	1.1	35	198.81	198.81	198.81	198.81	198.81	198.81
8	1.05	28.70	198.81	198.81	198.81	198.81	198.81	198.81
9	1.05	60	169.22	152.29	135.37	118.45	101.53	84.61
10	2.1	60.36	169.22	152.29	135.37	118.45	101.53	84.61
11	1.5	70.36	154.19	138.81	132.38	107.96	92.54	77.12
12	1.01325	70.36	154.36	138.92	123.49	108.05	92.62	77.18
13	1.1	70.78	154.36	138.92	123.49	108.05	92.62	77.18
14	1.05	40	154.36	138.92	123.49	108.05	92.62	77.18
15	2.05	100	169.22	152.29	135.37	118.45	101.53	84.61
16	1.96	122	143.58	129.24	114.88	100.52	86.16	71.8
17	1.96	119.57	154.19	138.81	132.38	107.96	92.54	77.12
18	2	120.29	154.19	138.81	132.38	107.96	92.54	77.12
19	2.03	122	169.22	152.29	135.37	118.45	101.53	84.61
20	2.01	125	169.22	152.29	135.37	118.45	101.53	84.61
21	3	135.00	26.33	23.59	20.97	18.35	15.73	13.12
22	2.9	132.37	26.33	23.59	20.97	18.35	15.73	13.12
23	1.99	125	25.64	23.05	20.49	17.93	15.37	12.81
24	1.96	30	15.03	13.49	11.99	10.49	8.99	7.5
25	1.96	30	10.61	9.56	8.5	7.44	6.38	5.31
26	7.84	150.45	15.03	13.49	11.99	10.49	8.99	7.5
27	7.79	30.00	14.93	13.39	11.9	10.42	8.93	7.44
28	31.16	150.14	14.93	13.39	11.9	10.42	8.93	7.44
29	31.11	30	14.90	13.37	11.88	10.4	8.92	7.43
30	110.05	138.57	14.90	13.37	11.88	10.4	8.92	7.43
31	110	22	14.90	13.37	11.88	10.4	8.92	7.43

Table B.7: PCCS parameters for treating flue gas from 50% N_2 rich gas mixture with syngas under different load conditions using AMP-PZ solvent

Point	Pressure (bar)	Temperature (°C)	Mass flow rate (kg/s)					
			100%	90%	80%	70%	60%	50%
0	0.885	104.64	268.60	241.74	214.88	188.02	161.16	134.3
1	1.15	137.82	268.60	241.74	214.88	188.02	161.16	134.3
2	1.1	65.40	268.60	241.74	214.88	188.02	161.16	134.3
3	1.05	40.00	266.50	239.85	213.20	186.55	159.90	133.25
4	0.895	40.40	250.43	225.39	200.34	175.30	150.26	125.21
5	0.885	118.08	250.43	225.39	200.34	175.30	150.26	125.21
5a	0.885	105.00	0.00	26.86	53.72	80.58	107.44	134.3
5b	0.885	118.08	250.43	252.25	254.06	255.88	257.7	259.52
5c	1.15	152.96	250.43	252.25	254.06	255.88	257.7	259.52
6	1	35	198.81	198.81	198.81	198.81	198.81	198.81
7	1.1	35	198.81	198.81	198.81	198.81	198.81	198.81
8	1.05	28.75	198.81	198.81	198.81	198.81	198.81	198.81
9	1.05	60	183.01	164.71	146.40	128.11	109.81	91.51
10	2.1	60.36	183.01	164.71	146.40	128.11	109.81	91.51
11	1.5	70.36	166.76	150.20	133.44	116.76	100.08	83.4
12	1.01325	70.36	166.94	150.25	133.55	116.86	100.16	83.47
13	1.1	70.78	166.94	150.25	133.55	116.86	100.16	83.47
14	1.05	40	166.94	150.25	133.55	116.86	100.16	83.47
15	2.05	100	183.01	164.71	146.40	128.11	109.81	91.51
16	1.96	123	155.29	139.78	124.24	106.72	93.18	77.65
17	1.96	119.57	166.76	150.20	133.44	116.76	100.08	83.40
18	2	120.29	166.76	150.20	133.44	116.76	100.08	83.40
19	2.03	123	183.01	164.71	146.40	128.11	109.81	91.51
20	2.01	125	183.01	164.71	146.40	128.11	109.81	91.51
21	3	135.00	28.48	25.51	22.68	19.84	17.01	14.17
22	2.9	132.37	28.48	25.51	22.68	19.84	17.01	14.17
23	1.99	125	27.73	24.93	22.16	19.39	16.62	13.85
24	1.96	30	16.26	14.58	12.97	11.34	9.73	8.1
25	1.96	30	11.47	10.35	9.19	8.05	6.89	5.75
26	7.84	150.45	16.26	14.58	12.97	11.34	9.73	8.1
27	7.79	30.00	16.15	14.48	12.88	11.27	9.66	8.05
28	31.16	150.14	16.15	14.48	12.88	11.27	9.66	8.05
29	31.11	30	16.12	14.46	12.86	11.25	9.64	8.03

Table B.7: PCCS parameters for treating flue gas from 50% N_2 rich gas mixture with syngas under different load conditions using AMP-PZ solvent

Point	Pressure (bar)	Temperature (°C)	Mass flow rate (kg/s)					
			100%	90%	80%	70%	60%	50%
30	110.05	138.57	16.12	14.46	12.86	11.25	9.64	8.03
31	110	22	16.12	14.46	12.86	11.25	9.64	8.03

Table B.8: PCCS parameters for treating flue gas from 25% N_2 rich gas mixture with syngas under different load conditions using AMP-PZ solvent

Point	Pressure (bar)	Temperature (°C)	Mass flow rate (kg/s)					
			100%	90%	80%	70%	60%	50%
0	0.885	104.64	268.60	241.74	214.88	188.02	161.16	134.3
1	1.15	137.75	268.60	241.74	214.88	188.02	161.16	134.3
2	1.1	65.40	268.60	241.74	214.88	188.02	161.16	134.3
3	1.05	40.00	265.89	239.3	212.71	186.12	159.53	132.95
4	0.895	40.40	248.57	223.71	198.85	173.99	149.14	124.28
5	0.885	118.67	248.57	223.71	198.85	173.99	149.14	124.28
5a	0.885	105	0.00	26.86	53.72	80.58	107.44	134.3
5b	0.885	118.67	248.57	250.57	252.57	254.58	256.58	258.58
5c	1.15	153.60	248.57	250.57	252.57	254.58	256.58	258.58
6	1	35	198.81	198.81	198.81	198.81	198.81	198.81
7	1.1	35	198.81	198.81	198.81	198.81	198.81	198.81
8	1.05	28.80	198.81	198.81	198.81	198.81	198.81	198.81
9	1.05	60	197.27	177.54	157.81	138.08	118.36	98.63
10	2.1	60.36	197.27	177.54	157.81	138.08	118.36	98.63
11	1.5	70.36	179.74	161.81	143.83	125.86	107.87	89.89
12	1.01325	70.36	179.94	161.95	143.95	125.96	107.96	89.97
13	1.1	70.78	179.94	161.95	143.95	125.96	107.96	89.97
14	1.05	40	179.94	161.95	143.95	125.96	107.96	89.97
15	2.05	100	197.27	177.54	157.81	138.08	118.36	98.63
16	1.96	122	167.38	150.66	133.92	117.18	100.44	83.7
17	1.96	119.57	179.74	161.81	143.83	125.86	107.87	89.89
18	2	120.29	179.74	161.81	143.83	125.86	107.87	89.89
19	2.03	122	197.27	177.54	157.81	138.08	118.36	98.63
20	2.01	125	197.27	177.54	157.81	138.08	118.36	98.63
21	3	135.00	30.69	27.5	24.45	21.38	18.33	15.28

Table B.8: PCCS parameters for treating flue gas from 25% N_2 rich gas mixture with syngas under different load conditions using AMP-PZ solvent

Point	Pressure (bar)	Temperature (°C)	Mass flow rate (kg/s)					
			100%	90%	80%	70%	60%	50%
22	2.9	132.37	30.69	27.5	24.45	21.38	18.33	15.28
23	1.99	125	29.89	26.87	23.89	20.9	17.92	14.93
24	1.96	30	17.52	15.72	13.98	12.23	10.49	8.74
25	1.96	30	12.37	11.15	9.91	8.67	7.43	6.19
26	7.84	150.45	17.52	15.72	13.98	12.23	10.49	8.74
27	7.79	30.00	17.40	15.81	13.88	12.15	10.41	8.87
28	31.16	150.14	17.40	15.81	13.88	12.15	10.41	8.87
29	31.11	30	17.37	15.6	13.86	12.13	10.4	8.66
30	110.05	138.57	17.37	15.6	13.86	12.13	10.4	8.66
31	110	22	17.37	15.6	13.86	12.13	10.4	8.66

Table B.9: PCCS parameters for treating flue gas from syngas under different load conditions using AMP-PZ solvent

Point	Pressure (bar)	Temperature (°C)	Mass flow rate (kg/s)				
			100%	90%	80%	70%	60%
0	0.885	104.64	268.60	241.74	214.88	188.02	161.16
1	1.15	137.68	268.60	241.74	214.88	188.02	161.16
2	1.1	65.40	268.60	241.74	214.88	188.02	161.16
3	1.05	40.00	265.26	238.74	212.21	185.68	159.16
4	0.895	40.40	246.65	221.98	197.32	172.65	147.98
5	0.885	119.30	246.65	221.98	197.32	172.65	147.98
5a	0.885	105	0.00	26.86	53.72	80.58	107.44
5b	0.885	119.30	246.65	248.84	251.04	253.23	255.43
5c	1.15	154.27	246.65	248.84	251.04	253.23	255.43
6	1	35	198.81	198.81	198.81	198.81	198.81
7	1.1	35	198.81	198.81	198.81	198.81	198.81
8	1.05	28.90	198.81	198.81	198.81	198.81	198.81
9	1.05	60	212.00	190.80	169.60	148.40	127.20
10	2.1	59.65	212.00	190.80	169.60	148.40	127.20
11	1.5	69.48	193.17	173.90	154.58	135.26	115.93
12	1.01325	69.48	193.38	174.04	154.71	135.37	116.03
13	1.1	69.90	193.38	174.04	154.71	135.37	116.03

Table B.9: PCCS parameters for treating flue gas from syngas under different load conditions using AMP-PZ solvent

Point	Pressure (bar)	Temperature (°C)	Mass flow rate (kg/s)				
			100%	90%	80%	70%	60%
14	1.05	40	193.38	174.04	154.71	135.37	116.03
15	2.05	100	212.00	190.80	169.60	148.40	127.20
16	1.96	122	179.88	161.92	143.93	125.93	107.94
17	1.96	119.57	193.17	173.90	154.58	135.26	115.93
18	2	120.29	193.17	173.90	154.58	135.26	115.93
19	2.03	122	212.00	190.80	169.60	148.40	127.20
20	2.01	125	212.00	190.80	169.60	148.40	127.20
21	3	135.00	32.99	29.55	26.27	22.99	19.70
22	2.9	132.37	32.99	29.55	26.27	22.99	19.70
23	1.99	125	32.12	28.88	25.67	22.46	19.26
24	1.96	30	18.83	16.90	15.02	13.14	11.27
25	1.96	30	13.29	11.98	10.65	9.32	7.99
26	7.84	150.45	18.83	16.90	15.02	13.14	11.27
27	7.79	30.00	18.70	16.78	15.10	13	11.19
28	31.16	150.14	18.70	16.78	15.10	13	11.19
29	31.11	30	18.67	16.76	14.90	13.03	11.17
30	110.05	138.57	18.67	16.76	14.90	13.03	11.17
31	110	22	18.67	16.76	14.90	13.03	11.17

Bibliography

[1] IEA (2024). World Energy Outlook 2024, IEA, Paris. https://www.iea.org/reports/world-energy-outlook-2024. Licence: CC BY 4.0 (report); CC BY NC SA 4.0 (Annex A).

[2] IEA. World Energy Statistics and Balances, IEA, Paris. https://www.iea.org/data-and-statistics/data-product/world-energy-statistics-and-balances. Licence: CC BY 4.0.

[3] IEA (2023). World Energy Outlook 2023, IEA, Paris. https://www.iea.org/reports/world-energy-outlook-2023. Licence: CC BY 4.0 (Annex A).

[4] IEA (2024). Electricity 2024, IEA, Paris. https://www.iea.org/reports/electricity-2024. Licence: CC BY 4.0.

[5] T. Liu, J. Xu, Y. Li. Analyzing the economic, social, and technological determinants of renewable and nonrenewable electricity production in China: Findings from time series models. *Energy*, 282, 2023. doi:10.1016/j.energy.2023.128888.

[6] R. Hino, L. X. Yan. Nuclear Hydrogen Production Handbook. *CRC Press*, 2011. doi:10.1201/b10789.

[7] S. Suman. Hybrid nuclear-renewable energy systems: A review. *J Clean Prod*, 181, 2018. doi:10.1016/j.jclepro.2018.01.262.

[8] IEA (2024). Electricity Mid-Year Update - July 2024, IEA, Paris. https://www.iea.org/reports/electricity-mid-year-update-july-2024. Licence: CC BY 4.0.

[9] IEA (2022). World Energy Outlook 2022, IEA, Paris. https://www.iea.org/reports/world-energy-outlook-2022. Licence: CC BY 4.0 (report); CC BY NC SA 4.0 (Annex A).

[10] IEA (2024). Electricity 2024, IEA, Paris. https://www.iea.org/reports/electricity-2024. Licence: CC BY 4.0.

[11] R. York, S. E. Bell. Energy transitions or additions?: Why a transition from fossil fuels requires more than the growth of renewable energy. *Energy Research Social Science*, 15, 2019. doi:10.1016/j.erss.2019.01.008.

[12] F. Martins, C. Felgueiras, M. Smitkova, N. Caetano. Analysis of Fossil Fuel Energy Consumption and Environmental Impacts in European Countries. *Energies*, 12(6), 2019. doi:10.3390/en12060964.

[13] IEA (2022). Electricity Security Policy, IEA, Paris. https://www.iea.org/reports/electricity-security-policy. Licence: CC BY 4.0.

[14] IEA (2022). Coal Mid-Year Update - July 2024, IEA, Paris. https://www.iea.org/reports/coal-mid-year-update-july-2024. Licence: CC BY 4.0.

[15] S. Sammarchi, J. Li, D. Izikowitz, Q. Yang, D. Xu. China's coal power decarbonization via CO_2 capture and storage and biomass co-firing: A LCA case study in Inner Mongolia. *Energy*, 261, 2022. doi:10.1016/j.energy.2022.125158.

[16] NS Energy. Profiling the top five biggest coal power plants in the world, Accessed: 10/09/2024. https://www.nsenergybusiness.com/analysis/biggest-coal-power-plants/?cf-view.

[17] H. S. Jung, S. G. Ryoo, Y. T. Kang. Life cycle environmental impact assessment of Taean coal power plant with CO_2 capture module. *Journal of Cleaner Production*, 357:131663, 2022. doi:10.1016/j.jclepro.2022.131663.

[18] Dubai Electricity Water Authority. Jebel Ali Power and Desalination Complex enhances generation efficiency and meets energy and water demand in Dubai, Accessed: March. 25, 2025. https://www.dewa.gov.ae/en/about-us/media-publications/latest-news/2021/07/jebel-ali-power-and-desalination-complex?utm_source=chatgpt.com.

[19] A. Farnoosh. *Power Generation from Coal, Oil, Gas, and Biofuels.* Hafner, M., Luciani, G. (eds) The Palgrave Handbook of International Energy Economics. Palgrave Macmillan, Cham, 2022. doi:10.1007/978-3-030-86884-0_6.

[20] IEA (2023). The Oil and Gas Industry in Net Zero Transitions, IEA, Paris. https://www.iea.org/reports/the-oil-and-gas-industry-in-net-zero-transitions. Licence: CC BY 4.0.

[21] M. A. Sayegh et al. Trends of European research and development in district heating technologies. *Renewable and Sustainable Energy Reviews*, 68, 2017. doi:10.1016/j.rser.2016.02.023.

[22] S. Gendelis, E. Dace, J. Ziemele. Impact of global warming and building renovation on the heat demand and district heating capacity: Case of the city of Riga. *Energy*, 276, 2023. doi:10.1016/j.energy.2023.127567.

[23] IEA (2022). 350 million building units connected to district energy networks by 2030, provide about 20% of space heating needs, IEA, Paris. https://www.iea.org/. Licence: CC BY 4.0.

[24] S. Kuntuarova, T. Lickleder, T. Huynh, D. Zinsmeister, T. Hamacher, V. Perić. Design and simulation of district heating networks: A review of modeling approaches and tools. *Energy*, 305, 2024. doi:10.1016/j.energy.2024.132189.

[25] H. Lund, S. Werner, R. Wiltshire, S. Svendsen, J. E. Thorsen, F. Hvelplund, B. V. Mathiesen. 4th Generation District Heating (4GDH): Integrating smart thermal grids into future sustainable energy systems. *Energy*, 68, 2014. doi:10.1016/j.energy.2014.02.089.

[26] S. Buffa, M. Cozzini, M. D'Antoni, M. Baratieri, R. Fedrizzi. 5th generation district heating and cooling systems: A review of existing cases in Europe. *Renewable and Sustainable Energy Reviews*, 104:504 – 522, 2019. doi:10.1016/j.rser.2018.12.059.

[27] N. Lamaison, D. Chèze, J.-F. Robin, F. Bruyat, F. Lefrancois. Operational behaviour of a solar-fed bidirectional substation for 4GDH networks. *ISES SWC 2021 - Solar World Congress 2021, Virtual, France*, pages 1 – 10, 2021. doi:10.18086/swc.2021.28.03.

[28] M. Pipiciello, F. Trentin, A. Soppelsa, D. Menegon, R. Fedrizzi, M. Ricci, B. Di Pietra, P. Sdringola. The bidirectional substation for district heating users: experimental performance assessment with operational profiles of prosumer loads and distributed generation. *Energy and Buildings*, 305:113872, 2024. doi:10.1016/j.enbuild.2023.113872.

[29] J. Barco-Burgos, J.C. Bruno, U. Eicker, A.L. Saldaña-Robles, V. Alcántar-Camarena. Review on the integration of high-temperature heat pumps in district heating and cooling networks. *Energy*, 239:122378, 2022. doi:10.1016/j.energy.2021.122378.

[30] T. Deng, L. Tian, B. Hu, Xinping Liu, J. Liu, G. Zhou, Y. Zhao. Dynamic availability of energy storage in district heating networks for automatic generation control of a CHP plant. *Applied Thermal Engineering*, 183, 2021. doi:10.1016/j.applthermaleng.2020.116198.

[31] L. Tian, Y. Xie, B. Hu, X. Liu, T. Deng, H. Luo, F. Li. A Deep Peak Regulation Auxiliary Service Bidding Strategy for CHP Units Based on a Risk-Averse Model and District Heating Network Energy Storage. *Energies*, 12(17):3314, 2019. doi:10.3390/en12173314.

[32] I. Opriș, V.-E. Cenușă. Design optimization of cogeneration steam power plants with supercritical parameters. *Sustainable Energy Technologies and Assessments*, 64, 2024. doi:10.1016/j.seta.2024.103727.

[33] A. Chakraborty, M. Joshi, S. Manjare, I. A. Karimi. An Industrial Perspective of Cogeneration – A Comprehensive Review. *Chemical Engineering and Processing - Process Intensification*, page 109974, 2024. doi:10.1016/j.cep.2024.109974.

[34] IEA (2011). Co-Generation and Renewables, IEA, Paris. https://www.iea.org/reports/co-generation-and-renewables. Licence: CC BY 4.0.

[35] M. Kabeyi, O. Olanrewaju. Preliminary design of a cogeneration plant for a 120 MW diesel engine power plant. *12th annual Istanbul international conference on industrial engineering and operations management, Istanbul, Turkey*, 411, 2022. doi:10.46254/AN12.20220411.

[36] H. Chen, Y. Wu, S. Xu, G. Xu, Y. Yang, W. Liu. Thermodynamic and economic evaluation of a novel heat supply design using low-pressure feedwater in a cogeneration plant. *Applied Thermal Engineering*, 166:114672, 2020. doi:10.1016/j.applthermaleng.2019.114672.

[37] R. De Souza, M. Casisi,D. Micheli, M. Reini. A review of small–medium combined heat and power (CHP) technologies and their role within the 100 *Energies*, 14(17):5338, 2021. doi:10.3390/en14175338.

[38] J. Beiron, R. M. Montañés, F. Normann, F. Johnsson. Flexible operation of a combined cycle cogeneration plant – A techno-economic assessment. *Applied Energy*, 278:115630, 2020. doi:10.1016/j.apenergy.2020.115630.

[39] U.S. Commercial Service Poland. Poland - Country Commercial Guide: Energy Sector, Accessed: Sep. 30, 2024. https://www.trade.gov/country-commercial-guides/poland-energy-sector.

[40] ARE (Energy Market Agency) for MKiŚ, URE. Electricity generation capacity in Poland. https://energy.instrat.pl/en/electrical-system/generation-capacity-are/.

[41] Instrat. Power plants database for Poland expanded, Accessed: Sep. 30, 2024. https://docs.google.com/spreadsheets/d/10CGXI3JlGY2_xKGERF5LA8AzFi8OQlgu43Y9RASRJqo/edit?gid=1215954284#gid=1215954284.

[42] A. Konvalinová. *Polish Coal Sector: Beginning of a Phase-out Era?* PhD thesis, Masaryk University, 2021.

[43] Tauron. TAURON Capital Group's Strategy and its assumptions. https://raport.tauron.pl/en/strategy-and-outlook/tauron-capital-groups-strategy-and-its-assumptions/.

[44] Tauron. Competitive environment. https://raport.tauron.pl/en/conditions-of-activity/competitive-environment/.

[45] PGE. PGE Group's strategy. https://www.gkpge.pl/en/pge-group/about-group/pge-group-s-strategy.

[46] Ministry of Climate and Environment. Energy Policy of Poland until 2040 (EPP2040), Accessed: Oct. 01, 2024. https://www.gov.pl/web/climate/.

[47] A. C. Marques, D. S. Pereira. Could electricity demand contribute to diversifying the mix and mitigating CO_2 emissions? A fresh daily analysis of the French electricity system. *Energy Policy*, 142, 2020. doi:10.1016/J.ENPOL.2020.111475.

[48] S. Zafar, S. Ammara. Variations in climate change views across Europe: An empirical analysis. *J Clean Prod*, 442, 2024. doi:10.1016/J.JCLEPRO.2024.141157.

[49] S. Tadadjeu, H. Njangang, A. Woldemichael. Are resource-rich countries less responsive to global warming? Oil wealth and climate change policy. *Energy Policy*, 182, 2023. doi:10.1016/J.ENPOL.2023.113774.

[50] R. Wu, Jieyu Wang, S. Wang, K. Feng. The drivers of declining CO_2 emissions trends in developed nations using an extended STIRPAT model: A historical and prospective analysis. *Renewable and Sustainable Energy Reviews*, 149:111328, 2021. doi:10.1016/j.rser.2021.111328.

[51] IEA (2024). CO_2 Emissions in 2023, IEA, Paris. https://www.iea.org/reports/co2-emissions-in-2023. Licence: CC BY 4.0.

[52] IEA (2025). Global Energy Review 2025, IEA, Paris. https://www.iea.org/reports/global-energy-review-2025. Licence: CC BY 4.0.

[53] M. A. Aktar, M. M. Alam, A. Q. Al-Amin. Global economic crisis, energy use, CO_2 emissions, and policy roadmap amid COVID-19. *Sustainable Production and Consumption*, 26:770 – 781, 2021. doi:10.1016/j.spc.2020.12.029.

[54] IEA (2023). CO_2 Emissions in 2022, IEA, Paris. https://www.iea.org/reports/co2-emissions-in-2022. Licence: CC BY 4.0.

[55] R. M. Hannun, H. H. Razzaq. Air Pollution Resulted from Coal, Oil and Gas Firing in Thermal Power Plants and Treatment: A Review. *IOP Conference Series Earth and Environmental Science*, 1002(1):012008, 2022. doi:10.1088/1755-1315/1002/1/012008.

[56] H. Ritchie, M. Roser. CO_2 emissions. https://ourworldindata.org/co2-emissions, 2020.

[57] M. Guevara, S. Enciso1, Carles Tena, Oriol Jorba1, S. Dellaert, H. D. van der Gon, C. P. García-Pando. A global catalogue of CO_2 emissions and co-emitted species from power plants, including high-resolution vertical and temporal profiles. *Earth System Science Data*, 16:337 – 373, 2024. doi:10.5194/essd-16-337-2024.

[58] G. Han, Y. Huang, T. Shi, H. Zhang, S. Li, H. Zhang, W. Chen, J. Liu, W. Gong. Quantifying CO_2 emissions of power plants with Aerosols and Carbon Dioxide Lidar onboard DQ-1. *Earth System Science Data*, 16:337 – 373, 2024. doi:10.5194/essd-16-337-2024.

[59] P. Brandl, M. Bui, J. P. Hallett, N. M. Dowell. Beyond 90 *International Journal of Greenhouse Gas Control*, 105:103239, 2021. doi:10.1016/j.ijggc.2020.103239.

[60] H. Ritchie, P. Rosado, M. Roser. CO_2 emissions by fuel. https://ourworldindata.org/emissions-by-fuel, 2020.

[61] IEA (2021). The IEA at COP26, IEA, Paris. https://www.iea.org/commentaries/the-iea-at-cop26. Licence: CC BY 4.0.

[62] M. E. Kahn, K. Mohaddes, R. N. C. Ng, M. H. Pesaran, M. Raissi, J. C. Yang. Long-term macroeconomic effects of climate change: A cross-country analysis. *Energy Econ*, 104, 2021. doi:10.1016/J.ENECO.2021.105624.

[63] D. Welsby, J. Price, S. Pye, P. Ekins. Unextractable fossil fuels in a 1.5 ℃ world. *Nature*, 597(7875):230 – 234, 2021. doi:10.1016/J.ENECO.2021.105624.

[64] IEA (2023). Credible pathways to 1.5℃, IEA, Paris. https://www.iea.org/reports/credible-pathways-to-150c. Licence: CC BY 4.0.

[65] IEA (2023). Net Zero Roadmap: A Global Pathway to Keep the 1.5 ℃ Goal in Reach, IEA, Paris. https://www.iea.org/. Licence: CC BY 4.0.

[66] IRENA (2021). World Energy Transitions Outlook: 1.5℃ Pathway, International Renewable Energy Agency, Abu Dhabi. https://www.irena.org/publications.

[67] IEA (2024). Clean Energy Market Monitor – March 2024, IEA, Paris. https://www.iea.org/reports/clean-energy-market-monitor-march-2024. Licence: CC BY 4.0.

[68] A. Sharif, N. Saqib, K. Dong, S.A.R. Khan. Nexus between green technology innovation, green financing, and CO_2 emissions in the G7 countries: the moderating role of social globalisation. *Sustainable Development*, 30(6):1934 – 1946, 2022. doi:10.1002/sd.2360.

[69] I. Tatarewicz et al. The Role of BECCS in Achieving Climate Neutrality in the European Union. *Energies (Basel)*, 14, 2021. doi:10.3390/en14237842.

[70] de Coninck, H., A. Revi, M. Babiker, P. Bertoldi, M. Buckeridge, A. Cartwright, W. Dong, J. Ford, S. Fuss, J.-C. Hourcade, D. Ley, R. Mechler, P. Newman, A. Revokatova, S. Schultz, L. Steg, and T. Sugiyama. Strengthening and Implementing the Global Response. In: Global Warming of 1.5℃. An IPCC Special Report on the impacts of global warming of 1.5℃ above pre-industrial levels and related global greenhouse gas emission pathways, in the context of strengthening the global response to the threat of climate change, sustainable development, and efforts to eradicate poverty. *Cambridge University Press, Cambridge, UK and New York, NY, USA*, pages 313 – 444, 2018. doi:10.1017/9781009157940.006.

[71] J. Penman, M. Gytarsky, T. Hiraishi, W. Irving, T. Krug. 2006 IPCC GUIDELINES FOR NATIONAL GREENHOUSE GAS INVENTORIES. https://www.ipcc-nggip.iges.or.jp.

[72] IEA (2011). Combining Bioenergy with CCS, IEA, Paris. https://www.iea.org/reports/combining-bioenergy-with-ccs. Licence: CC BY 4.0.

[73] IEA (2023). Tracking Clean Energy Progress 2023, IEA, Paris. https://www.iea.org/reports/tracking-clean-energy-progress-2023. Licence: CC BY 4.0.

[74] IEA (2023). Operational and planned BECCS capture capacity vs. the Net Zero Scenario, 2022-2030, IEA, Paris. https://www.iea.org/. Licence: CC BY 4.0.

[75] T. Hossain, P. Burli, J. Pin, D. Jones, D. Hartley, R. Hess. Deployment of BECCUS value chains in the United States - A case study of sequestering CO2 from ethanol production. https://www.ieabioenergy.com/.

[76] M. A. Gonzalez-Salazar, T. Kirsten, L. Prchlik. Review of the operational flexibility and emissions of gas- and coal-fired power plants in a future with growing renewables. *Renewable and Sustainable Energy Reviews*, 82:1497 – 1513, 2018. doi:10.1016/j.rser.2017.05.278.

[77] E. Assareh, S. Hoseinzadeh, D. E. Ghersi, et al. Energy, exergy, exergoeconomic, exergoenvironmental, and transient analysis of a gas-fired power plant-driven proposed system with combined Rankine cycle: thermoelectric for power production under different weather conditions. *J Therm Anal Calorim*, 148:8283 – 8307, 2023. doi:10.1007/s10973-022-11651-7.

[78] B. Zaporowski. Energy Effectiveness and Economic Performance of Gas and Gas-Steam Combined Heat and Power Plants Fired with Natural Gas. *Acta Energetica 1/26*, pages 152 – 157, 2016.

[79] M. Jamróz., M. Piwowarski, P. Ziemiański, G. Pawlak. Technical and Economic Analysis of the Supercritical Combined Gas-Steam Cycle. *Energies*, 14(11):2985, 2021. doi:10.3390/en14112985.

[80] Modern Power Systems. CC efficiency record broken at Keadby PS, Accessed: 11/10/2024. https://www.modernpowersystems.com/.

[81] J. Garcet, R. De Meulenaere, J. Blondeau. Enabling flexible CHP operation for grid support by exploiting the DHN thermal inertia. *Applied Energy*, 316:119056, 2022. doi:10.1016/j.apenergy.2022.119056.

[82] H. Li, S. Svendsen. Energy and exergy analysis of low temperature district heating network. *Energy*, 45, 2012. doi:10.1016/j.energy.2012.03.056.

[83] G. Peridas, B. Mordick Schmidt. The role of carbon capture and storage in the race to carbon neutrality. *The Electricity Journal*, 34, 2021. doi:10.1016/j.tej.2021.106996.

[84] P. Madejski, K. Chmiel, N. Subramanian, T. Kuś. Methods and Techniques for CO_2 Capture: Review of Potential Solutions and Applications in Modern Energy Technologies. *Energies*, 15(3):887, 2022. doi:10.3390/en15030887.

[85] D. Mullen, M. Lucquiaud. On the cost of zero-carbon electricity: A techno-economic analysis of combined cycle gas turbines with post-combustion CO_2 capture. *Energy Reports*, 11:5104 – 5124, 2024. doi:10.1016/j.egyr.2024.04.067.

[86] M. Sharif, T. Zhang, X. Wu, Y. Yu, Z. Zhang. Evaluation of CO_2 absorption performance by molecular dynamic simulation for mixed secondary and tertiary amines. *International Journal of Greenhouse Gas Control*, 97:103059, 2020. doi:10.1016/j.ijggc.2020.103059.

[87] B. Aghel, S. Janati, S. Wongwises, M. S. Shadloo. Review on CO_2 capture by blended amine solutions. *International Journal of Greenhouse Gas Control*, 119:103715, 2022. doi:10.1016/j.ijggc.2022.103715.

[88] S. Janati, B. Aghel, M. S. Shadloo. The effect of alkanolamine mixtures on CO_2 absorption efficiency in T-Shaped microchannel. *Environmental Technology Innovation*, 24:102006, 2021. doi:10.1016/j.eti.2021.102006.

[89] A. Ayyad, A. Abbas, N. Elminshawy. A simulation study of the effect of post-combustion amine-based carbon-capturing integrated with solar thermal collectors for combined cycle gas power plant. *Discover Sustainability*, 2(1):9, 2021. doi:10.1007/s43621-021-00018-x.

[90] A. Baudoux, F. Demeyer, W. De Paepe. Advanced configurations of amine based post-combustion carbon capture process applied to combined cycle gas turbine. *Energy Conversion and Management*, 22:100537, 2024. doi:10.1016/J.ECMX.2024.100537.

[91] M. Shahbaz, A. AlNouss, I. Ghiat, G. Mckay, H. Mackey, S. Elkhalifa, T. Al-Ansari. A comprehensive review of biomass based thermochemical conversion technologies integrated with CO_2 capture and utilisation within BECCS networks. *Resources, Conservation and Recycling*, 173:105734, 2021. doi:10.1016/j.resconrec.2021.105734.

[92] E.I. Koytsoumpa, D. M. Skouloudi, S. Karellas, E. Kakaras. Bioenergy with carbon capture and utilization: A review on the potential deployment towards a European circular bioeconomy. *Renewable and Sustainable Energy Reviews*, 152:111641, 2021. doi:10.1016/j.rser.2021.111641.

[93] NCO2PP. Negative CO2 Post-Combustion Project, 2024. Accessed: 25 March 2025. URL: https://nco2pp.mech.pg.gda.pl/pl.

[94] K. Lisiecka. Elektrociepłownia Gorzów pełna dobrej energii. PGE GiEK S.A. Oddział Elektrociepłownia Gorzów, 2017.

[95] N. Subramanian, P. Madejski. Analysis of CO_2 capture process from flue-gases in combined cycle gas turbine power plant using post-combustion capture technology. *Energy*, 282, 2023. doi:10.1016/j.energy.2023.128311.

[96] M. Wójcik. Analysis of the natural gas distribution infrastructure in the BSR countries, 2012.

[97] A. Manowska, A. Rybak, A. Dylong, J. Pielot. Forecasting of Natural Gas Consumption in Poland Based on ARIMA-LSTM Hybrid Model. *Energies*, 14(24):8597, 2021. doi:10.3390/en14248597.

[98] R. Wojtowicz, J. Jaworski. Operation Analysis of Selected Domestic Appliances Supplied with Mixture of Nitrogen-Rich Natural Gas with Hydrogen. *Sustainability*, 13(24):13577, 2021. doi:10.3390/su132413577.

[99] PGNiG Grupa Orlen. Natural gas, Accessed: Oct. 23, 2024. https://pgnig.pl/czym-jest-gaz-ziemny.

[100] P. Grzymislawski, P. Czyzewski, R. Slefarski. Nitrogen Dilution Effect on Swirl Stabilized Methane Burning in Gas Turbine Conditions. *Heat Transfer Engineering*, 44:11-12:1053 – 1060, 2023. doi:10.1080/01457632.2022.2113443.

[101] J. D. Bień and B. Bień. Thermal sewage sludge utilization in Poland in the context of circular economy. *Desalination Water Treat*, 186:10 – 18, 2020. doi:10.5004/dwt.2020.25135.

[102] A. Khakbaz et al. Monitoring of heavy metals, EOX and LAS in sewage sludge for agricultural use: A case study. *Detritus*, 12:160 – 168, 2020. doi:10.31025/2611-4135/2020.13993.

[103] M. J. Kacprzak, I. Kupich. The specificities of the circular economy (CE) in the municipal wastewater and sewage sludge sector—local circumstances in Poland. *Clean Technologies and Environmental Policy*, 2021. doi:10.1007/s10098-021-02178-w.

[104] The 2030 Agenda for Sustainable Development. Proportion of municipal waste generated according to the treatment operation to total municipal generated, Accessed: Oct. 24, 2024. https://sdg.gov.pl/.

[105] N. L. Enebe, C. B. Chigor, K. Obileke, M. S. Lawa, M. C. Enebe. Biogas and Syngas Production from Sewage Sludge: A Sustainable Source of Energy Generation. *Methane*, 2(2):192 – 217, 2023. doi:10.3390/methane2020014.

[106] K. Śpiewak. Gasification of Sewage Sludge — A Review. *Energies*, 17(17):4476, 2024. doi:10.3390/en17174476.

[107] Vishwajeet et al. Entrained Flow Plasma Gasification of Sewage Sludge– Proof-of-Concept and Fate of Inorganics. *Energies (Basel)*, 15, 2022. doi:10.3390/en15051948.

[108] Z. Wołoncewicz, J. Buraczewski. Experience of exploitation of gas-steam cycle in EC Gorzów S.A. 1999-2003. In: Konferencja Elektrownie i elektrociepłownie gazowe i gazowo - parowe, Poznań – Kierz 2003 (in Polish).

[109] ChemicalBook. Chemical properties. https://www.chemicalbook.com/.

[110] Siemens AG. SGT-800 Gas Turbine, Accessed: Aug. 25, 2024. https://refman.energytransitionmodel.com/publications/1954/download.

[111] Siemens AG. SST-400 Industrial Steam Turbines, Accessed: Aug. 25, 2024. [Online] Available: https://www.hgpauction.com/wp-content/uploads/2014/01/Siemens-Industrial-Steam-Turbine-SST-400-Brochure.pdf.

[112] Siemens. Gas turbine SGT - 800 for power generation applications. https://consult.environment-agency.gov.uk/.

[113] R. Shahouni, M. Abbasi, M. Akrami. A comprehensive review on control and mitigating the foam formation in amine-based solvents. *Chemical Engineering Journal Advances*, 19, 2025. doi:10.1016/j.ceja.2024.100618.

[114] M. Afkhamipour, M. Mofarahi. Review on the mass transfer performance of CO_2 absorption by amine-based solvents in low-and high-pressure absorption packed columns. *Royal Society of Chemistry*, 7, 2017. doi:10.1039/c7ra01352c.

[115] BTS Engineering. Use of recuperative cycles for closed heating of the brew column. https://bts.net.ua/eng/column/obogrev-brazhnoy-kolonny/.

[116] M. Caplow. Kinetics of carbamate formation and breakdown. *Journal of the American Chemical Society*, 90(24):6795 – 6803, 1968. doi:10.1021/ja01026a041.

[117] P. V. Danckwerts. The reaction of CO_2 with ethanolamines. *Chemical Engineering Science*, 34(4):443 – 446, 1979. doi:10.1016/0009-2509(79)85087-3.

[118] R. T. J. Porter, M. Fairweather, M. Pourkashanian, R. M. Woolley. The range and level of impurities in CO_2 streams from different carbon capture sources. *International Journal of Greenhouse Gas Control*, 36:161 – 174, 2015. doi:10.1016/j.ijggc.2015.02.016.

[119] P. H. M. Feron, A. Cousins, K. Jiang, R. Zhai, M. Garcia. An update of the benchmark post-combustion CO_2-capture technology. *Fuel*, 273, 2020. doi:10.1016/j.fuel.2020.117776.

[120] J. Jung, Y. S. Jeong, Y. Lim, C. S. Lee, and C. Han. Advanced CO_2 Capture Process Using MEA Scrubbing: Configuration of a Split Flow and Phase Separation Heat Exchanger. *Energy Procedia*, 37:1778 – 1784, 2013. doi:10.1016/j.egypro.2013.06.054.

[121] J. Andersson. An investigation of carbon capture technologies for Sävenäs waste-to-energy plant. *Natural Resources Engineering, Luleå University of Technology*, 2020.

[122] J. C. Morgan et al. Development of a framework for sequential Bayesian design of experiments: Application to a pilot-scale solvent-based CO_2 capture process. *Appl Energy*, 262:114533, 2020. doi:10.1016/j.apenergy.2020.114533.

[123] S. Hasan, A. J. Abbas, G. G. Nasr. Improving the Carbon Capture Efficiency for Gas Power Plants through Amine-Based Absorbents. *Sustainability*, 13:72, 2020. doi:10.3390/su13010072.

[124] J. Oexmann, A. Kather. Post-combustion CO_2 capture in coal-fired power plants: Comparison of integrated chemical absorption processes with piperazine promoted potassium carbonate and MEA. *Energy Procedia*, 1:799 – 806, 2009. doi:10.1016/j.egypro.2009.01.106.

[125] Dariusz Obarski. Siemens Sp. z o.o. Energy Sector Oil Gas industry Technical conditions of the investment for Construction of a new gas and steam unit in PGE GiEK S.A. Gorzów Branch, VIII Scientific and Technical Conference - i-MITEL, 2014.

[126] P. Madejski, P. Żymełka. *Introduction to computer calculations and simulation of energy systems operation in STEAG Ebsilon®Professional (in Polish).* The AGH University of Science and Technology Press, Kraków, 2020.

[127] Z. Liu, I. A. Karimi. Simulating combined cycle gas turbine power plants in Aspen HYSYS. *Energy Convers Manag*, 171:1213 – 1225, 2018. doi:10.1016/j.enconman.2018.06.049.

[128] R. Canepa, M. Wang, C. Biliyok, A. Satta. Thermodynamic analysis of combined cycle gas turbine power plant with post-combustion CO_2 capture and exhaust gas recirculation. *Proceedings of the Institution of Mechanical Engineers*, 227:89 – 105, 2013. doi:10.1177/0954408912469165.

[129] Z. Aminov, N. Nakagoshi, T. D. Xuan, O. Higashi, and K. Alikulov. Evaluation of the energy efficiency of combined cycle gas turbine. Case study of Tashkent thermal power plant, Uzbekistan. *Appl Therm Eng*, 103:501 – 509, 2016. doi:10.1016/j.applthermaleng.2016.03.158.

[130] P. Ziółkowski, Paweł Madejski, M. Amiri, T. Kuś, K. Stasiak, N. Subramanian, H. P. -Kruczek,J. Badur, Ł. Niedźwiecki, D. Mikielewicz. Thermodynamic Analysis of Negative CO_2 Emission Power Plant Using Aspen Plus, Aspen Hysys, and Ebsilon Software. *Energies*, 14(19):6304, 2021. doi:10.3390/en14196304.

[131] N. Subramanian P. Madejski. Carbon dioxide capture in large-scale CCGT power plant from flue gases obtained from various fuel mixtures. *Archives of Thermodynamics*, 45(4):85 – 93, 2024. doi:10.24425/ather.2024.151999.

[132] A. Tatarczuk, M. Szega, J. Zuwała. Thermodynamic analysis of a post-combustion carbon dioxide capture process in a pilot plant equipped with a heat integrated stripper. *Energy*, 278:127907, 2023. doi:10.1016/j.energy.2023.127907.

[133] C. Madeddu, M. Errico, R. Baratti. *CO_2 Capture by Reactive Absorption-Stripping: Modeling, Analysis and Design.* Springer, 2018.

[134] Aspen Plus. *Rate-Based Model of the CO_2 Capture Process by MEA using Aspen Plus.* Aspen Technology, Inc., USA, 2008.

[135] European Commission. Market analysis, Accessed: 21/11/2024. https://energy.ec.europa.eu/data-and-analysis/market-analysis_en.

[136] European Commission – DG Energy A4. Final Report – LCOE LCOH: Energy costs, taxes and the impact of government interventions on investments. https://trinomics.eu/, 2020.

[137] C. Fu, G d. A. Serrano, P. Ziółkowski, K. Stasiak, M. Kaszuba, M. Amiri, P. Dąbrowski, H. P. Kruczek, M. Ostrycharczyk, M. Baranowski, K. Krochmalny, M. Czerep, M. Kowal, P. Madejski, L.

Niedzwiecki, N. Subramanian, D. Mikielewicz. Comparative techno-economic analysis of negative emission CO_2 power plant versus combined cycle gas turbine with carbon capture and storage. *Energy*, 2025. doi:10.2139/ssrn.5087251.

[138] IEA (2020). Projected Costs of Generating Electricity 2020, IEA, Paris. https://www.iea.org/reports/projected-costs-of-generating-electricity-2020. Licence: CC BY 4.0.

[139] Polskie Sieci Elektroenergetyczne S.A. Balancing Market Operation - Energy Prices on Balancing Market, Accessed on: 19/11/2024. https://www.pse.pl/.

[140] Energy Regulatory Office. The role of the President of URE in the process of approving prices and fee rates in the heat market, Accessed: 26/11/2024. https://www.ure.gov.pl/.

[141] Ember energy. The price of emissions allowances in Europe, Accessed on: 19/11/2024. https://ember-energy.org/data/european-electricity-prices-and-costs/.

[142] Towarowa Giełda Energii S.A. Natural gas market price, Accessed on: 26/11/2024. https://tge.pl/gas-dam.

[143] nCO2PP. Project on Negative CO2 emission gas power plant. https://nco2pp.mech.pg.gda.pl/pl/dokumenty/raporty-techniczne.

[144] Główny Urząd Statystyczny. Sewage sludge from industrial and municipal wastewater treatment plants, Accessed: 24/11/2024. https://dbw.stat.gov.pl/.

[145] B. Zhang, S. Xiong, B. Xiao, D. Yu, X. Jia. Mechanism of wet sewage sludge pyrolysis in a tubular furnace. *International Journal of Hydrogen Energy*, 36(1):355 – 363, 2011. doi:10.1016/j.ijhydene.2010.05.100.

[146] X. Wu, M. Wang, P. Liao, J. Shen, Y. Li. Solvent-based post-combustion CO_2 capture for power plants: A critical review and perspective on dynamic modelling, system identification, process control and flexible operation. *Applied Energy*, 257:113941, 2020. doi:10.1016/j.apenergy.2019.113941.

[147] K. R. Simonsen, D. S. Hansen, S. Pedersen. Challenges in CO_2 transportation: Trends and perspectives. *Renewable and Sustainable Energy Reviews*, 191:114149, 2024. doi:10.1016/j.rser.2023.114149.

[148] Global CCS institute. TRANSPORTING CO_2. https://www.globalccsinstitute.com/wp-content/uploads/2018/12/Global-CCS-Institute-Fact-Sheet_Transporting-CO2-1.pdf, 2018.

[149] S. Peletiri, N. Rahmanian, I. Mujtaba. CO_2 Pipeline Design: A Review. *Energies*, 11(9):2184, 2018. doi:10.3390/en11092184.

[150] R. T. J. Porter, M. Fairweather, M. Pourkashanian, R. M. Woolley. The range and level of impurities in CO_2 streams from different carbon capture sources. *International Journal of Greenhouse Gas Control*, 36:161 – 174, 2015. doi:10.1016/j.ijggc.2015.02.016.

[151] L. Quynh Hoa, R. Baessler, D. Bettge. On the Corrosion Mechanism of CO_2 Transport Pipeline Steel Caused by Condensate: Synergistic Effects of NO_2 and SO_2. *Materials*, 12(3):364, 2019. doi:10.3390/ma12030364.